Functional and structural studies of the Abruptex region of the Notch receptor



Zhi Han Bo

Department of Biochemistry and St Cross College

University of Oxford

A thesis submitted for the degree of

Doctor of Philosophy (DPhil)

Michaelmas term 2024

Functional and structural studies of the Abruptex region of the Notch receptor

A thesis submitted for the degree of Doctor of Philosophy by Zhi Han Bo, Department of Biochemistry, St Cross College, Michaelmas term 2024

Abstract

This project aimed to study the function and structure of the Abruptex (Ax) region (EGF24-29) within the Notch receptor, where missense mutations induce a phenotype indicative of enhanced Notch signalling in *Drosophila*. These mutations can be further divided into three classes (homozygous lethal, *N* suppressor, *N* enhancer) based on the phenotype when expressed with a null allele of Notch.

Assays to study Notch1 (N1) cell surface level, ligand binding, trans-activation and cis-inhibition were developed and performed on N1 reporter cells carrying Ax mutations. Homozygous lethal mutations reduced cell surface N1 level. While not reducing cell surface N1 level or amount of ligand constructs bound to the cell, *N* suppressor and *N* enhancer mutations reduced N1 trans-activation by Jag1 and Dll4.

Cis-inhibition assays suggested that *N* suppressors reduced JAG1-mediated N1 cis-inhibition when grown with either trans-Jag1 or trans-Dll4, while *N* enhancers reduced JAG1-mediated cis-inhibition when grown with trans-Jag1 but not trans-Dll4. In addition, while *N* suppressors did not affect cis-inhibition by cis-DLL4, *N* enhancer H1129Y reduced it. These results suggest that *N* suppressors and *N* enhancers may affect different properties of the receptor.

Activation assays performed in the presence of the glycosyltransferase Lfng discovered that Ax variants were less sensitive than WT to the negative effect of Lfng on Jag1-mediated N1 trans-activation. Also, when grown with trans-Jag1, Ax variants showed higher activation levels than WT upon co-expression of cis-JAG1 and Lfng, which may help to explain the Notch-enhancing *Ax* phenotype in the *Drosophila* wing.

SAXS analysis of hN1 EGF20-27 and EGF20-29 fragments suggested an extended structure for EGF24-27 but a potentially bent or flexible structure for EGF27-29. This finding showed that *N* suppressors in EGF24-25 and *N* enhancers in EGF27-29 may be located in regions of different structures.

These data establish new information on the structure and function of the Ax region and the mechanism underlying the Notch-enhancing phenotypes caused by the Ax variants in *Drosophila*. The native property of the Ax region has a role in optimising trans-activation and cis-inhibition of N1 both in the presence and absence of Lfng.

Acknowledgement

I would like to express my sincere thanks to my supervisor Prof Penny Handford for giving me the opportunity to do my DPhil project with her and for being such a responsible supervisor. I am grateful for the continuous generous support, guidance and help she has given me during my time in her lab and for the valuable suggestions, criticisms and encouragement she provided during the writing process of this thesis.

I would like to thank Prof Christina Redfield and Dr Edward D. Lowe for their guidance in the collection and analysis of SEC-SAXS data in this thesis and for the comments they provided on the related thesis chapter. I gratefully thank Prof Christina Redfield and Prof Alison Woollard for being my thesis committee members and for their genuine feedback on my progress and plan during the DPhil study. I would like to thank my secondary supervisor, Prof Catherine Pears, for providing useful assessments of my progress each term in graduate supervision reports. I want to thank my thesis examiners, Prof Sarah J. Bray and Dr Michael Ranes, for their time and effort spent on assessing my work. Also, I wish to thank Prof Robert S. Haltiwanger and Dr Steven John Berardinelli for generously sharing their Fringe-encoding plasmids.

I would like to thank my current and previous lab members, Xinyi Feng, Dr Hilman Nurmhadi, Dr Yao Meng and Dr Shrutti Mittal for their support both to my research and to the atmosphere of the lab. I hope our friendship will continue after my DPhil study. I wish to thank Xinyi Feng for her help with my experiments, the quality time we spent on discussion about science and troubleshooting, and daily emotional support. I wish to thank Dr Hilman Nurmhadi for helping me maintain cell lines and prepare proteins for the SEC-SAXS project, and for collaborating on the EGF33 project. I wish to thank Dr Yao Meng and Dr Shruti Mittal for their guidance on experimental techniques in the first year of my DPhil study. Also, I am grateful for the opportunity Yao provided to write a review together and for her suggestions on my research even after she left Handford lab.

I would like to express my deep gratitude to my family, especially my parents, Ke Li and Sen Bai, and my siblings, Zhiyan Bo and Jinghan Bo, for their support both mentally and financially during my DPhil study, for their patience and care when I am not at my best, and for their endless and generous love. Also, I would like to thank all my friends, including Ruohan Zhang, Gege Yang, Qian Li, Yuhan Zheng and Zishan Zhang for their emotional support and encouragement. I am deeply grateful for all the challenges and gains God has given me throughout my time in Oxford.

Table of Contents

List of Figures……..xi

List of Tables……xv

List of Abbreviations…….. xvii

1 Introduction 1

1.1 General Background of Notch Signalling 2

1.1.1 Overview of Notch signalling 2

1.1.2 Molecular mechanism of canonical Notch signalling 3

1.1.3 Notch in diseases 8

1.2 Notch Receptors 14

1.2.1 Overview of Notch receptors 14

1.2.2 EGF domains 15

1.2.2.1 Conserved structure of EGF domains 15

1.2.2.2 Calcium-binding EGF 18

1.2.2.3 Structure of tandem EGF repeats 19

1.2.3 Ligand-binding region 20

1.2.4 Abruptex region 21

1.2.5 Negative regulatory region 22

1.2.6 Structure of the Notch extracellular domain 23

1.2.7 Notch intracellular domain 26

1.2.8 Notch post-translational modification 27

1.2.8.1 Overview of Notch post-translational modification 27

1.2.8.2 O-fucosylation 30

1.2.8.3 Fringe modification of O-fucose 31

1.2.8.4 O-glucosylation 34

1.2.8.5 O-GlcNAcylation 36

1.2.8.6 N-linked glycosylation 37

1.2.8.7 β-hydroxylation 37

1.3 Canonical Notch Ligands 38

1.3.1 Overview of Notch ligands 38
1.3.2 The C2 domain 41
1.3.3 The Delta/Serrate/LAG-2 domain 42
1.3.4 Ligand post-translational modification 43
1.4 Interaction between Notch receptor and ligand 44
1.4.1 Insights from the structures of receptor-ligand complexes 44
1.4.2 Endocytosis and mechanical force 46
1.4.3 The binding affinity of ligands 49
1.5 Cis-inhibition 50
1.5.1 Molecular mechanism of Notch cis-inhibition 50
1.5.2 Onset and strength of cis-inhibition 54
1.5.3 Domains required for cis-interaction 55
1.5.4 Cis-inhibition in development 57
1.6 Abruptex region 59
1.6.1 Ax variants 59
1.6.2 Hypotheses of the effects of Ax variants 63
1.7 Thesis Aims 65
2 Materials and Methods 67
2.1 DNA manipulation 68
2.1.1 Polymerase chain reactions (PCR) 68
2.1.2 DNA gel electrophoresis 68
2.1.3 DNA extraction from agarose TBE gel 68
2.1.4 Genomic DNA extraction 69
2.1.5 DNA sequencing 69
2.1.6 DNA concentration determination 69
2.2 Cloning 69
2.2.1 Cloning strategy for mN1 variants 69
2.2.2 Mutagenesis by Overlap Extension 72

2.2.3 Restriction enzyme digestion 73
2.2.4 DNA ligation 73
2.3 Plasmid amplification 74
2.3.1 Transformation of competent *E. coli* 74
2.3.2 Plasmid purification 74
2.4 Reverse transcription polymerase chain reaction (RT-PCR) 75
2.4.1 RNA extraction 75
2.4.2 RNA concentration determination 75
2.4.3 Reverse transcription 75
2.4.4 cDNA PCR 76
2.5 Cell culture 76
2.5.1 General methods 76
2.5.2 Adherent cell lines 77
2.5.2.1 Adherent cell line maintenance 77
2.5.2.2 Adherent cell line sub-culturing 78
2.5.2.3 Adherent cell line freezing and thawing 78
2.5.3 HEK293F cell line 79
2.5.3.1 HEK293F maintenance and sub-culturing 79
2.5.3.2 HEK293F freezing and thawing 80
2.5.4 S2 cell line 80
2.5.4.1 S2 maintenance and sub-culturing 80
2.5.4.2 S2 freezing and thawing 81
2.6 Protein production 82
2.6.1 Large-scale transfection for protein purification 82
2.6.1.1 Large-scale transfection of HEK293T 82
2.6.1.2 Large-scale transfection of HEK293F 82
2.6.2 HEK-RBP mN1 stable cell line generation 83
2.6.2.1 HEK-RBP mN1 cell line 83
2.6.2.2 HEK-RBP transfection 84

2.6.2.3 HEK-RBP mN1 selection and maintenance 85
2.6.3 HEK cells transient transfection 85
2.6.4 S2 stable cell line generation 86
2.6.4.1 S2 cell transfection 86
2.6.4.2 S2 hN1 cell selection and maintenance 86
2.7 Protein purification 87
2.7.1 Protein purification process 87
2.7.2 Cell medium collection 88
2.7.3 Immobilised metal affinity chromatography (IMAC) 89
2.7.4 Size exclusion chromatography (SEC) 89
2.7.5 His tag removal by HRV 3C protease 90
2.8 Protein analysis 90
2.8.1 Protein Concentration Determination 90
2.8.2 Sodium dodecyl sulfate-polyacrylamide gel electrophoresis (SDS-PAGE) 91
2.8.3 Coomassie staining 91
2.8.4 Western blot 91
2.9 Notch activation assays 92
2.9.1 Ligand-independent activation assay 92
2.9.2 Ligand-dependent activation assay 93
2.9.2.1 Plate-based trans-activation assay 93
2.9.2.2 Co-culture-based trans-activation assay 93
2.9.3 Cis-inhibition assay 94
2.10 Cell surface protein staining 95
2.11 Ligand binding assay 95
2.12 Flow cytometry (FACS) analysis 96
2.13 Small angle X-ray scattering (SAXS) 98
2.13.1 Sample preparation and data collection 98

2.13.2 SAXS data analysis 98
2.14 Statistical analysis 99
3 Identifying the role of the Abruptex region in Notch1 trans-activation 100
3.1 Introduction 101
3.2 Ax region in human NOTCHs 102
3.3 HEK-RBP mN1 cell line establishment 104
3.3.1 Flp-In TRex 293 mN1-NLuc/CLuc-RBPJκ cell line 104
3.3.2 mN1 cell lines made in this project 105
3.3.3 Verification of stable cell line 106
3.4 Studying the effect of Ax variants on cell surface N1 level 110
3.4.1 Two assays for cell surface N1 quantification 110
3.4.2 Cell surface N1 level of Ax variants 112
3.5 Trans-activation of Ax variants with plate-coated protein 114
3.5.1 Assay design 114
3.5.2 Ligand protein production and purification 115
3.5.3 Ligand titration 118
3.5.4 Plate-based trans-activation of Ax variants 119
3.6 Trans-activation of Ax variants by co-culturing with ligand-expressing B16 cells 122
3.6.1 Assay design and optimisation 122
3.6.2 Co-culture trans-activation of Ax variants 128
3.7 Ligand binding ability of Ax variants 129
3.7.1 Assay design and optimisation 129
3.7.2 Ligand binding of Ax variants 132
3.8 Discussion 135

4 Investigating the role of the Abruptex region in Notch1 cis-inhibition by JAG1 141

4.1 Introduction 142

4.2 JAG1 cis-inhibition assay design and optimisation 142

4.3 *JAG1* RNA expression verification 145

4.4 Effect of cis-JAG1 expression on N1 WT activation 148

4.5 Cis-inhibition of Ax variants by JAG1 152

4.6 Discussion 157

5 Investigating the role of the Abruptex region in Notch1 cis-inhibition by DLL4 162

5.1 Introduction 163

5.2 DLL4 cis-inhibition assay design and optimisation 163

5.3 *DLL4* RNA expression verification 166

5.4 Effect of cis-DLL4 expression on N1 WT activation 168

5.5 Cis-inhibition of Ax variants by DLL4 170

5.6 Discussion 175

6 Studying the response of Ax variants to Fringe expression 181

6.1 Introduction 182

6.1.1 Overall assay design 184

6.1.2 Experimental setup 185

6.2 Studying the effects of Lfng expression on N1 trans-activation 189

6.2.1 Effects of Lfng expression on N1 WT trans-activation 189

6.2.2 Effects of Lfng expression on trans-activation of Ax variants 190

6.3 Studying the effects of Lfng expression on N1 cis-inhibition by JAG1 193

6.3.1 Effects of Lfng expression on N1 WT cis-inhibition by JAG1 193

6.3.2 Effects of Lfng expression on cis-inhibition of Ax variants by JAG1

194

6.3.2.1 Cis-Inhibition of N947I and H1129Y in the absence of Fng. 194

6.3.2.2 Cis-Inhibition of N947I in the presence of Lfng 195

6.3.2.3 Cis-inhibition of H1129Y in the presence of Lfng 196

6.4 Discussion 198

7 Low-resolution structural analysis of the Abruptex region 204

7.1 Introduction 205

7.2 SEC-SAXS sample preparation 206

7.2.1 Protein purification strategy 206

7.2.2 Purification of hN1 EGF20-27 and EGF20-29 209

7.2.3 SEC-SAXS preparation 214

7.3 SEC-SAXS for hN1 constructs 215

7.3.1 SEC-SAXS 215

7.3.2 Data analysis pipeline 218

7.3.3 SEC-SAXS for hN1 EGF20-27 222

7.3.3.1 Foldedness and length 222

7.3.3.2 Structural model generated by SREFLEX 224

7.3.3.3 Structural model generated by AlphaFold2 225

7.3.4 SEC-SAXS for hN1 EGF20-29 226

7.3.4.1 Foldedness and length 226

7.3.4.2 Structural model generated by SREFLEX 228

7.3.4.3 Structural model generated by AlphaFold2 230

7.4 Discussion 231

8 Discussion 236

8.1 Aim of this thesis 237

8.2 Assessment of experimental approaches employed in this project 237

8.2.1 Assay systems to test N1 signalling 237

8.2.2 Low-resolution structural analysis of N1 239

8.3 Structure of the Ax region 240

8.4 The role of the Ax region in Notch signalling 242

8.4.1 Misfolding of EGF24-25 affected receptor trafficking 242

8.4.2 The Ax region facilitates trans-activation of N1 243

8.4.3 The Ax region regulates cis-inhibition of N1 247

8.5 Ax variants in the presence of Lfng 250

8.6 Ax variants and the *Ax* phenotype 254

8.7 Future work 256

9 Bibliography 260

List of Figures

Figure 1.1. Schematic illustration of canonical Notch signalling. 6

Figure 1.2. Three modes of Notch signalling in tissues. 8

Figure 1.3. Domain arrangement of Notch receptors..... 15

Figure 1.4. Structures of EGF and cbEGF domains. 17

Figure 1.5. The *Notch* and *Abruptex* phenotypes in *Drosophila*..... 22

Figure 1.6. Structure of the NRR. 23

Figure 1.7. Structure of NECD and intramolecular interactions. 25

Figure 1.8. O-glycosylation of Notch receptor..... 29

Figure 1.9. Domain arrangement of Notch ligands. 40

Figure 1.10. Structure of the N terminus of canonical Notch ligands. 41

Figure 1.11. Structural basis of LBR-ligand interaction. 46

Figure 1.12. Bilateral endocytosis of receptor and ligand during trans-activation. 49

Figure 1.13. Potential mechanisms of cis-inhibition. 53

Figure 1.14. Receptor and ligand domains involved in cis-inhibition..... 57

Figure 1.15. Notch cis-inhibition during *Drosophila* photoreceptor differentiation 58

Figure 1.16. Protein sequence alignment for Ax region in Notch receptors across species. 60

Figure 1.17. Schematic illustration of the locations of Ax variants in *Drosophila*. 63

Figure 2.1. Cloning for pUC-19 mN1 (512-4131) plasmid..... 71

Figure 2.2. Cloning for pcDNA5/FRT-mN1-NLuc plasmid..... 72

Figure 2.3. mN1 was inserted in the FRT site encoded by the HEK-RBP cell line. 84

Figure 2.4. Protein purification process. 88

Figure 2.5. Gating strategies for flow cytometry 97

Figure 3.1. Protein sequence alignment for EGF16 and Ax regions across Notch receptors..... 103

Figure 3.2. DNA sequencing of HEK-RBP mN1 variant cell lines. 108

Figure 3.3. RT-PCR for HEK-RBP mN1 cell lines. 109
Figure 3.4. Cell surface mN1 level quantification by two assays 111
Figure 3.5. Cell surface mN1 level quantification for mN1 Ax variants. 113
Figure 3.6. mN1 trans-activation assays. 115
Figure 3.7. Ligand NE3-Fc-His purification. 117
Figure 3.8. Ligand NE3 titration for plate-based mN1 trans-activation assay. 119
Figure 3.9. Trans-activation of mN1 Ax variants by plate-coated purified protein. 121
Figure 3.10. Cell number and co-culturing time optimisations for activation by B16 mJag1. 124
Figure 3.11. Cell number and co-culturing time optimisations for activation by B16 mDll4. 125
Figure 3.12. Substrate incubation time optimisation for co-culture-based activation assays. 127
Figure 3.13. Trans-activation of mN1 Ax variants by ligands expressed in B16 cells. 129
Figure 3.14. Optimisation for ligand binding assay. 131
Figure 3.15. Quantification of hJAG1 NE3 bound to mN1 Ax variants. 134
Figure 3.16. Quantification of hDLL4 NE3 bound to mN1 Ax variants. 135

Figure 4.1. Optimisation for cis-inhibition assay using cis-JAG1. 144
Figure 4.2. RT-PCR for *JAG1* expressed in mN1 cells transfected with cis-JAG1 plasmid. 146
Figure 4.3. RT-PCR for *mN1* expressed in mN1 cells transfected with cis-JAG1 plasmid. 147
Figure 4.4. RT-PCR for *GAPDH* expressed in mN1 cells transfected with cis-JAG1 plasmid. 148
Figure 4.5. Trans-activation of mN1 WT cells transfected with cis-JAG1 plasmid. 151
Figure 4.6. Trans-activation of cis-JAG1-expressing mN1 Ax variant cells by B16 mJag1. 155
Figure 4.7. Trans-activation of cis-JAG1-expressing mN1 Ax variant cells by B16 mDll4.

..... 156

Figure 5.1. Optimisation for cis-inhibition assay using cis-DLL4. 165
Figure 5.2. RT-PCR of mN1 cells transfected with cis-DLL4 plasmid. 167
Figure 5.3. Trans-activation of mN1 WT cells transfected with cis-DLL4 plasmid. 169
Figure 5.4. Trans-activation of cis-DLL4-expressing mN1 Ax variant cells by B16 mJag1. 172
Figure 5.5. Trans-activation of cis-DLL4-expressing mN1 Ax variant cells by B16 mDll4. 174
Figure 5.6. Locations of *N* enhancer mutations in N1 EGF29..... 180

Figure 6.1. Schematic illustration of Lfng modifications of O-fucose on mN1. 183
Figure 6.2. Plasmids used to study Lfng's effects on Notch activation and cis-inhibition. 188
Figure 6.3. Trans-activation of mN1 WT cells transfected with Lfng plasmid. 189
Figure 6.4. Trans-activation of mN1 N947I cells transfected with Lfng plasmid. 191
Figure 6.5. Trans-activation of mN1 H1129Y cells transfected with Lfng plasmid. 192
Figure 6.6. Trans-activation of mN1 WT cells transfected with cis-JAG1 and Lfng plasmids. 194
Figure 6.7. Trans-activation of mN1 N947I cells transfected with cis-JAG1 and Lfng. 197
Figure 6.8. Trans-activation of mN1 H1129Y cells transfected with cis-JAG1 and Lfng. 198

Figure 7.1. Existing structural models of hN1ECD. 206
Figure 7.2. Preparation of protein samples for SEC-SAXS..... 208
Figure 7.3. Purification of hN1 EGF20-27. 211
Figure 7.4. Purification of hN1 EGF20-29. 213
Figure 7.5. SDS-PAGE for hN1 constructs after dialysis. 215
Figure 7.6. SEC-SAXS data collection. 217

Figure 7.7. Quality check for SEC-SAXS data..... 219
Figure 7.8. Determination of the shape and foldedness of a construct by SAXS. 221
Figure 7.9. Prediction of the foldedness and length of hN1 EGF20-27. 223
Figure 7.10. Structural model of hN1 EGF20-27 generated by SREFLEX..... 225
Figure 7.11. Structural model of hN1 EGF20-27 generated by AlphaFold2. 226
Figure 7.12. Prediction of the foldedness and length of hN1 EGF20-29. 228
Figure 7.13. Structural model of hN1 EGF20-29 generated by SREFLEX..... 229
Figure 7.14. Structural model of hN1 EGF20-29 generated by AlphaFold2. 230
Figure 7.15. Structural model of hN1 Ax region. 231
Figure 7.16. Structures of (cb)EGF-EGF pairs. 234

Figure 8.1. Structure of hN1ECD. 241
Figure 8.2. Structural model of hN1 EGF27-30 generated by AlphaFold2. 245
Figure 8.3. Activation of N1 WT and Ax variants by different trans-ligands under conditions with and without Lfng and cis-JAG1. 253

List of Tables

Table 1.1. Summary of cancer-related NOTCH mutations. Table adapted from Meng et al. (2023). 10

Table 1.2. Summary of genetic diseases associated with mutations in components of the Notch signalling pathway, including receptors, ligands, glycosyltransferases and RBPJk. Table adapted from Meng et al. (2023). 12

Table 1.3. Effects of Fng expression on N1 and N2 activation by different trans-ligands and the interaction between N1 and different cis-ligands. 33

Table 1.4. Abruptex variants identified in *Drosophila* with hN1 homolog shown (De Celis and Garcia-Bellido, 1994). 59

Table 2.1. List of restriction enzymes (NEB). 73

Table 2.2. Recipe for RT reaction. 76

Table 3.1. HEK-RBP mN1 cell lines established in this project. 106

Table 3.2. Summary of the effects of Ax variants on N1 cell surface level and ligand binding. 137

Table 3.3. Summary of the effects of Ax variants on N1 trans-activation. 138

Table 4.1. Summary for N1 WT trans-activation and cis-inhibition by JAG1. 158

Table 4.2. Summary of effects of cis-JAG1 expression on Jag1-mediated trans-activation of Ax variants. 159

Table 4.3. Summary of effects of cis-JAG1 expression on Dll4-mediated trans-activation of Ax variants. 160

Table 5.1. Summary for N1 WT trans-activation and cis-inhibition by DLL4. 176

Table 5.2. Summary of effects of cis-DLL4 expression on Jag1-mediated trans-activation of Ax variants. 178

Table 5.3. Summary of effects of cis-DLL4 expression on Dll4-mediated trans-activation of Ax variants. 178

Table 6.1. Effects of Lfng expression on N1 activation by different trans-ligands and the strength of interactions between N1 and different cis-ligands (LeBon *et al.*, 2014; Kakuda and Haltiwanger, 2017; Kakuda *et al.*, 2020; Kuintzle, Santat and Elowitz, 2023). 185

Table 6.2. Effects of Lfng expression on the trans-activation of mN1 WT and Ax variants. 199

Table 6.3. Changes in Jag1-mediated trans-activation of mN1 WT and Ax variants upon co-expression of cis-JAG1 and Lfng. 200

Table 6.4. Changes in DLL1-mediated trans-activation of mN1 WT and Ax variants upon co-expression of cis-JAG1 and Lfng. 201

Table 8.1. Summary of the effects of N1 Ax mutations on cis-inhibition. 248

Table 8.2. Proposed experiments to further characterise the effects of Ax substitutions on Notch signalling. 258

List of Abbreviations

A	Absorbance
Å	Ångstrom
ADAM	A disintegrin and metalloprotease-containing protein
AF488	Alexa Fluor 488
ANK	Ankyrin repeat
AOS	Adams-Oliver syndrome
APC	Allophycocyanin
AspH	Aspartate/asparagine β-hydroxylase
ASX	Asn/Asp
Ax	Abruptex
BAV	Bicuspid aortic valve
bp	Base pairs
BSA	Bovine serum albumin
c	*Caenorhabditis elegans*
CADASIL	Cerebral autosomal dominant arteriopathy with subcortical infarcts and leukoencephalopathy
cAMP	Cyclic adenosine 3′,5′-monophosphate
cbEGF	Calcium-binding EGF
CDK	Cyclin-dependent kinase
cDNA	Complementary DNA
CHO	Chinese hamster ovary cell
CLuc	C terminal half of the luciferase domain
CMV	Cytomegalovirus
Co-IP	Co-immunoprecipitation
CRD	Cysteine-rich region
d	*Drosophila melanogaster*
D/V	Dorsal/Ventral
Da	Dalton

DAPI	4′,6-diamidino-2-phenylindole
Dl	Delta
DLK1	Delta Like Non-Canonical Notch Ligand 1
Dll1	Delta-like1
Dll3	Delta-like3
Dll4	Delta-like4
D_{max}	Maximum dimension
DMEM	Dulbecco's Modified Eagle Medium
DMSO	Dimethyl sulfoxide
DNA	Deoxyribonucleic acid
DNER	Delta and Notch-like epidermal growth factor-related receptor
dNTPs	Deoxynucleotide triphosphates
DSL	Delta/Serrate/LAG-2
DTT	Dithiothreitol
DTX4	Deltex E3 Ubiquitin Ligase 4
DVNI	D909V/N947I
Dx	Deltex
ECD	Extracellular domain
EDTA	Ethylenediaminetetraacetic acid
EGF	Epidermal growth factor
EGTA	Ethylene glycol-bis(β-aminoethyl ether)-N,N,N′,N′-tetraacetic acid
EHBA	Extrahepatic biliary atresia
ELISA	Enzyme-linked immunosorbent assay
E(N)	*Ax N* enhancer allele
EOGT	EGF domain specific O-linked N-Acetylglucosamine transferase
ER	Endoplasmic reticulum
ESI-MS	Electron spray ionisation mass spectrometry
EV	Empty vector

EX-CELL 420 + FBS	EX-CELL 420 Serum-Free Medium supplemented with 10% FBS
FACS	Flow cytometry fluorescence-activated cell sorting
FAEK	F207A/E228K
FAYA	F195A/Y216A
FBS	Fetal bovine serum
FBW7	F-box/WD repeat-containing protein 7
Fib	Fibrillin
flgM	Negative regulator of flagellin synthesis
Fng	Fringe
g	gram
GlcNAc	β1,3-N-acetylglucosaminyl
GPI	Glycosylphosphatidylinositol
h	Human
HD	Heterodimerization domain
HEK	Human embryonic kidney cell
HEK-RBP	Flp-In TRex 293 CLuc-RBPJκ
HEK-RBP mN1	Flp-In TRex 293 mN1-NLuc/CLuc-RBPJκ
HEPES	4-(2-hydroxyethyl)-1-piperazineethanesulfonic acid
HES	Hairy/enhancer of split
HEY	Hairy/enhancer of split related with YRPW motif
hFA IX	Human coagulation factor IX
HRP	Horseradish peroxidase
HRV 3C	Recombinant type 14 3C protease from human rhinovirus
I	Intensity
I	Ionic strength
ICD	Intracellular domain
IgG	Immunoglobulin G
IMAC	Immobilised metal affinity chromatography

IP3-DAG	Inositol trisphosphate-diacylglycerol
Jag1	Jagged1
Jag2	Jagged2
K_d	Dissociation constant
l	litre
L-Ax	*Ax* homozygous lethal allele
LBR	ligand-binding region
LNR	LIN-12/Notch repeats
Lfng	Lunatic fringe
LTBP	Latent TGF-β binding protein
m	Mouse
M	Mole/dm3
mAb	Monoclonal antibody
MAML	Mastermind-like protein
Mfng	Manic fringe
MIB	Mindbomb
Min	Minutes
MNNL	Module at the N-terminal of Notch ligands
MQ	Milli-Q
MS	Mass spectrometry
MSP-1	Merozoite surface protein 1
MW	Molecular weight
N	Notch
N^r	Null Notch allele
N1	Notch1
N2	Notch2
N3	Notch3
N4	Notch4
NE3	N terminal C2 to EGF3

NECD	Extracellular domain of Notch
NEUR	Neuralized
NEXT	Notch extracellular truncation
NICD	Intracellular domain of Notch
NIH	Mouse NIH/Swiss embryo fibroblast cell
Ni-NTA	Nickel-nitrilotriacetic acid
NLS	Nuclear localisation sequence
NLuc	N terminal half of the luciferase domain
NMR	Nuclear Magnetic resonance
NRR	Negative regulatory region
ns	Not significant
O-fut1	O-fucosyltransferase 1
P(r)	Pair distance
PBS	Phosphate buffered saline
PBS-EDTA	Phosphate buffer saline with 1 mM EDTA
PBST	Phosphate buffered saline with 0.1% V/V Triton X-100
PCR	Polymerase chain reaction
PDB	Protein Data Bank
PE	Phycoerythrin
PEST	Proline/glutamic acid/serine/threonine-rich motif
pN	Piconewton
POFUT1	Protein O-fucosyltransferase 1
POGLUT1	Protein O-glucosyltransferase 1
POGLUT2	Protein O-glucosyltransferase 2
POGLUT3	Protein O-glucosyltransferase 3
PTM	Post-translational modification
r	Distance between scattering elements within the particle during SAXS analysis
RAM	RBPJk association module

RBPJk	Recombination signal binding protein for immunoglobulin kappa J region family
RDC	Residual dipolar coupling
Rfng	Radical fringe
RMSD	Root mean square deviation
RNA	Ribonucleic acid
rpm	Revolutions per minute
RPMI	Roswell Park Memorial Institute Medium
RT	Reverse transcription
S2	Schneider 2
SAXS	Small angle X-ray scattering
SCC	Squamous cell cancer
SD	Standard deviation
SDS-PAGE	Sodium dodecyl sulfate–polyacrylamide gel electrophoresis
SEC	Size exclusion chromatography
sEH	Soluble epoxide hydrolase
Ser	Serrate
SHARP	SMRT/HDAC1 associated repressor protein
SPR	Surface plasmon resonance
Su(N)	*Ax N* suppressor allele
SV40	Simian virus 40
TAD	Transcriptional activation domain
T-ALL	T-cell acute lymphoblastic leukaemia
TBE	Tris/borate/EDTA
TF	Transcription factor
Tris	Tris (hydroxymethyl) aminomethane
trypsin-PBS	0.33 g/l trypsin in PBS-EDTA
TSP2	Thrombospondin2
Ub	Ubiquitin

UV	Ultraviolet
V	Volt
V/V	Volume/volume
VDW	Van der Waals
W/V	Weight/volume
Wg	Wingless
WT	Wild type
xg	Number of times the gravitational force
XL-MS	Cross-linking mass spectrometry
ϵ	Extinction coefficient

Standard symbols from the Periodic Table have been used to represent the chemical elements.

List of amino acid abbreviations used

A	Ala	Alanine
C	Cys	Cysteine
D	Asp	Aspartic acid
E	Glu	Glutamic acid
F	Phe	Phenylalanine
G	Gly	Glycine
H	His	Histidine
I	Ile	Isoleucine
K	Lys	Lysine
L	Leu	Leucine
M	Met	Methionine
N	Asn	Asparagine
P	Pro	Proline
Q	Gln	Glutamine
R	Arg	Arginine
S	Ser	Serine
T	Thr	Threonine
V	Val	Valine
W	Trp	Tryptophan
Y	Tyr	Tyrosine

Metric prefixes

p	10^{-12}
n	10^{-9}
μ	10^{-6}
m	10^{-3}
c	10^{-2}
k	10^{3}

1 Introduction

1.1 General Background of Notch Signalling

1.1.1 Overview of Notch signalling

The Notch signalling pathway generates a juxtacrine short-range signal regulating many developmental and homeostatic processes, including the determination and maintenance of cell fate (reviewed by Kobia *et al.*, 2020; Porcheri *et al.*, 2020; Seymour *et al.*, 2020; Duvall *et al.*, 2022; Logeay *et al.*, 2022; Gozlan and Sprinzak, 2023).

The importance of Notch signalling was first reported by Dexter et al. in 1914 when mutations linked to a single gene locus, later named *Notch*, in *Drosophila melanogaster* induced the development of notched wing edges in mutant flies, known as the *Notch (N)* phenotype (Dexter, 1914). Subsequent studies discovered that these mutations were homozygous lethal, sex-linked, and dominant with regard to the wing phenotype (Morgan, 1917). Further studies of Notch mutation revealed the gene's involvement in the embryonic development of *Drosophila*, including the development of the wing veins, central nervous system, eyes, and the maintenance of the Dorsal/Ventral (D/V) boundary (Lehmann *et al.*, 1983, p. 198; Xu *et al.*, 1990; Artavanis-Tsakonas, 1999; Singh and Choi, 2003).

The key components of the Notch signalling pathway are Notch receptors and their canonical ligands, which are both Type I transmembrane proteins. The primary structure of *Drosophila* Notch (dN) was first characterised in 1985 when it was discovered that there was amino acid sequence homology of its extracellular domain with epidermal

growth factor (EGF) (Wharton *et al.*, 1985). Two types of ligands, Delta (Dl) and Serrate (Ser) that directly bind to dN were identified in *Drosophila* (Vässin *et al.*, 1987; Fleming *et al.*, 1990). Homologues of dN were found subsequently in other species including *Caenorhabditis elegans* (Yochem, Weston and Greenwald, 1988; Austin and Kimble, 1989), *Xenopus* (Coffman, Harris and Kintner, 1990), human (Ellisen *et al.*, 1991), rat (Weinmaster, Roberts and Lemke, 1991), mouse (Del Amo *et al.*, 1992), and zebrafish (Bierkamp and Campos-Ortega, 1993), suggesting Notch signalling is evolutionarily conserved in metazoan species. *Drosophila* remains the best-characterised model organism for Notch signalling with only one Notch receptor and two ligands. Mammals have four Notch receptors (N1 to 4), in which Notch1 (N1) and Notch2 (N2) share structural homology with dN, five ligands, in which Jagged1 (Jag1) and Jagged2 (Jag2) belong to the Jagged/Serrate family and Delta-like1, 3, 4 (Dll1, 3, 4) belong to the Delta family.

1.1.2 Molecular mechanism of canonical Notch signalling

A schematic overview of canonical Notch signalling is shown in Figure 1.1. After translation at the ribosome, the extracellular domains of Notch receptors and ligands are imported via a signal peptide into the lumen of the endoplasmic reticulum (ER), where they undergo posttranslational modifications, and are translocated to the Golgi and then the cell surface membrane, where they interact with other proteins, leading to activation or inhibition of Notch signalling.

Most Notch receptors (200-350 kDa) except dN are processed by a furin-dependent cleavage (S1) in the trans-Golgi network, forming a heterodimeric structure before being transported to the cell surface membrane (Blaumueller *et al.*, 1997; Logeat *et al.*, 1998). The two fragments produced by S1 cleavage are associated non-covalently, where the shorter 120-kDa fragment contains the transmembrane and intracellular domain of the receptor and the longer 200-kDa fragment is extracellular (Blaumueller *et al.*, 1997; Sanchez-Irizarry *et al.*, 2004).

Direct interactions of the extracellular domain of Notch (NECD) and ligand expressed on neighbour cells (in trans), along with a pulling force generated by ligand ubiquitination and endocytosis, induce a conformational change of the receptor, changing the autoinhibitory conformation of the membrane-proximal negative regulatory region (NRR) to expose a proteolytic cleavage (S2) site to ADAM family metalloproteases (Brou *et al.*, 2000; Stephenson and Avis, 2012), which release majority of the NECD. This S2-cleaved product, termed Notch extracellular truncation (NEXT), is subsequently cleaved at the S3 site by the γ-secretase complex at the remaining intramembrane region (Schroeter, Kisslinger and Kopan, 1998; Struhl and Adachi, 2000). The intracellular domain of Notch (NICD) is released and translocated to the nucleus, where it binds to the transcription factor (TF), the recombination signal binding protein for immunoglobulin kappa J region family (RBPJk, also known as CSL or CBF1/Su(H)/Lag-1), displacing the corepressor proteins, such as Hairless (Barolo *et al.*, 2002) and SHARP (Oswald *et al.*, 2002), and inviting coactivators, such as Mastermind-like proteins (MAML1-3) (Bray and Gomez-

Lamarca, 2018; Falo-Sanjuan *et al.*, 2019). RBPJk, in complex, binds to specific DNA binding sites (5' (C/T)GTGGAA 3') and activates the expression of primary target genes such as *HES* and *HEY,* which are transcriptional regulators mainly acting as repressors to control multiple key steps in development (Iso, Kedes and Hamamori, 2003; Kopan and Ilagan, 2009; Oswald and Kovall, 2018; Henrique and Schweisguth, 2019; Sprinzak and Blacklow, 2021).

While Notch activation by ligands in trans leads to stimulation of the signalling pathway, ligands expressed in the same cell (in cis) are capable of forming cis-inhibitory complexes with Notch receptors in a cell-type-dependent manner. Cis-inhibition has important physiological roles and regulates wing development and sensory organ precursor cell selection in *Drosophila* amongst other developmental processes (de Celis and Bray, 1997; Sprinzak *et al.*, 2010; Del Gaudio, Liu and Lendahl, 2022; Troost *et al.*, 2023). Recently, cis-activation has been detected in various cell lines and has been shown to impact neural stem cell survival *in vitro* (Nandagopal, Santat and Elowitz, 2019).

The multiple modes of ligand-receptor interactions enhance the sensitivity, complexity and capacity of Notch signalling, integrating signals from within the cell, adjacent cells and the environment. With no secondary messenger cascades or enzymatic steps that amplify the signal, as occurs in other pathways such as the cAMP signalling pathway (Sutherland and Rall, 1958) and the IP3-DAG signalling pathway (Streb *et al.*, 1983), the number of receptors activated, thus the nuclear concentration of NICD, is directly

proportional to the signal strength.

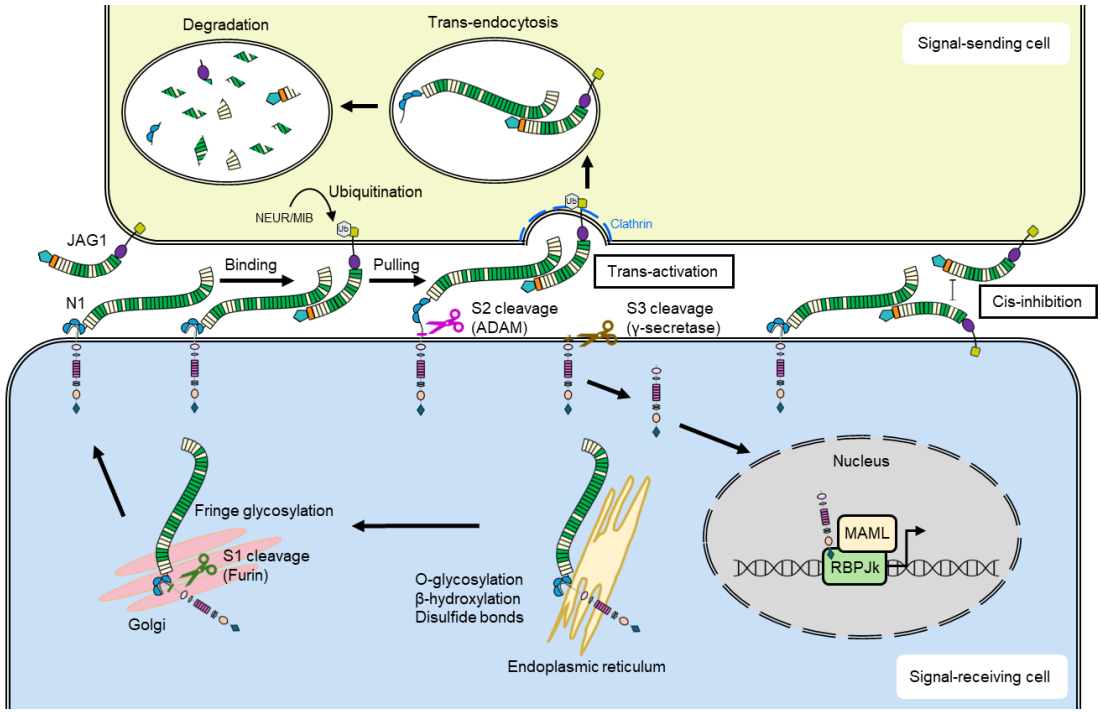


Figure 1.1. Schematic illustration of canonical Notch signalling.

The Notch (N1 in this figure) receptor is transported to the cell surface after post-translational modifications and S1 cleavage by furin in the ER and Golgi apparatus. Upon binding of NECD to canonical ligand (JAG1 in this figure) on the neighbour cell, a pulling force is generated by ligand ubiquitination by E3 ubiquitin (Ub) ligases, Neuralized (NEUR) and Mindbomb (MIB), and subsequent clathrin-dependent trans-endocytosis of ligand-receptor extracellular complex, which leads to the exposure of the S2 cleavage site in the NRR. ADAM metalloprotease cleaves at the S2 site and releases the NECD. This is followed by S3 cleavage by γ-secretase. The NICD is released and translocated to the nucleus where it interacts with transcription factor RBPJk and coeffectors such as MAML to switch on downstream genes. In contrast, ligands expressed in the same cell bind to the receptor and cause cis-inhibition. Cis-activation has recently been described but the basis for this interaction and its physiological importance are unclear.

Notch signalling's relative simplicity and flexibility allow it to be widely involved in the complex organisation and maintenance of tissues. Mediated by the short-range cell-cell or within-cell interactions between Notch receptors and ligands, the roles Notch

signalling plays in development and homeostasis can be divided into three modes (Bray, 1998): 1) lateral inhibition, which regulates the differentiation of sensory hair cells in the inner ear into hair cells and support cells (Kiernan, 2013); 2) lineage decision, which facilitates the differentiation of sensory organ precursor cells in *Drosophila* into anterior pIIb cell and posterior pIIa cell (Guo, Jan and Jan, 1996); and 3) boundary formation, which regulates the development of the D/V boundary in *Drosophila* wing and eye (Kim, Irvine and Carroll, 1995; Papayannopoulos *et al.*, 1998) (Figure 1.2).

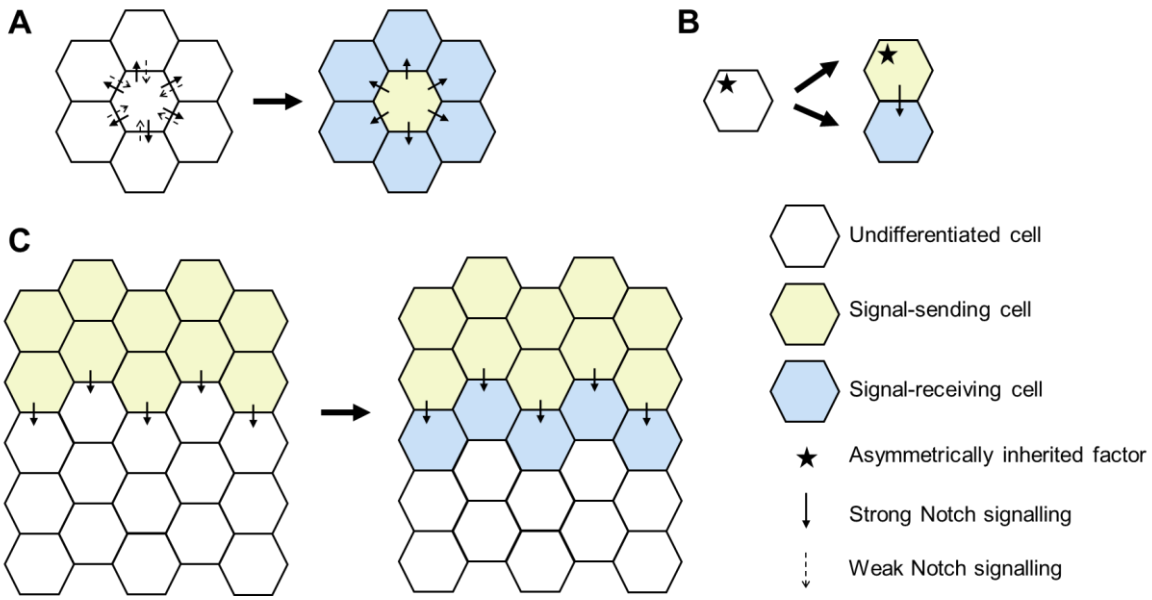


Figure 1.2. Three modes of Notch signalling in tissues.

Notch signalling regulates cell fate determination via three modes, lateral inhibition, lineage decision and boundary formation. White hexagons represent undifferentiated precursor cells. Green hexagons represent signal-sending cells expressing canonical Notch ligands. Blue hexagons represent signal-receiving cells expressing Notch receptors. (A) In lateral inhibition mode, in a population of undifferentiated precursors population, one cell stochastically expresses slightly more ligands and induces strong Notch signalling (green arrow) in neighbouring cells. The difference in Notch signalling intensity between cells is amplified by a feedback mechanism, leading to the differentiation of cells into different cell types. (B) In lineage decision mode, asymmetric inheritance of Notch signalling regulator (star icon) produces differential expressions of Notch signalling components and signalling levels in daughter cells, thus leading to the adoption of different cell fates. (C) In boundary formation mode, ligand-expressing cells on one side can only induce Notch signalling in cells at the junction with another population of cells. Therefore, the cells at the junction adopt a new cell fate and form a boundary that separates the two cell populations.

1.1.3 Notch in diseases

Notch signalling abnormality has been shown to contribute to the development of various types of cancer in either an oncogenic or tumour-suppressive manner depending on the cellular/tissue context and cancer type (Table 1.1). Notch plays

an oncogenic role in T-cell acute lymphoblastic leukaemia (T-ALL), colorectal cancer, breast cancer, ovarian cancer, prostate cancer, pancreatic adenocarcinoma, splenic marginal zone lymphoma, lung adenocarcinoma, hepatocellular carcinoma, adenoid cystic carcinoma, and glioma, where poor prognosis, lower survival and increase in the risk of developing resistance to endocrine therapy, chemotherapy and radiotherapy have been associated with abnormal Notch activation (Santagata *et al.*, 2004; Weng *et al.*, 2004; Reedijk *et al.*, 2005; Choi *et al.*, 2008; Guo *et al.*, 2009; Westhoff *et al.*, 2009; Gao *et al.*, 2011; Jubb *et al.*, 2012; Ho *et al.*, 2013; Stephens *et al.*, 2013; Kim *et al.*, 2015; Yuan *et al.*, 2015; Zheng *et al.*, 2015; Bernasconi-Elias *et al.*, 2016; Bray, 2016; Sugiyama *et al.*, 2016; Strati *et al.*, 2017; Vaish, Kim and Shim, 2017; Bonfiglio *et al.*, 2022). Notch activation in these cancers can be caused either by constitutive Notch and ligand expression or mutations that activate Notch in a ligand-independent manner (Santagata *et al.*, 2004; Weng *et al.*, 2004; Aster, Pear and Blacklow, 2017). Alternatively, frameshift and nonsense mutations creating truncated Notch receptors without the NICD or loss-of-function missense mutations of Notch have been discovered in cancers where Notch plays a tumour-suppressive role, including head and neck, oesophageal, cutaneous and lung squamous cell cancers (SCC), urothelial carcinomas, small cell lung cancers, low-grade gliomas, and pancreatic ductal adenocarcinomas (Agrawal *et al.*, 2011; Stransky *et al.*, 2011; Hammerman *et al.*, 2012; Alcolea *et al.*, 2014; Rampias *et al.*, 2014; Brat *et al.*, 2015; George *et al.*, 2015; Bailey *et al.*, 2016; Sawangarun

et al., 2018).

Table 1.1. Summary of cancer-related NOTCH mutations. Table adapted from Meng et al. (2023).

Cancer	Genes	Mutations	References
GOF (oncogene)			
T-cell acute lymphoblastic leukemia (T-ALL)	*NOTCH1*, *NOTCH3* (rare)	Missense in the NRR and late truncation leading to PEST mutations, frequent frameshift or nonsense mutations	(Weng *et al.*, 2004; Xu *et al.*, 2015)
Early T cell progenitor acute lymphoblastic leukaemia	*NOTCH1*	Missense in the NRR and late truncation leading to PEST mutations	(Van Vlierberghe *et al.*, 2011; Zhang *et al.*, 2012; Neumann *et al.*, 2013)
Adult T-cell leukaemia/ lymphoma (ATL)	*NOTCH1*	Missense, nonsense mutations, and deletions affecting the PEST domain	(Shimizu *et al.*, 2007; Pancewicz *et al.*, 2010)
B-cell Chronic Lymphocytic Leukemia (B-CLL)	*NOTCH1*	Late truncation leading to PEST mutations in *NOTCH1*	(Di Ianni *et al.*, 2009; Sportoletti *et al.*, 2010; Puente *et al.*, 2011, 2015)
Mantle cell lymphoma	*NOTCH1, NOTCH2*	Late truncation leading to PEST mutations	(Kridel *et al.*, 2012; Beà *et al.*, 2013)
Marginal zone B cell lymphoma	*NOTCH2*	Missense and late truncation leading to PEST mutations	(Trøen *et al.*, 2008; Kiel *et al.*, 2012; Rossi *et al.*, 2012)
Breast carcinoma/ triple-negative breast cancer	*NOTCH1, NOTCH2*	Missense mutations, deletions, and gene rearrangement affecting NRR or PEST domains	(Robinson *et al.*, 2011; Stoeck *et al.*, 2014)
Adenoid cystic carcinoma	*NOTCH1*	Missense, frameshift mutations in *NOTCH1*, truncating mutations in *NOTCH2*	(Ho *et al.*, 2013; Stephens *et al.*, 2013)
Glomus tumour	*NOTCH1* (rare), *NOTCH2, NOTCH3*	Gene rearrangement leading to significant expression of the NICD	(Mosquera *et al.*, 2013)
LOF (tumor suppressor)			

Squamous cell carcinoma	*NOTCH1, NOTCH2, NOTCH3*	Missense, in-frame deletions in *NOTCH1/3*, and early truncation resulting from nonsense or frameshift mutations before or within the ANK domain	(Agrawal *et al.*, 2011; Durinck *et al.*, 2011; Wang *et al.*, 2011; Cancer Genome Atlas Research Network, 2012)
Bladder transitional cell carcinoma/ urothelial carcinoma	*NOTCH1, NOTCH2, NOTCH3*	Missense, in-frame deletions in *NOTCH1/2*, and early truncation resulting from nonsense or frameshift mutations before or within the ANK domain	(Rampias *et al.*, 2014)
Small-cell lung carcinoma	*NOTCH1, NOTCH2*	Missense and early truncation resulting from nonsense or frameshift mutations before or within the ANK domain	(George *et al.*, 2015)
Esophageal carcinoma	*NOTCH1, NOTCH2, NOTCH3*	Missense, frameshift, and splice site mutations in *NOTCH1*	(Song *et al.*, 2014)
Lower-grade glioma	*NOTCH1*	Missense, in-frame deletions, and early truncation resulting from nonsense or frameshift mutations before or within the ANK domain	(Brat *et al.*, 2015)
Chronic myelomonocytic leukemia	*NOTCH2*	Missense	(Klinakis *et al.*, 2011)

Several genetic diseases have been linked to abnormal expression or functioning of Notch signalling components (Table 1.2). Adams-Oliver syndrome (AOS) is associated with autosomal dominant mutations of N1, DLL4, and RBPJk and induces symptoms such as terminal limb-reduction defects, absence or scarred skin, partial absence or thin skull and central nervous system and cardiovascular anomalies (Adams and Oliver, 1945; Hassed *et al.*, 2012, 2017; Stittrich *et al.*, 2014; Meester *et al.*, 2015; Southgate *et al.*, 2015). Autosomal dominant N1 mutations have been associated with familial and sporadic cases of bicuspid aortic valve (BAV) disease, which usually involve a reduction in strength/size/number of aortic valve leaflets and increased risk of thoracic aortic

aneurysm and infective endocarditis (Garg *et al.*, 2005; Mohamed *et al.*, 2006; Debiec *et al.*, 2022). N3 mutations that alter the number of cysteine residues in EGF repeats by substitution or addition of cysteine are the major causes of cerebral autosomal dominant arteriopathy with subcortical infarcts and leukoencephalopathy (CADASIL), which causes abnormal development of small cerebral arteries and can lead to subcortical infarcts, white matter damage, lateral meningocele syndrome, and infantile myofibromatosis (Joutel *et al.*, 1996; Chabriat *et al.*, 2009; Yuan *et al.*, 2024).

Table 1.2. Summary of genetic diseases associated with mutations in components of the Notch signalling pathway, including receptors, ligands, glycosyltransferases and RBPJk. Table adapted from Meng et al. (2023).

Disease	Genes	Mutations	Phenotypes	References
Alagille syndrome	*JAG1, NOTCH2*	Missense/frameshift/splice site leading to decay/retention of JAG1	Hepatic, skeletal, cardiac, renal developmental disorders.	(Hassed *et al.*, 2012; Shaheen *et al.*, 2013; Stittrich *et al.*, 2014; Meester *et al.*, 2015; Southgate *et al.*, 2015)
Extrahepatic biliary atresia	*JAG1*	Missense site leading to reduced ability to activate Notch	Partial or total absence of bile duct.	(Kohsaka *et al.*, 2002)
Tetralogy of Fallot	*JAG1*	Missense/frameshift mutation, most reported missense mutations cluster at the extreme N-terminus	Hole in septum of heart.	(Eldadah *et al.*, 2001; Guarnaccia *et al.*, 2009; Bauer *et al.*, 2010)
Congenital Muscular Dystrophy	*JAG2, POGLUT 1*	Missense, frameshift, nonsense, in-frame deletion, and a larger deletion encompassing	Progressive muscle weakening.	(Servián-Morilla *et al.*, 2016, 2020; Coppens *et al.*, 2021)

		JAG2		
Charcot-Marie-Tooth disease type 2	*JAG1*	Missense mutations in *JAG1*	Partial paralysis of vocal fold and peripheral neuropathy.	(Sullivan *et al.*, 2020)
CADASIL	*NOTCH3*	Predominantly cysteine-related missense mutations in EGF domains	Impaired differentiation and maturation of vascular smooth muscle cells, accumulation of proteins in matrix around vascular smooth muscle cells.	(Joutel *et al.*, 1996; Chabriat *et al.*, 2009; Yuan *et al.*, 2024)
Adams-Oliver syndrome	*NOTCH1, DLL4, EOGT, RBPJ*	Addition/deletion of a cysteine residue in EGF domains	Terminal limb-reduction defects, skin/skull absence and cardiovascular anomalies.	(Hassed *et al.*, 2012; Shaheen *et al.*, 2013; Stittrich *et al.*, 2014; Meester *et al.*, 2015; Southgate *et al.*, 2015)
Bicuspid aortic valve disease	*NOTCH1*	Missense/frameshift mutation	Abnormal aortic valve leaflets and aorta.	(Garg *et al.*, 2005; Mohamed *et al.*, 2006; Debiec *et al.*, 2022)
Dowling-Degos disease	*POFUT1, POGLUT 1*	Non-sense, frameshift and missense mutations contributing to haploinsufficiency of POFUT1 and POGLUT1	Lacy/net-like pattern of abnormally darkened skin.	(Yao *et al.*, 2011; Li *et al.*, 2013; Basmanav *et al.*, 2014; Wang *et al.*, 2017)
Spondylocostal dysostosis	*LFNG, DLL3*	Missense mutation, in-frame deletion of *LFNG* leading to loss of the enzyme activity; in-frame deletion/insertion of *DLL3* leading to truncations of ECD or missense mutations disrupt EGF repeats of DLL3	Fused/deleted/uneven/severe curvature spine, truncal shortening.	(Bulman *et al.*, 2000; Umair *et al.*, 2022)

Hajdu Cheney syndrome	*NOTCH2*	Frameshift/deletion mutations in exon 34 that disrupt or remove the PEST domain	Progressive focal bone destruction.	(Isidor *et al.*, 2011; Simpson *et al.*, 2011; Canalis and Zanotti, 2016)

1.2 Notch Receptors

1.2.1 Overview of Notch receptors

Four mammalian Notch receptors were identified with NECD comprising varying numbers of multiple tandem EGF repeats at the N terminus, some of which are calcium-binding EGFs (cbEGFs) (Downing *et al.*, 1996; Hambleton *et al.*, 2004; Cordle, Johnson, *et al.*, 2008). Schematic presentations of Notch receptors in *C. elegans, Drosophila* and human are shown in Figure 1.3. The alleles of human *N1* (*hN1*) to *N4* are located on chromosomes 9, 1, 19 and 6 accordingly. hN1 and hN2 have 36 EGF repeats, which is the same as dN, while hN3 has 34 and hN4 has 29 EGF repeats. EGF11-12 (from the 36 domain NECDs), named as the ligand-binding region (LBR) form the core site of ligand interaction and are essential for trans-activation (Rebay *et al.*, 1991). Missense mutations in the Abruptex region (Ax) of dN, which includes EGF24-29, can induce a unique Notch-enhancing phenotype in *Drosophila*, suggesting the importance of this region in Notch signalling regulation (De Celis and Garcia-Bellido, 1994). After EGF repeats is the membrane-proximal NRR where the S2 cleavage site is located. NICD is released after S3 cleavage and subsequently interacts with RBPJk and co-activators in the nucleus to induce transcription of downstream genes.

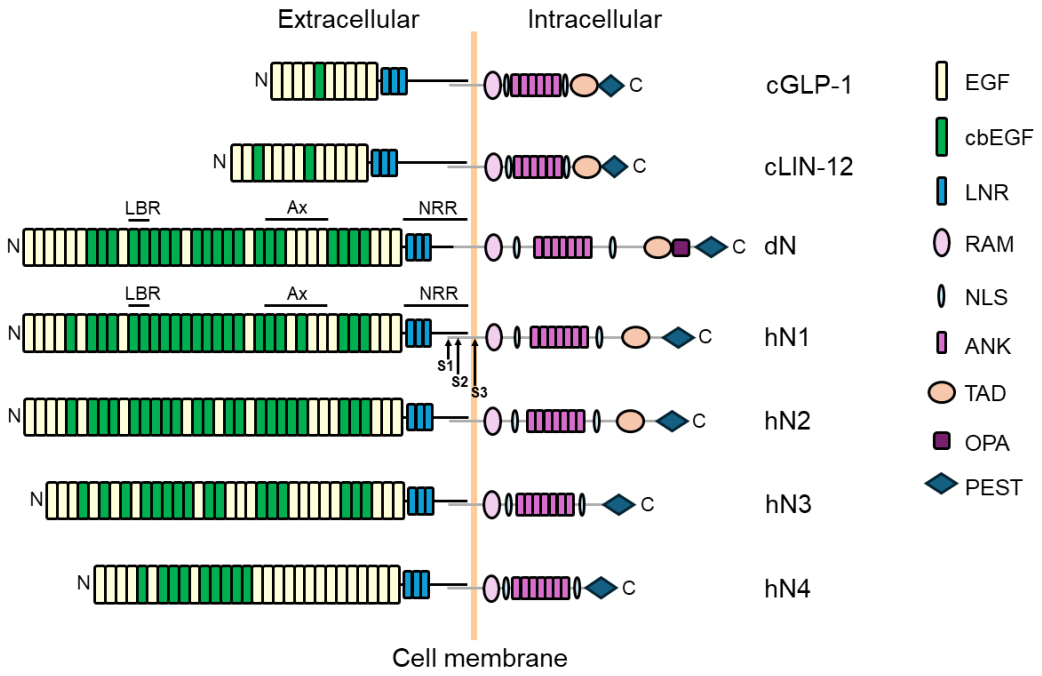


Figure 1.3. Domain arrangement of Notch receptors.

Notch receptors in *C. elegans* (cGLP-1 and cLIN-12), *Drosophila* (dN) and humans (hN1, 2, 3 and 4) have ECDs with varying numbers of EGF and cbEGF repeats. cbEGFs are labelled based on the consensus sequence D/N/E-x-D/N-D/N/E/Q-x_m-D/N/Q*-x_n-Y/F (* denotes possible β-hydroxylation, m/n denote variable numbers of residues). The core ligand-binding region (LBR) EGF11-12, the Abruptex region (Ax) EGF24-29, and the Negative Regulatory region (NRR) consisting of three LIN-12/Notch repeats (LNRs) are indicated in dN and hN1. The intracellular domains of Notch receptors consist of an RBPJk association module (RAM), nuclear localisation sequences (NLS), ankyrin repeats (ANKs), a transcriptional activation domain (TAD) (absent in hN3 and 4) and a conserved proline/glutamic acid/serine/threonine-rich motif (PEST). S1, S2 and S3 cleavage sites are indicated with black arrows.

1.2.2 EGF domains

1.2.2.1 Conserved structure of EGF domains

EGF domains are structurally conserved modular protein subunits present in many proteins in the extracellular milieu, including extracellular matrix proteins, such as fibrillin (Fib) and Latent TGF-β binding proteins (LTBPs), and components of the blood

coagulation system including factors VII, IX, X, protein C and thrombomodulin (Handford *et al.*, 1995; Wouters *et al.*, 2005). An EGF repeat usually contains 30-40 amino acids with the native structure comprising a central β-hairpin (Figure 1.4A). An EGF comprises six conserved cysteines connected by three disulfide bonds with a 1-3, 2-4, 5-6 arrangement (Cooke *et al.*, 1987; Handford *et al.*, 1990; Baron *et al.*, 1992; Rao *et al.*, 1995). The disulfide bonds formed in the ER and stabilise the EGF fold.

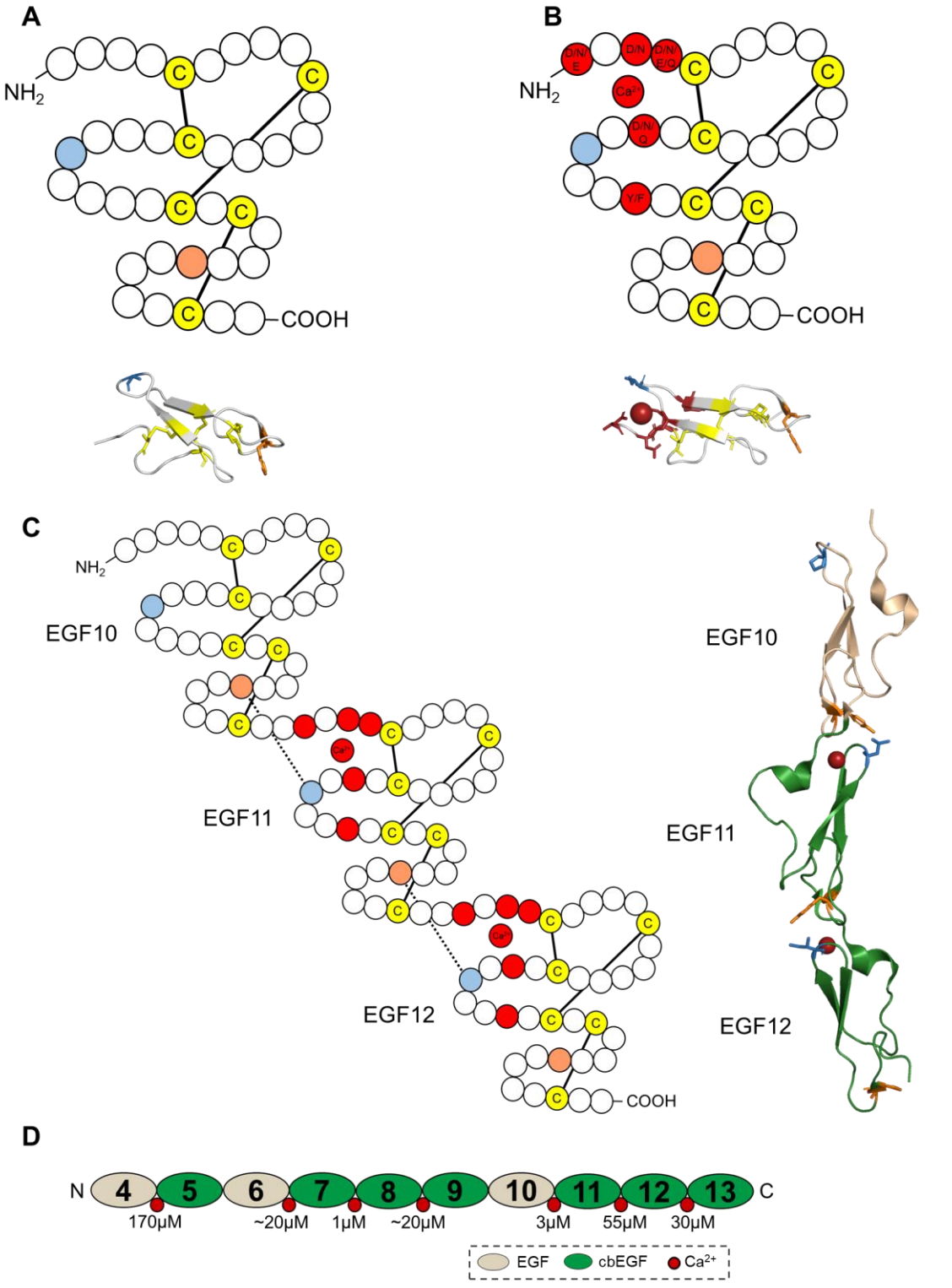


Figure 1.4. Structures of EGF and cbEGF domains.

Conserved residues are shown in schematic illustrations and X-ray crystallography structures of EGF (A) and cbEGF (B) domains. X-ray crystallography structures of hN1 EGF6 (Protein Data Bank (PDB): 5FMA) (Weisshuhn *et al.*, 2016) and hN1 EGF12 (PDB: 2VJ3) (Cordle, Johnson, *et al.*, 2008), which is Ca^{2+}-binding, are used as examples of EGF and cbEGF.

Cysteine residues required for forming the β-hairpins are coloured yellow. Disulfide bonds are shown as black lines. The consensus residues for Ca^{2+} binding and Ca^{2+} ions are shown in red. Consensus aliphatic residue (blue) and aromatic residue (orange) mediate the interaction between adjacent cbEGF domains. (C) Structure of EGF/cbEGF-cbEGF pairs. The conserved aliphatic residue and aromatic residue are shown in schematic illustrations and the X-ray crystallography structure of EGF10-12 from rat N1/Jag1 complex (PDB: 5UK5). Hydrophobic packing interactions (black dashed line) and Ca^{2+} binding stabilise EGF10-11 and EGF11-12 interfaces producing a near-linear structure. (D) The Ca^{2+} dissociation constants (pH 7.5, I = 0.15) for hN1 EGF4–13 (Weisshuhn *et al.*, 2016).

1.2.2.2 Calcium-binding EGF

In EGF repeats, consensus residue sequence D/N/E-x-D/N-D/N/E/Q-x_m-D/N/Q*-x_n-Y/F (* denotes possible β-hydroxylation, m/n denote variable numbers of residues) is predictive for Ca^{2+} binding (Handford *et al.*, 1991; Meng *et al.*, 2023) (Figure 1.4B). Up to seven intradomain ligands, which are donated by the oxygen atoms in the side chain carboxylates and carboxyamides of consensus residues, and potentially by the backbone carbonyl oxygens of the residues adjacent to the Ca^{2+} ion or a water molecule, are required to coordinate the Ca^{2+} ion in a pentagonal bipyramidal arrangement (Rao *et al.*, 1995; Lee *et al.*, 2004; Jensen *et al.*, 2005). Though not directly interacting with the Ca^{2+} ion, the second D/N and the fifth aromatic consensus residues help stabilise the Ca^{2+} binding site (Rao *et al.*, 1995). The second consensus residue's carboxylate or carboxyamide side chain forms a hydrogen bond with the main-chain amide nitrogen of Cys1 which is 2 residues after it, creating an ASX turn. The fifth consensus residue, which is aromatic, forms strong hydrophobic interactions with other hydrophobic residues between Cys1 and Cys2. A study of hN1 EGF4-13 suggested the dissociation constant

(K_d) values for Ca^{2+} of typical Notch EGF domains are between 1-200 μM at pH 7.5 and ionic strength (I) = 0.15, therefore should be saturated under physiological concentrations in the extracellular region (free Ca^{2+} ~ 1.5 mM) (Weisshuhn *et al.*, 2016) (Figure 1.4D). However, Ca^{2+} binding of Notch EGF domains may be unsaturated in other cellular compartments with lower Ca^{2+} concentrations, such as the ER (free Ca^{2+} 100 μM - 1 mM), endosome (free Ca^{2+} < 30 μM) and lysosome (free Ca^{2+} 500 μM – 600 μM) (Albrecht *et al.*, 2015; Raffaello *et al.*, 2016; Lloyd-Evans and Waller-Evans, 2020).

1.2.2.3 Structure of tandem EGF repeats

The diverse contexts of EGF domains create a variety of inter-domain angles and flexibilities in tandem EGF domains, which are likely to influence the shape of the NECD and its interactions with other molecules (Downing *et al.*, 1996; Weisshuhn *et al.*, 2016). Most cbEGF domains in Notch receptor are Class II cbEGFs as they have two residues linking the cbEGF-cbEGF pair or EGF-cbEGF pair, forming a ~119° interdomain twist (Downing *et al.*, 1996). The N terminus of a cbEGF is rigidified by Ca^{2+} binding and hydrophobic packing interactions between the conserved aromatic residue at the end of the previous EGF/cbEGF and the conserved aliphatic residue in the central β-hairpin of the cbEGF (Figure 1.4C). A linear rod-like structure is formed as a consequence of these pairwise interactions between EGF/cbEGF and cbEGF domains (Downing *et al.*, 1996; Hambleton *et al.*, 2004; Cordle, Johnson, *et al.*, 2008; Cordle, Redfield, *et al.*, 2008). For example, X-ray crystallography revealed an extended rod-like structure for calcium-

binding N1 EGF11-13 both with and without ligand binding (Cordle, Johnson, *et al.*, 2008; Luca *et al.*, 2015, 2017).

The interfaces in cbEGF-EGF pairs are more variable. For example, an angle of 80-90° was detected between calcium-binding hN1 EGF5, and non-calcium-binding EGF6 (Weisshuhn *et al.*, 2016). This angle was created by the interactions of A208 (EGF5) with V239 (EGF6) and Y219 (EGF5) with P221 (EGF6) (Weisshuhn *et al.*, 2016). On the other hand, the interface between calcium-binding hN1 EGF9 and non-calcium-binding EGF10 was shown to be flexible by nuclear magnetic resonance (NMR) residual dipolar coupling (RDC) studies (Weisshuhn *et al.*, 2016).

1.2.3 Ligand-binding region

EGF11-12 of NECDs of the long forms of the receptor is the key site of ligand interaction (Rebay *et al.*, 1991; Whiteman *et al.*, 2013; Luca *et al.*, 2015, 2017). It was initially identified in dN by cell aggregation assays (Rebay *et al.*, 1991) and was extensively studied by NMR and X-ray crystallography of hN1, hN2 and dN fragments (Hambleton *et al.*, 2004; Cordle, Johnson, *et al.*, 2008; Taylor *et al.*, 2014; Suckling *et al.*, 2017). These studies suggested, despite having only 67% sequence identity, hN1 and hN2 share a similar rod-like rigid structure in EGF11-13, where EGF11-13 of hN2 has a root mean square deviation (RMSD) of 1.55Å when superimposed on hN1 (Suckling *et al.*, 2017). Surface plasmon resonance (SPR) was used to determine the K_d of Jag1 C2-EGF3 (NE3) and Dll4 NE3 for N1 EGF8-12 and EGF11-12 and suggested an extended

interface of N1 EGF8-10 contributes to N1-Jag1 binding but had a minimal contribution in N1-Dll4 binding (Luca *et al.*, 2017), However, results of cellular assays suggested EGF8-10 were essential for optimal Notch1 activation by Dll4 (Andrawes *et al.*, 2013).

1.2.4 Abruptex region

EGF 24-29 of the Notch receptor, known as the Abruptex region (Ax), has also been shown to be essential for receptor-ligand interaction (Foster, 1975; Portin, 1975; Kelley *et al.*, 1987; De Celis and Garcia-Bellido, 1994). The region was first defined in *Drosophila* where missense mutations in this region can generate phenotypes opposite to the well-known *Drosophila N* phenotype (Nasarenko, 1930; Kelley *et al.*, 1987). While the *N* phenotype caused by a null allele of the *dN* gene has enlarged wing veins, more bristles, and notches along the edge of the wing, the *Abruptex* (*Ax*) phenotype caused by single nucleotide polymorphisms in EGF 24-29 has interrupted wing veins and fewer micro and macrochaetae on the scutum of the fly (De Celis and Garcia-Bellido, 1994; Fryxell, Soderlund and Jordan, 2001) (Figure 1.5). The *Ax* phenotype is commonly considered to be caused by hyperactivation of Notch signalling (De Celis and Bray, 2000), although some studies suggested alternative theories (Brennan *et al.*, 1999). Two variants in the EGF16 of dN were found to also generate phenotypes with enhanced Notch signalling though the Ax region is still confined as EGF24-29 (Yamamoto *et al.*, 2012).

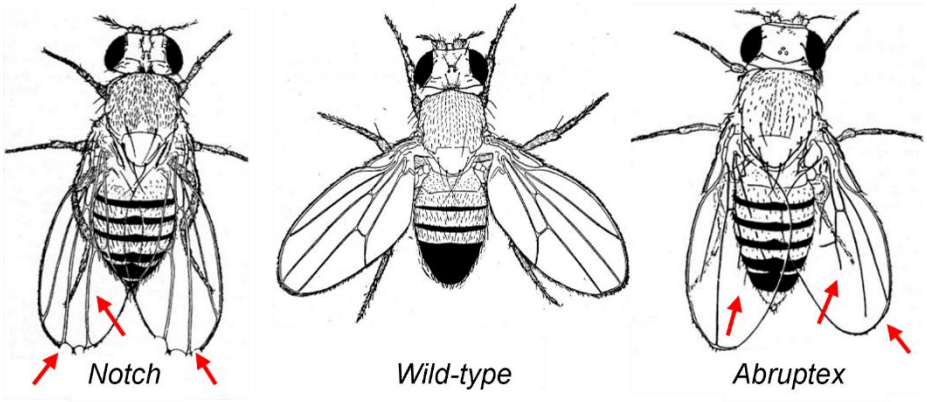


Figure 1.5. The *Notch* and *Abruptex* phenotypes in *Drosophila.*

The *Notch* phenotype caused by a null *NOTCH* allele possesses enlarged wing veins, more bristles, and notches along the edge of the wing. The *Ax* phenotype caused by heterozygous missense mutations in the Ax region of the Notch receptor has thinner and fewer wing veins, as well as fewer bristles. The wild-type (WT) fly has moderate wing vein thickness and a suitable number of bristles. Key phenotypes are shown by red arrows. The figure was adapted from Fryxell et al. (2001) (Fryxell, Soderlund and Jordan, 2001) and flypress.gen.cam.ac.uk (*FlySox « Russell Lab*).

1.2.5 Negative regulatory region

Following the EGF repeats is the NRR, which contains three LIN-12/Notch repeats (LNRs) and a heterodimerization domain (HD) (Figure 1.6). In its natural autoinhibited conformation, the HD was wrapped around and stabilised by the LNRs. The helices in the HD pack against the top of the 4-stranded β-sheets at the base of the HD, forming a hydrophobic core (Gordon *et al.*, 2009). Each LNR binds to a Ca^{2+} ion, which stabilises and rigidifies the structure to cap over the hydrophobic core. This structure sterically occludes the S2 cleavage site in the last β-sheet of the HD. Upon ligand binding, a mechanical pulling force is generated by ligand endocytosis (see Section 1.4.2), inducing a conformational change of the NRR, exposing the shielded S2 site, which is then accessible by ADAM metalloprotease, ADAM10 and ADAM17 (Meloty-Kapella *et al.*,

2012). ADAM metalloprotease cleaves between the conserved alanine and valine in HD, such as A1720 and V1721 in N1, generating the intermediate cleavage product NEXT (Brou *et al.*, 2000). Also, removal of the Ca^{2+} from the LNRs by mutation or chelating agents can disengage LNRs from the HD, allowing ADAM protease to access the S2 site, and increasing ligand-independent activation of the receptor (Rand *et al.*, 2000; Gordon *et al.*, 2009). NEXT is subsequently cleaved by γ-secretase complex at the S3 site, such as between G1753 and V1754 in N1, in the transmembrane region, releasing the NICD from the cell surface membrane (Schroeter, Kisslinger and Kopan, 1998; De Strooper *et al.*, 1999).

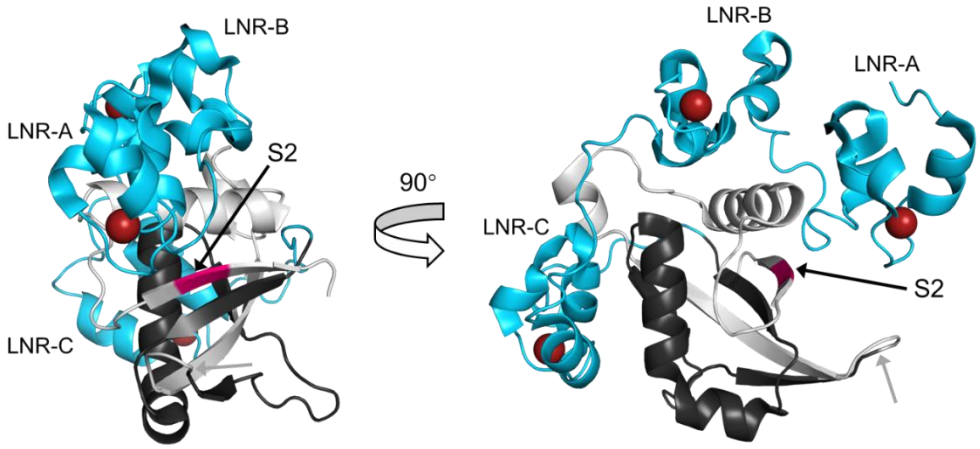


Figure 1.6. Structure of the NRR.

The X-ray structure of furin-cleaved hN1 NRR (PDB: 3ETO) (Gordon *et al.*, 2009) is shown with the three LNR modules (A-C) in blue, the region of the HD domain preceding the S1 cleavage site in light grey, and the region after in dark grey. Ca^{2+} ions are shown in red. The S2 cleavage site between A1721 and V1722 (coloured purple) is shown by a black arrow. The position of a deleted loop (residues 1623–1669) containing the S1 cleavage site is denoted by a grey arrow.

1.2.6 Structure of the Notch extracellular domain

Though commonly depicted as a straight rod in simplified figures, many studies provided

evidence for a non-linear architecture of NECD (Figure 1.7A). SAXS of monomeric NECD of N1 suggested a flexible/non-linear molecule with a maximum distance (D_{max}) of 380 Å (Zeronian *et al.*, 2021). As the dimension of an EGF domain is around 30 Å x 15 Å x 15 Å, the length of N1 NECD should be around 1027 Å if fully extended.

Several studies identified intramolecular interactions between different regions of NECD, supporting a folded structure of the molecule (Figure 1.7B). Enzyme-linked immunosorbent assay (ELISA)-based binding assays discovered that dN EGF21-30 and EGF22-27 could directly bind to dN EGF11-14 and EGF11-20 which contain the LBR but not to ligands (Pei and Baker, 2008). This is supported by *in vitro* assays showing hN1 EGF21-30 could bind to hN1 EGF11-15 but not to ligands (Sharma, Rangarajan and Dighe, 2013). In addition, competition of dN and hN1 EGF21-30 with the extracellular domain of Dl and JAG1 for binding to EGF11-20 have been detected (Pei and Baker, 2008; Sharma, Rangarajan and Dighe, 2013). These results suggested that Ax can physically interact with the LBR but not with ligands and it competes with the ligands for the LBR. An SPR study conducted by Zeronian et al. (2021) detected a direct interaction of N1 EGF8–EGF13 with N1 EGF33–NRR with a K_d of 115 μM, which is not strong enough for dimerisation but indicates the possibility for intramolecular binding (Zeronian *et al.*, 2021). Those studies suggested that the NECD may bend after the extended LBR region, which could enable potential interactions of LBR with Ax or the C terminus of the NECD. However, it should be noted that these experiments were conducted using protein fragments in solution and not in a native cellular context, thus further evidence is needed

to reach a conclusion.

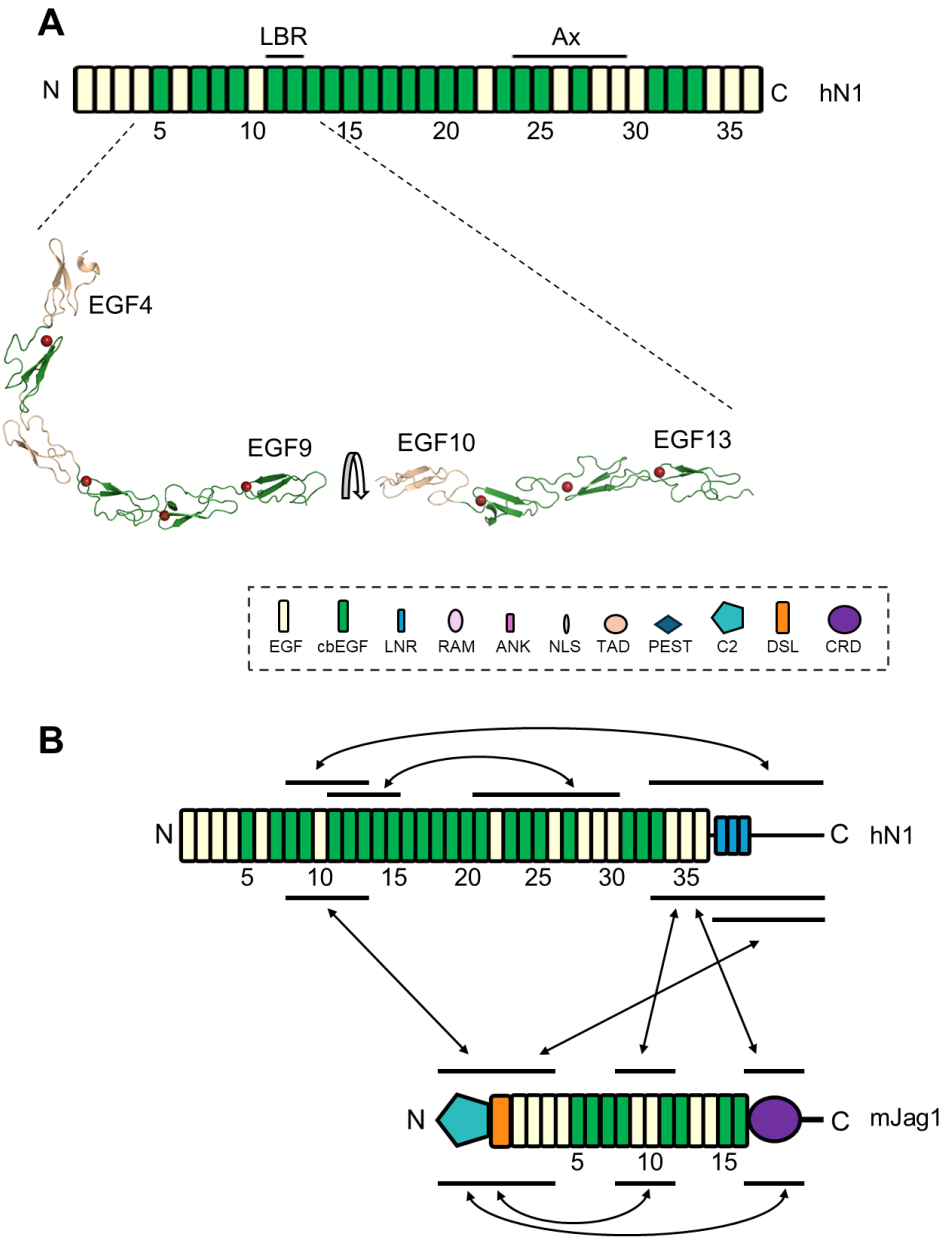


Figure 1.7. Structure of NECD and intramolecular interactions.

(A) Existing structural models of hN1ECD. X-ray structures for the EGF4–7 (PDB: 5FMA) and EGF10–13 (PDB: 2VJ3) and RDC measurements were employed to construct the model for EGF4-13 by Weisshuhn et al. (2016), which suggested a flexible linker between EGF9 and 10 (Cordle, Johnson, *et al.*, 2008; Weisshuhn *et al.*, 2016). EGF domains are shown in wheat. cbEGF domains are shown in green. The Ca^{2+} ions are shown as red spheres. (B) Schematic illustration of the reported inter- and intra-molecular interactions between hN1 and mJag1 detected by cross-linking mass spectrometry (XL-MS) and quantitative interaction assays (Sharma, Rangarajan and Dighe, 2013; Zeronian *et al.*, 2021). Direct interactions between fragments (black lines) are shown by arrows.

1.2.7 Notch intracellular domain

After S3 cleavage, NICD translocates into the nucleus where it interacts with transcriptional regulators to affect the expression of target genes. The NICD is formed from the N terminus to the C terminus by an RBPJk association module (RAM), nuclear localisation sequences (NLS), seven ankyrin repeats (ANKs), a transcriptional activation domain (TAD) (absent in N3 and N4) and a conserved proline/glutamic acid/serine/threonine-rich motif (PEST) (Figure 1.3). Initially, the conserved WxP motif in RAM binds to the β-trefoil domain of RBPJk (Tamura *et al.*, 1995; Tani *et al.*, 2001; Lubman *et al.*, 2007). This increases the local concentration of ANK, enabling ANK repeats to interact with RBPJk and displace transcriptional corepressors, such as Hairless in *Drosophila* (Barolo *et al.*, 2002; Yuan *et al.*, 2016) and SHARP and KyoT2 in mammals (Oswald *et al.*, 2002; Collins, Yuan and Kovall, 2014), previously bound to RBPJk (Bertagna *et al.*, 2008; Friedmann, Wilson and Kovall, 2008). Transcriptional coactivator MAML1-3 recognises the RBPJk-ANK interface, forming a ternary complex that employs other co-effectors, such as histone acetyltransferases and chromatin remodelling factors. TAD also facilitate the interaction between NICD, RBPJk and MAML (Gerhardt *et al.*, 2014).

An active transcriptional complex is created which binds to target promoters to initiate the expression of genes including the *Hes/Hey* family of TFs (Fryer, White and Jones, 2004; Nam *et al.*, 2006; Wilson and Kovall, 2006; Kopan and Ilagan, 2009; Gomez-Lamarca *et al.*, 2018). While both suppress the expression of tissue-specific TFs to

negatively regulate stem cell differentiation, HES TFs regulate the development and homeostasis of the nervous system and sensory organs, while HEY TFs function mainly in the cardiovascular system (Fischer and Gessler, 2003; Hu and Zou, 2022).

The PEST domain at the C terminus of NICD can be phosphorylated by kinases CDK1, 2, and 8, which enables it to be recognised by E3 ubiquitin ligase FBW7, leading to ubiquitination and subsequent proteasomal degradation of NICD (Fryer, White and Jones, 2004; Tsunematsu *et al.*, 2004; O'Neil *et al.*, 2007; Carrieri *et al.*, 2019). TAD can also be phosphorylated which assists the turnover of NICD (Fryer, White and Jones, 2004). The degradation of NICD disassembles the ternary complex, releases and resets RBPJk and other co-effectors, and stops Notch-mediated transcriptional changes.

1.2.8 Notch post-translational modification

1.2.8.1 Overview of Notch post-translational modification

As cell surface transmembrane proteins, Notch receptors traffic through the secretory pathway where they undergo various post-translational modifications (PTMs) due to the presence of suitable enzymes and consensus sequences for enzyme recognition. In the ER, disulfide bonds are formed to stabilise the native fold of EGF domains and the LNRs and O-glycosylation (O-fucosylation, O-glucosylation, O-GlcNAcylation) and β-hydroxylation of these domains may take place. Subsequently, the receptors are transported to the Golgi where the O-glycans may be further modified by other

glycosyltransferases. Post-translational modifications can affect the structure and function of Notch receptors and modulate the strength of Notch signalling (reviewed by Takeuchi *et al.*, 2017; Matsumoto, Luther and Haltiwanger, 2021; Pandey, Niknejad and Jafar-Nejad, 2021a). The consensus sequences for O-glycosylation and O-glycosylation sites in the EGF repeats of the hN1 and mouse N1 (mN1) ECD predicted by consensus sequence matching are shown in Figure 1.8.

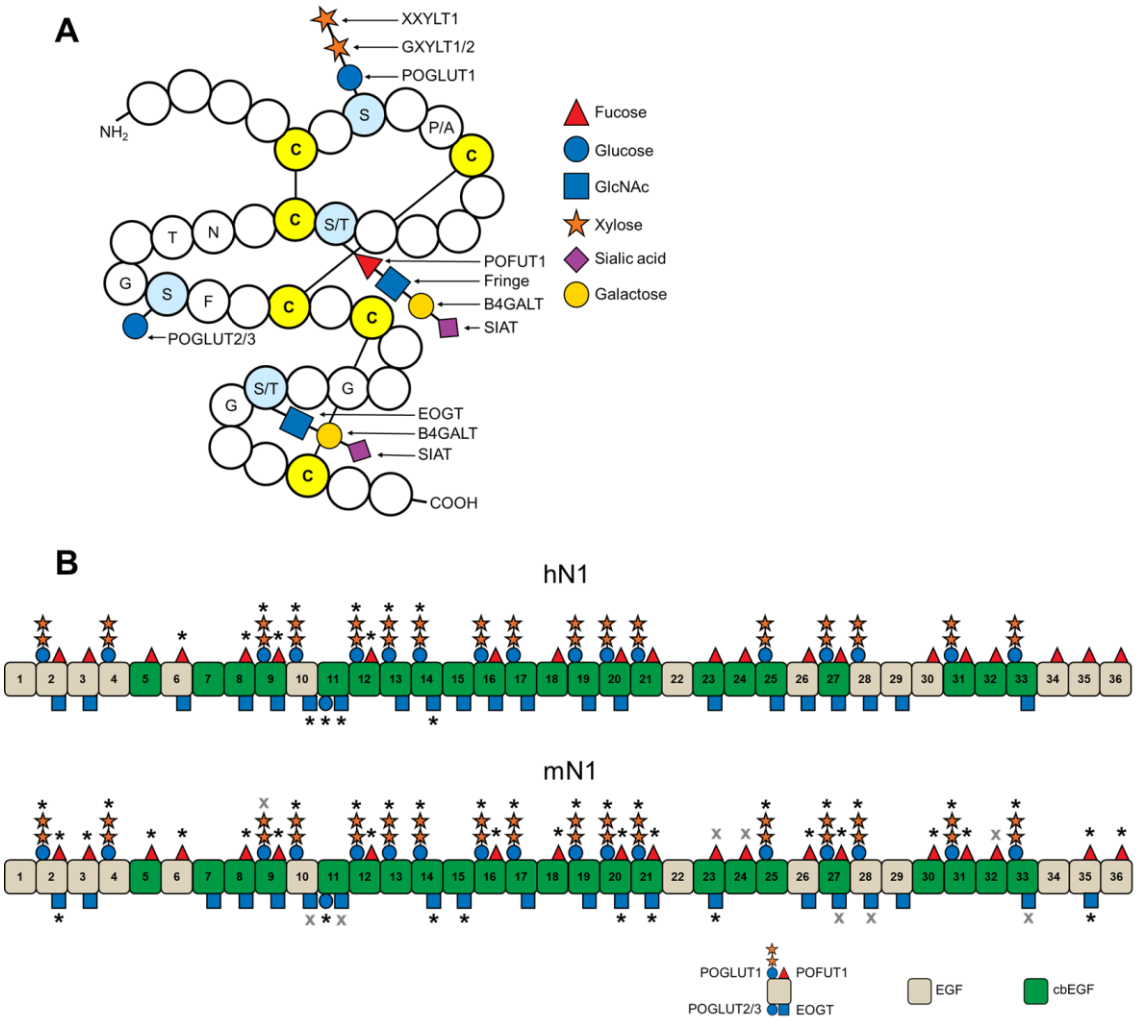


Figure 1.8. O-glycosylation of Notch receptor.

(A) Schematic diagram of an EGF domain showing the locations and consensus sequences for O-glycosylation. The structures of O-glycans and the enzymes catalysing the additions are shown. The conserved cysteine residues of the EGF domain are coloured yellow. Disulfide bonds formed between the cysteine residues are shown as black lines. (B) Schematic diagrams showing the O-glycosylation sites in the EGF repeats of hN1 and mN1 ECDs predicted by consensus sequence matching. EGF repeats harbouring the recognition consensus sequences for POGLUT1, POGLUT2/3, POFUT1, and EOGT are shown. O-glycosylation sites that have been confirmed experimentally are indicated by asterisks (Andrawes *et al.*, 2013; Taylor *et al.*, 2014; Kakuda and Haltiwanger, 2017; Ogawa *et al.*, 2018; Takeuchi *et al.*, 2018; Urata *et al.*, 2020; Yokoi and Nishimura, 2020; Pennarubia *et al.*, 2022). Predicted sites that have been confirmed as unmodified are indicated by grey crosses. Fuc: fucose; Glc: glucose; Xyl: xylose; XXYLT: xyloside xylosyltransferases; GXYLT: glucoside xylosyltransferases; B4GALT: b-1,4-galactosyltransferases; SIAT: sialyltransferases. Figure adapted from Meng et al. (2023).

1.2.8.2 O-fucosylation

O-fucosyltransferase 1, such as POFUT1 in mammals and O-fut1 in *Drosophila*, adds O-fucose to the consensus site C^2-X_{4-5}-(S/T)-C^3 (Wang *et al.*, 1996, 2001; Holdener and Haltiwanger, 2019). Mass spectrometry of mN1 produced by HEK293T cells suggested that most O-fucose sites in the EGF repeats are modified except for EGF 23, 24, 32 (Kakuda and Haltiwanger, 2017). Knockout of O-fucosyltransferase 1 repressed expression of Notch target genes during the development of *Drosophila* wing discs and mouse embryo somitogenesis, and induced developmental abnormalities similar to those of Notch-null phenotypes, such as wing notching in flies and fusion of somites adjacent to presomitic mesoderm in mouse embryos (note the phenotypes might not be solely due to the reduced O-fucosylation of Notch), supporting that O-fucosylation is required for receptor functioning (Okajima and Irvine, 2002; Shi and Stanley, 2003).

O-fucosylation can stabilise the EGF repeat as shown by folding assays of the first EGF repeat in human coagulation factor IX (hFA IX), which contains a similar number of amino acids as EGF repeats in Notch (Takeuchi *et al.*, 2017). Some studies suggested that O-fucosylation, such as O-fucose in EGF9 of N1 and N2, facilitates Notch trafficking to the cell surface in *Drosophila* and mammalian cells and the absence of POFUT1 led to Notch accumulation in ER in mouse presomitic mesoderm cells (Okajima *et al.*, 2008; Okamura and Saga, 2008; Kakuda and Haltiwanger, 2017; Takeuchi *et al.*, 2017). Moreover, O-fucose regulates the interaction of Notch with its ligands. For example, Fng-modified O-

fucose at T466 in EGF12 enhances the binding to Jag1, Dll1 and Dll4 (Taylor *et al.*, 2014; Kakuda and Haltiwanger, 2017; Luca *et al.*, 2017). O-fucose at T311 in EGF8 also enhances the activation of N1 by Jag1 and Dll1 (Kakuda and Haltiwanger, 2017; Luca *et al.*, 2017). O-fucose in EGF9 and EGF27 facilitate activation by Jag1 but not Dll1 while O-fucose in EGF26 facilitates activation by Dll1 but not Jag1 (Kakuda and Haltiwanger, 2017).

1.2.8.3 Fringe modification of O-fucose

O-fucose can be further extended by the β1,3-N-acetylglucosaminyl (GlcNAc) transferase, Fringe (Fng), which adds GlcNAc onto O-fucose through β1,3 bond to form GlcNAcβ1-3Fucose disaccharide (Moloney, Panin, *et al.*, 2000; Rampal *et al.*, 2005). The disaccharide can subsequently be extended to form tri- and then tetra-saccharide Siaα2-6Galβ1-4GlcNAcβ1-3Fuc (Moloney, Panin, *et al.*, 2000). *Drosophila* possess one Fng while mammals possess three Fng homologs, Lunatic Fringe (Lfng), Manic (Mfng) and Radical (Rfng) (Cohen *et al.*, 1997; Johnston *et al.*, 1997). Fng modification coordinates Notch signalling intensity during the development of several tissues in both *Drosophila* and mammals. For example, through differentially regulating Ser's and Dl's abilities to activate Notch in the *Drosophila* wing disc, Fng facilitates the formation of the D/V boundary (Irvine and Wieschaus, 1994; Fleming, Gu and Hukriede, 1997; Klein and Arias, 1998).

Fng modifications have different impacts on trans-activation by different ligands. In *Drosophila*, Fng expression in receptor-expressing cells reduces Notch trans-activation by Ser but increases that by Dl (Panin *et al.*, 1997). This may be explained by S2 cell-based ligand binding assays which found Fng expression improved Dl-dN binding but reduced Ser-dN binding (Brückner *et al.*, 2000; Pérez *et al.*, 2005; Pandey *et al.*, 2019). In mammals, the effects of Fngs are complicated by the diversity of Fngs, receptors and ligands (Table 1.3). For N1, in CHO-K1 and/or NIH3T3 cells, Lfng and Mfng expression reduced trans-activation by JAG1 and JAG2 but enhanced trans-activation by DLL1; Rfng expression increased trans-activation by DLL1 and JAG1 but had minimal effect on trans-activation by DLL4 and JAG2 (LeBon *et al.*, 2014; Kakuda and Haltiwanger, 2017; Kakuda *et al.*, 2020; Kuintzle, Santat and Elowitz, 2023). While Kakuda et al. (2020) found that DLL4-mediated N1 activation was not affected by Lfng or Mfng expression in NIH3T3 cells, Kuintzle et al. (2023) found that DLL4-mediated N1 activation was improved by Lfng expression in CHO-K1 cells, suggesting the response to Fng may be affected by cell type (Kakuda *et al.*, 2020; Kuintzle, Santat and Elowitz, 2023).

Table 1.3. Effects of Fng expression on N1 and N2 activation by different trans-ligands and the interaction between N1 and different cis-ligands.

"↓" or "↑" represent decrease or increase. "=" represents no effect (LeBon *et al.*, 2014; Kakuda and Haltiwanger, 2017; Kakuda *et al.*, 2020; Kuintzle, Santat and Elowitz, 2023; Thambyrajah *et al.*, 2024).

Trans-ligand	Effect on N1 trans-activation			Effect on N2 trans-activation			Effect on N1 cis-interaction		
	Lfng	Mfng	Rfng	Lfng	Mfng	Rfng	Lfng	Mfng	Rfng
JAG1	↓	↓	↑	↓	↓	=	↓	↓	↑
JAG2	↓	↓	=	↓	↓	=	Not tested	Not tested	Not tested
DLL1	↑	↑	↑	↑	↑	=	↑	↑	↑
DLL4	= (NIH3T3) ↑ (CHO-K1)	=	=	↑	=	=	Not tested	Not tested	Not tested

Mutation studies showed that the inhibitory effect of Lfng and Mfng on N1 trans-activation by Jag1 depends mainly on their modification of O-fucose in EGF6 and EGF36, while the stimulatory effect of all three Fngs on N1 trans-activation by Dll1 depends on their modification of EGF8 and EGF12 (Kakuda and Haltiwanger, 2017). Interestingly, the addition of GlcNAc to O-fucose modifications by all three Fngs enhanced the binding of both JAG1 and DLL1 to N1 in cell- and molecular-based assays (Taylor *et al.*, 2014; Kakuda and Haltiwanger, 2017; Kuintzle, Santat and Elowitz, 2023). While this increase in binding affinity may explain the enhanced trans-activation by DLL1, it does not explain the inhibitory effect of Lfng and Mfng on N1 trans-activation by JAG1. Therefore, the inhibitory effect of Lfng and Mfng on N1 trans-activation may be caused by the molecular effect of the O-glycan at another position independent of ligand binding. Furthermore, Fng modification does not enhance the binding of DLL4, potentially because the DLL4 already has a strong binding affinity for Notch before Fng modification (Taylor *et al.*, 2014; Kuintzle, Santat and Elowitz, 2023).

Several studies suggested that Fngs affect Notch cis-inhibition in a similar pattern as in trans-activation. In *Drosophila*, phenotypic analysis and cell-based aggregation assay of O-fucose site mutations suggested that Fng modifications of EGF8 and EGF12 reduced Notch inhibition by cis-Ser (Pandey *et al.*, 2019). In CHO-K1 cells, shown by changes in the level of trans-ligand binding, Lfng and Mfng strengthened the N1-Dll1 cis-interaction but reduced the N1-Jag1 cis-interaction, while Rfng preserved or enhanced N1 cis-interactions with both ligands (LeBon *et al.*, 2014). In cells in the intra-aortic hematopoietic clusters, knock-down experiments suggested that Rfng enhanced N1-Jag1 cis-interaction to maintain hematopoietic stem cell phenotype (Thambyrajah *et al.*, 2024). The interplay of Fng's effects on trans- and cis-interactions of receptors with different ligands increases the complexity and diversity of Notch signalling.

1.2.8.4 O-glucosylation

O-glucosyltransferase 1, such as POGLUT1 in mammals and Rumi in *Drosophila*, adds O-glucose to the consensus site C^1-X-S-X-(P/A)-C^2 in EGF domains (Acar *et al.*, 2008; Takeuchi *et al.*, 2011). Mass spectrometric analyses of dN, N1 and N2 suggested that most EGF repeats with this consensus sequence have been modified (Harvey *et al.*, 2016; Urata and Takeuchi, 2020; Urata *et al.*, 2020). Mammals have two other O-glucosyltransferase homologs, POGLUT2 and POGLUT3 (also known as KDELC1 and KDELC2), which add O-glucose to the consensus site C^3-x-N-T-x-G-S-F-x-C^4. Only N1

EGF11 and N3 EGF10 are glucosylated by POGLUT2 and POGLUT3 (Takeuchi *et al.*, 2018; Williamson and Haltiwanger, 2022).

O-glucosylation helps to stabilise the EGF domain fold as O-glucosylation of mN1 EGF28 enhanced the resistance to unfolding induced by Dithiothreitol (DTT) (Lee *et al.*, 2013; Takeuchi *et al.*, 2017). Overall O-glucosylation enhances Notch trafficking as suggested by Rumi mutations, which led to a temperature-dependent dN intracellular accumulation and Notch loss-of-function phenotype in *Drosophila*, and by POGLUT1 knockout in HEK293T cells, which led to N1 ER accumulation (Acar *et al.*, 2008; Matsumoto *et al.*, 2016; Takeuchi *et al.*, 2017).

Furthermore, several studies in *Drosophila* suggested that the absence of O-glucose does not reduce cell surface Notch level at a lower temperature (18 °C) but still leads to a Notch loss-of-function phenotype (Acar *et al.*, 2008; Leonardi *et al.*, 2011; Perdigoto, Schweisguth and Bardin, 2011). Rumi or POGLUT1 knockouts did not affect ligand binding but led to aberrant Notch S2 cleavage pattern in S2 cells, mouse models and mammalian cell lines, suggesting O-glucosylation regulates S2 cleavage by stabilising the autoinhibitory conformation of NECD and the transmission of pulling force generated by ligand (Acar *et al.*, 2008; Jafar-Nejad, Leonardi and Fernandez-Valdivia, 2010; Fernandez-Valdivia *et al.*, 2011; Leonardi *et al.*, 2011; Ma *et al.*, 2011; Chu, Liu and Wang, 2013; Ramkumar *et al.*, 2015; Servián-Morilla *et al.*, 2016, 2020; Pandey, Niknejad and Jafar-Nejad, 2021).

While most O-glucosylation residues of N1 are peripheral to the ligand interface, O-glucosylation of S435 in N1 EGF11 located at the interface with Dll4 DSL domain may potentially enhance binding affinity (Andrawes *et al.*, 2013; Luca *et al.*, 2015). In addition, mutation of this O-glycosylation site exacerbated the negative effect of EGF8 O-fucosylation site mutation on N1 activation by DLL1 and their binding (Takeuchi *et al.*, 2018). It was proposed that the other O-glucose modifications may inhibit the aggregation of receptors via hydrophobic surfaces (Luca *et al.*, 2015).

1.2.8.5 O-GlcNAcylation

EGF domain-specific O-linked GlcNAc transferase (EOGT1 in mammals and EOGT in *Drosophila*) adds O-GlcNAc to the consensus sequence C^5-X-X-G-X-(S/T)-G-X-X-C^6, which can be further extended with galactose and sialic acid (Matsuura *et al.*, 2008; Sakaidani *et al.*, 2011). Mass spectrometric analyses of mN1 suggested that most of the seventeen EGFs with the consensus sequence are O-GlcNAcylated, while only five out of eighteen EGFs with consensus sequence in dN are modified (Sakaidani *et al.*, 2012; Harvey *et al.*, 2016; Ogawa *et al.*, 2018; Ogawa and Okajima, 2019). The function of O-GlcNAc in Notch remains unclear as loss of EOGT function in mouse and *Drosophila* led to different phenotypes, with the former having a phenotype resembling reduced Notch signalling and the latter showing enhanced Notch signalling in wing (Müller, Jenny and Stanley, 2013; Sawaguchi *et al.*, 2017; Varshney and Stanley, 2018). In addition, loss of

EOGT function reduces DLL1 and DLL4 binding to N1 but has no effect on JAG1 binding (Sawaguchi *et al.*, 2017). Structural study of the Jag1-N1 interface suggests the O-GlcNAc at T445 in EGF11 does not facilitate binding to Jag1 (Luca *et al.*, 2017).

1.2.8.6 N-linked glycosylation

N-linked glycans can be added to the consensus sequence N-X-S/T (X is not proline) or N-X-C (Bause and Hettkamp, 1979; Lowenthal *et al.*, 2016). There are several consensus sites for N-glycan in the EGF repeats of Notch receptors, many of which are modified, while their function remains unclear or insignificant (Moloney, Shair, *et al.*, 2000; Takeuchi and Haltiwanger, 2014). CHO cell lines defective in N-glycan modification did not show altered Notch signalling (Moloney, Panin, *et al.*, 2000; Chen, Moloney and Stanley, 2001). Also, Notch signalling in mice incapable of producing complex N-glycan remained normal during embryonic development (Stanley, 2007).

1.2.8.7 β-hydroxylation

Aspartate/asparagine β-hydroxylase (AspH or BAH) can hydroxylate EGF domains at the consensus sequence C^3-X-(D/N)-X-X-X-X-(Y/F)-X-C^4, which overlaps with parts of the calcium-binding consensus sequence in cbEGF (Ohlin *et al.*, 1988; Stenflo *et al.*, 1988, 1989; Korioth, Gieffers and Frey, 1994). Mice lacking AspH manifested phenotypes resembling the phenotypes in Jag2 knockout mice, suggesting β-hydroxylation may be required for Notch signalling (Dinchuk *et al.*, 2002). Also, AspH

overexpression or inhibition is linked with upregulated or impaired Notch signalling pathway activity in cancer tissues, mouse models and both primary and reporter cell lines (Cantarini et al., 2006; Gundogan et al., 2011; Iwagami et al., 2016; Lin et al., 2019; Ogawa et al., 2020). Co-immunoprecipitation (co-IP) showed that AspH can physically interact with N1 NECD, JAG1, JAG2, ADAM10 and ADAM17 in pancreatic and breast cancer cell lines (Dong *et al.*, 2015; Lin *et al.*, 2019). Moreover, AspH expression enhances N1-JAG1 binding via an unknown mechanism in breast cancer cell lines, thus increasing the trans-activation of the receptor (Lin *et al.*, 2019). It was found that AspH preferably hydroxylase EGF with the non-canonical disulfide bond, suggesting AspH may be involved in the protein folding pathway (Pfeffer *et al.*, 2019).

1.3 Canonical Notch Ligands

1.3.1 Overview of Notch ligands

Canonical Notch ligands can be divided into 2 families, Jagged/Serrate and Delta. They are single-pass type I transmembrane proteins with large extracellular domains and small intracellular domains (Figure 1.9 and 1.10). The extracellular domain of ligands consists of the N-terminal C2 domain, followed by a Delta/Serrate/LAG-2 (DSL) domain, and varying numbers of EGF and cbEGF domains. The Jagged/Serrate family has an extra cysteine-rich region (CRD) after the EGF repeats (Vitt, Hsu and Hsueh, 2001; D'souza, Miyamoto and Weinmaster, 2008). Mammals have five canonical Notch ligands, including three of the Delta family, Dll1, Dll3 and Dll4, and two of the Jagged/Serrate

family, Jag1 and Jag2.

Notch receptors may also be activated or inhibited via noncanonical ligands, such as: 1. integral membrane proteins, e.g. DLK1 and DNER which resemble canonical ligands but lack a C2 and DSL domain; 2. glycosylphosphatidylinositol (GPI)-linked membrane proteins, e.g. Contactin1 and Contactin6; 3. secreted proteins, e.g. Wingless (Wg) in *Drosophila*, Thrombospondin2 (TSP2) in mammals and OSM11 in *C. elegans* (reviewed by D'Souza et al., 2010).

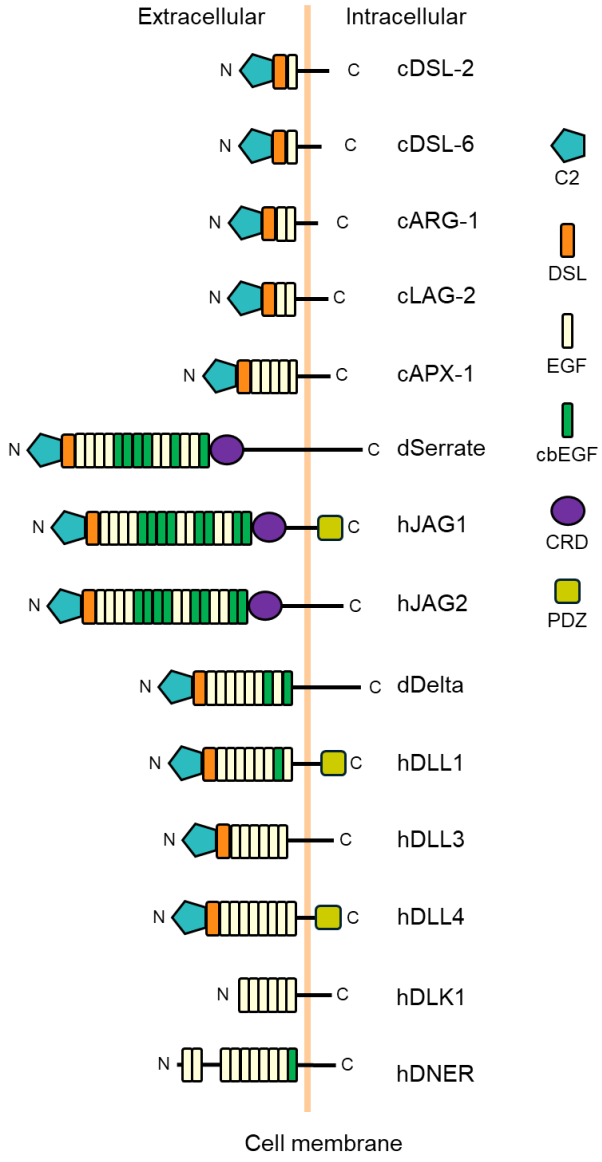


Figure 1.9. Domain arrangement of Notch ligands.

Canonical Notch ligands in *C. elegans* (cDSL-2, 6, cARG-1, cLAG-2 and cAPX-1), *Drosophila* (dSerrate and dDelta) and humans (hJAG1, hJAG2, hDLL1, hDLL3 and hDLL4) can be divided into two families. Their NECD contains from the N terminus a C2 domain, a Delta/Serrate/LAG-2 (DSL) domain, multiple EGF domains and an additional cysteine-rich domain (CRD) only in the Jagged/Serrate family ligands. Some ligands possess a C-terminal PSD-95/Dlg/ZO-1 (PDZ) motif in the intracellular domain. Soluble *C. elegans* ligands (cDSL-1/3/4/5/7) are not shown (Komatsu *et al.*, 2008). The extracellular domains of non-canonical ligands DLK1 and DNER consist of multiple EGF repeats but lack the N terminal C2 and DSL domains (Gubina *et al.*, 1999; Eiraku *et al.*, 2002; D'Souza, Meloty-Kapella and Weinmaster, 2010).

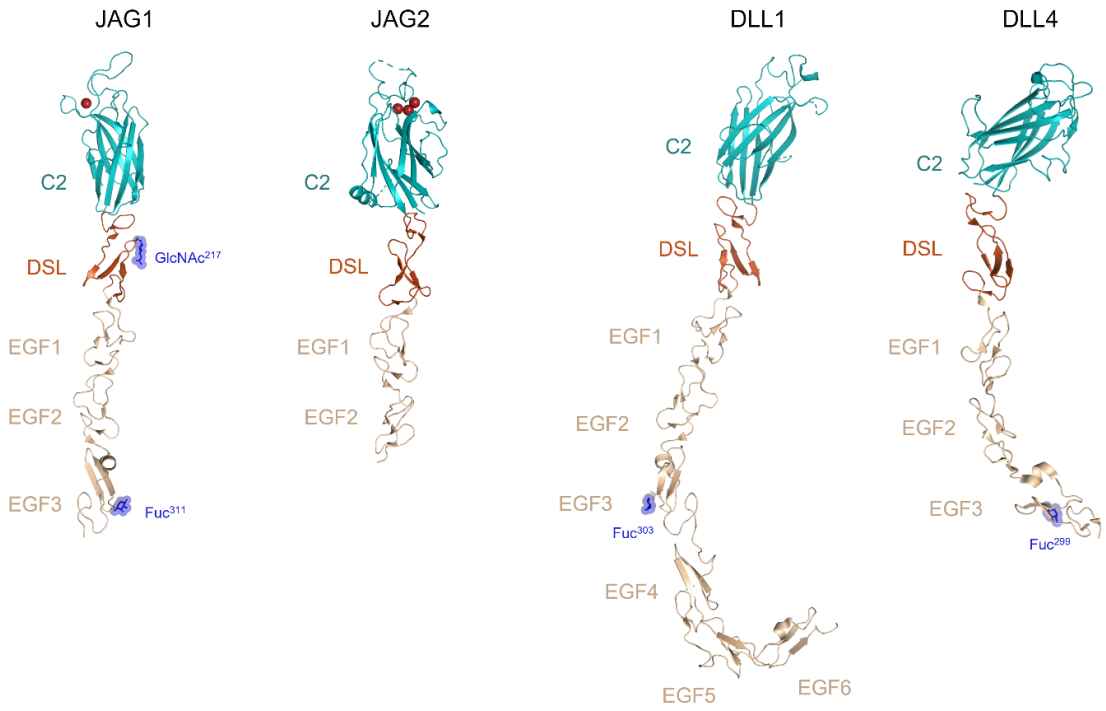


Figure 1.10. Structure of the N terminus of canonical Notch ligands.

X-ray structures of human JAG1 C2-EGF3 (PDB: 4CC1), JAG2 C2-EGF2 (PDB: 5MWF), DLL1 C2-EGF6 (PDB: 4XBM), DLL4 C2-EGF3 (PDB: 5MVX) (Chillakuri *et al.*, 2013; Kershaw *et al.*, 2015; Suckling *et al.*, 2017). C2 domain and DSL domain are shown in teal and brown. EGF domains are shown in wheat. The Ca^{2+} ions are shown as red spheres. O-glycans are coloured blue.

1.3.2 The C2 domain

The C2 domain, which was formerly known as the “module at the N-terminal of Notch ligands” (MNNL), not only facilitates receptor binding but also interacts with phospholipids in keeping with its role as a common lipid-binding module in other proteins (Chillakuri *et al.*, 2013; Corbalan-Garcia and Gómez-Fernández, 2014; Luca *et al.*, 2015, 2017; Suckling *et al.*, 2017). The C2 domain consists of two sets of four-stranded antiparallel β-strands creating a β-sandwich hydrophobic core with various loops connecting the strands. The loop connecting β-strands 2 and 3 of the C2 domain binds

to EGF12 of N1, whilst the apical β1-2 and β5-6 loops confer lipid binding properties (Taylor *et al.*, 2014; Luca *et al.*, 2017; Suckling *et al.*, 2017).

All C2 domains of mammalian Notch ligands except DLL3 can bind to liposomes consisting of a mixture of phospholipids commonly found in the cell surface membrane (Suckling *et al.*, 2017). While the C2 domains of Jag1 and Jag2 can bind Ca^{2+}, the C2 domains of Delta family ligands cannot (Figure 1.10). Several JAG1 C2 mutations identified in the disease extrahepatic biliary atresia (EHBA) have been shown to reduce Notch activation but do not affect binding to receptor (Suckling *et al.*, 2017). Alternatively, they reduced the ligand's capacity to bind lipids. In addition, Yao et al. (2022) discovered that mutations abolishing N-glycosylation of JAG1 N143 decreased the ligand's ability to activate Notch. Also, the removal of this N-glycan in JAG1 C2 reduces its interaction with phospholipids. These results suggested a role for the C2 domain in membrane binding, which facilitates Notch activation by JAG family ligands.

1.3.3 The Delta/Serrate/LAG-2 domain

The DSL domain shares a similar structure fold with an EGF and consists of double-stranded anti-parallel β-sheets with six conserved cysteine residues, forming disulfide bonds with 1-2, 3-4, and 5-6 arrangement. A surface loop of the DSL with conserved charged and aromatic residues, such as JAG1 F199, R201, R203, D205 and F207, formed the binding site for Notch EGF11 (Cordle, Johnson, *et al.*, 2008). The effects of DSL mutations on *Drosophila* wing disc development upon Ser overexpression, such as

reduced Notch activation in ventral cells and reduced repressing of Notch activity at the D/V boundary, suggested that those residues are essential for both trans-activation and cis-inhibition, indicating the DSL regulates both cis- and trans-interactions between receptor and ligand (Cordle, Johnson, *et al.*, 2008). DLL3 has a degenerate DSL domain and is unable to activate Notch (Ladi *et al.*, 2005; Geffers *et al.*, 2007; Serth *et al.*, 2015). It functions as a negative regulator of Notch (Chapman *et al.*, 2011). While other mammalian ligands are located in the cell surface membrane, DLL3 is mainly located in the trans-Golgi (Geffers *et al.*, 2007).

1.3.4 Ligand post-translational modification

O-glycosylation modifications have been found in Notch ligands by structural and mass spectrometric analyses, though their functions remain less studied (Panin et al., 2002; Luca et al., 2015, 2017). Both *Drosophila* Ser and Dl and mammalian Jag1 and Dll1 have O-fucose modifications that can be elongated by Fng (Panin et al., 2002). The effect of O-fucosylation varies between ligands. Structural studies suggested the O-fucose at T311 of Jag1 EGF3 facilitates the interaction with N1 EGF8 (Luca et al., 2017). As shown by mutations of O-fucosylation sites, O-fucose modifications in EGF2 and EGF5 of Dll3, which are extended by Lfng are essential for embryonic somitogenesis in mice despite having no impact on the cis-interaction of Dll3 with Notch1 (Serth et al., 2015). Also, mutations of mDll1 O-fucosylation sites at EGF3, 4, 7 and 8 induce some extent of ligand intracellular accumulation (Müller et al., 2014). Dl and Ser are O-GlcNAcylated by Eogt in S2 cells though the function of these modifications remains unclear (Müller, Jenny and

Stanley, 2013). EGF4, 8, 11 and 16 of Jag1 are O-glucosylated by Poglut1 in the C57BL/6 mouse model (Thakurdas et al., 2016). Loss of one copy of Poglut1 reduced the deleterious effect of Jag1 haploinsufficiency on intrahepatic bile duct development (Thakurdas et al., 2016). Ligands also possess consensus sites for N-glycosylation although their glycosylation status and functions are mostly unclear. N-glycosylation of N143 in the JAG1 C2 domain has been shown to be required for Notch activation by facilitating, directly or indirectly, the ligand/membrane interaction (Meng et al., 2022).

1.4 Interaction between Notch receptor and ligand

1.4.1 Insights from the structures of receptor-ligand complexes

N1 EGF12 interacts directly with the C2 domain of ligands. This interface is known as Site 1 (Figure 1.11). Mutagenesis studies and structures of receptor-ligand complexes suggested that L468, D469, and I477 in EGF12 are essential for ligand binding (Whiteman *et al.*, 2013; Luca *et al.*, 2015). Additionally, Fng-mediated elongation of O-fucose at T466 in EGF12, which forms hydrogen bonds with residues such as Y65 in Dll4 and Y82 in Jag1, enhances the binding to both types of ligands by participating in interface anchorage (Taylor *et al.*, 2014; Luca *et al.*, 2015, 2017). N1 EGF11 interacts directly with the DSL domain of ligands. This interface is known as Site 2 (Figure 1.11). The centre of this interaction is R448 in N1 EGF11, whose side chain buries deeply into the groove in the DSL domain and interacts with residues such as F195, Y216 and D218 in Dll4 (Luca *et al.*, 2015). Also, P422 and F436 in the hydrophobic pocket in EGF11 form

Van der Waals (VDW) interactions with F195 in the DSL domain of Dll4 (Luca *et al.*, 2015). The O-glycan at Ser435 of N1 EGF11 may also contribute to its interaction with Dll4 (Luca *et al.*, 2015).

As mentioned in Section 1.2.3, EGF1-3 of Jag1 appears to play a more important role in receptor binding than the equivalent fragment from Dll4, though it should be noted that the Dll4-N1 interface was defined using a structure formed by a shorter N1 EGF11-13 fragment instead of the N1 EGF8-12 fragment used during Jag1-N1 interface determination (Luca *et al.*, 2015, 2017). Luca et al. (2017) proposed that Y255 in EGF1 of Jag1, which protrudes outward to help anchor N1 EGF10, may reinforce the difference in receptor-binding interface as it is not conserved in Dll1 and Dll4. The O-fucose at T311 in N1 EGF8 facilitates ligand binding by forming a hydrogen bond with the side chain of Jag1 N298 in EGF3 (Luca *et al.*, 2017). Removal of this O-fucose in N1 EGF8 has a stronger impact on Notch activation than removal of the O-fucose at T466 in EGF12 (Luca *et al.*, 2017). The O-fucose at T311 of Jag1 EGF3 also facilitates the interaction with N1 EGF8 (Luca *et al.*, 2017).

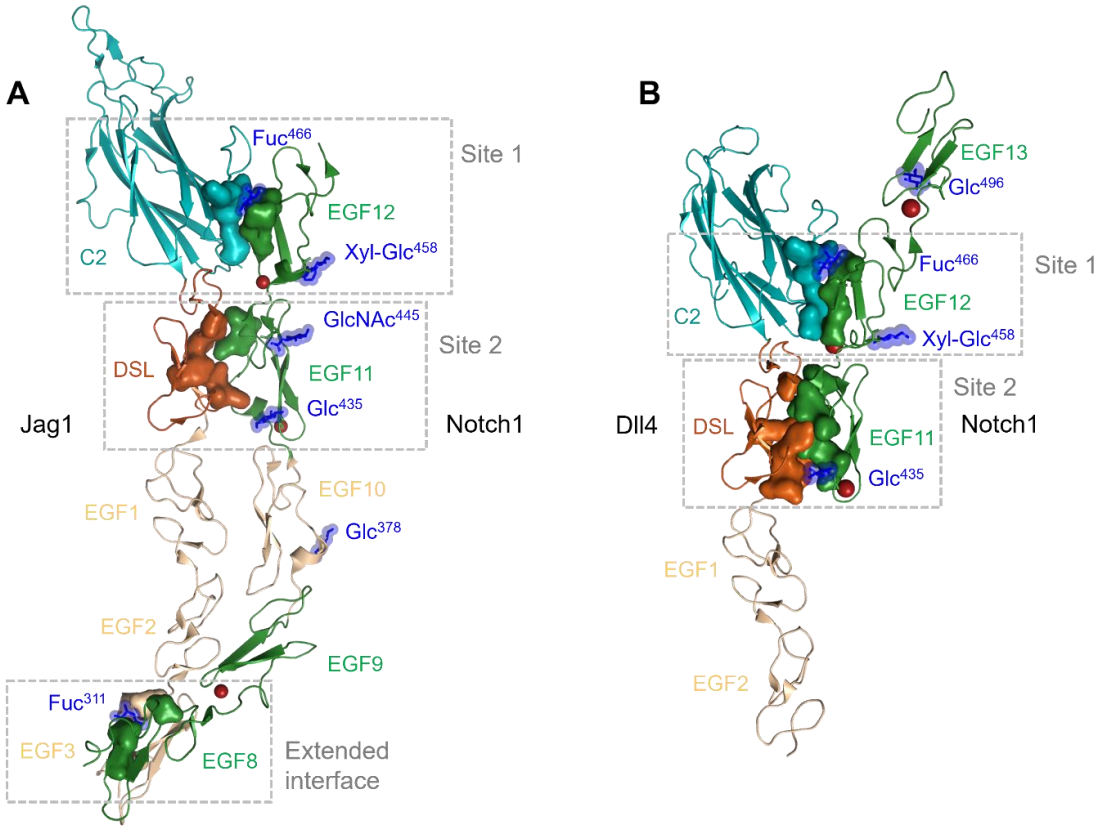


Figure 1.11. Structural basis of LBR-ligand interaction.

(A) X-ray structure of rat Notch1 EGF8–12/Jag1 C2-EGF3 complex (PDB: 5UK5) (Luca *et al.*, 2017). (B) X-ray structure of rat Notch1 EGF11–13/Dll4 C2-EGF2 complex (PDB: 4XLW) (Luca *et al.*, 2015). C2 domain and DSL domain are shown in teal and brown. EGF domains are shown in wheat. cbEGF domains are shown in green. The Ca^{2+} ions are shown as red spheres. Key residues involved in the binding between ligand and receptor at Site 1 and Site 2 and a third Jag1-specific site are shown as surface representations. O-glycans on the receptor are coloured blue.

1.4.2 Endocytosis and mechanical force

The intracellular domain of ligands can be ubiquitinated at the cell membrane by two families of RING-domain-containing E3 ubiquitin (Ub) ligases, Neuralized (Neur), such as Neur1 and Neur2 in mammals, and Mindbomb (Mib), such as Mib1 and Mib2 in mammals, leading to ligand endocytosis (Deblandre, Lai and Kintner, 2001; Kang *et al.*, 2012). Ligand endocytosis is suggested to be essential for Notch activation, shown by

reduced Notch signalling in the absence of Neur and Mib (Parks *et al.*, 2000; Deblandre, Lai and Kintner, 2001; Itoh *et al.*, 2003; Lai *et al.*, 2005; Le Borgne, 2005). It was proposed that ligand endocytosis exerts a pulling force on the NECD, leading to a conformational change that exposes the S2 cleavage site in the NRR. Following S2 cleavage, NECD can be trans-endocytosed into the signal-sending cells for degradation in pair with the ligand (Figure 1.12) (Klueg and Muskavitch, 1999; Parks *et al.*, 2000; Nichols *et al.*, 2007).

Notch is thus regarded as a mechanosensor which activates upon a mechanical trigger. In support of this, tension gauge tether assay and magnetic tweezer assay showed that N1 trans-endocytosis induces a pulling force between 5.4 to 12 pN, which is sufficient to initiate S2 cleavage (Wang and Ha, 2013; Gordon *et al.*, 2015). Furthermore, the bilateral endocytosis model suggests that Deltex E3 ubiquitin ligase 4 (DTX4)-mediated ubiquitination and subsequent endocytosis of Notch into the signal-receiving cell can generate a pulling force in the opposite direction on the Notch-ligand complex, thereby enhancing the pulling force induced by ligand endocytosis into the signal-sending cell (Chapman *et al.*, 2016; Chastagner, Rubinstein and Brou, 2017).

Tension gauge tether assays for the N1-Jag1/Dll4 complex discovered that the lifetime of the Notch-ligand complex is improved along with an increase in pulling force up to 10 pN, which includes the predicted range of pulling force generated by Notch trans-endocytosis (Luca *et al.*, 2017). This bond stabilisation by mechanical force indicates a

catch bond property. The formation of this catch bond may involve changes in relative domain positions at the receptor-ligand interface which enhance the binding affinity or docking of the binding sites (Luca *et al.*, 2017; Suckling *et al.*, 2017). The combined effects of pulling force and catch bond formation help to amplify the interaction between receptor and ligand, transmitting the mechanical trigger along the lengthy NECD towards the NRR.

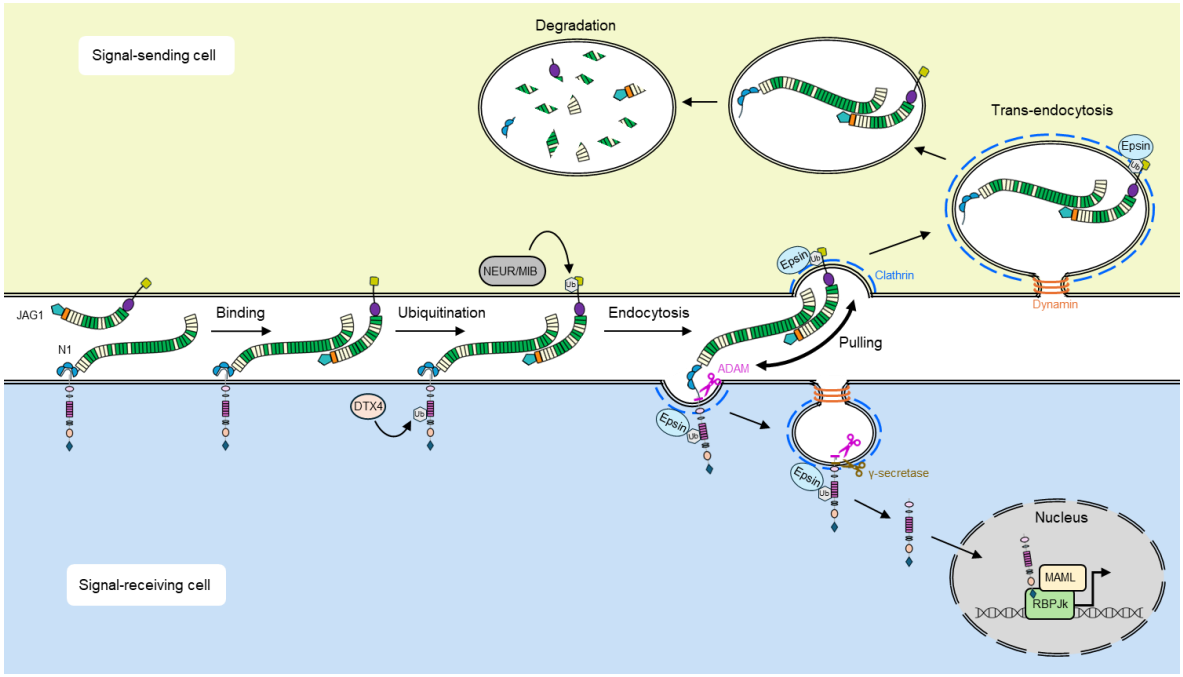


Figure 1.12. Bilateral endocytosis of receptor and ligand during trans-activation.

E3 ligases NEUR or MIB catalyse the ubiquitination of ligand intracellular domain (JAG1 in this figure), and upon receptor-ligand binding, initiate the clathrin-dependent endocytosis of the ligand-receptor complex into the signal-sending cell (Deblandre, Lai and Kintner, 2001; Kang *et al.*, 2012). According to Chastagner et al. (2017), DTX4-mediated ubiquitination of receptor (N1 in this figure) induces the endocytosis of the receptor into the signal-receiving cell (Chastagner, Rubinstein and Brou, 2017). This bilateral endocytosis creates a strong pulling force on the NECD, leading to a conformational change that exposes the S2 cleavage site in the NRR. In consequence, S2 cleavage by ADAM and S3 cleavage by γ-secretase take place, releasing the NICD into the cytoplasm. NICD then travels to the nucleus to initiate the transcription of target genes. Epsin interacts with both the ubiquitin on the ligand and receptor intracellular domains and clathrin to organise the invagination (Gupta-Rossi *et al.*, 2004, p. 200; Wang and Struhl, 2004, 2005; Chen *et al.*, 2009; Sorensen and Conner, 2010; Xie, Cho and Fischer, 2012). The GTPase dynamin excises the nascent clathrin-coated pit from the cell membrane to form the endocytic vesicle (Vaccari *et al.*, 2008; Windler and Bilder, 2010). NECD is trans-endocytosed into the signal-sending cell in complex with ligand extracellular domains and subsequently degraded in the lysosome.

1.4.3 The binding affinity of ligands

Ligands bind to receptors with different affinity. Biolayer interferometry and SPR studies

showed that DLL4's affinity for N1 is over 10-fold stronger than that of DLL1 (Andrawes *et al.*, 2013). A recent molecular dynamic simulation study suggested that the loop β2-3 with disulfide bond in the C2 domain of Dll4 has higher flexibility and a wider range of motion than that of Dll1 and may contribute to more effective interaction with N1 EGF12 (Hirano *et al.*, 2020). Also, SPR studies revealed that Dll4 has a higher affinity to N1 than Jag1, which may explain why Dll4 requires a lower tension (F < 4pN) than Jag1 (4pN < F < 12pN) for N1 activation (Luca *et al.*, 2017). On the other hand, while DLL4 has a lower affinity to N2 than N1, DLL1 has a similar affinity for N1 and N2 and a stronger affinity than DLL4 for N2 (Tveriakhina *et al.*, 2018). The different binding affinities observed across ligands may ensure that Notch activation can occur over a wide range of physiological conditions.

1.5 Cis-inhibition

1.5.1 Molecular mechanism of Notch cis-inhibition

When Notch receptors and ligands are expressed in the same cell, Notch may be inhibited. Ligands in neighbouring cells can no longer activate the receptor. The exact molecular mechanism of Notch cis-inhibition remains controversial, with evidence supporting multiple modes (Fleming, 2020) (Figure 1.13). Firstly, early studies detected a reduction in cell surface Notch level upon expression of cis-ligands (Pérez *et al.*, 2005; Glittenberg *et al.*, 2006). Also, only full-length Notch was detected in the complexes of Dl/N and Ser/N, suggesting the complexes were formed before S1 cleavage (Sakamoto

et al., 2002) (see Section 1.1.2). It was proposed that receptors and ligands may form complexes in the ER or the Golgi and be targeted for degradation (Figure 1.13A). The fact that DLL3, the cis-inhibiting ligand, is primarily located in the Golgi, further supports this theory (Geffers *et al.*, 2007).

On the other hand, Ser carrying an ER retention signal has a reduced ability to cis-inhibit dN, indicating retention of receptor/ligand complexes in the secretory pathway is insufficient for generating full-scale cis-inhibition (Glittenberg *et al.*, 2006). Also, when Dll1 and Dll3 were expressed in cis, the cell surface Notch level did not decrease (Sakamoto *et al.*, 2002; Ladi *et al.*, 2005). These studies suggested that cis-inhibition may also take place on the cell surface. This theory is supported by the finding that elevated cis-ligand endocytosis through the expression of E3 ligase Neur or Mib1 (see Section 1.4.2) damaged cis-inhibition in *Drosophila* cells and wing disc and neural tube in chick embryos (Glittenberg *et al.*, 2006; Berndt *et al.*, 2017; Baek *et al.*, 2018).

Cis-ligand is not expected to activate Notch on the cell surface due to the lack of a pulling force (Fleming, 2020). There are several possible ways cis-ligands may interact with the Notch receptors on the cell surface. Firstly, as cis-ligand may bind to the same domains in the receptor involved in its interaction with trans-ligand, it may compete with the trans-ligand and weaken the interaction of trans-ligand with the receptor (Figure 1.13B). As a result, not enough “trigger” is received by the receptor, thus no activation is induced. Evidence supporting this model includes S2 cell aggregation assay showing reduced

aggregation between Ser-expressing cells and cells coexpressing dN and Ser, though no measurement for cell surface dN level was taken (Fleming *et al.*, 2013).

Alternatively, trans-ligand may still bind to the receptor at the cell surface in the presence of cis-ligand, shown by aggregation of S2 cells expressing Dl with S2 cells coexpressing dN and Dl (Fiuza *et al.*, 2010). Therefore, cis-interaction between ligand and receptor may still enable trans-interaction but repress S2 or S3 cleavage (Figure 1.13C). While not affecting cell surface Notch level in S2 cells, cis-ligands reduced ethylenediaminetetraacetic acid (EDTA)-induced Notch activation (Fiuza *et al.*, 2010). As EDTA is a calcium chelator that activates Notch by disrupting the calcium-dependent folded structure of the NRR, this result suggested the possibility that cis-interaction between ligand and receptor may block the access of ADAM to Notch NRR despite its calcium-binding status.

Though evidence supporting different mechanisms has been found, these mechanisms may operate in parallel to enhance the inhibitory effect of cis-ligands (Glittenberg *et al.*, 2006; Fleming, 2020).

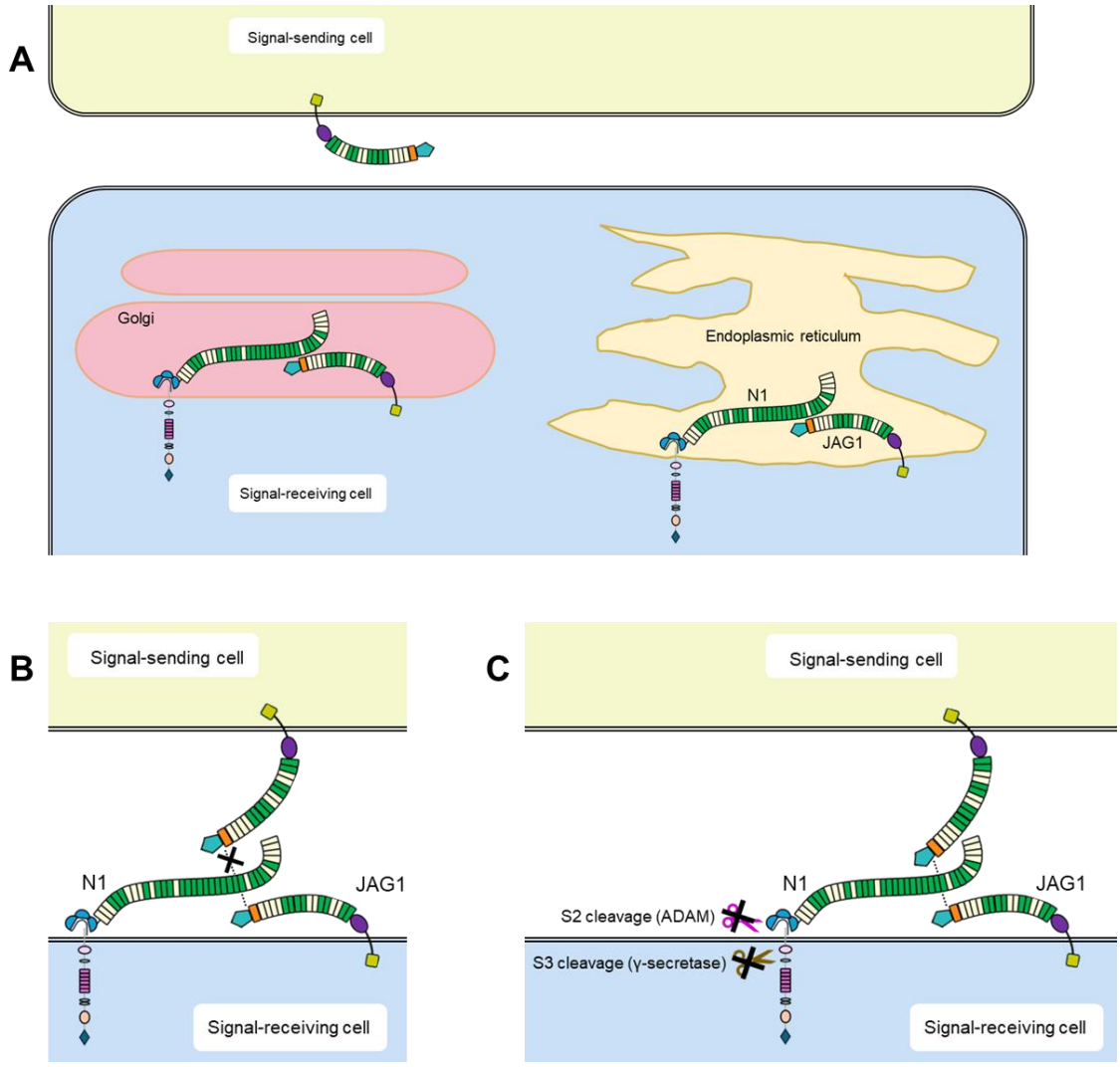


Figure 1.13. Potential mechanisms of cis-inhibition.

Three potential mechanisms of cis-inhibition are illustrated by schematic presentations using N1 and JAG1. (A) Notch receptors may form complexes with ligands and be trapped in the ER (yellow) or Golgi (red) on their way to the cell surface, thus reducing the number of receptors available on the cell surface to interact with and be activated by trans-ligands (Sakamoto *et al.*, 2002; Pérez *et al.*, 2005; Glittenberg *et al.*, 2006). (B) Notch receptors and cis-ligands may reach the cell surface. If a similar interaction site is involved, the competition between cis- and trans- ligand-receptor complexes would favour the cis-complex over the trans-complex, thus preventing or weakening the interaction between receptors and trans-ligands (Fleming *et al.*, 2013). Therefore no pulling force is received by the receptor and no trans-activation takes place. (C) Notch receptors and cis-ligands may reach the cell surface and the receptors may still be able to interact with the trans-ligands despite the presence of cis-ligand. However, the cis-interaction between receptor and ligand inhibits S2 and S3 cleavage potentially by blocking the cleavage sites (Fiuza *et al.*, 2010). As a result, the NECD

cannot be cleaved to release the NICD.

1.5.2 Onset and strength of cis-inhibition

Early studies observed that cis-inhibition could be overcome by an increase in dN expression in the *Drosophila* wing, indicating that the cis-interaction simultaneously inhibits both the receptor and the ligand (Doherty *et al.*, 1996; Klein, Brennan and Arias, 1997). This titration-based mutual inactivation model was further confirmed by computational studies (Sprinzak *et al.*, 2010, 2011; del Álamo, Rouault and Schweisguth, 2011). The most direct proof of the model was obtained using quantitative time-lapse microscopy that detected a sharp onset of cis-inhibition once the concentration of cis-Dl reached a certain threshold, which depended on the concentration of N1 but not the concentration of trans-Dl (Sprinzak *et al.*, 2010).

The strength of cis-inhibition can be influenced by multiple factors, including receptor-ligand affinity, trans and cis-ligands pairing, receptor identity and Fng status. DLL4 was found to be more efficient than DLL1 in cis-inhibition of N1 (CHO-K1 and HeLa cells) (Preuße *et al.*, 2015; Nandagopal, Santat and Elowitz, 2019). This was attributed to DLL4 having a higher affinity for the receptor than DLL1. On the other hand, JAG2 cis-inhibits N1 most effectively across all ligands in CHO-K1 cells, suggesting cis-inhibition strength does not depend solely on binding affinity (Kuintzle, Santat and Elowitz, 2023). Unlike JAG family ligands, DLL1 and DLL4 can only cis-inhibit N1 but not N2 in CHO-K1 cells (Kuintzle, Santat and Elowitz, 2023). The strength of cis-inhibition may also depend on the identity of the trans-ligand as the ligand can more efficiently cis-inhibit N1 when

antagonising the same ligand in trans (Kuintzle, Santat and Elowitz, 2023). Furthermore, similar to trans-interaction, Fng modifications of O-fucose of Notch affect the strength of cis-interaction between ligand and receptor and the efficiency of cis-inhibition (see Section 1.2.8.3) (Pandey *et al.*, 2019; Kakuda *et al.*, 2020).

More recently, in some cell types, ligands have been shown to induce cis-activation of Notch (Nandagopal, Santat and Elowitz, 2019). N1 and N2 could be activated by cis-DLL1 and DLL4 when their concentrations were below certain thresholds (Nandagopal, Santat and Elowitz, 2019; Kuintzle, Santat and Elowitz, 2023). Comparisons between ligands and Fng modification of Notch indicated the level of cis-activation increased along with ligand-receptor affinity (Nandagopal, Santat and Elowitz, 2019). Only minimal JAG1 and JAG2-mediated cis-activation were detected, suggesting this cis-activation mechanism may be less important for JAG family ligands (Kuintzle, Santat and Elowitz, 2023).

1.5.3 Domains required for cis-interaction

Firstly, it has been proposed that a similar interface is required for both trans-activation and cis-inhibition. EGF12 in the LBR of the dN and the DSL domain of Ser are required for cis-inhibition as missense mutations in those domains led to reduced trans-activation and cis-inhibition in the *Drosophila* wing disc (Cordle, Johnson, *et al.*, 2008; Becam *et al.*, 2010). While a mutation in EGF8 of dN disrupted both Ser-induced trans-activation and cis-inhibition, it did not affect Dl-induced Notch activation or inhibition, indicating that

EGF8 is required for cis-interaction of Notch with Ser but not with Dl (Yamamoto *et al.*, 2012). This may be explained by the finding that an extended interface which includes EGF8 in N1 and EGF3 in Jag1 contributes to N1-Jag1 binding but not N1-Dll4 binding (Luca *et al.*, 2017) (see Section 1.2.3). In support of this, the deletion of EGF3 in Ser reduced the ligand's ability to cis-inhibit dN as measured by Cut expression upon ectopic Ser expression in the wing disc (Fleming *et al.*, 2013).

On the other hand, several regions in the ligand may only be involved in cis-interaction but not trans-interaction (Figure 1.14). Removals of each EGF in EGF4-6 of Ser were found to abolish cis-inhibition but not trans-activation in *Drosophila* wing discs and S2 cells (Fleming *et al.*, 2013). While EGF4-6 are conserved in other Jagged/Serrate family ligands, it is not conserved in the Delta family ligands, suggesting that the cis-interaction interface may differ between the two ligand families. Chen et al. (2023) discovered that deletion of EGF8 of DLL4 significantly reduced cis-inhibition of N2 by DLL4 but deletion of EGF6 or 7 did not, suggesting that DLL4 EGF8 is required for cis-inhibition of N2 (Chen *et al.*, 2023). None of those EGF deletions impacted trans-activation.



Figure 1.14. Receptor and ligand domains involved in cis-inhibition.

Schematic illustrations of the extracellular regions of dN (A), Ser (B) and DLL4 (C) with domains that have been shown to participate in cis-inhibition indicated by asterisks. EGF8 and EGF12 in dN have been shown to be required for dN cis-inhibition by Ser (Cordle, Johnson, *et al.*, 2008; Becam *et al.*, 2010; Yamamoto *et al.*, 2012). For cis-inhibition by Dl, dN EGF8 has been shown to be dispensable and the role of EGF12 is unknown. Ser DSL and EGF3-6 (Fleming *et al.*, 2013) and DLL4 EGF8 (Tveriakhina *et al.*, 2018) have been shown to regulate cis-inhibition.

1.5.4 Cis-inhibition in development

The role of cis-inhibition in development was initially characterised in *Drosophila* where it is involved in the development of the wing vein (de Celis and Bray, 1997; Miller, Lyons and Herman, 2009; Troost *et al.*, 2023). In the wing disc, the expression of Wg in the D/V boundary induces the expression of Ser and Dl in cells adjacent to the D/V boundary, which cis-inhibit Notch signalling in those cells, limiting Notch signalling only to the D/V boundary (de Celis and Bray, 1997; Micchelli, Rulifson and Blair, 1997). This pattern is essential for the maintenance of the lineage restriction of dorsal and ventral cells (Micchelli and Blair, 1999; Becam and Milán, 2008). Also, cis-inhibition helps regulate the development of photoreceptors in the eye (Figure 1.15) and sensory bristles in

Drosophila (Voas and Rebay, 2004; Miller, Lyons and Herman, 2009). Cis-inhibition has also been found to regulate vertebrate development, such as during angiogenesis, haematopoiesis, pancreatic development and neural fate decision (Boareto *et al.*, 2015; Baek *et al.*, 2018; Xu *et al.*, 2023; Thambyrajah *et al.*, 2024). For example, while N1 activation by Dll4 initiates the transition of hemogenic endothelial cells to intra-aortic hematopoietic clusters, an increasing Jag1 level in the clusters leads to N1 cis-inhibition and a gradual decrease in Notch signalling, maintaining a hematopoietic stem cell fate (Thambyrajah *et al.*, 2024).

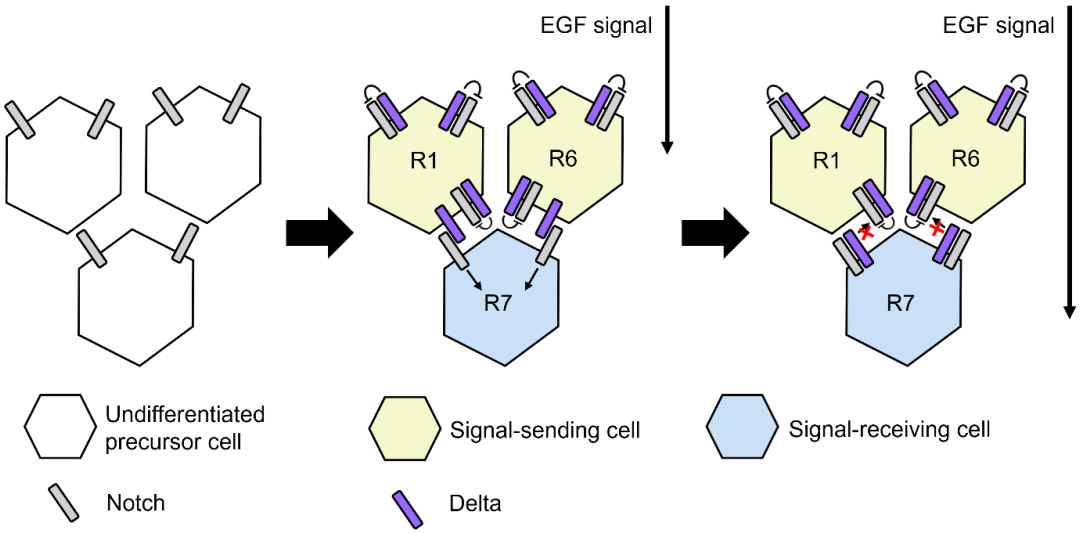


Figure 1.15. Notch cis-inhibition during *Drosophila* photoreceptor differentiation

Three undifferentiated precursor cells of photoreceptor (white hexagon) form a cluster. dN (grey rod) is expressed in precursor cells. Dl expression (purple rod) is induced in the first two cells receiving the EGF signal. These two cells differentiate into R1 and R6 cells which become signal-sending cells (green hexagon). Dl expressed on the cell surface of R1 and R6 activates dN on the third precursor cell in their cluster, which differentiates into R7 cell due to Notch activation (blue hexagon). When the EGF signal reaches the R7 cell, which then starts to express Dl, this Dl expressed by R7 can no longer activate dN in R1 and R6 as their receptors are already cis-inhibited, further maintaining their R1 and R6 cell fate (Miller, Lyons and Herman, 2009).

1.6 Abruptex region

1.6.1 Ax variants

Ax variants that can induce the *Ax* phenotype in *Drosophila* can be divided into three classes, known as homozygous lethal (*L-Ax*), *N* suppressor (*Su(N)*), and *N* enhancer (*E(N)*) (Foster, 1975; Portin, 1975; De Celis and Garcia-Bellido, 1994) (Table 1.4). Residues affected by Ax variants identified in dN are conserved in Notch receptors across multiple species (Figure 1.16), except for dN S1088, which corresponds to hN1 Q1049.

Table 1.4. Abruptex variants identified in *Drosophila* with hN1 homolog shown (De Celis and Garcia-Bellido, 1994).

Ax variant	EGF	Residue change in dN	Effect	hN1 homologue
Ax9	24	D948V	*N* suppressor	D909V
Ax59b	24	C972G	homozygous lethal	C933G
Ax59d	24	C972S	homozygous lethal	C933S
Ax1	25	N986I	*N* suppressor	N947I
Ax-M1	25	C999Y	homozygous lethal	C960Y
Ax71d	27	S1088I	*N* enhancer	Q1049I
Ax-E2	29	H1167Y	*N* enhancer	H1129Y
Ax16	29	G1174A	*N* enhancer	G1136A

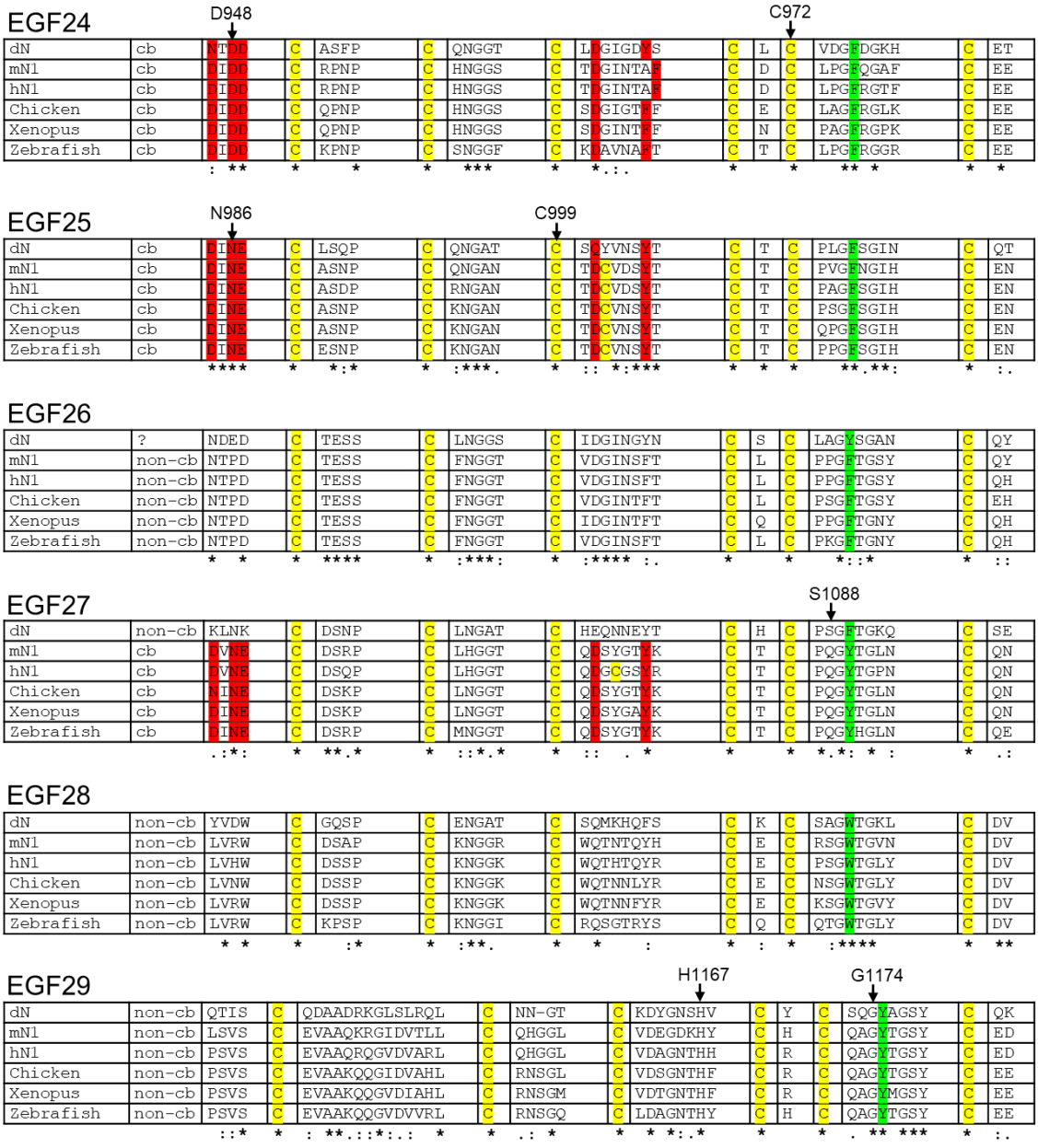


Figure 1.16. Protein sequence alignment for Ax region in Notch receptors across species.

NCBI reference protein sequences for (from top to bottom) dN (NP_476859.2), mN1 (NP_032740.3), hN1 (NP_060087.3), Chicken N1 (NP_001384725.1), *Xenopus* N1.L (XP_018084977.1) and Zebrafish N1.b (NP_571377.2) were aligned by Clustal Omega available on EMBL-EBI website (Sievers and Higgins, 2021; Madeira *et al.*, 2022; *Clustal Omega < EMBL-EBI*, no date). Alignment result was shown for each EGF domain. Fully conserved residues are shown by asterisks (*). Conserved positions where aligned residues are strongly similar in biochemical properties are indicated by colons (:). Conserved positions where aligned residues are weakly similar in biochemical properties are indicated by periods

(.). Cysteine residues are highlighted in yellow, with conserved cysteines involved in forming the EGF fold aligned in columns. Consensus aromatic residues that may be involved in hydrophobic packing are highlighted in green. Ca^{2+}-binding consensus residues D/N/E-x-D/N-D/N/E/Q-x_m-D/N/Q-x_n-Y/F (m/n denote variable numbers of residues) are highlighted in red if the complete consensus is predicted or shown to bind Ca^{2+}. EGF26 in dN have one residue different to the known Ca^{2+}-binding consensus sequence. Its Ca^{2+}-binding status is uncertain (indicated by "?"). Sites of missense mutations generating the *Ax* phenotype are shown by arrows, which are conserved in Notch receptors across species, except for S1088.

When homozygous (*L-Ax/L-Ax*), or when heterozygous with a null *dN* allele (*L-Ax/N*$^-$) or an *Ax* allele from a different class (*L-Ax/Su(N), L-Ax/E(N)*), Ax homozygous lethal alleles confer lethality (Portin, 1975). Since they substitute cysteine residues involved in disulfide bonding of the EGF domain (Figure 1.17), they will likely generate large structural change. An earlier study suggested that the homozygous lethal C999Y reduces Notch availability on the cell surface membrane in *Drosophila* S2 cells (Pérez *et al.*, 2005).

When heterozygous with a null *dN* allele (*Su(N)*/*N*$^-$ *or E(N)*/*N*$^-$), the *N* suppressor and enhancer alleles cause differential effects on the *N* phenotype (Foster, 1975; Portin, 1975; Kelley *et al.*, 1987). Though the *Ax* phenotype is suppressed, *N* suppressors suppress wing nicking caused by the *N* phenotype, while *N* enhancers enhance the extent of wing nicking. *N* suppressors and *N* enhancers are both homozygous viable (*Su(N)/Su(N)* or *E(N)/E(N)*) inducing the same phenotype as their heterozygote form (*Su(N)*/*N*$^+$ *or E(N)*/*N*$^+$) (Foster, 1975; Portin, 1975). They are also viable when heterozygous with Ax variants of the same class, such as D948V/N986I or H1167Y/G1174A, but are hardly viable when heterozygous with Ax variants of another

class (*Su(N)/E(N)*), such as D948V/H1167Y (Foster, 1975; Portin, 1975). The fact that combinations of *N* suppressors and *N* enhancers cause negative complementation has led to the suggestion that these variants may affect alternative functions of the receptor (De Celis and Garcia-Bellido, 1994).

None of the Ax variants affects the consensus sequence for O-glycosylation in dN (see Section 1.2.8), suggesting the *Ax* phenotypes are not caused by changes in the glycosylation pattern of Notch. However, the homologous mutation of dN G1174A in hN1 and hN2 affects the consensus sequence of O-GlcNAcylation in EGF29, which was tested as partially O-GlcNAcylated in mN1 by liquid chromatography with tandem mass spectrometry (Tsukamoto *et al.*, 2022).

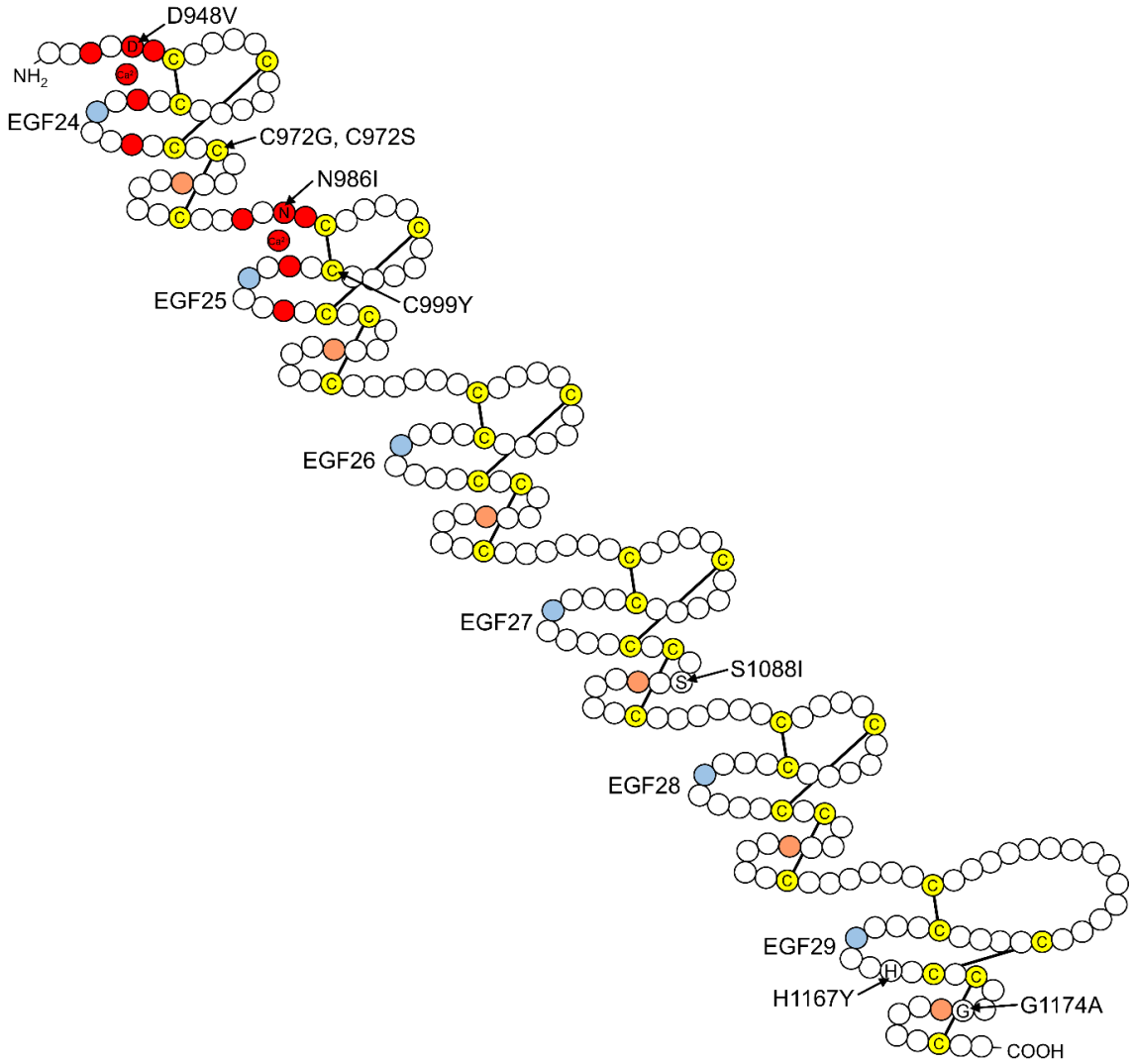


Figure 1.17. Schematic illustration of the locations of Ax variants in *Drosophila*.

Homozygous lethal and *N* suppressor variants are located in the Ca^{2+}-binding N terminus EGF24-25 of the Ax, while *N* enhancers are located in non-calcium-binding EGF27 and 29. Homozygous lethal variants affect cysteine residues essential for the maintenance of the EGF fold. *N* suppressors affect residues forming the Ca^{2+}-binding consensus sequence and are likely to reduce the Ca^{2+}-binding affinity (Handford *et al.*, 1991). *N* enhancer G1174A affects the glycine residue required for a conserved β-turn of the core EGF structure (Campbell *et al.*, 1990; Baron *et al.*, 1992). Cysteine residues (yellow), disulfide bonds (black lines), consensus residues for Ca^{2+} binding and Ca^{2+} ion (red), conserved aliphatic residue (blue) and aromatic residue (orange) are shown.

1.6.2 Hypotheses of the effects of Ax variants

Different hypotheses were proposed to explain the effects of Ax variants on *Drosophila*

wing development. Firstly, studies have shown that the loss of function of E3 ubiquitin ligase Deltex (Dx) can suppress the gain of function phenotypes of some Ax variants and rescue the lethal combinations of Ax variants, suggesting that the way those Ax variants enhance Notch signalling involves Notch ubiquitination and endocytosis (Xu and Artavanis-Tsakonas, 1990; Gorman and Girton, 1992; Busseau *et al.*, 1994; Diederich *et al.*, 1994).

On the other hand, the Ax variants are proposed to reduce Notch cis-inhibition since they have a similar effect as the removal of the ligands Dl and Ser at the D/V boundary in *Drosophila* wings where the ligands cis-inhibit Notch signalling (De Celis and Bray, 2000). While Wg and Cut expression, which is downstream of Notch activation, is only detected in the D/V boundary in WT flies, they are expressed broadly in Ax wing discs, suggesting Notch activation is ectopically upregulated (Celis, Garcia-Bellido and Bray, 1996). Furthermore, reduction of Cut level by ectopic expression of Dl and Ser was significantly mitigated in Ax variants, leading to the hypothesis that when disrupted by amino acid substitutions, the cis-inhibitory function of the Ax region is lost (Heitzler and Simpson, 1993; De Celis and Bray, 2000). In addition, Ax variants N986I (*N* suppressor), C999Y (homozygous lethal) and G1174A (*N* enhancer) were insensitive to the ectopic expression of Fng (see Section 1.2.8.3) which functioned to inhibit Notch signalling at the D/V boundary (De Celis and Bray, 2000). Nonetheless, other studies did not find an effect of C999Y on cis-inhibition or sensitivity to Fng (Pérez *et al.*, 2005; Becam *et al.*, 2010; Fiuza *et al.*, 2010).

An early study in S2 cells showed that the *N* enhancer H1167Y reduced dN's affinity for Dl in cell aggregation assays, suggesting Ax variants may affect receptor-ligand binding (Lieber *et al.*, 1992). Though no direct interaction was detected between the Ax region and ligands (see Section 1.2.6), Sharma et al. (2013) found that hJAG1 and hDLL4 competed with antibodies against hN1 EGF21-30 and EGF25-26 for binding to full-length N1 in flow cytometry (Sharma, Rangarajan and Dighe, 2013). They proposed that the Ax region may be a second ligand-binding site that is only exposed upon the presence of ligands.

In conclusion, current theories suggest that the Ax region may facilitate the binding or positioning of the Notch receptor to ligands, especially when the ligands function in cis to inhibit Notch activation. However, the interpretation of these data is not straightforward with other contradictory studies also published. These data demonstrate that there is a need to understand the molecular properties of the Ax region, how this affects NECD architecture and the ability to form cis-inhibitory and trans-activatory complexes.

1.7 Thesis Aims

Previous functional studies of the NECD mainly focused on regions close to the LBR and the NRR. Early phenotypic studies in *Drosophila* showed an important role of the Ax region in modulating Notch signalling, which suggests a study of this region may yield

important mechanistic insights. In this study, I aim to investigate the molecular basis for the effects of mutations in the Ax region in the mammalian system. The individual result chapters (Chapters 3-7) detailing these studies are:

Chapter 3: Establishment of stable cell lines expressing full-length mN1 carrying mutations homologous to *Drosophila* Ax variants. Investigation of the effects of Ax variants on cell surface Notch level and Notch trans-activation by luciferase complementation-based assays. Investigation of the effects of Ax variants on ligand binding using soluble fragments of ligands.

Chapter 4: Establishment of cis-inhibition assay using cis-JAG1. Assessment of the effect of Ax variants on N1 cis-inhibition by JAG1.

Chapter 5: Establishment of cis-inhibition assay using cis-DLL4. Assessment of the effect of Ax variants on N1 cis-inhibition by DLL4.

Chapter 6: Studying the effects of Lfng expression on trans-activation and cis-inhibition of N1 WT and selected Ax variants in the reporter cell system.

Chapter 7: Purification and SEC-SAXS analysis of hN1 EGF20-27 and EGF20-29 to study the shape of the Ax region

2 Materials and Methods

2.1 DNA manipulation

2.1.1 Polymerase chain reactions (PCR)

KOD Hot-Start Polymerase kit (Merck) was used for PCR following the suggested protocol provided by the manufacturer (Appendix A). Primers (Appendix A), which were designed to have a melting temperature between 60 °C and 65 °C, were ordered from Thermo Fisher Scientific. 10 ng of plasmid DNA, 100 ng of genomic DNA or 5 µl of reverse transcription sample was used as the DNA template in each 50 µl PCR reaction.

2.1.2 DNA gel electrophoresis

Agarose TBE gels were made with TBE buffer (90 mM Tris-HCl, 90 mM Boric acid, 2 mM EDTA), 0.8-2.5% agarose, and 1:10,000 SYBR™ Safe stain (Invitrogen™). DNA samples and DNA ladders (1 kb or 100 bp, NEB) were diluted with 6x Purple Gel Loading Dye (NEB) before adding to wells in gels, which were run at 70-90v for 25-80 minutes in a DNA electrophoresis tank (Bio-Rad) before visualisation by a UV transilluminator (Uvitec) with or without a gel documentation system.

2.1.3 DNA extraction from agarose TBE gel

The band of interest was cut out from agarose TBE gel over a UV transilluminator (Uvitec). DNA extraction was performed with a Qiagen QIAquick Gel Extraction kit following the kit's handbook. DNA was eluted in 30 µl Milli-Q (MQ) water and stored at -20 °C.

2.1.4 Genomic DNA extraction

Genomic DNA was extracted from 5 x 10^6 cultured cells using a Qiagen QIAamp DNA Mini Kit following the kit's handbook. DNA was eluted in 200 µl MQ water and stored at -20 °C.

2.1.5 DNA sequencing

DNA samples were submitted to Source Bioscience PLC for Sanger sequencing following the instructions shown on the Source Bioscience PLC website. Sequencing results were read by SnapGene® Viewer.

2.1.6 DNA concentration determination

DNA concentration was determined by a NanoDrop Lite Spectrophotometer (Thermo Scientific) using the Beer-Lambert law, assuming an absorbance reading of 1.0 at a wavelength of 260 nm (A260) is equivalent to ~50 µg/ml double-stranded DNA. DNA samples with an A260nm/A280nm ratio over 1.80, which suggests good DNA purity, were used.

2.2 Cloning

2.2.1 Cloning strategy for mN1 variants

To generate mN1 variants, overlap extension PCR mutagenesis was performed using a cDNA fragment from 521 bp to 4131 bp of the full-length mN1 (Figure 2.1). The mN1

cDNA fragments carrying the mutations were restriction digested and ligated into a pUC19 vector, which is relatively small (6.3 kbp including mN1 insert), for ease of ligation. The ligation mixtures were transformed into Competent *E. coli* for the selection, amplification and preparation of successfully constructed plasmids. After sequencing the entire mN1 fragment inserted to ensure the sequence was correct, the mN1 fragment carrying the Ax variant was restriction digested from the pUC19 plasmid and ligated into a pcDNA5/FRT plasmid containing the rest of the mN1 sequence and NLuc (Figure 2.2). The constructed pcDNA5/FRT plasmid (12.6 kbp) will encode a full-length mN1 carrying the designed mutation. The pcDNA5/FRT-mN1 variant plasmids were sequenced before transfected into HEK-RBP cells to generate cell lines stably expressing mN1 variants.

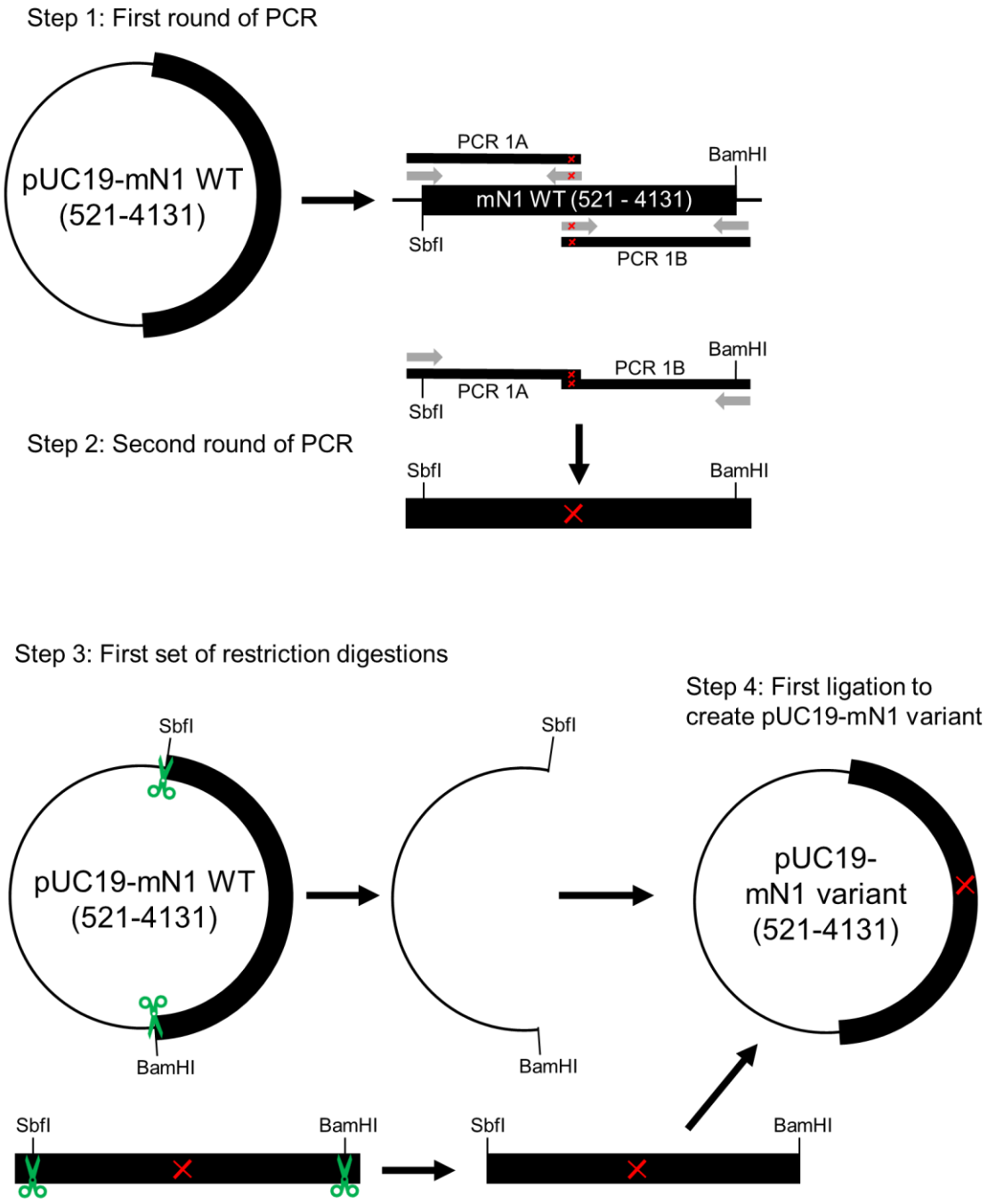


Figure 2.1. Cloning for pUC-19 mN1 (512-4131) plasmid.

An overview of the cloning process taken to produce pUC19 plasmid carrying mN1 variant used for stable cell line transfection. Overlap extension mutagenesis was employed to create mN1 fragment with required variation through two rounds of PCR reactions (Step 1 and 2). The mN1 fragment was digested with SbfI and BamHI (Step 3) and ligated into a pUC19 vector (Step 4). Vector backbone is shown as black thin line. mN1 from amino acid 521 to 4131 is shown as black thick line. Primers are shown as grey arrows. Substitution is shown as red cross. Restriction enzyme sites (SbfI and BamHI) are indicated with restriction enzymes shown as green scissors.

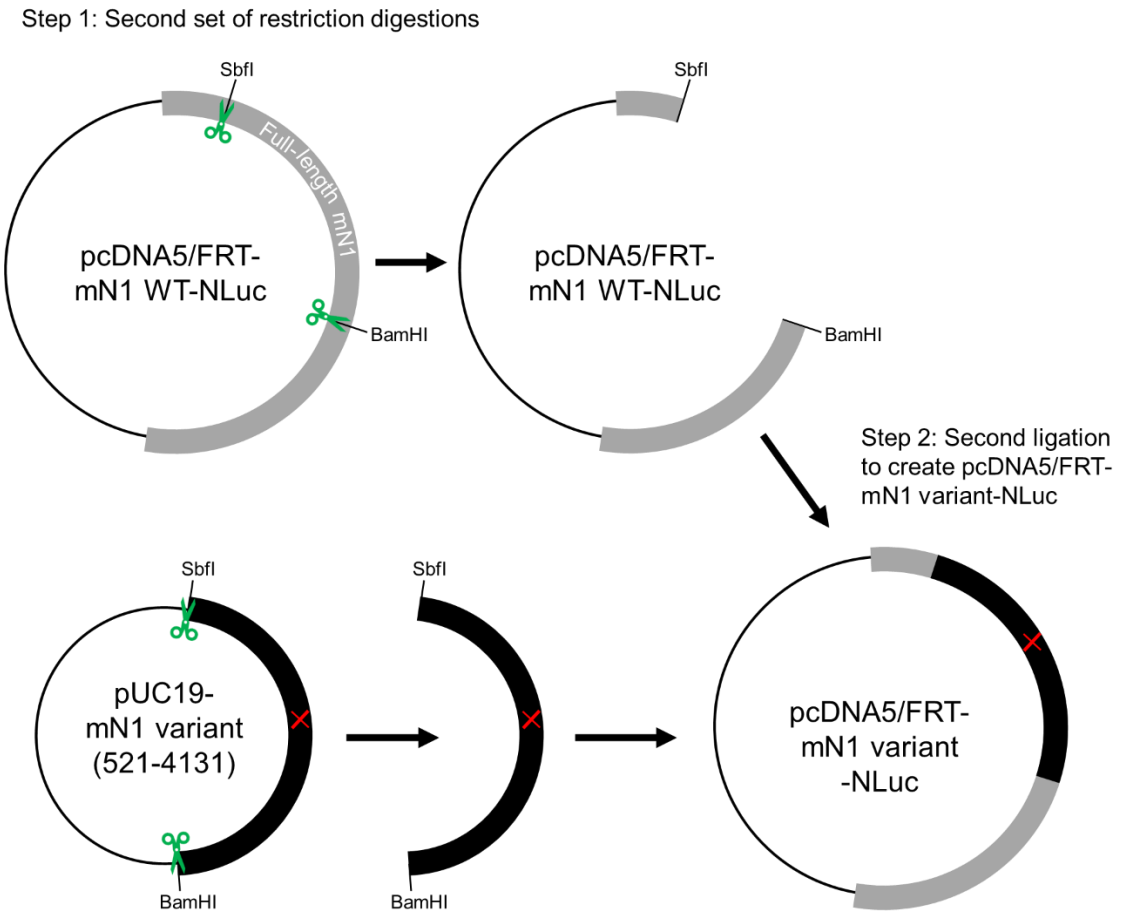


Figure 2.2. Cloning for pcDNA5/FRT-mN1-NLuc plasmid.

pUC19-mN1 variant plasmid and pcDNA5/FRT-mN1-NLuc plasmid were digested with SbfI and BamHI (Step 1). The pcDNA5/FRT vector and the mN1 variant (521-4131) fragment from the pUC19 plasmid were ligated (Step 2). The successfully constructed pcDNA5/FRT plasmid encoded a full-length mN1 carrying the substitution. The pcDNA5/FRT-mN1 variant-NLuc plasmid was then used to transfect HEK RBP cells to generate cell lines stably expressing mN1 variant-NLuc. Vector backbone is shown as black thin line. mN1 from amino acid 512 to 4131 is shown as black thick line. Substitution is shown as red cross. Restriction enzyme sites (SbfI and BamHI) are indicated with restriction enzymes shown as green scissors.

2.2.2 Mutagenesis by Overlap Extension

Overlap extension mutagenesis involving two rounds of PCRs was employed to create mN1 variants using the pUC19-mN1 WT (521-4131) plasmid (Figure 2.1). Firstly, The

left and right arms were produced by two PCRs each using one mutagenesis primer containing the substitution at their 3' ends and one backbone primer containing the recognition site of restriction enzyme SbfI for left arm PCR and BamHI for right arm PCR at their 5' ends. The second round of PCR, using the left and right arms as templates and backbone primers, created the whole mN1 521-4131 sequence with SbfI recognition site at the 5' end and BamHI recognition site at the 3' end.

2.2.3 Restriction enzyme digestion

Restriction mixture (0.5 – 1 µg DNA, 0.7 µl of each restriction enzyme (Table 2.1), 1x NEB CutSmart Buffer, made up to 35 µl by MQ water) were incubated at 37 °C for one hour and run on an agarose gel to visualise and extract DNA bands representing the inserts and vectors.

Table 2.1. List of restriction enzymes (NEB).

Usage	Upstream restriction enzyme	Downstream restriction enzyme
Mutagenesis for mN1 LBR, EGF16 and Ax variants	SbfI-HF	BamHI-HF
Creation of pcDNA3.1(+)- full-length hDLL4	EcoRI-HF	NotI-HF

2.2.4 DNA ligation

Restriction-digested insert DNA and vector were ligated together using a Roche Rapid DNA Ligation Kit (Merck) following the manufacturer's suggested protocol. The molar ratio of vector DNA to insert DNA is 1:3. A negative control ligation with MQ water instead of insert DNA was performed alongside. Ligation mixture was incubated at room temperature for one hour and subsequently stored at -20 °C in long term.

2.3 Plasmid amplification

2.3.1 Transformation of competent *E. coli*

1 µl purified plasmid or 2.5 µl ligation mixture for PUC19, pcDNA5/FRT, pOG44, pcDNA3.1(+), pHLsec, and pEXS2.2 plasmids were transformed into 50 µl NEB® 5-alpha Competent *E. coli* (NEB) following the supplier's protocol (Appendix B). 5 µl purified pAPtag2 plasmids were transformed into 100 µl MC1061 P3 Competent *E. coli* (DSMZ, DSM 7123) following the protocol shown in Appendix B. Transformed cells were plated on a sterile 2xYT (MP Biomedicals) 1.5% agar plate containing suitable selective antibiotics (Appendix B) and incubated overnight at 37 °C to select successfully transformed colonies. Transformation and plate selection were also performed for negative control ligation mixtures. Colonies were expanded in antibiotic-containing 2xYT medium at 37 °C, 150 rpm for 16 hours before plasmid extraction.

2.3.2 Plasmid purification

100 ml and 200 ml of *E. coli* expansion culture were processed with Qiagen Plasmid Midiprep kit and Maxiprep kit respectively following the supplier's protocol. DNA pellets were resuspended in 400 µl (Midiprep) or 1 ml (Maxiprep) MQ water. Purified plasmid stocks were sequenced and stored at -20 °C.

2.4 Reverse transcription polymerase chain reaction (RT-PCR)

2.4.1 RNA extraction

RNA was extracted using the RNeasy mini kit following the kit protocol. 1 – 3 x 10^6 cells were lysed in 350 µl Buffer RLT containing 1% V/V β-mercaptoethanol. The lysates were homogenised using the Qiagen QIAshredder column and directly processed with subsequent RNA extraction steps. One round of on-column DNase digestion was performed with the Qiagen RNase-free DNase set for stable cell lines. Two rounds of on-column DNase digestion were performed for transiently transfected cell lines. RNAs were eluted in 50 µl RNase-free water.

2.4.2 RNA concentration determination

RNA concentration was determined by a NanoDrop Lite Spectrophotometer using the Beer-Lambert law, assuming an A260 reading of 1.0 is equivalent to ~40 µg/ml single-stranded RNA. RNA samples with an A260nm/A280nm ratio between 2.00 and 2.10, which suggests good RNA purity, were used.

2.4.3 Reverse transcription

Reverse transcription (RT) was performed with the Qiagen Omniscript RT kit with each reaction (20 µl) prepared on ice following the kit protocol and recipe (Table 2.2). RT reactions were incubated at 37 °C for 1 hour, and stored on ice temporarily or at -20 °C in the long term.

Table 2.2. Recipe for RT reaction.

Component	Per 20 µl reaction (µl)
10x Buffer RT	2
dNTP Mix (5 mM each dNTP)	2
Oligo-dT primers (Qiagen #79237)	2
10 units/µl Recombinant RNasin™ Ribonuclease Inhibitor (Promega #N251A)	1
0.25 µg/ul Template RNA	8 (total 2 µg)
Omniscript Reverse Transcriptase	1
RNase-free water	4

2.4.4 cDNA PCR

cDNA PCRs were performed using the KOD Hot-Start Polymerase kit (Merck) (see Section 2.1.1) with 2.5 µl of RT reaction used per 25 µl PCR reaction. To check if the extracted RNA samples had DNA contamination, control PCRs were performed with 2.5 µl of 0.1 µg/µl purified RNA samples per 25 µl PCR reaction. The PCR products were visualised by gel electrophoresis (see Section 2.1.2).

2.5 Cell culture

2.5.1 General methods

Freshly thawed cells were recognised as of passage one. Cell line passage number increased by one after each round of sub-culturing. For every cell line, cells between passage four and passage 20 (B16 cells) or 30 (HEK293T, HEK-RBP, CHO-K1, HEK293F, S2) were used for assays, transfection and protein production. Cell culture works were conducted in a laminar flow sterile hood using sterilised equipment. Bright-line™ hemacytometer (Sigma) was used for cell density determination. Cell cultures with

over 90% viability were used for assays and transfections.

2.5.2 Adherent cell lines

2.5.2.1 Adherent cell line maintenance

HEK293T and CHO-K1 cells were maintained in Dulbecco's modified Eagle's Medium (DMEM, Gibco) supplemented with 10% fetal bovine serum (FBS, Gibco), 50 U/ml penicillin and 0.05 mg/ml streptomycin (Sigma), and 2 mM L-glutamine (Gibco) (DMEM complete). Flp-In TRex 293 CLuc-RBPJκ cells (HEK-RBP) were maintained in DMEM complete with 0.2 µg/ml puromycin (Gibco). Flp-In TRex 293 CLuc-RBPJκ cells stably transfected to express mN1 (HEK-RBP mN1) were maintained in DMEM complete with 0.2 µg/ml puromycin (Gibco) and 100 µg/ml hygromycin (Sigma). CHO-K1 cells stably transfected to express hDLL1 were maintained in DMEM complete with 0.5 mg/ml geneticin (Gibco). B16 (WT, mJag1, mDll4) mouse melanoma cells were maintained in RPMI 1640 medium (Gibco) supplemented with 10% FBS (Gibco), 50 U/ml penicillin and 0.05 mg/ml streptomycin (Sigma), and 2 mM L-glutamine (Gibco) (RPMI complete). Adherent cell lines were grown in a 37 °C humidified incubator with 5% CO_2 in 25 cm^2, 75 cm^2, or 175 cm^2 tissue culture flasks (Greiner or Sarstedt) with 5 ml, 15 ml, or 25 ml medium per flask, or 12-well or 6-well cell culture plates (Corning or Costar) with 1 ml or 2.5 ml medium per well. Culture medium was changed every 3-4 days if no sub-culturing was required.

2.5.2.2 Adherent cell line sub-culturing

When cells reached ~90% confluency, culture medium was aspirated and cells were gently washed with ~0.05 ml/cm^2 phosphate buffer saline with 1 mM EDTA (PBS-EDTA), which was then aspirated. Cells were then incubated with 0.05 ml/6-well, 0.1 ml/6-well, 0.3 ml/25 cm^2, 1 ml/75 cm^2, or 2ml/175 cm^2 of 0.33 g/l trypsin (Sigma) diluted in PBS-EDTA (trypsin-PBS) in the 37 °C incubator for 2 minutes (HEK293T and HEK-RBP) or 5 minutes (CHO-K1). B16 cells were incubated with a double volume of trypsin-PBS for 5 minutes in the incubator. Cells were resuspended in fresh culture medium of over 5 times the volume of trypsin-PBS previously added. An appropriate amount of this cell culture was added to a new cell culture flask with fresh culture medium and gently mixed before incubating in the incubator. In general, HEK293T cells were split 1:10 every 3-4 days. HEK-RBP cells were split 1:10 every 6-7 days. CHO-K1 and B16 cells were split 1:20 every 3-4 days. For protein production (see Section 2.6), Notch activation assays (see Section 2.9) and ligand binding assay (see Section 2.11), after trypsinisation and resuspension in medium, cells were centrifuged at 1000 rpm for 3 minutes. The cell pellet was resuspended in fresh medium before splitting into new containers.

2.5.2.3 Adherent cell line freezing and thawing

To prepare long-term frozen cell line storage, when reached ~90% confluency, cells were washed, trypsinised and resuspended in fresh culture medium. Cell culture was centrifuged at 1000 rpm for 3 minutes. The cell pellet was resuspended in ice-cold freshly

made freezing medium containing 90% FBS and 10% DMSO (Sigma). 1 ml freezing medium was used per 25 cm^2 of cells. 1 ml cell suspension was aliquoted into each cryotube and frozen in a cryofeezer (Corning) overnight at -80 °C. The cryotubes were subsequently transferred to liquid nitrogen for long-term storage.

Cryotubes from liquid nitrogen were temporarily stored on dry ice before defreezed in a 37 °C water bath. The cell culture inside each cryotube was mixed with 9 ml of fresh culture medium and centrifuged at 1000 rpm for 3 minutes. The cell pellet was resuspended in fresh culture medium and grown in a 75 cm^2 flask overnight in the incubator to allow cell attachment. The culture medium was replaced with fresh medium on the next day.

2.5.3 HEK293F cell line

2.5.3.1 HEK293F maintenance and sub-culturing

HEK293F cells were maintained in 40 ml or 80 ml FreeStyle™ 293 Expression Medium (Thermo Fisher Scientific) per 125 ml or 250 ml polycarbonate Erlenmeyer flask with vented cap (Corning) in a 37 °C incubator with 8% CO_2, rotating at 135 rpm. HEK293F cells were counted and directly split into a new flask with fresh medium every 3 to 4 days to a cell density of 0.1-0.2 x 10^6 cells/ml.

2.5.3.2 HEK293F freezing and thawing

HEK293F cell culture with a cell density between 0.5-1 x 10^6 viable cells/ml was counted and centrifuged at 100 xg for 5 minutes. The cell pellet was resuspended in a freezing medium of 90% FreeStyle™ 293 Expression Medium and 10% DMSO to a final density of 1 x 10^7 cells/ml. 1 ml cell suspension was aliquoted into each cryotube and frozen in a cryofeezer (Corning) overnight at -80 °C. The cryotubes were subsequently transferred to liquid nitrogen for long-term storage.

Cryotubes from liquid nitrogen were temporarily stored on dry ice before defreezed in a 37 °C water bath. The cell culture inside each cryotube was added into a 125 ml Erlenmeyer flask with 40 ml fresh medium. After being grown overnight in a 37 °C incubator with 8% CO_2, rotating at 135 rpm, cell viability was checked and culture with over 70% viability was maintained for future usage.

2.5.4 S2 cell line

2.5.4.1 S2 maintenance and sub-culturing

S2 cells (Expres2ion Biotechnologies) were maintained in 25 ml, 50 ml or 500 ml EX-CELL 420 Serum-Free Medium (Sigma) per 125 ml, 250 ml or 2l polycarbonate Erlenmeyer flask with vented cap (Corning) in a 25 °C incubator rotating at 100 rpm. S2 cells were counted and directly split into a new flask with fresh medium every 3 to 4 days to a cell density of 8 x 10^6 cells/ml. S2 hN1 EGF20-27 cell line was maintained by Dr

Hilman Nurmahdi (University of Oxford).

2.5.4.2 S2 freezing and thawing

S2 cells were split into 5 x 10^6 cells/ml in EX-CELL 420 Serum-Free Medium supplemented with 10% FBS (EX-CELL 420 + FBS) and allowed to grow for two days. Cells were counted and centrifuged at 125 xg for 3 minutes. The cell pellet was resuspended in a freezing medium of 40% EX-CELL 420 Serum-Free Medium, 50% FBS and 10% DMSO to a final density of 40-250 x 10^6 cells/ml. 1 ml cell suspension was aliquoted into each cryotube and frozen in a cryofeezer (Corning) overnight at -80 °C. The cryotubes were subsequently transferred to liquid nitrogen for long-term storage.

Cryotubes from liquid nitrogen were temporarily stored on dry ice before defreezed in a 25 °C water bath. The cell culture inside each cryotube was added into a 125 ml Erlenmeyer flask with 25 ml EX-CELL 420 + FBS. After being grown for 1 to 2 days in a 25 °C incubator rotating at 100 rpm, cells were counted and collected by centrifugation at 330 xg for 5 minutes and resuspended in 25 ml EX-CELL 420 + FBS to 5 x 10^6 cells/ml. Cells were grown for another 2 passages in EX-CELL 420 + FBS during which cells were split every 3 to 4 days to a cell density of 5 x 10^6 cells/ml. FBS was removed from the medium afterwards.

2.6 Protein production

2.6.1 Large-scale transfection for protein purification

2.6.1.1 Large-scale transfection of HEK293T

HEK293T cells in 90% confluent 75 cm^2 flasks were split 1:5 in DMEM complete into two 875 cm^2 5-layer cell culture flasks (Falcon) and a 175 cm^2 flask, which was used to check cell confluency. Cells were transfected when reaching 80-90% confluency. Transfection mixture (500 µg pHLsec-hJAG1 NE3-Fc-His plasmid, 1 mg polyethylenimine, made up to 50 ml by DMEM with no additives) was prepared in a Falcon tube and mixed by inverting the tube and incubated at room temperature for 20 minutes. Old medium in the 5-layer flasks was replaced with 100 ml fresh DMEM without additives per flask. 25 ml transfection mixture was added to each 5-layer flask and gently mixed with the fresh DMEM inside the flask. Medium was collected for protein purification after around 90 hours of incubation.

2.6.1.2 Large-scale transfection of HEK293F

HEK293F cells were split into two 250 ml Erlenmeyer flasks 24 hours before transfection to 0.6–0.7 x 10^6 cells/ml. Before transfection, cells were split to have 1 x 10^6 cells/ml in 80 ml per 250 ml Erlenmeyer flask. 224 µg sterile-filtered pcDNA3.1(+)-hDLL4 NE3-Fc-His plasmid was diluted in OptiPro™ SFM (Gibco) to a total volume of 3.2 ml in a 15 ml Falcon tube. 224 µl of FreeStyle™ MAX Transfection Reagent (Gibco) was diluted in

OptiPro™ SFM in another 15 ml Falcon tube. To prepare the transfection mixture, the two solutions were mixed gently followed by incubation at room temperature for 10 minutes. 3.2 ml of transfection mixture was added to each flask dropwise while slowly swirling the flask. Medium was collected for protein purification after 4 days of incubation.

2.6.2 HEK-RBP mN1 stable cell line generation

2.6.2.1 HEK-RBP mN1 cell line

HEK-RBP cells were used to create cell lines stably expressing mN1-NLuc. The genome of the Flp-In cell has a single FRT site. HEK-RBP cells were transfected simultaneously with a pOG44 plasmid encoding the Flp recombinase and a pcDNA5/FRT plasmid encoding an FRT site, mN1-NLuc downstream of a CMV promoter, and a hygromycin resistance gene (Figure 2.3). The Flp recombinase encoded by the pOG44 plasmid catalysed the homologous recombination between the host cell's and the pcDNA5/FRT plasmid's FRT sites, so the construct in the pcDNA5/FRT plasmid could be integrated into the cell's genome at the FRT site. Successfully transfected cells were resistant to hygromycin as the inserted hygromycin resistance gene is downstream of an SV40 promoter in the host cell genome. Transfected cells were selected and maintained in the cell medium containing puromycin (0.2 µg/ml), for stable expression of CLuc-RBPJκ, and hygromycin (100 µg/ml), for stable expression of mN1-NLuc. HEK-RBP cells, POG44 plasmid, and pcDNA5/FRT-mN1 WT-NLuc plasmid were a kind gift from Kopan lab, University of Cincinnati College of Medicine.

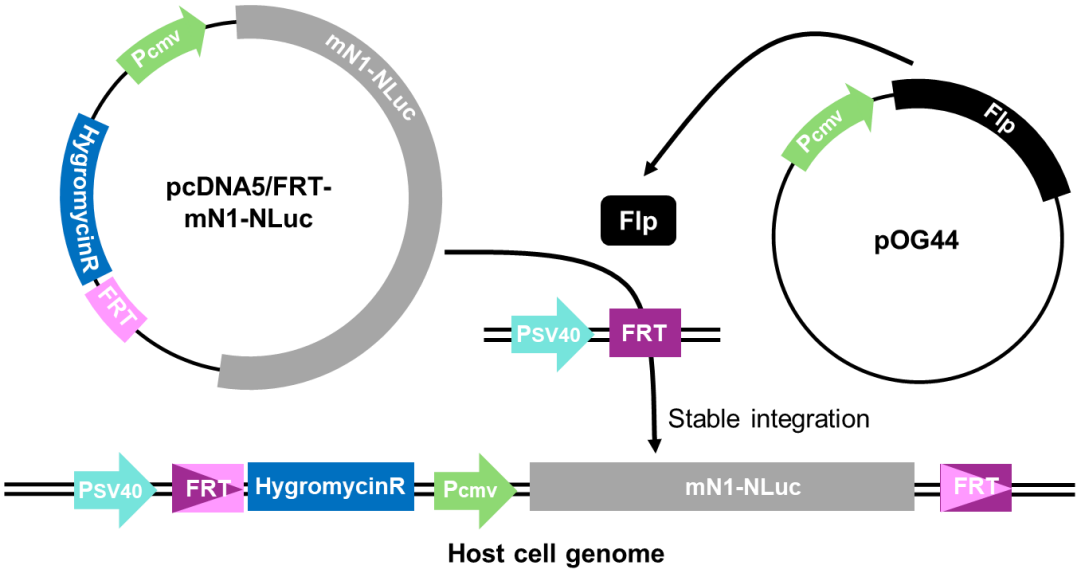


Figure 2.3. mN1 was inserted in the FRT site encoded by the HEK-RBP cell line.

The Flp recombinase encoded by the pOG44 plasmid catalyses the homologous recombination between the host cell's and the pcDNA5/FRT plasmid's FRT sites, so the construct in the pcDNA5/FRT plasmid can be integrated into the cell's genome at the FRT site. Successfully transfected cells were resistant to hygromycin as the inserted hygromycin resistance gene is downstream of an SV40 promoter in the host cell genome. The mN1-NLuc inserted into the host cell genome is downstream of the CMV promoter, which is encoded in the pcDNA5/FRT plasmid.

2.6.2.2 HEK-RBP transfection

HEK-RBP cells were transfected using Mirus TransIT-293 transfection reagent following the supplier's recommended protocol. HEK-RBP cells were split in 2.5 ml DMEM complete to each well of a 6-well plate 18-24 hours before transfection to have 70-80% confluency at the time of transfection. 900 ng of pOG44 plasmid and 100 ng pcDNA5/FRT mN1-NLuc plasmid were mixed with 250 µl of Opti-MEM I Reduced-Serum Medium (Gibco) and 7.5 µl of Mirus TransIT-293 transfection reagent and incubated at

room temperature for 20 minutes. The transfection mixture was then added dropwise to different areas of a well. The 6-well plate is then rocked gently to distribute the transfection mixture evenly and incubated at 37 °C for 24 hours.

2.6.2.3 HEK-RBP mN1 selection and maintenance

Post 24-hour incubation with transfection mixture, cells from each well were transferred to a 15 cm cell culture dish in 20 ml DMEM complete to allow cell attachment. On the next day, the culture medium was replaced with 20 ml DMEM complete with selection antibiotics (0.2 µg/ml puromycin and 100 µg/ml hygromycin). A well of untransfected cells was also transferred to 15 cm dishes at the same time and grown with antibiotics to check for efficient antibiotic selection. Cells were grown with selection antibiotics for around 3 weeks until the establishment of resistant colonies, with medium changing every 3 – 4 days. Single colonies were transferred to a 6-well plate and expanded for further investigation.

2.6.3 HEK cells transient transfection

HEK-RBP mN1 and HEK293T cells were transiently transfected in the same procedure as HEK-RBP cells (see Section 2.6.2.2). HEK-RBP mN1 cells were transfected with 4 µg of pcDNA3.1(+)-hJAG1 or 2.5 µg of pcDNA3.1(+)-hDLL4 or 2 µg of pcDNA3.1(+)-hJAG1 plus 2µg of pAPtag2 plasmid DNA per well. HEK293T cells were transfected with 4 µg of pcDNA3.1(+) plasmid DNA and 12 µl of Mirus TransIT-293 reagent per well. Cells

were used in assays immediately after 24 hours of incubation with transfection mixture.

2.6.4 S2 stable cell line generation

2.6.4.1 S2 cell transfection

One day before transfection, S2 cells were centrifuged at 450 xg for 3 minutes and resuspended in EX-CELL 420 + FBS to a density of 5 x 10^6 cells/ml. Before transfection, cells were centrifuged and resuspended in EX-CELL 420 to a density of 2 x 10^6 cells/ml. 5 ml of cell culture was transferred to a 25 cm^2 flask. 50 µl of ExpreS^2 Insect-TR 5x were added to the culture and mixed by gently swirling the flask. Subsequently, 12.5 µg pEXS2-2 plasmid was added to the culture and mixed by gentle swirling. The cells were then incubated at 25 °C on top of an empty 75 cm^2 flask for 2 – 4 hours, after which 1 ml of FBS was added to the culture.

2.6.4.2 S2 hN1 cell selection and maintenance

Geneticin was added to the culture at a concentration of 4 mg/ml one day after transfection. After 2 days, 3 ml cell culture was replaced with fresh EX-CELL 420 + FBS with 4 mg/ml geneticin. 3 ml of cell culture was replaced with 3 ml of fresh EX-CELL 420 + FBS with geneticin every 3 - 4 days for two weeks, after which the culture was expanded to a 75 cm^2 flask with 4 ml of fresh EX-CELL 420 + FBS with geneticin. 5 ml of fresh EX-CELL 420 + FBS with geneticin was added to the flask once the cells recovered. After 26 days of selection, 15 ml of resuspended cell culture was transferred

to a 125 ml Erlenmeyer flask with 10 ml EX-CELL 420 + FBS without geneticin and grown in 25 °C incubator rotating at 100 rpm. Cells were further expanded for protein production and frozen for long-term storage. Selection was also performed for untransfected cells alongside transfected cells to check selection efficiency.

2.7 Protein purification

2.7.1 Protein purification process

Ligand N terminus to EGF3 (NE3) fragments with C-terminal Fc and His-tag produced by transient transfection of HEK293T or HEK293F cells (see Section 2.6.1) and hN1 EGF20-27 and EGF20-29 fragments with C-terminal BirA and His-tag produced by stably transfected S2 cells (see Section 2.6.4) were purified as previously described (Chillakuri *et al.*, 2013; Suckling *et al.*, 2017) (Figure 2.4). Buffers used in protein purification are shown in Appendix C.

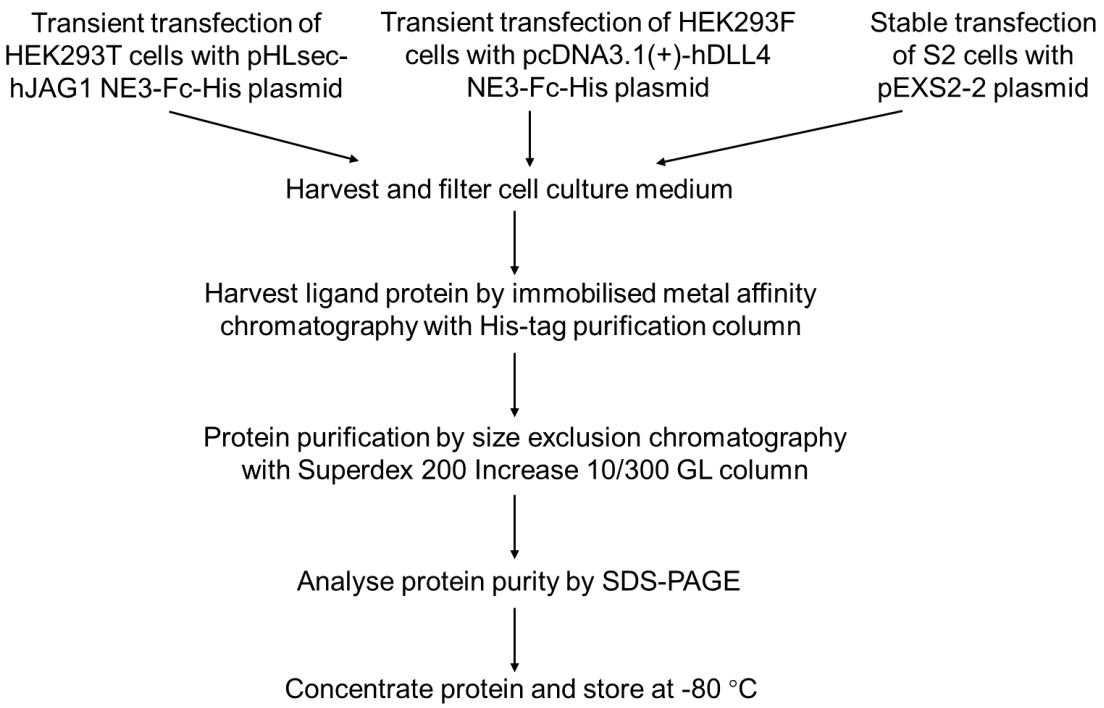


Figure 2.4. Protein purification process.

Cell culture medium post-transfection of HEK293 cells or from stably transfected S2 cells was filtered and processed by IMAC with His-tag purification column. His-tagged proteins attached to the column were eluted from the column and further purified by SEC with Superdex 200 Increase 10/300 GL column. Protein-containing fragments were then analysed by reducing and non-reducing SDS-PAGE. Fragments containing protein with correct molecular weight (MW) and high homogeneity were combined and concentrated for long-term storage at -80 °C.

2.7.2 Cell medium collection

To collect secreted protein fragments, cell medium of transiently transfected HEK293T (~250 ml, see Section 2.6.1.1), HEK293F (~160 ml, see Section 2.6.1.2) and stably transfected S2 cells after 4 days of incubation in EX-CELL 420 Serum-Free Medium (~ 1L) were collected and centrifuged at 4 °C, at 4400 rpm for 10 minutes (HEK293T), 3500 rpm for 10 minutes (HEK293F), or 4400 xg for 20 minutes (S2). The supernatant was collected and filtered with a 0.2 μm bottle-top filter (Nalgene). HEK293T's supernatant was mixed with 3 times volumes of 4 °C Tris gel filtration buffer (pH 9.0) (Appendix C).

HEK293F's supernatant was mixed with 2 times volumes of 4 °C MES gel filtration buffer (pH 6.5) (Appendix C). S2's supernatant was used directly for subsequent purification steps. Supernatants were stored at 4 °C.

2.7.3 Immobilised metal affinity chromatography (IMAC)

IMAC was performed at 4 °C using buffers and water filtered with 0.22 µm bottle-top filters. 1 ml His-tag purification column (Roche) connected to a peristaltic P-1 pump (Cytiva) was equilibrated with 15 ml Tris gel filtration buffer (pH 9.0) for HEK293T- and S2-produced protein, or MES gel filtration buffer (pH 6.5) for HEK293F-produced protein. Filtered supernatant was run through the purification column at 1–0.5 ml/minute. Subsequently, the purification column was washed with 50 ml wash buffer (Appendix C). Proteins were eluted from the purification column with 20 ml elution buffer (Appendix C) and concentrated to around 1 ml for HEK293T- and HEK293F-produced proteins and 2.5 ml for S2-produced protein using a 10000 MW protein concentrator spin column (Vivaspin) by centrifugation at 3000 xg at 4 °C. Concentrated eluates were stored on ice. After elution, the column was washed with MQ water and 20% ethanol and stored at 4 °C. Different columns were used for each protein.

2.7.4 Size exclusion chromatography (SEC)

SEC was performed at room temperature with AKTA Pure 25 L1 system (Cytiva) using buffers and water filtered with 0.22 µm bottle-top filters. A Superdex 200 Increase 10/300 GL column (Cytiva) was washed with MQ water and equilibrated with SEC gel filtration

buffer (Appendix C). 0.3–0.6 ml concentrated IMAC eluate was injected and ran through the column at 0.7 ml/minute. Fractions with a UV detection over 1 mAU were collected and analysed by SDS-PAGE. Fractions containing the target proteins were frozen in liquid nitrogen and stored at -80 °C. After SEC, the column was washed with MQ water and 20% ethanol and stored at room temperature.

2.7.5 His tag removal by HRV 3C protease

To remove the His-BirA tag at the C terminus after the HRV 3C protease recognition sequence in S2-produced proteins, 0.5 units of N-terminal His-tagged HRV 3C protease (Sigma) were mixed with each nanomole of substrate peptide and incubated at 4 °C overnight. Ni-NTA agarose (Qiagen) was centrifuged at 2000 rpm for 2 minutes and equilibrated by resuspending in SEC gel filtration buffer at least 2 times the original volume of the aliquoted agarose. Protease-protein mixture was mixed with 100 µl original volume of agarose per mg protein at 4°C for one hour on a rotary shaker. The supernatant containing the cleaved S2 protein construct was collected by centrifuging the agarose mixture at 2000 rpm for 2 minutes. The protein sample was further concentrated and purified by SEC.

2.8 Protein analysis

2.8.1 Protein Concentration Determination

Protein concentration was calculated using the A280 reading of a NanoDrop Lite

Spectrophotometer following the equation:

$$Protein\ concentration = \frac{A280\ absorbance}{Extinction\ coefficient\ (\epsilon)} \times Molecular\ weight\ (MW)$$

The theoretical extinction coefficient (ϵ) and molecular weight (MW) for each protein construct were calculated by the Expasy ProtParam tool (Gasteiger *et al.*, 2005).

2.8.2 Sodium dodecyl sulfate-polyacrylamide gel electrophoresis (SDS-PAGE)

SDS-PAGE gels were prepared in a 1.5 mm gel casting system (Bio-Rad). The stacking gel (Appendix D) was cast on top of the resolving gel (Appendix D). Solidified gels were used immediately or stored in running buffer (Appendix D) at 4 °C for usage within 1 months. Protein samples were mixed with a suitable volume of loading dye (Appendix D) with or without 5% V/V β-mercaptoethanol and heated at 100 °C for 10 minutes. Samples were cooled to room temperature before being loaded onto the SDS-PAGE. Gels were run at 150-175V in running buffer until the dye front reached the end of the gel.

2.8.3 Coomassie staining

SDS-PAGE gels were washed and stained with SimplyBlue SafeStain (Thermo Fisher Scientific) following the manufacturer's recommended protocol on a rocking or orbital shaker. Gels were imaged with a scanner (Canon LiDE).

2.8.4 Western blot

The protein in the acrylamide gel obtained after SDS-PAGE was transferred onto a nitrocellulose membrane (Amersham) by running in a Mini Trans-Blot Cell (Bio-Rad) in prechilled blotting buffer (Appendix D) at 100V for 90 minutes on ice. The nitrocellulose membrane was blocked in PBST (Appendix D) with 5% W/V skimmed milk powder (blocking buffer) for one hour at room temperature on a rocking shaker or overnight at 4°C and incubated in blocking buffer with 1:2000 V/V HRP Anti-6X His tag antibody (Abcam #ab1187) for one hour at room temperature on a roller mixer. The membrane was then washed in PBST on a rocking shaker three times each for 5 minutes and incubated in ECL Western Blotting Detection Reagents (Amersham) for 1 minute. After removing excess reagents, the membrane was sealed in cling film, stored in light-tight film cassette and exposed to chemiluminescent films (Amersham) in a dark room. The films were processed by OPTIMAX 2010 X-Ray Film Processor (PROTEC X-ray technology).

2.9 Notch activation assays

2.9.1 Ligand-independent activation assay

HEK-RBP mN1 cells to be assayed were split 1:3 into DMEM complete. After two days, 40,000 cells to be assayed were added to each well of a 96-well Costar black clear bottom plate in 200 µl DMEM complete. 48 hours later, wells were washed with 200 µl HBS buffer (20 mM HEPES, 150 mM NaCl, 0.9 mM $CaCl_2$, pH7.4, autoclaved), and 100 µl HBS with 150 µg/ml D-luciferin potassium salt (Life Technologies)) and 10 mM

ethylene glycol-bis(β-aminoethyl ether)-N,N,N′,N′-tetraacetic acid (EGTA) (Sigma) was added to each well with pipetting to resuspend cells. Control wells had the same solution without EGTA. Luciferase activity was monitored using a PHERAstar FS plate reader (BMG LABTECH) at 40 mins after the addition of EGTA for monitoring luminescence for 10 seconds per well.

2.9.2 Ligand-dependent activation assay

2.9.2.1 Plate-based trans-activation assay

HEK-RBP mN1 cells to be assayed were split 1:3 into DMEM complete. The following day, a 96-well Costar black clear bottom was coated with 50 µl of 10 µg/ml hJAG1 or hDLL4 NE3-Fc-His protein in HBS buffer and incubated overnight at 4 °C. Control wells were incubated without protein. The following day, wells were washed with 200 µl/well HBS buffer, and 40,000 cells to be assayed were added to each well in 200 µl DMEM complete. After 24 hours, each well was washed with 200 µl HBS buffer, and 100 µl substrate solution (1 mg/ml $MgCl_2$, 0.1% W/V D-glucose, 150 µg/ml D-luciferin potassium salt (Life Technologies) in HES buffer) per well was added with pipetting to resuspend cells. Luciferase activity was monitored using a PHERAstar FS plate reader for monitoring luminescence for 5 seconds per well.

2.9.2.2 Co-culture-based trans-activation assay

HEK-RBP mN1 cells to be assayed were split 1:3 into DMEM complete. B16 cells to be

assayed were split 1:15 or 20 into RPMI complete. CHO-K1 cells to be assayed were split 1:15 into DMEM complete. Two days later, 40,000 HEK-RBP cells to be assayed were added to each well of a white 96-well Nunc MicroWell plate in 125 µl DMEM complete. The following day, 40,000 B16 cells or CHO-K1 cells in 125 µl DMEM complete were added gently to each well of the MicroWell plate. 24 hours later, each well was washed with 200 µl HBS and 100 µl substrate solution was added. Luciferase activity was monitored using a PHERAstar FS plate reader for monitoring luminescence for 2 seconds per well.

2.9.3 Cis-inhibition assay

HEK-RBP mN1 cells to be assayed were split to have 12.5 x 10^5 cells in 2.5 ml DMEM complete per well in a 6-well plate. B16 cells to be assayed were split 1:15 or 20 into RPMI complete. CHO-K1 cells to be assayed were split 1:15 into DMEM complete. The following day, HEK-RBP mN1 cells were transfected with pcDNA3.1(+) empty vector or pcDNA3.1(+)-full-length hJAG1 or hDLL4 (see Section 2.6.3). On the next day, 40,000 (for JAG1 cis-inhibition) or 10,000 (for DLL4 cis-inhibition) transfected HEK-RBP cells to be assayed were added to each well of a white 96-well Nunc MicroWell plate in 125 µl DMEM complete. The following day, 40,000 B16 cells or CHO-K1 cells in 125 µl DMEM complete were added to each well of the plate. 24 hours later, each well was washed with 200 µl HBS, and 100 µl substrate solution was added. Luciferase activity was monitored using a PHERAstar FS plate reader for monitoring luminescence for 2 seconds per well.

2.10 Cell surface protein staining

All staining steps were performed with prechilled buffer solutions on ice or at 4°C. For each sample, 5–10 x 10^5 cells to be assayed were harvested in a microcentrifuge tube and washed 2 times by repeating centrifuging at 2500-3000 rpm for 5 minutes and resuspending in 400 µl with FACS buffer (0.1% W/V NaN_3, 2% V/V FBS in PBS, 0.22 µm filtered). For JAG1 staining, cells were resuspended in 100 µl FACS buffer with 10 µg/ml anti-JAG1 (J1-65D) antibody (Masiero *et al.*, 2019) and incubated for 1 hour. Cells were then washed 2 times with FACS buffer and incubated for 1 hour in the dark in 200 µl FACS buffer with 1:500 V/V phycoerythrin (PE) goat anti-mouse IgG (H+L) secondary antibody (Invitrogen #A10543). For mN1 staining, after the initial washing steps, cells were incubated for 1 hour in the dark in 100 µl FACS buffer with 2 µg/ml allophycocyanin (APC)-conjugated anti-mN1 (22E5) antibody (Invitrogen #17-5765-82). Since this step, samples were kept in the dark. Cells were washed 2 times with FACS buffer, resuspended in 400 µl PBS with 1 µg/ml DAPI and incubated for 10–15 minutes before flow cytometry analysis. Samples with no staining and stained with only DAPI were prepared as controls.

2.11 Ligand binding assay

HEK-RBP mN1 cells were split into 12-well plates with 228,000 cells per well in DMEM

complete. After two days, ligand conjugate solution was prepared by mixing 50 nM or 200 nM JAG1 or DLL4 NE3-Fc-His proteins with 75 nM or 300 nM anti-human IgG- Alexa Fluor 488 (AF488) antibody (Invitrogen #A11013) in PBS and rotated in the dark at 4°C for minimum 1 hour. Meanwhile, cell medium was aspirated and cells were blocked with 400 µl per well DMEM complete with 1% W/V BSA and 10% V/V goat serum for 45 min at 37°C. After blocking, 100 µl ligand conjugate solution was added dropwise into each well and cells were resuspended by gentle pipetting. After 2 hours of incubation in the dark at 37°C, cells were harvested into microcentrifuge tubes. Since this step, samples were kept on ice in the dark. Cells were washed 2 times by repeating centrifuging at 3000 rpm for 5 minutes at 4°C and resuspending in 300 µl HEPES buffered saline solution stored at 4°C (Lonza). Cells were resuspended in 300µl HEPES buffered saline solution with 1µg/ml DAPI and incubated for 10–15 minutes before flow cytometry analysis. Samples incubated without ligand conjugate solution and with only anti-human IgG-AF488 antibody were prepared as controls.

2.12 Flow cytometry (FACS) analysis

Samples were analysed with a CytoFLEX LX flow cytometer (Beckman Coulter) with a flow rate between 200–1000 events/second. Data for 30,000 events or 10,000 viable cells were collected for each sample. DAPI fluorescence was measured with excitation at 405 nm and emission at 450 nm. AF488 fluorescence was measured with excitation at 488 nm and emission at 525 nm. PE fluorescence was measured with excitation at

561 nm and emission at 585 nm. APC fluorescence was measured with excitation at 638 nm and emission at 660 nm. Data was analysed by FlowJo™ v10.8 Software (BD Life Sciences). Median fluorescence intensities of fluorophores of interest were quantified for single viable cells selected by a series of fluorescence gating (Figure 2.5).

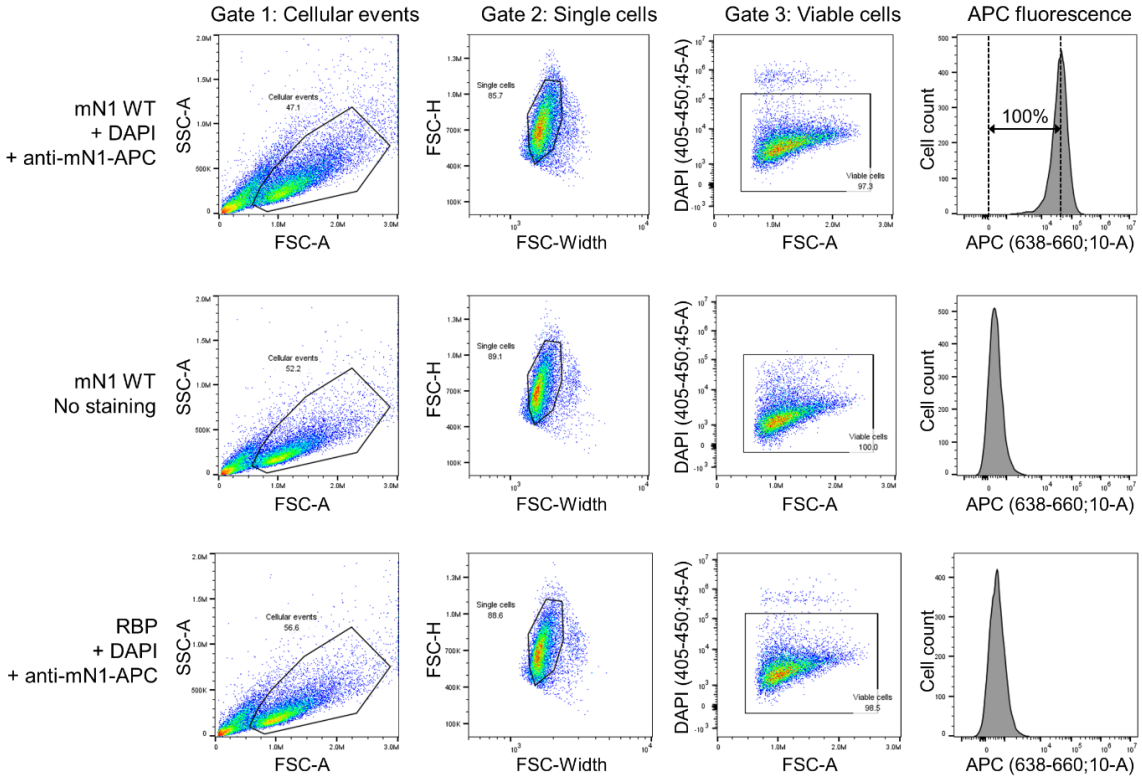


Figure 2.5. Gating strategies for flow cytometry

Gating for cellular events was performed on a forward scatter vs side scatter plot of all events detected by the flow cytometer. Gating for single cells was then performed on a forward scatter height vs width plot of cellular events. Subsequently, viable cells, which showed lower fluorescence intensity for DAPI were gated from single cells. The median fluorescence intensity for the fluorophore of interest (APC in this figure) was then quantified for viable cells. Flow cytometry gatings for HEK-RBP mN1 WT cells stained with both DAPI and anti-mN1-APC (top panel) and with no staining (middle panel) and HEK-RBP cells stained with both DAPI and anti-mN1-APC (lower panel) are shown as examples. Only cells stained with DAPI possessed a subpopulation with high DAPI signal, which should indicate dead cells. Median fluorescence intensity for APC in each case is shown relative to the mN1 WT stained with

anti-mN1-APC (set as 100%).

2.13 Small angle X-ray scattering (SAXS)

2.13.1 Sample preparation and data collection

S2-produced hN1 EGF20-27 and EGF20-29 proteins cleaved to remove the BirA-His tag (see Section 2.7.5) were dialysed overnight at 4 °C in 2 litres of SAXS buffer (5 mM Tris-HCl, 15 mM $CaCl_2$, pH 7.5, 0.22 µm filtered) and concentrated by a 10,000 MW protein concentrator spin column by centrifugation at 3000 xg to 2.5 mg/ml. Protein samples were frozen at -80 °C and stored on dry ice for transport to the beamline. Scattering data were collected using Beamline B21 at the Diamond Light Source using a SEC-SAXS method. 50 µl freshly thawed protein sample was autoloaded onto a Shodex 402.5 analytical SEC column. The SAXS buffer used for overnight dialysis (0.22 µm filtered) was used as the SEC buffer. 1 mg/ml BSA diluted in SAXS buffer was used as the blank. The eluent from the column was passed through the X-ray beam and the scatter pattern was recorded. Data were collected up to a scattering vector of 0.37$Å^{-1}$.

2.13.2 SAXS data analysis

SAXS data were processed and analysed using the ATSAS 3.0 software package (Manalastas-Cantos *et al.*, 2021). Scattering data was initially processed by Chromixs to subtract the scattering attributed to the buffer from that of the protein peak. Semi-flexible models of EGF20-27 and EGF20-29 created using the Coot software (Emsley *et al.*, 2010) were used for structure fitting by SREFLEX (Panjkovich and Svergun, 2016) based

on the scattering data. The structure models generated by SREFLEX and AlphaFold2 (Jumper *et al.*, 2021) were then evaluated using CRYSOL (Svergun, Barberato and Koch, 1995).

2.14 Statistical analysis

Statistical analyses were performed with Prism 10 (GraphPad, San Diego, CA, USA). D'Agostino and Pearson tests were employed to confirm the data's normal distribution. Brown-Forsythe tests were used to check if datasets have equal variance. Parametric and nonparametric tests used are indicated in each figure legend, together with (where appropriate) the post hoc test used for multiple comparisons. Values are presented together with the mean ± standard deviation (SD). Statistical significance are shown are: ns = not significant; * $p<0.05$; ** $p<0.01$; *** $p<0.001$; **** $p < 0.0001$.

3 Identifying the role of the Abruptex region in Notch1 trans-activation

3.1 Introduction

Missense mutations in dN EGF24-29 have been shown to induce a unique phenotype distinct from the *N* phenotype during *Drosophila* wing development (Nasarenko, 1930; Kelley *et al.*, 1987). The *Ax* phenotype includes interrupted wing veins and fewer dorsal bristles, which is commonly considered a representation of enhanced Notch signalling (De Celis and Bray, 2000), compared to the notches end enlarged wing veins observed in dN haploinsufficiency (Dexter, 1914). Mutations causing the *Ax* phenotype can be divided into three categories (*N* suppressor, *N* enhancer and homozygous lethal) each generating a different phenotype in combination with an N^- allele (Foster, 1975; Portin, 1975; Kelley *et al.*, 1987) (see Section 1.6.1).

Since these data suggest the Ax region has a distinct role in Notch function, the impact of different homologous Ax variants on mammalian Notch receptor trans-activation was studied in this chapter. Luciferase reporter cell lines stably expressing WT or variant mN1 were established and employed in various assays. Firstly, the number of N1 on the cell surface was quantified by both a ligand-independent Notch activation assay and detecting immunostaining using an anti-NECD antibody followed by flow cytometry. Secondly, the impact of Ax variants on N1 trans-activation was investigated by culturing HEK-RBP mN1 cells with plate-coated purified ligand constructs or ligand-expressing B16 mouse melanoma cells. Finally, the effect of Ax substitutions on receptor-ligand binding was quantified by a FACS-based ligand binding assay.

3.2 Ax region in human NOTCHs

Sequence alignment of dN Ax region (EGF24-29) with human NOTCHs identified homologous regions in all 4 receptors, which are EGF24-29 in hN1 and hN2, EGF22-27 in hN3, and EGF20-23 in hN4 (Figure 3.1). No homologous sequences to dN EGF25-26 are found in hN4. Despite sequence homology, the number of EGF domains that bind Ca^{2+}, according to consensus sequence matching (see Section 1.2.2.2) varies between different receptors. The first two EGFs in the Ax region of dN, hN1, hN2 and hN3 all have the consensus sequence for calcium binding. Additionally, EGF27 of hN1 and EGF26-27 of hN2 also have the consensus sequence for cbEGF. dN EGF26 has a glutamic acid at the second position of the calcium-binding consensus sequence, which hasn't been seen in previously identified cbEGF domains, and thus is classified as non-calcium-binding. Interestingly, hN1 has an additional cysteine in EGF25 and EGF27 apart from the structurally conserved six cysteine residues per EGF that form the three native disulfide bonds (see Section 1.2.2.1). The extra cysteine residues lie between Cys3 and Cys4. The extra cysteine in EGF25 is conserved in mouse and rat N1 while the extra cysteine in EGF27 is not. Residues affected by *Drosophila* Ax substitutions are conserved in human NOTCHs except for dN S1088. Two mutations in EGF16 also induced a phenotype similar to the *Ax* phenotype in *Drosophila* (Yamamoto *et al.*, 2012) (see Section 1.2.4). Sequence alignment identified regions homologous to dN EGF16 in human NOTCHs, which all lack the consensus aromatic residue between Cys5 and Cys6 (Figure 3.1). The residues affected by the two mutations are conserved in human NOTCHs.

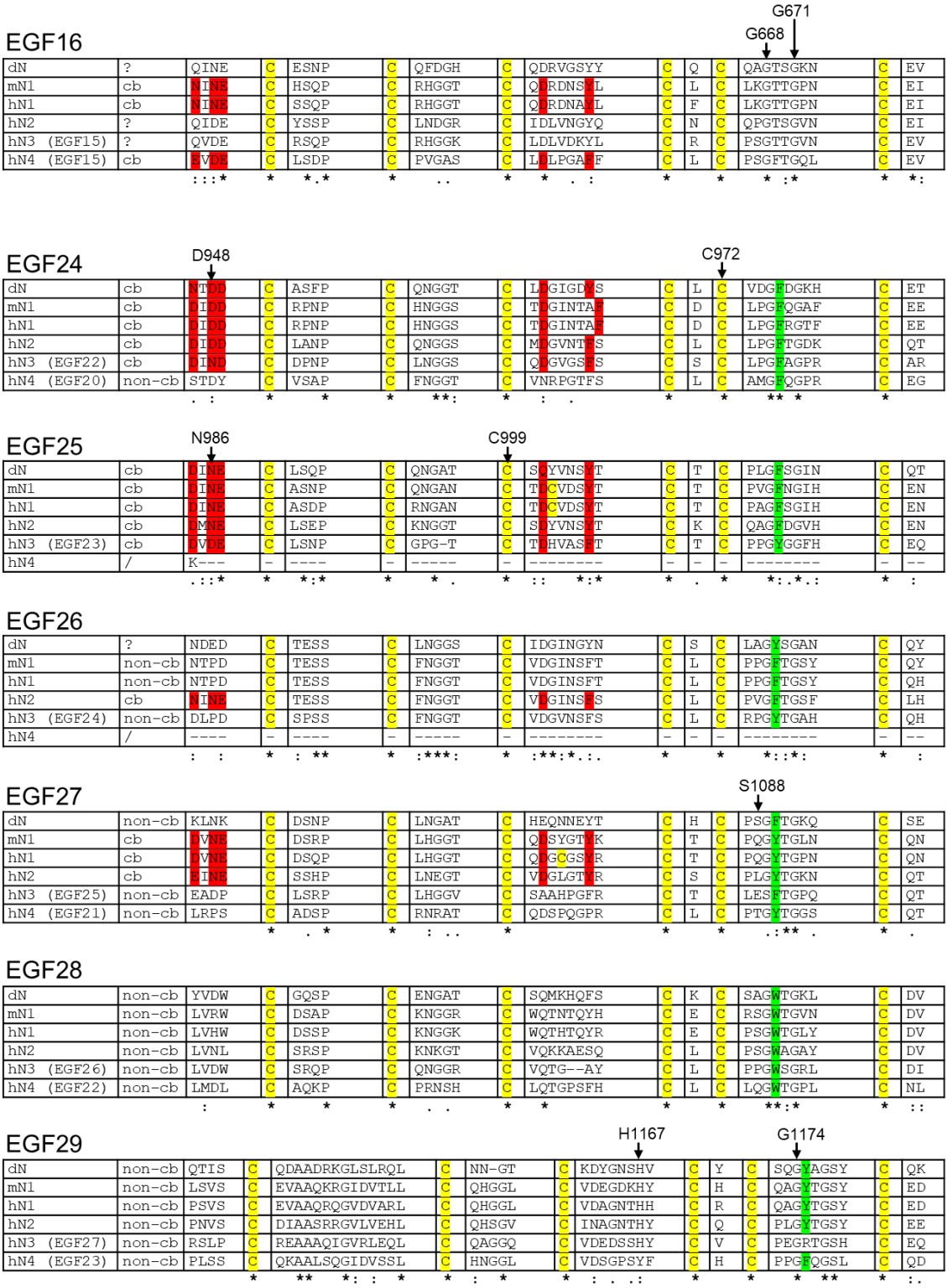


Figure 3.1. Protein sequence alignment for EGF16 and Ax regions across Notch receptors.

NCBI reference protein sequences for (from top to bottom) dN (NP_476859.2), mN1 (NP_032740.3), hN1 (NP_060087.3), hN2 (NP_077719.2), hN3 (NP_000426.2) and hN4 (NP_004548.3) were aligned by Clustal Omega available on EMBL-EBI website (Sievers and

Higgins, 2021; Madeira *et al.*, 2022; *Clustal Omega* < *EMBL-EBI*, no date). Alignment result was shown for each EGF domain. Fully conserved residues are shown by asterisks (*). Conserved positions where aligned residues are strongly similar in biochemical properties are indicated by colons (:). Conserved positions where aligned residues are weakly similar in biochemical properties are indicated by periods (.). Cysteine residues are highlighted in yellow, with conserved cysteine involved in forming the EGF fold aligned in columns. Consensus aromatic residues that may be involved in hydrophobic packing are highlighted in green. Ca^{2+}-binding consensus residues D/N/E-x-D/N-D/N/E/Q-x_m-D/N/Q-x_n-Y/F (m/n denote variable numbers of residues) are highlighted in red if the complete consensus is predicted or shown to bind Ca^{2+}. EGF16 in dN, hN2, hN3 and EGF26 in dN each have one residue different to the known Ca^{2+}-binding consensus sequence. Their Ca^{2+}-binding status is uncertain (indicated by "?"). hN4 lacks a homologous sequence to EGF25-26. Sites of missense mutations generating the *Ax* phenotype are shown by arrows, which are conserved in dN, mN1, hN1 and hN2, except for S1088.

3.3 HEK-RBP mN1 cell line establishment

3.3.1 Flp-In TRex 293 mN1-NLuc/CLuc-RBPJκ cell line

Flp-In TRex 293 CLuc-RBPJκ cells stably expressing WT or variant mN1-NLuc (HEK-RBP mN1) were established using the Flp-in system (see Section 2.2 and 2.6.2) and used in different assays. The cell line expresses the DNA-binding protein RBPJκ with the C-terminal half of the firefly luciferase attached to its N terminus (CLuc-RBPJκ) and a mN1 receptor with the N-terminal half of luciferase attached to the C terminus of its intracellular domain (mN1-NLuc). S2 and S3 cleavage takes place upon ligand-dependent or independent activation (similar to WT Notch) and the NICD-NLuc is released and transported to the nucleus where it interacts with CLuc-RBPJκ to form an active luciferase. When substrate, such as D-luciferin, is provided in excess, luminescence is produced, proportional to the amount of NICD cleavage and therefore

N1 activation. Quantification of the luminescence signal provides a numerical readout of N1 activation which can be analysed directly using a luminescence plate reader. This luciferase complementation-based assay, which was initially designed by Ilagan et al. (2011), offers a good platform to compare the effects of different variants of mN1 on Notch signalling using a full-length Notch receptor and RBPJκ in a native cellular context.

3.3.2 mN1 cell lines made in this project

Cell lines established in this project are listed in Table 3.1. To study the role of the Ax region in Notch signalling, mN1 cell lines carrying variants homologous to *Drosophila* Ax variants were created, including two homozygous lethal variants C933S and C960Y, two *N* suppressor variants[1] D909V and N947I and a D909V/N947I (DVNI) double variant, and two *N* enhancer variants H1129Y and G1136A (see Section 1.6.1). Since dN S1088 is not conserved in mammalian Notch (Figure 3.1), to study the *N* enhancer variant dN S1088I, mN1 Q1049I with isoleucine replacing glutamine in the same position as S1088 in EGF27 was made. Additionally, S990N, a variant in hN1 EGF26 that was found in ageing oesophageal and skin tissues was made (Martincorena *et al.*, 2018). As a negative control for ligand binding and trans-activation, a cell line expressing mN1 L468A, which replaces a key residue in EGF12 previously shown to be essential for ligand binding was used (Whiteman *et al.*, 2013). EGF16 variants, G632R and G635D, homologous to *Drosophila* variants that generated a phenotype similar to the *Ax* phenotype were also created (Yamamoto *et al.*, 2012) (see Section 1.2.4). For each cell

[1] N suppressor variants D909V and N947I change residues within the Ca^{2+}-binding consensus.

line, at least three clones were established and tested to confirm successful DNA incorporation and consistent RNA expression (see Section 3.3.3).

Table 3.1. HEK-RBP mN1 cell lines established in this project.

Plasmids used to construct HEK-RBP mN1 L468A, D909V, and DVNI were made by Dr Thomas J W Rowntree (University of Oxford). The plasmids used to construct the other mN1 variant cell lines were made in this project. All variant cell lines were made in this project, except for the L468A cell line, which was made by Dr Thomas J W Rowntree (University of Oxford).

EGF	Residue change	Category	dN homologue
12	L468A	Ligand-binding deficient	/
16	G632R	dN signal enhancing	G668R
16	G635D	dN signal enhancing	G671D
24	D909V	*Ax N* suppressor	D948V
24	C933S	*Ax* homozygous lethal	C972G
25	N947I	*Ax N* suppressor	N986I
24-25	D909V/N947I (DVNI)	*Ax N* suppressor double variant	D948V/N986I
25	C960Y	*Ax* homozygous lethal	C999Y
26	S990N	Human aging tissue	/
27	Q1049I	*Ax N* enhancer	S1088I
29	H1129Y	*Ax N* enhancer	H1167Y
29	G1136A	*Ax N* enhancer	G1174A

3.3.3 Verification of stable cell line

Genomic DNA was extracted from each stable cell line (see Section 2.1.4) and following PCR amplification of the region spanning the introduced mutation, was sequenced to ensure the cell line had the correct genotype (see Section 2.1.5) (Figure 3.2). To ensure mN1 RNA was expressed at a similar level in stable cell lines, RNA extracted from each cell line was reverse-transcribed and subjected to PCR amplification of a region of cDNA

encoding mN1 EGF20-22 (337 bp) (see Section 2.4). The RT-PCR products were examined by gel electrophoresis (Figure 3.3). RT-PCRs for mN1 produced bands of similar intensity, suggesting mN1 variant RNA was expressed at a similar level to mN1 WT. No band for mN1 was observed for RT-PCR using the RNA sample extracted from HEK-RBP cell, showing the primers used were specific to mN1. RT-PCRs for GAPDH, producing a band of 237 bp, were performed alongside to ensure each reverse transcription reaction was performed with the same starting concentration of RNA across all cell lines. In addition, PCRs for RNA samples without reverse transcription were performed to confirm the RNA samples were not contaminated with DNA. It should be noted that RT-PCR serves as a test of mN1 RNA expression but not a direct measurement of protein.

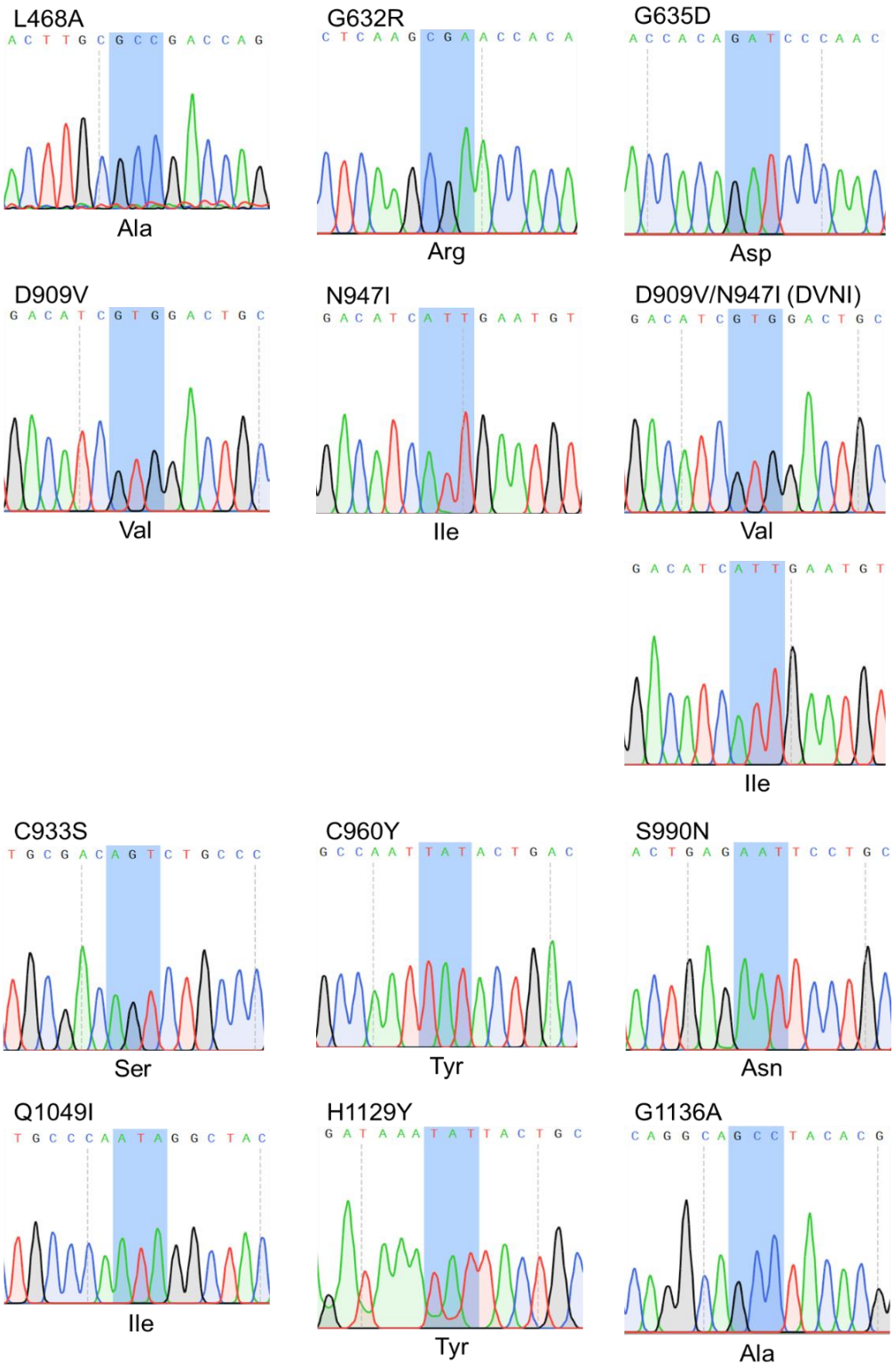


Figure 3.2. DNA sequencing of HEK-RBP mN1 variant cell lines.

Genomic DNA was extracted from each newly established stable cell line. Different regions of mN1 were amplified by PCR using primers specific to mN1 and sequenced to confirm genotype. The DNA sequences that encode the introduced substitutions are shown for each variant cell line indicated by labels.

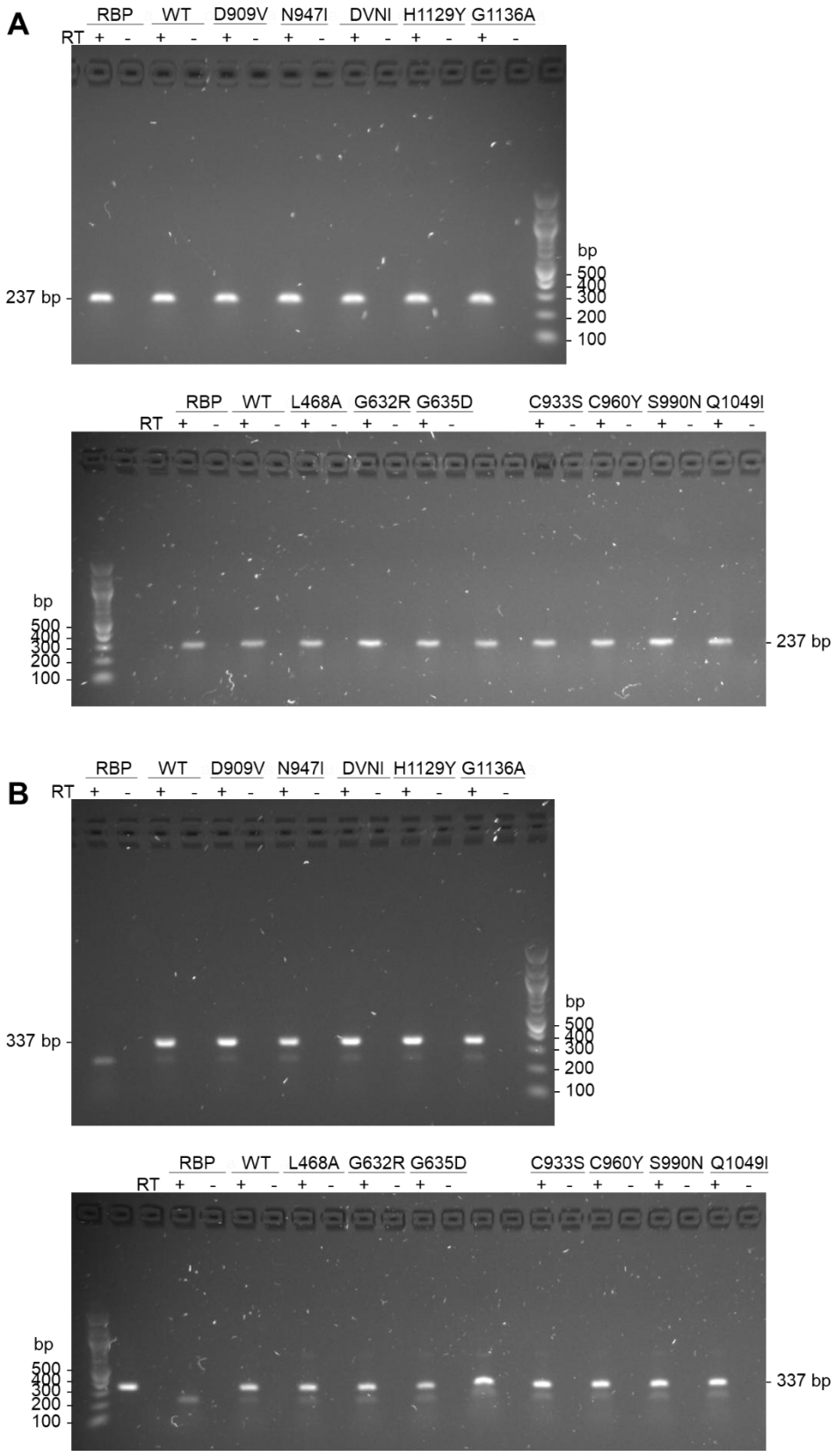


Figure 3.3. RT-PCR for HEK-RBP mN1 cell lines.

RNA was extracted from each newly established cell line. PCRs to amplify (A) a 237 bp region in GAPDH cDNA and (B) a 337 bp region in mN1 cDNA were performed for RNA

samples from all cell lines (indicated by labels) with and without RT (indicated by + and -). PCR products were run on a 2.5% agarose TBE gel. No bands were observed for PCRs of RNA samples without RT, suggesting there was no DNA contamination in the RNA samples.

3.4 Studying the effect of Ax variants on cell surface N1 level

3.4.1 Two assays for cell surface N1 quantification

Following genotype and RNA expression verification, HEK-RBP mN1 variant cell lines were employed in two assays to study the effect of substitutions on N1 cell surface protein level. Firstly, a ligand-independent activation assay initially developed by Ilagan et al. (2011) was used to quantify N1 when cells were incubated with an excess of the Ca^{2+} ion chelator EGTA (Figure 3.4A) (see Section 2.9.1) (Ilagan *et al.*, 2011). EGTA serves to remove the Ca^{2+} ions from the NRR of mN1, which induces conformational changes to expose the S2 cleavage site leading to subsequent γ-secretase-mediated release of the NICD-NLuc and the formation of an active luciferase. Upon substrate addition, the luminescence signal produced, which indicates NICD released, is proportional to the total number of mN1 receptors on the cell surface. This ligand-independent activation level for each variant was compared with that of mN1 WT to identify any changes in cell surface expression caused by the amino acid substitution.

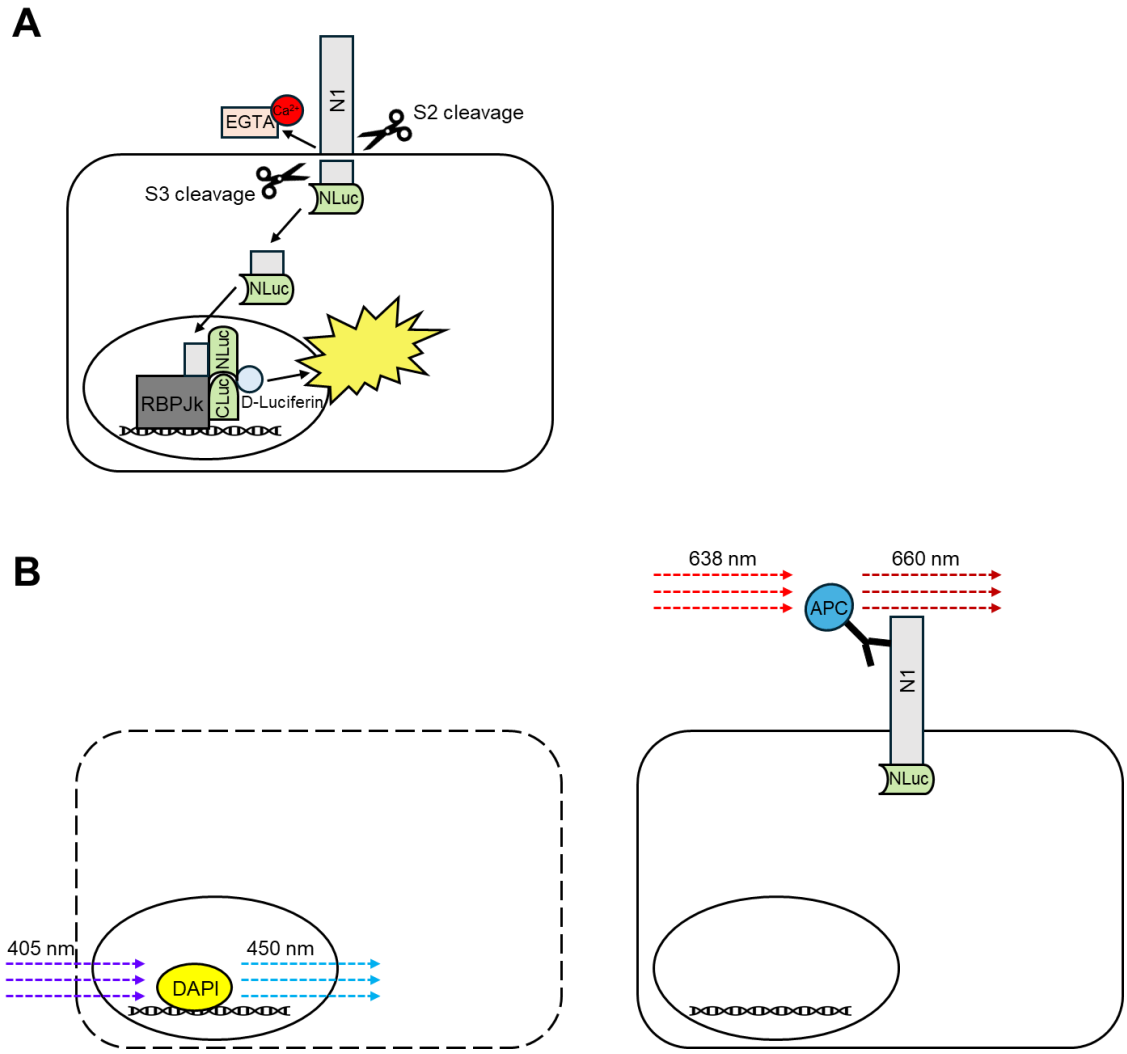


Figure 3.4. Cell surface mN1 level quantification by two assays

(A) A ligand-independent activation assay was employed to quantify the amount of activable mN1 receptors on the cell surface. An excess amount of EGTA was added to HEK-RBP mN1 cells to activate mN1 and induce the release of NICD-NLuc. NICD-NLuc migrated to the nucleus to bind with CLuc-RBPJk, forming a functional luciferase. (B) A FACS-based assay was employed to quantify cell surface mN1 level by immunostaining. HEK-RBP mN1 cells were incubated with a fluorophore APC-conjugated anti-mN1 antibody (anti-mN1-APC) and DAPI, which can diffuse into dead cells with truncated cell membranes. Excitation and emission wavelengths for APC and DAPI are indicated.

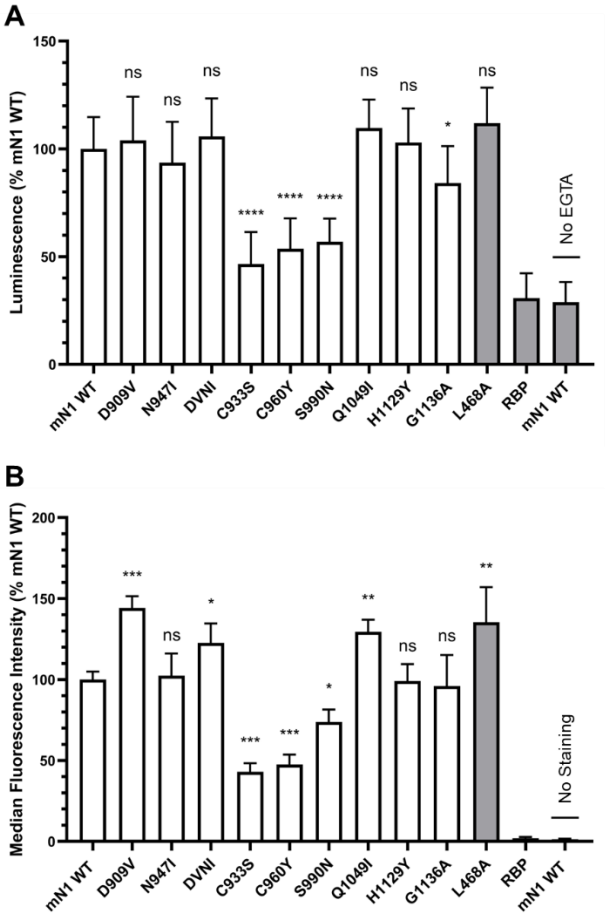
In the second assay, cells were incubated with an APC-conjugated antibody against mN1 EGF1-12 in the extracellular region (see Section 2.10) without permeabilization and analysed by flow cytometry (FACS) (Figure 3.4B) (see Section 2.12). Viable single cells

which exclude DAPI were selected by a series of fluorescence gating (Figure 2.5) and the median APC fluorescence level of the cell population, which indicates the amount of bound anti-mN1 antibody, was used as the measurement of cell surface mN1 level. This median APC fluorescence intensity for each variant was compared with that of mN1 WT to identify any changes in cell surface expression.

3.4.2 Cell surface N1 level of Ax variants

Both the ligand-independent activation and FACS-based assays were first performed for the negative control HEK-RBP cell lines, which produced, as expected, a significantly lower activation and fluorescence level compared to the mN1 WT cell line, suggesting the assays were able to distinguish differences in cell surface mN1 level (Figure 3.5). For both methods, very similar trends were observed for all variants in the Ax region. Both assays suggested that homozygous lethal variants C933S and C960Y and the ageing-related variant S990N reduced cell surface levels to around 50%-60% of that seen in the mN1 WT cell line. The *N* suppressor N947I and the *N* enhancer H1129Y did not significantly affect cell surface level in either assay. Whilst showing no significant effect in the ligand-independent activation assay, the binding-deficient L468A variant, *N* suppressor D909V, the DVNI double variant and *N* enhancer Q1049I were shown to increase fluorescence intensity by 20-40% compared to WT in the FACS-based assay. *N* enhancer G1136A showed a slight decrease of 15% in ligand-independent assay but no significant difference in FACS-based assay. Ligand-independent activation assay performed for EGF16 variants suggested that they did not affect cell surface expression

of the receptor (Appendix E, Figure E.1).



Cell line	Luminescence (% mN1 WT)	Statistical significance
mN1 WT	100 ± 14.8	
D909V	104 ± 20.2	ns
N947I	93.6 ± 18.9	ns
DVNI	105.8 ± 17.7	ns
C933S	46.5 ± 14.9	****
C960Y	53.7 ± 14.04	****
S990N	56.9 ± 10.8	****
Q1049I	109.7 ± 13.2	ns
H1129Y	102.9 ± 15.8	ns
G1136A	84.1 ± 17.2	*
L468A	112 ± 16.5	ns

Cell line	Median fluorescence intensity (% mN1 WT)	Statistical significance
mN1 WT	100 ± 7.2	
D909V	144.3 ± 7.2	***
N947I	102.4 ± 13.7	ns
DVNI	122.7 ± 11.9	*
C933S	43 ± 5.3	***
C960Y	47.6 ± 6	***
S990N	73.9 ± 7.6	*
Q1049I	129.5 ± 7.5	**
H1129Y	99.2 ± 10.4	ns
G1136A	95.9 ± 19.2	ns
L468A	135.4 ± 21.7	**

Figure 3.5. Cell surface mN1 level quantification for mN1 Ax variants.

(A) A ligand-independent activation assay was performed for mN1 Ax variants. Graph (left panel) and table (right panel) show the combined results of four independent plates (biological repeats), each with five repeat wells (technical repeats). Signal in each case is shown relative to the mN1 WT incubated with EGTA. (B) Flow cytometry-based quantification of cell surface mN1 level was performed for Ax variants. Graph (left panel) and table (right panel) show the combined results of four biological repeats, each with at least two technical repeats. Median fluorescence intensity for APC in each case is shown relative to the mN1 WT cells stained with anti-mN1-APC. Data presented as mean ± SD. Statistical significance compared to mN1 WT was determined by Kruskal-Wallis test and Dunn's post hoc test (ns = not significant, * = $P < 0.05$, ** = $P < 0.01$, *** = $P < 0.001$, **** = $P < 0.0001$).

3.5 Trans-activation of Ax variants with plate-coated protein

3.5.1 Assay design

To study the effect of substitutions on ligand-dependent N1 trans-activation, an activation assay (Ilagan *et al.*, 2011) utilising purified ligand fragments was performed for all mN1 variant cell lines (see Section 2.9.2.1). HEK-RBP mN1 cells were grown overnight on a 96-well plate immobilised with purified C-terminal Fc-His-tagged hJAG1 or hDLL4 C2 to EGF3 (NE3) constructs (hJAG1 or hDLL4 NE3-Fc-His) (Figure 3.6A). Although this plate-based assay has some limitations since it uses a shortened form of ligand which is not presented on a cell surface, many previous studies have demonstrated that purified ligand NE3 constructs are necessary and sufficient for full Notch activation (Andrawes *et al.*, 2013). Furthermore, NE3 ligands can be purified to near homogeneity and accurately quantified, facilitating experimental analysis.

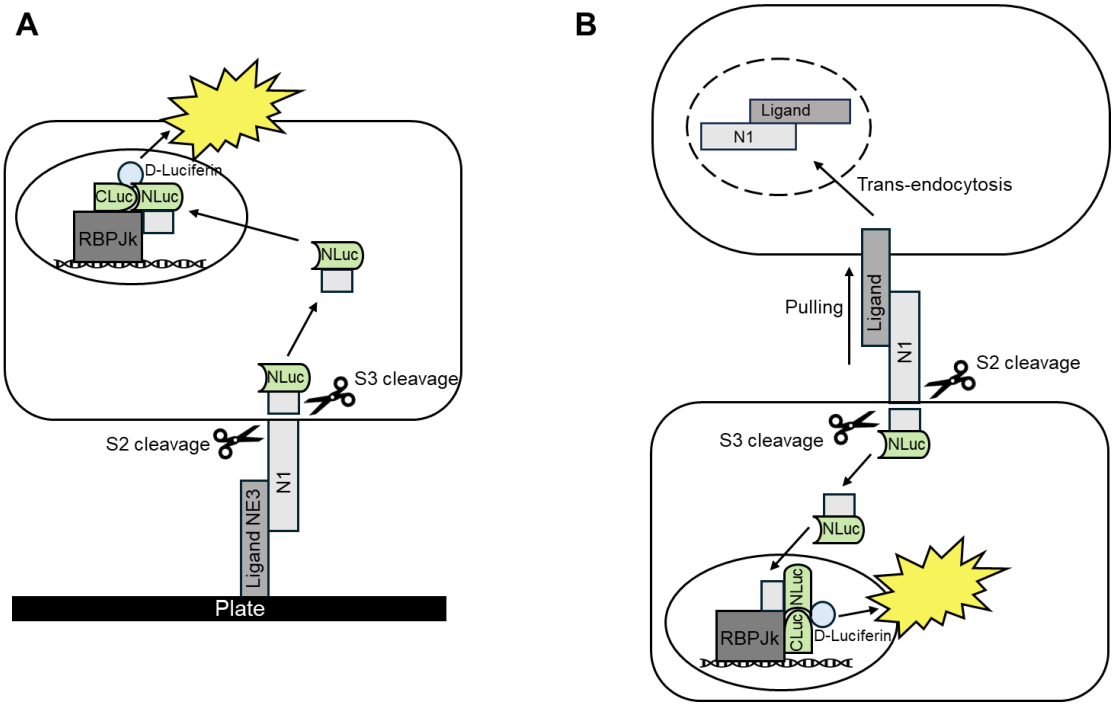


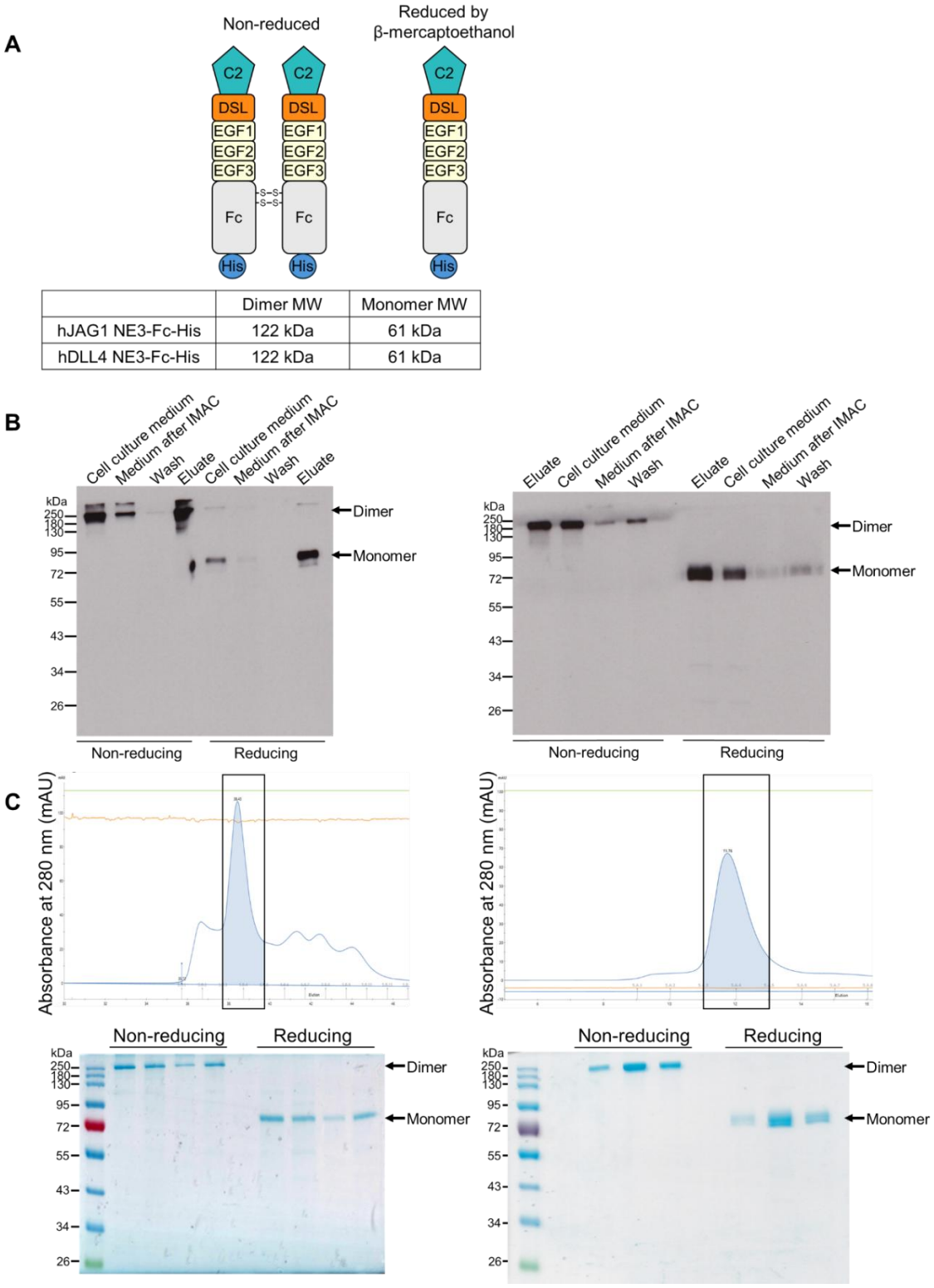
Figure 3.6. mN1 trans-activation assays.

Two ligand-dependent activation assays (plate-based and co-culture-based) were employed to quantify the level of mN1 trans-activation by Jag1 and Dll4. (A) An excess amount of ligand NE3 protein was coated by adsorption on a 96-well plate. HEK-RBP mN1 cells were grown on the protein-coated plate overnight to allow mN1 activation and induce the release of NICD-NLuc. (B) HEK-RBP mN1 cells were grown on a 96-well plate. 24 hours later, B16 cells expressing full-length mJag1 or mDll4 were coated directly on the top of mN1 cells and co-cultured overnight. Interactions between mN1 and ligands coupled with trans-endocytosis of NECD-ligand complex into the B16 cells expose the S2 cleavage site of mN1 and induce the release of NICD-NLuc.

3.5.2 Ligand protein production and purification

hJAG1 and hDLL4 NE3-Fc-His constructs (Figure 3.7A) were produced by transient transfection of HEK293T or HEK293F cells with pHLsec or pcDNA3.1(+) plasmids (see Section 2.6.1) and purified using a well- established protocol (Chillakuri *et al.*, 2013) (see Section 2.7). The cell medium containing the secreted His-tagged ligand proteins was filtered and subjected initially to IMAC with samples analysed by western blotting (Figure 3.7B). The protein sample eluted from the column was further purified by SEC. Purified

samples were initially analysed by reducing and non-reducing SDS-PAGE to estimate purity (Figure 3.7C). Bands differing in MW dependent on monomer or dimer form were observed with purity over 90%. Reducing and non-reducing bands for both ligands were higher in MW than predicted due to the presence of post-translational modifications. This was observed consistently between different batches of ligands.



	Dimer MW	Monomer MW
hJAG1 NE3-Fc-His	122 kDa	61 kDa
hDLL4 NE3-Fc-His	122 kDa	61 kDa

Figure 3.7. Ligand NE3-Fc-His purification.

(A) Schematic illustration of ligand NE3-Fc-His constructs. Estimated MWs without post-translational modifications are shown in the table. In the non-reducing condition, disulfide bonds formed between Fc regions lead to the formation of ligand dimer with a higher MW. When the disulfide bonds are reduced by β-mercaptoethanol, ligand monomer with a lower

MW is obtained. (B) Western blots were performed on samples taken during IMAC purification (indicated by labels) for hJAG1 (left panel) and hDLL4 NE3-Fc-His (right panel). An anti-His-tag antibody was used to show a predominant dimer (>180 kDa, indicated by arrow and label) under non-reducing conditions and a monomer (>72 kDa, indicated by arrow and label) under reducing conditions. The presence of His-tagged proteins suggested NE3 ligands were successfully produced and purified. (C) hJAG1 (left panel) and hDLL4 (right panel) NE3-Fc-His sample eluted from His-tag column was further purified by SEC using a Superdex 200 Increase 10/300 GL column. The chromatograms (top panel) show the peaks automatically collected by the AKTA Pure machine for one injection. The indicated peaks were collected and analysed by SDS-PAGE and Coomassie staining for protein identity and purity. SDS-PAGE (bottom panel) showed that the fragments containing the proteins were relatively pure (>90%) and showed the expected MW difference between dimer and monomer forms (indicated by arrows and labels).

3.5.3 Ligand titration

To ensure the 96-well plate was saturated with ligand NE3 construct for optimal N1 activation, titration experiments were conducted. 50 µl of different concentrations of hJAG1 or hDLL4 NE3 protein in HBS buffer was added to each well and incubated overnight at 4 °C. Results of subsequent activation assays suggested that activation saturated at around 5 µg/ml of hJAG1 NE3 and 3.75 µg/ml of hDLL4 NE3 (Figure 3.8). An excess concentration of 10 µg/ml was therefore employed in assays with N1 variants.

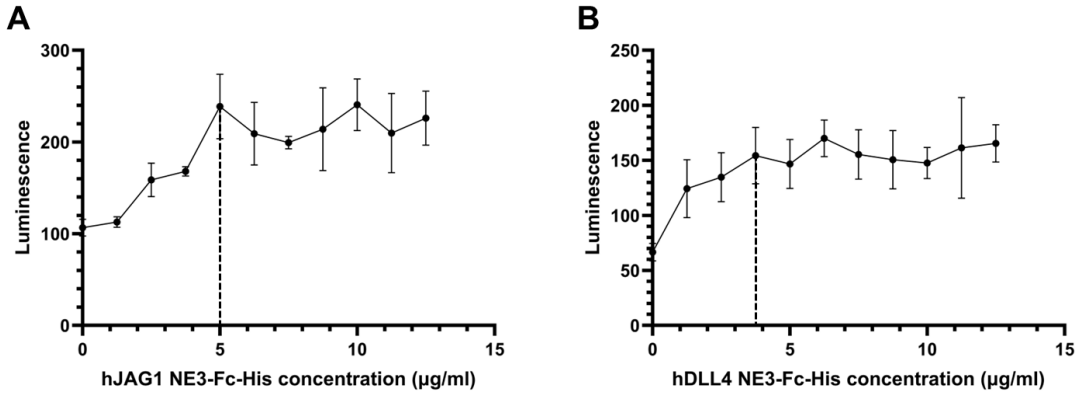


Figure 3.8. Ligand NE3 titration for plate-based mN1 trans-activation assay.

Activation assays were performed with mN1 WT cell line using (A) hJAG1 and (B) hDLL4 NE3-Fc-His concentrations ranging from 1.25 µg/ml to 12.5 µg/ml. Luminescence measured was shown as mean ± SD. Luminescence level started to plateau when protein concentration exceeded 5 µg/ml for hJAG1 and 3.75 µg/ml for hDLL4 NE3 (indicated by dashed line) suggestive of plate saturation.

3.5.4 Plate-based trans-activation of Ax variants

Initial experiments performed for the ligand binding-deficient N1 variant L468A showed substantially lower activation by both hJAG1 NE3 (Figure 3.9A) and hDLL4 NE3 (Figure 3.9B), compared to the N1 WT line. These data suggested that ligand constructs purified had native-like properties, and the assay distinguished clearly between the positive and negative controls. For *N* suppressor variants, D909V showed no significant changes in activation while N947I showed a 25% decrease in activation by both ligands. The DVNI double variant showed a 30% decrease in activation by hJAG1 NE3 only. The *N* enhancer H1129Y showed a 20% decrease in activation by both ligands. The *N* enhancer G1136A showed a 30% decrease in activation by hJAG1 NE3 only but no changes in activation by hDLL4 NE3. The *N* enhancer Q1049I showed no significant changes in activation by both ligands. As *N* suppressor and *N* enhancer variants did not significantly

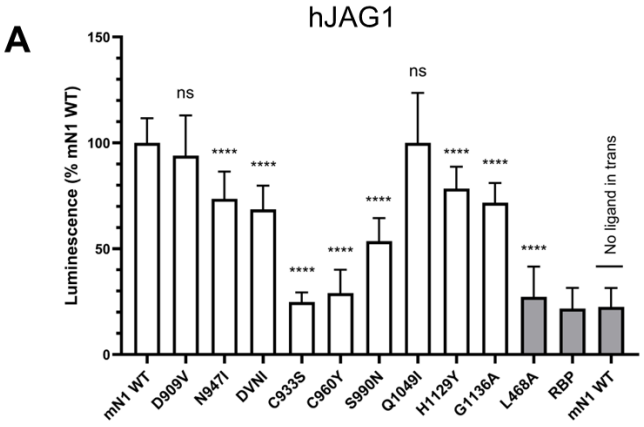
affect cell surface mN1 level as demonstrated by previous assays, these data suggest detrimental effects on activation but at a level less pronounced than that observed for L468A.

The homozygous lethal variants C933S and C960Y reduced activation by both ligands by 75%, similar to that of L468A. The ageing-related variant S990N led to a substantial 50% reduction in activation by both ligands. As these variants all reduced cell surface mN1 level (Figure 3.5), these changes were likely to be caused by reduced cell surface expression.

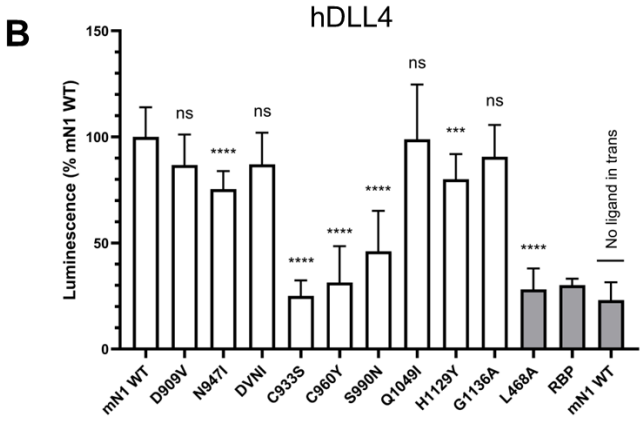
The EGF16 variant G635D led to a 20% reduction in activation by both ligands while G632R only led to a 15% reduction in hDLL4 activation (Appendix E, Figure E.2). As suggested by previous cell surface N1 quantification, their reductions in ligand-dependent activation were unlikely to be caused by changes in cell surface expression. Due to the number of variants studied in this study, EGF16 variants were not carried forward in later experiments.

Raw luminescence levels for cell lines grown in the absence of trans-ligands were also measured to check whether or not N1 variants increase receptor auto-activation similar to that seen in some T-ALL variants (Weng *et al.*, 2004) (Appendix E, Figure E.3). *N* suppressor and enhancer variants showed similar auto-activation compared with WT. C933S, C960Y and S990N showed reduced auto-activation, consistent with their

reduced cell surface expression.



Cell line	Luminescence (% mN1 WT)	Statistical significance
mN1 WT	100 ± 11.6	
D909V	94 ± 19	ns
N947I	73.6 ± 12.9	****
DVNI	68.6 ± 11.2	****
C933S	24.8 ± 4.5	****
C960Y	29 ± 11	****
S990N	53.6 ± 10.9	****
Q1049I	99.9 ± 23.6	ns
H1129Y	78.4 ± 10.4	****
G1136A	71.7 ± 9.3	****
L468A	27.3 ± 14.3	****



Cell line	Luminescence (% mN1 WT)	Statistical significance
mN1 WT	100 ± 14	
D909V	86.8 ± 14.4	ns
N947I	75.4 ± 8.4	****
DVNI	87.1 ± 14.9	ns
C933S	25.1 ± 7.3	****
C960Y	31.4 ± 17.1	****
S990N	46.1 ± 19.1	****
Q1049I	98.9 ± 25.8	ns
H1129Y	80.1 ± 11.8	***
G1136A	90.7 ± 15	ns
L468A	28.2 ± 9.9	****

Figure 3.9. Trans-activation of mN1 Ax variants by plate-coated purified protein.

Activation assays for mN1 Ax variants grown with plate-coated (A) hJAG1 or (B) hDLL4 NE3 protein or no coated protein (indicated by "No ligand in trans"). Graph (left panel) and table (right panel) show the combined results of four independent plates, each with five repeat wells. Signal in each case is shown relative to the mN1 WT. Data presented as mean ± SD. Statistical significance compared to mN1 WT was determined by Welch's ANOVA and Dunnett's post hoc test (ns = not significant, *** = $P < 0.001$, **** = $P < 0.0001$).

3.6 Trans-activation of Ax variants by co-culturing with ligand-expressing B16 cells

3.6.1 Assay design and optimisation

Alongside the plate-based assay, a co-culture-based trans-activation assay (see Section 2.9.2.2) was developed to study the properties of N1 variants in a more native condition, where ligands expressed on an opposing cell surface are able to exert a pulling force important for receptor activation (see Section 1.4.2). An equal number of B16 cells stably expressing mJag1 or mDll4 (gift from Prof. Adrian Harris, University of Oxford) were layered onto HEK-RBP mN1 cells and co-cultured overnight on a 96-well plate (Figure 3.6B). Expressions of mJag1 and mDll4 were validated by binding of hN1 EGF11-13-BirA-His construct to the B16 cells (results not shown). However, no direct comparison was performed for the expression levels of mJag1 and mDll4.

For assay optimisation, titrations of cell number were performed with either 24 or 48 hours of co-culture for mN1 WT and the negative control L468A cell lines (Figure 3.10 and 3.11). For both ligands, 24 hours of culturing produced results with larger differences between mN1 WT cells grown with ligand-expressing B16 cells and those grown with B16 WT control cells (without ligand). Also, a larger difference in the activation level of WT and L468A was obtained after 24 hours of co-culture compared with the 48-hour condition. At 24 hours of co-culture with equal numbers of ligand-expressing B16 cells, between 20,000 and 80,000 mN1-expressing cells per well generated similar results. When fewer than 20,000 mN1 cells were cultured per well, wider error bars and smaller

differences between mN1 WT cells and L468A cells were observed when grown with ligand-expressing B16 cells (results not shown). Therefore, conditions of 24 hours of co-culture with 40,000 mN1 cells and the equivalent number of B16 cells, which showed better cell attachment and more even cell distribution in the plate, were selected.

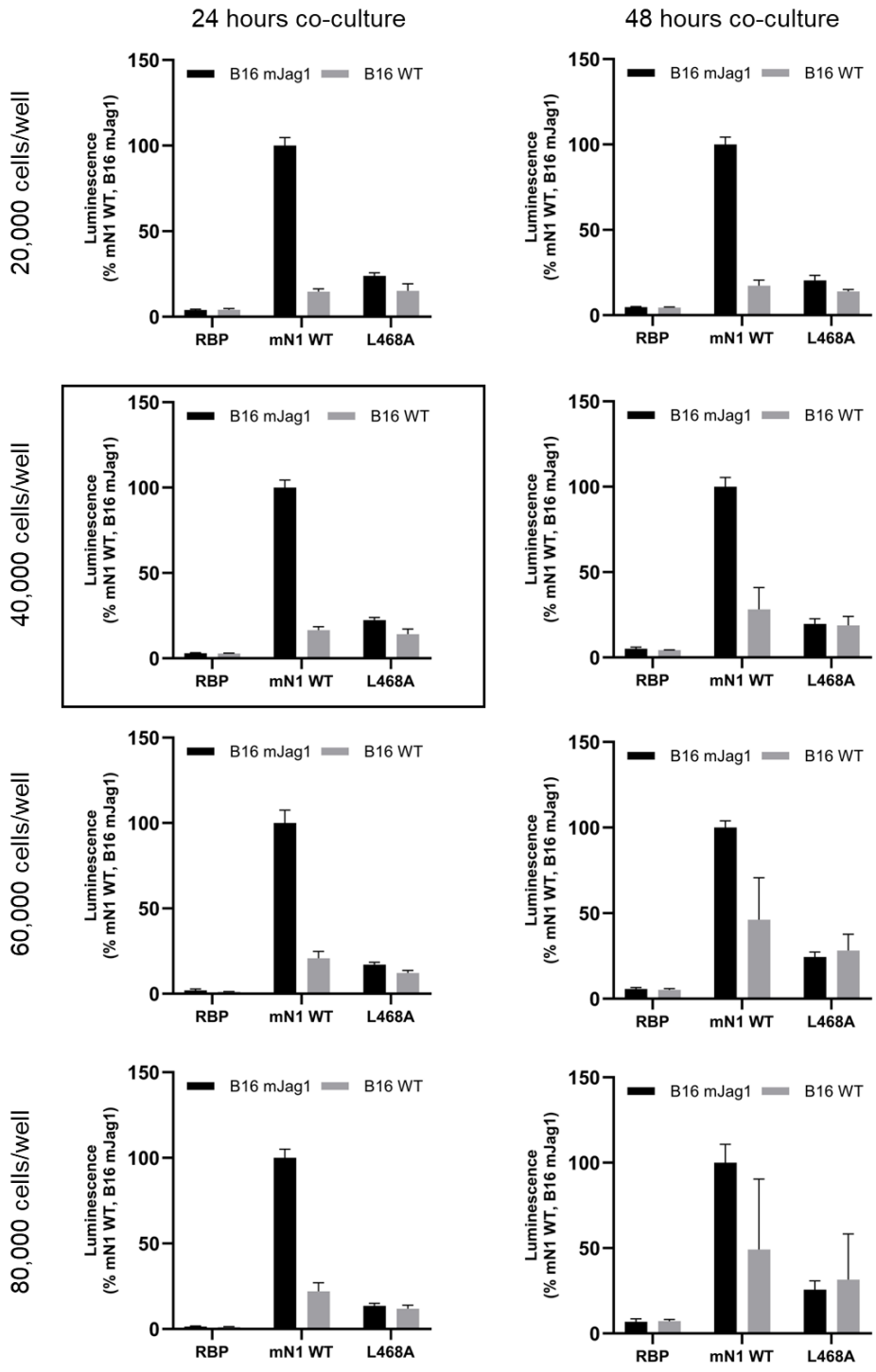


Figure 3.10. Cell number and co-culturing time optimisations for activation by B16 mJag1.

Activation assays for HEK-RBP, mN1 WT, and L468A cell lines grown with an equal number of B16 WT or mJag1 cells using 20,000 to 80,000 mN1 cells per well and 24 or 48 hours of co-culture. Signal in each case is shown relative to the mN1 WT co-cultured with B16 mJag1. Data presented as mean ± SD of 5 wells. Selected optimal condition which showed better cell attachment and more even cell distribution in the plate is indicated with a frame.

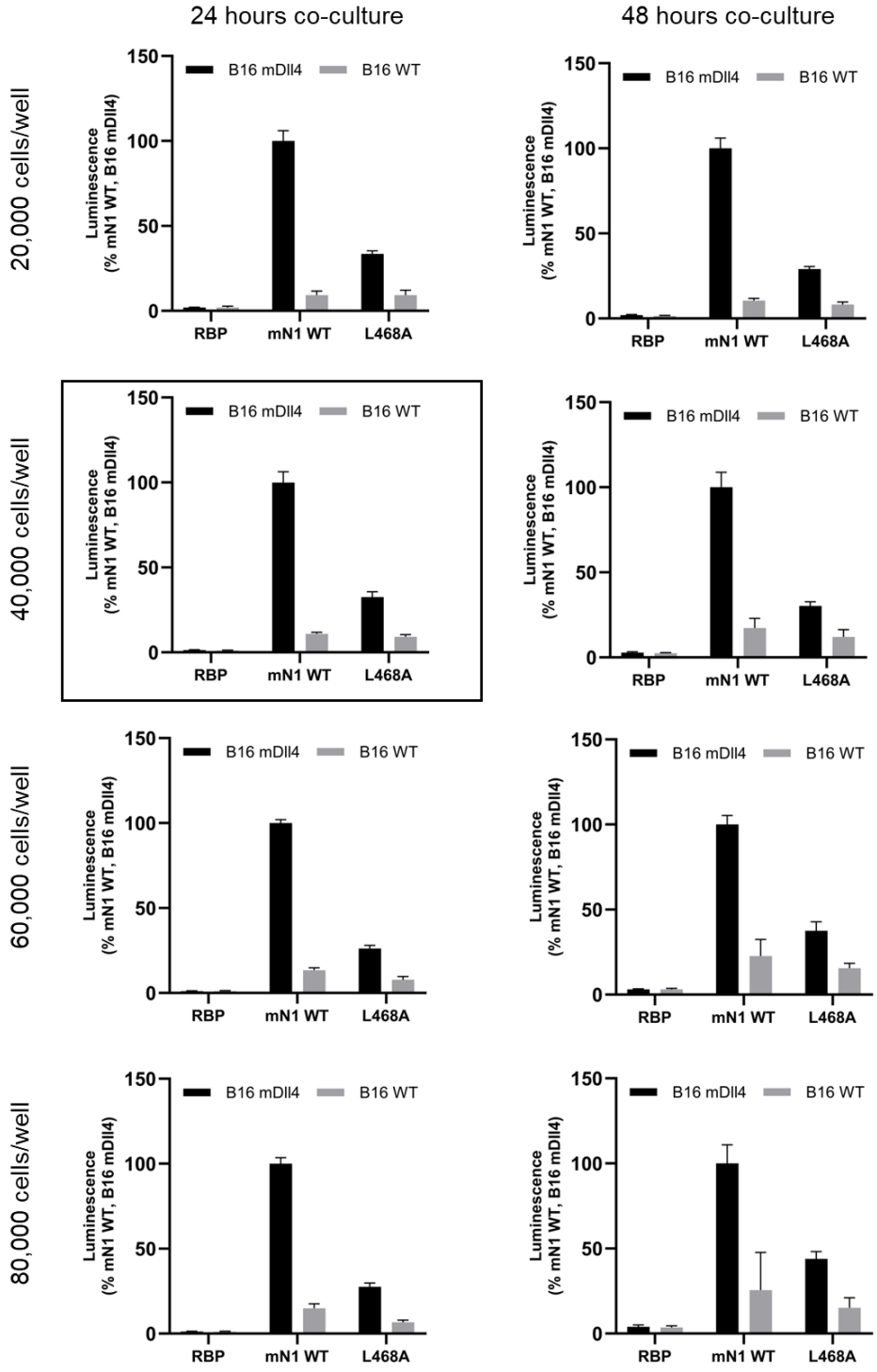


Figure 3.11. Cell number and co-culturing time optimisations for activation by B16 mDll4.

Activation assays for HEK-RBP, mN1 WT, and L468A cell lines grown with an equal number of B16 WT or mDll4 cells using 20,000 to 80,000 mN1 cells per well and 24 or 48 hours of co-culture. Signal in each case is shown relative to the mN1 WT co-cultured with B16 mDll4. Data presented as mean ± SD of 5 wells. Selected optimal condition which showed better cell attachment and more even cell distribution in the plate is indicated with a frame.

Substrate incubation time was also optimised with luminescence measured at 5-minute intervals after the addition of substrate solution to the 24-hour-co-cultured cells (Figure 3.12). For mJag1 co-culture, raw luminescence gradually increased after the addition of substrate and reached a maximum after 5-10 minutes. For mDll4 co-culture, raw luminescence gradually increased and started to plateau after 30 minutes of substrate incubation. When luminescence was shown relative to mN1 WT co-cultured with each ligand, the difference in luminescence between mN1 WT and L468A remained stable after 5 minutes of substrate incubation. In co-culture assays with mN1 variants, luminescence was measured 10 minutes after substrate addition.

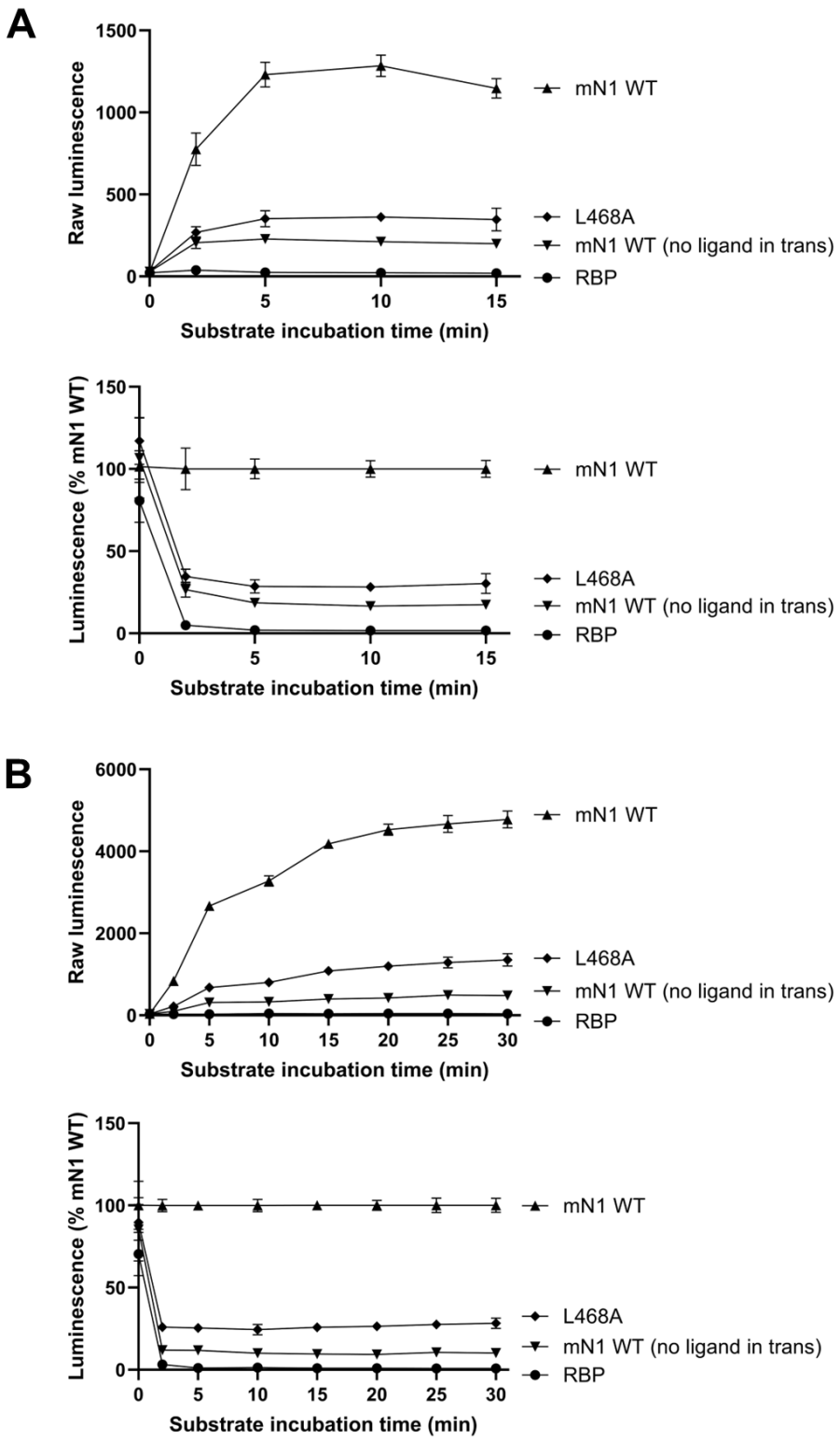
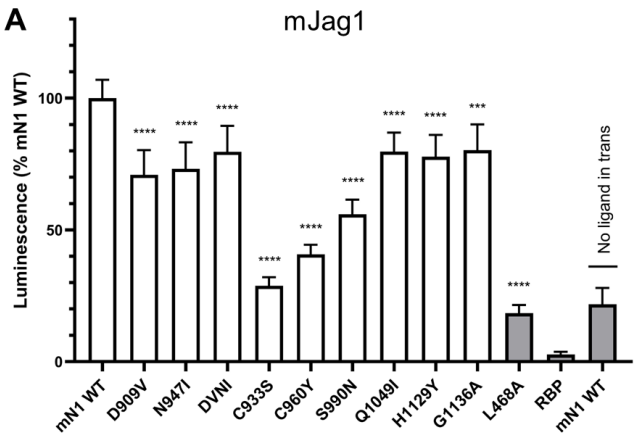


Figure 3.12. Substrate incubation time optimisation for co-culture-based activation assays.

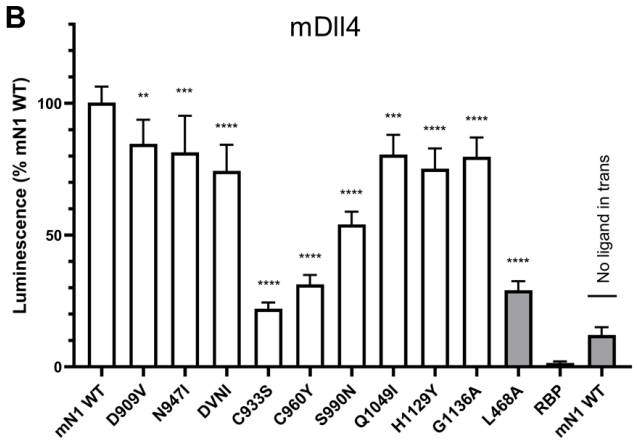
Luminescence was measured for HEK-RBP, mN1 WT and L468A cells co-cultured with (A) B16 mJag1 or (B) B16 mDll4 cells. Data for raw luminescence (top panel) and luminescence relative to mN1 WT (bottom panel) were presented as mean ± SD of 5 wells.

3.6.2 Co-culture trans-activation of Ax variants

Initial experiments using optimised conditions performed for the ligand binding-deficient L468A variant showed substantially lower activation by both mJag1 (Figure 3.13A) and mDll4 (Figure 3.13B), which was 20% (mJag1) to 30% (mDll4) of the signal obtained with N1 WT. All Ax variants reduced N1 activation by both ligands to different extents. The homozygous lethal variants reduced activation by mJag1 by 60-70% and mDll4 by 70-80%. The ageing-related variant S990N also led to a 45% reduction in activation by both ligands. *N* suppressor and *N* enhancer variants all showed a relatively modest (20-30%) but statistically significant decrease in activation by both ligands. The results were similar to those of plate-based activation assays, although the spread of the data was noticeably less marked than in the assay using purified ligands.



Cell line	Luminescence (% mN1 WT)	Statistical significance
mN1 WT	100 ± 7	
D909V	70.9 ± 9.4	****
N947I	73.2 ± 10	****
DVNI	79.6 ± 9.9	****
C933S	28.8 ± 3.2	****
C960Y	40.7 ± 3.7	****
S990N	55.9 ± 5.6	****
Q1049I	79.7 ± 7.3	****
H1129Y	77.8 ± 8.2	****
G1136A	80.3 ± 9.8	***
L468A	18.4 ± 3.1	****



Cell line	Luminescence (% mN1 WT)	Statistical significance
mN1 WT	100 ± 6.1	
D909V	84.6 ± 9.1	**
N947I	81.4 ± 13.9	***
DVNI	74.4 ± 9.9	****
C933S	22.1 ± 2.3	****
C960Y	31.3 ± 3.6	****
S990N	54.1 ± 4.8	****
Q1049I	80.5 ± 7.5	***
H1129Y	75.2 ± 7.7	****
G1136A	79.7 ± 7.3	****
L468A	29.1 ± 3.4	****

Figure 3.13. Trans-activation of mN1 Ax variants by ligands expressed in B16 cells.

Activation assays for mN1 Ax variants grown with B16 cells expressing (A) mJag1 or (B) mDll4 or B16 WT control cells (indicated by "No ligand in trans"). Graph (left panel) and table (right panel) show the combined results of four independent plates, each with five repeat wells. Signal in each case is shown relative to the mN1 WT. Data presented as mean ± SD. Statistical significance compared to mN1 WT was determined by Kruskal-Wallis test and Dunn's post hoc test (** = P < 0.01, *** = P < 0.001, **** = P < 0.0001).

3.7 Ligand binding ability of Ax variants

3.7.1 Assay design and optimisation

To study the effect of N1 variants on ligand binding, an assay comprising soluble ligands (in dimer form) and N1-expressing cell lines was developed based on the protocol used previously by Meng et al. (2022) (see Section 2.11). HEK-RBP mN1 cells were incubated

with hJAG1 or hDLL4 NE3-Fc-His proteins preincubated with anti-human IgG-AF488 antibody (Figure 3.14A) and analysed by flow cytometry in the presence of DAPI, which diffused into dead cells with truncated cell membranes (see Section 2.12). The median AF488 fluorescence intensity for viable cells of each variant was compared with that of mN1 WT to identify any changes in ligand binding ability.

Titrations of ligand concentration were performed with mN1 WT cell lines to determine the suitable concentration used for cell incubation (Figure 3.14B). hJAG1 NE3 binding reached a plateau at 200 nM while hDLL4 NE3 binding kept increasing even up to 1 μM. Two ligand concentrations, an unsaturated 50 nM (for both ligands) and a saturated (for hJAG1 NE3) 200 nM, were selected for use in assays with mN1 variants. To optimise ligand incubation time, mN1 WT and L468A cells which were used as the positive and negative controls were tested in incubations with 50 nM hJAG1 NE3 for one or two hours before analysis by flow cytometry (Figure 3.14C). The result suggested two hours of ligand incubation led to a greater difference in the quantities of ligand bound to mN1 WT and L468A cells.

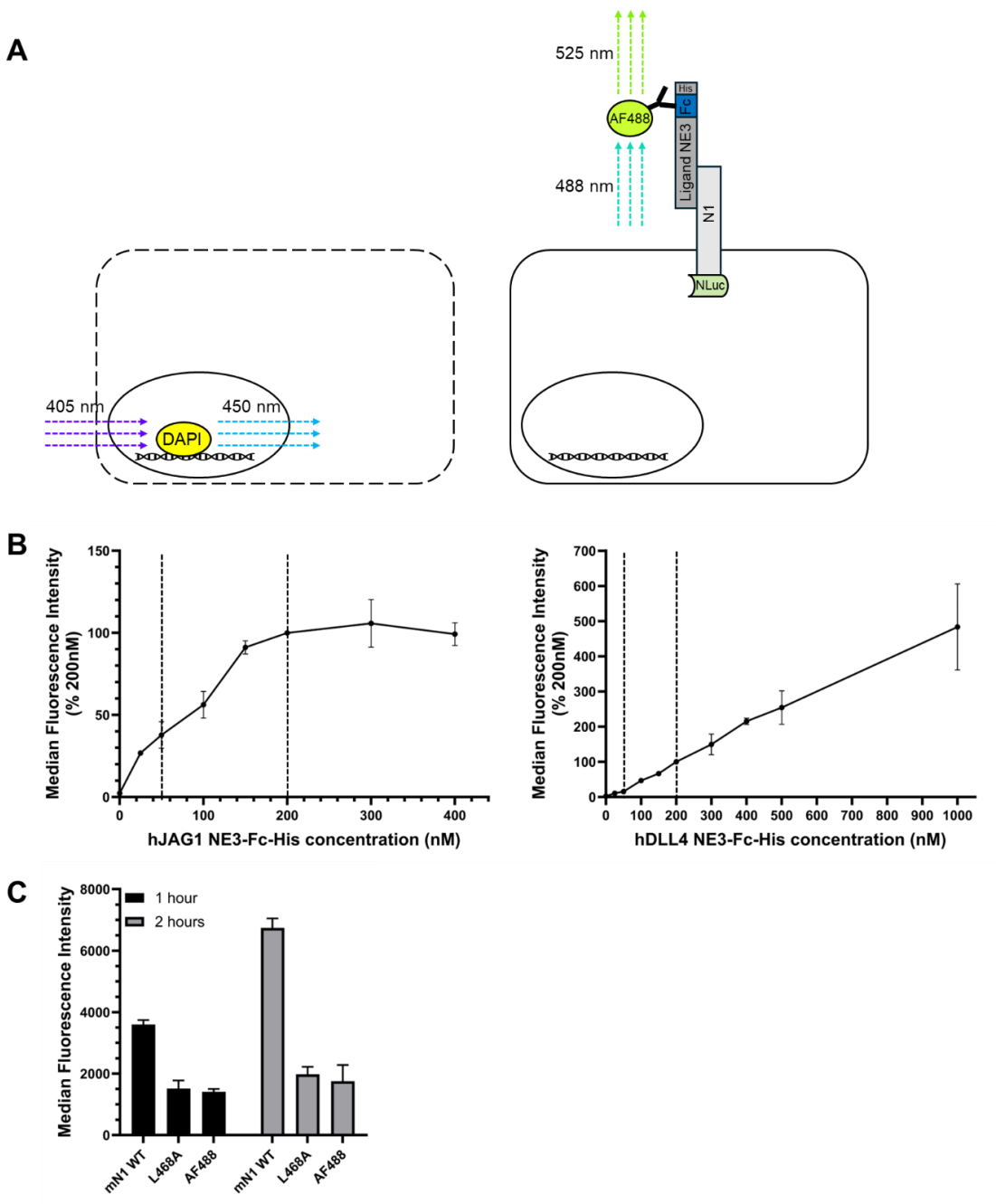


Figure 3.14. Optimisation for ligand binding assay.

(A) HEK-RBP mN1 cells were incubated with hJAG1 or hDLL4 NE3-Fc-His proteins preincubated with anti-human IgG-AF488 antibody and DAPI. Excitation and emission wavelengths for AF488 and DAPI are indicated. (B) Binding assay for mN1 WT cells incubated with different concentrations of hJAG1 (left panel) and hDLL4 NE3-Fc-His (right panel) for two hours. Signal in each case is shown relative to cells incubated with 200 nM ligand. Data presented as mean ± SD. Concentrations selected for use in assays (50 nM and 200 nM) are indicated by dashed lines. (C) Binding assay for mN1 WT cells incubated with 50 nM of hJAG1 NE3-Fc-His for one or two hours. Data presented as mean ± SD.

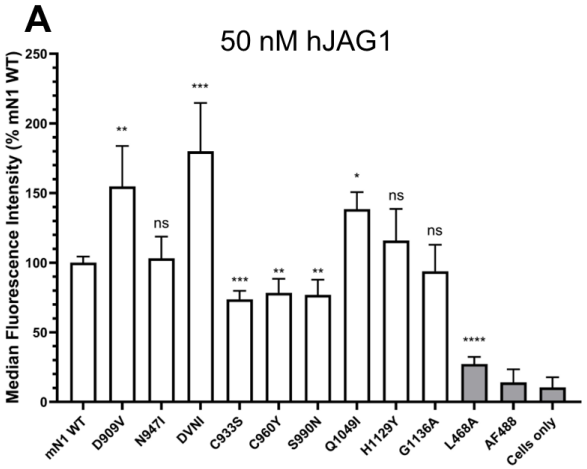
3.7.2 Ligand binding of Ax variants

Initial experiments performed for the ligand binding-deficient L468A variant showed a 90% reduction in binding of both hJAG1 NE3 (Figure 3.15) and hDLL4 NE3 (Figure 3.16) at both ligand concentrations used, suggesting the assay can discriminate on the basis of binding ability. Overall trends observed for both ligands at each concentration tested are similar, with some differences in statistical significance.

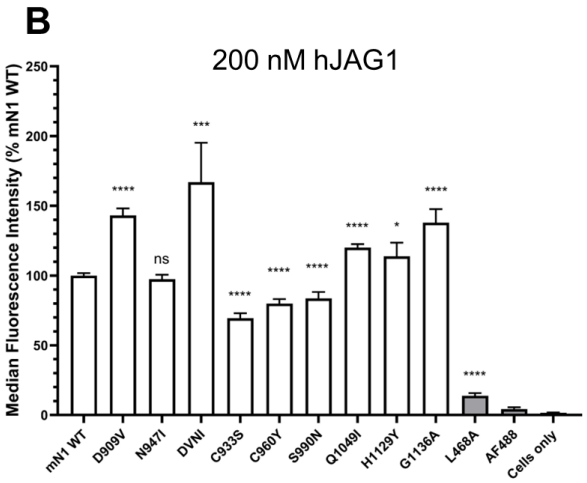
The variants shown previously in FACS-based measurements of cell surface N1 level to have reduced cell surface levels (Figure 3.5B), also showed reduced levels of ligand binding. However, their reductions in ligand binding were smaller than their reductions in cell surface expression. The homozygous lethal variants C960Y and C933S reduced the binding of both ligands by 30-40% while reducing N1 surface expression by 50-60%. Also, while the ageing-related variant S990N reduced cell surface level by 30%, it reduced the binding of both ligands by 20% (though the decrease was not statistically significant at 200 nM hDLL4 NE3).

Variants which showed WT levels of Notch cell surface expression showed either similar binding of ligands (N947I), or increased binding (G1136A, H1129Y). The *N* enhancer G1136A appeared to increase hJAG1 NE3 binding at 200 nM ligand concentrations by 35%, but had a similar ligand binding level compared to WT in other assay conditions. Also, the *N* enhancer H1129Y increased binding to hJAG1 NE3 by 15% (statistically significant at 200 nM concentration) but had no significant effect on the N1 binding to

hDLL4 NE3. The *N* suppressor N947I showed similar ligand binding levels compared to WT at both ligand concentrations. Variants which showed moderate increases in their cell surface expression, *N* suppressor D909V, DVNI double variant and the *N* enhancer Q1049I all showed increased ligand binding levels for both ligands, though this was not statistically significant for D909V and Q1049I at 200 nM hDLL4 NE3. This is most likely due to the higher levels of expression on the cell surface.



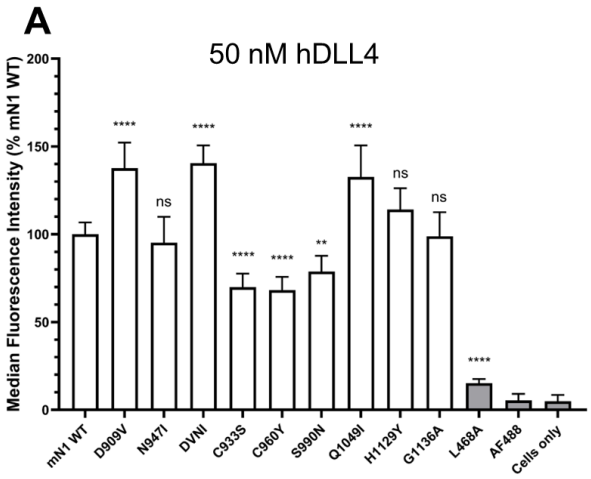
Cell line	Median fluorescence intensity (% mN1 WT)	Statistical significance
mN1 WT	100 ± 4.4	
D909V	154.8 ± 29	**
N947I	103.1 ± 15.6	ns
DVNI	180 ± 34.7	***
C933S	73.8 ± 6	***
C960Y	78.4 ± 10.1	**
S990N	76.9 ± 11	**
Q1049I	138.5 ± 12.2	*
H1129Y	115.9 ± 22.6	ns
G1136A	93.8 ± 19	ns
L468A	27.2 ± 5.1	****



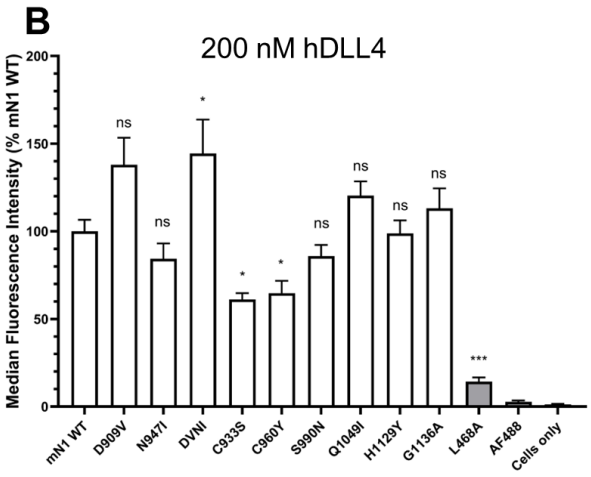
Cell line	Median fluorescence intensity (% mN1 WT)	Statistical significance
mN1 WT	100 ± 1.7	
D909V	143.2 ± 5	****
N947I	97.4 ± 3.3	ns
DVNI	166.9 ± 28.3	***
C933S	69.5 ±3.5	****
C960Y	79.9 ± 3.2	****
S990N	83.7 ± 4.5	****
Q1049I	120.1 ± 2.5	****
H1129Y	113.8 ± 9.8	*
G1136A	138 ± 9.6	****
L468A	13.8 ± 1.9	****

Figure 3.15. Quantification of hJAG1 NE3 bound to mN1 Ax variants.

mN1 cells were incubated with (A) 50 nM or (B) 200 nM hJAG1 NE3-Fc-His and analysed by flow cytometry. Graph (left panel) and table (right panel) for 50 nM ligand show the combined results of four biological repeats, each with at least two technical repeats. Graph (left panel) and table (right penal) for 200 nM ligand show the combined results of three biological repeats, each with three technical repeats. Median fluorescence intensity for AF488 in each case is shown relative to the mN1 WT. Data presented as mean ± SD. Statistical significance compared to mN1 WT was determined by Kruskal-Wallis test and Dunn's post hoc test (50nM) or Welch's ANOVA and Dunnett's post hoc test (200nM) (ns = not significant, * = $P < 0.05$, ** = $P < 0.01$, *** = $P < 0.001$, **** = $P < 0.0001$).



Cell line	Median fluorescence intensity (% mN1 WT)	Statistical significance
mN1 WT	100 ± 6.8	
D909V	137.7 ± 14.5	****
N947I	95.2 ± 14.7	ns
DVNI	140.5 ± 10.1	****
C933S	69.9 ± 7.8	****
C960Y	68.2 ± 7.5	****
S990N	78.8 ± 9	**
Q1049I	132.7 ± 17.9	****
H1129Y	114.1 ± 12.1	ns
G1136A	98.9 ± 13.7	ns
L468A	15.2 ± 2.4	****



Cell line	Median fluorescence intensity (% mN1 WT)	Statistical significance
mN1 WT	100 ± 6.5	
D909V	138 ± 15.4	ns
N947I	84.4 ± 8.7	ns
DVNI	144.4 ± 19.3	*
C933S	61.2 ± 3.6	*
C960Y	64.7 ± 7	*
S990N	85.9 ± 6.3	ns
Q1049I	120.4 ± 8.1	ns
H1129Y	98.8 ± 7.4	ns
G1136A	113.2 ± 11.3	ns
L468A	14.3 ± 2.4	***

Figure 3.16. Quantification of hDLL4 NE3 bound to mN1 Ax variants.

mN1 cells were incubated with (A) 50 nM or (B) 200 nM hDLL4 NE3-Fc-His and analysed by flow cytometry. Graph (left panel) and table (right panel) show the combined results of four biological repeats, each with at least two technical repeats. Median fluorescence intensity for AF488 in each case is shown relative to the mN1 WT. Data presented as mean ± SD. Statistical significance compared to mN1 WT was determined by ordinary one-way ANOVA and Dunnett's post hoc test (50nM) or Kruskal-Wallis test and Dunn's post hoc test (200nM) (ns = not significant, * = P < 0.05, ** = P < 0.01, *** = P < 0.001, **** = P < 0.0001).

3.8 Discussion

Assays validation and confidence

In this chapter, the impact of mN1 variants on cell surface expression, trans-activation

and ligand binding were studied by optimised cell-based assays in order to understand the involvement of different receptor domains in Notch signalling (Table 3.2 and 3.3). The ligand binding-deficient variant mN1 L468A was employed as a negative control for all assays. Cell surface N1 quantification suggested the L468A variant had a comparable cell surface number to WT (Figure 3.5), while having substantially reduced trans-activation (Figure 3.9 and 3.13) and ligand-binding ability (Figure 3.15 and 3.16). The reduction in trans-activation levels was consistent with the observed reduced ability to bind ligands.

Similar trends were observed in the two methods (ligand-independent activation and FACS-based direct cell surface quantification) used to measure the effects of Ax variants on cell surface N1 level (Table 3.2). In ligand-independent activation, the *N* suppressor D909V, DVNI double variant and the *N* enhancer Q1049I results were not statistically significantly different from WT but the error bars in this experiment were generally wider than for direct cell surface quantification (Figure 3.5). Results for G1136A did show a small difference from WT ($P < 0.05$) but not in direct quantification (Figure 3.5). The results of plate-based and co-culture-based activation assays agreed well, indicating confidence in the conclusions drawn for the variants' effects on N1 trans-activation (Table 3.3, compare Figure 3.9 and 3.13). Ligand binding assays also showed similar trends with two ligand concentrations used (Table 3.2, Figure 3.15 and 3.16).

Table 3.2. Summary of the effects of Ax variants on N1 cell surface level and ligand binding.

The results for cell surface level measured by ligand-independent activation (EGTA) and FACS-based assay (Figure 3.5) and ligand binding level using 50 nM and 200 nM ligand concentrations (Figure 3.15 and 3.16) for N1 Ax variants compared with N1 WT. Results for *N* suppressor, homozygous lethal and *N* enhancer variants are coloured in blue, red and green respectively. Variants showing no statistically significant change compared with WT are indicated by "ns". Variants showing statistically significant reductions or increases are indicated by "-" or "+" with one sign equals to a change of 10% of N1 WT.

N1 variant	Cell surface level		Binding to JAG1 NE3		Binding to DLL4 NE3	
	EGTA	FACS	50 nM	200nM	50 nM	200nM
D909V	ns	++++	+++++	++++	++++	ns
N947I	ns	ns	ns	ns	ns	ns
DVNI	ns	++	++++++++	+++++++	++++	++++
C933S	-----	-----	---	---	---	----
C960Y	-----	-----	--	--	---	----
S990N	----	---	--	--	--	ns
Q1049I	ns	++	++++	++	+++	ns
H1129Y	ns	ns	ns	+	ns	ns
G1136A	-	ns	ns	++++	ns	ns
L468A	ns	+++	-------	--------	--------	--------

Ax homozygous lethal and ageing-related variants reduced cell surface N1 levels

mN1 homologues of dN *Ax* homozygous lethal variants (C933S and C960Y) and S990N identified in ageing oesophageal and skin tissues showed reduced expression levels on the cell surface in both assays. These variants showed reduced trans-activation (Table 3.3) and ligand binding consistent with lower cell surface levels, although the reduction in ligand binding (e.g. ~30% less than WT for C933S) was smaller than one might expect from the measured cell surface level (e.g. ~50% less than WT for C933S) (Table 3.2). This may be due to an overcompensation for decreases in binding caused by the conditions of the ligand binding assay, which is avidity-driven, or due to variant receptors

in a different form compared to WT on the cell surface, possibly aggregating due to misfolding.

Table 3.3. Summary of the effects of Ax variants on N1 trans-activation.

The results for plate-based (Figure 3.9) and co-culture-based (Figure 3.13) trans-activation assays for N1 Ax variants compared with N1 WT. Results for *N* suppressor, homozygous lethal and *N* enhancer variants are coloured in blue, red and green respectively. Variants showing no statistically significant change compared with WT are indicated by "ns". Variants showing statistically significant reductions or increases are indicated by "-" or "+" with one sign equals to a change of 10% of N1 WT.

N1 variant	Trans-activation by Jag1		Trans-activation by Dll4	
	Plate	Co-culture	Plate	Co-culture
D909V	ns	- - -	ns	- -
N947I	- - -	- - -	- -	- -
DVNI	- - -	- -	ns	- - -
C933S	- - - - - - -	- - - - - - -	- - - - - - -	- - - - - - - -
C960Y	- - - - - - -	- - - - - -	- - - - - - -	- - - - - - -
S990N	- - - - -	- - - - -	- - - - -	- - - -
Q1049I	ns	- -	ns	- -
H1129Y	- -	- -	- -	- -
G1136A	- - -	- -	ns	- -
L468A	- - - - - - -	- - - - - - - -	- - - - - - -	- - - - - - -

<u>*Ax N* suppressor and enhancer variants reduced N1 trans-activation levels</u>

While having WT or raised cell surface levels, mN1 homologues of dN *Ax N* suppressor variants in EGF24-25 (D909V and N947I and the DVNI double variant) which affect calcium-binding consensus residues, and *N* enhancer variants in EGF 27-29 (Q1049I, H1129Y and G1136A) which do not, all reduced N1 trans-activation by 20-30% (Table 3.3). This loss of activation was however less pronounced than that observed for L468A. This suggests the native properties of the Ax region are required for optimal trans-

activation, but play a less critical role than the LBR.

Ax N suppressor and enhancer variants did not reduce the amount of ligand binding

The amount of ligand NE3 construct bound to *N* suppressor and enhancer variant cell lines mainly followed the trend observed for Notch cell surface expression measured by FACS-based assay (Table 3.2), Overall the binding assays revealed no major reduction in ligand binding as seen for L468A, which would explain the reduction in trans-activation seen in the Ax variants expressed at WT or higher levels on the cell surface. However, the increased JAG1 NE3 binding shown by *N* enhancer variants H1129Y and G1136A suggested these substitutions may affect a property of the receptor which impacts the ability of ligands to bind.

It should be noted that ligand NE3 constructs, instead of full-length ligands, were used in ligand binding assays. While previous studies demonstrated that C2 and DSL domains (and EGF1-3 in Jag1) form the main interfaces with Notch (Taylor *et al.*, 2014; Luca *et al.*, 2015, 2017), other domains in the ligand may also interact with the receptor (Zeronian *et al.*, 2021). Therefore, using ligand NE3 instead of full-length constructs may overlook the effect of N1 mutations on interaction with other domains of the ligands or when the ligands are in their native full-length conformation. The assay also assumes that the Notch variants are all presented on the cell surface in the same form (monomer/dimer). In addition, while hJAG1 NE3 binding reached a plateau at 200 nM, hDLL4 NE3 binding kept increasing even up to 1 mM, which might be due to aggregation of hDLL4 NE3 and

N1 on the cell surface or aggregation of hDLL4 NE3 via Fc tags in the constructs. Full-length ligand constructs without Fc tags could be used in future to include the effect of N1 variants on interaction with other domains of the ligands. Additionally, binding assays where ligands are presented on a cell membrane, such as the cell aggregation assay (Brückner *et al.*, 2000), may be conducted to confirm the effect of variants on binding when the ligands are in the native orientation.

4 Investigating the role of the Abruptex region in Notch1 cis-inhibition by JAG1

4.1 Introduction

In Chapter 3, activation assays performed for mN1 cell lines suggested Ax substitutions had negative effects on ligand-dependent trans-activation. For the Ax variants expressed at normal levels on the cell surface, these data do not provide an obvious explanation as to why they induce phenotypes in flies that may be perceived as Notch-enhancing and opposite to that caused by a null *Notch* allele (see Section 1.2.4) (Nasarenko, 1930; Kelley *et al.*, 1987). They may alter Notch signalling in a more complex way than just an effect on trans-activation. One possibility is that these Ax variants may change Notch cis-inhibition by ligands expressed in the same cell, as cis-inhibition is known to contribute to the regulation of the D/V boundary formation in the wing (de Celis and Bray, 1997; Micchelli, Rulifson and Blair, 1997) (see Section 1.5.4). To study the effect of JAG1 expressed in cis on Ax variant activity, quantitative assays were developed in this chapter using initially a mN1 WT reporter cell line transiently transfected to express either WT or receptor binding-deficient ligand variants. Following the establishment of the cis-inhibition assay, experiments were performed with Ax variants to investigate their response.

4.2 JAG1 cis-inhibition assay design and optimisation

HEK-RBP mN1 cells were transiently transfected in a 6-well plate with a pcDNA3.1(+) plasmid encoding native full-length hJAG1 (cis-JAG1) or an empty vector (EV) (see Section 2.6.3) and split into a 96-well plate (40,000 cells per well) 24 hours after the

transfection. B16 cells stably expressing mJag1 or mDll4 or non-ligand-expressing control cells (B16 WT control) were layered onto transfected HEK-RBP mN1 cells the next day and co-cultured overnight (Figure 4.1A). Interaction of the receptor with cis-JAG1 expressed in full-length form in transfected cells should inhibit mN1 trans-activation, shown by a reduction in luminescence relative to the signal obtained with EV transfection.

For assay optimisation, a titration of cis-JAG1 plasmid quantity was initially performed to determine the relationship between the amount of cis-JAG1 plasmid transfected and cell surface expression of ligand. JAG1 levels on non-permeabilised mN1 WT cells were measured by flow cytometry using an anti-JAG1 (J1-65D) antibody targeting the NE3 region (Masiero *et al.*, 2019) (see Section 2.10 and 2.12). The median fluorescence intensity measured for each cell showed that the cell surface JAG1 level observed was dependent upon cis-JAG1 plasmid concentration and had not yet reached a plateau when 4 µg was added per well (Figure 4.1B). Concomitantly, when co-cultured with B16 ligand-expressing cells (either mJag1 or mDll4), the Notch activation signal of transfected mN1 WT cells decreased and started to plateau at around 4 µg cis-JAG1 plasmid per well, indicative of effective cis-inhibition (Figure 4.1C). Therefore, 4 µg cis-JAG1 plasmid per well was added during subsequent transfections (see Section 2.9.3). It should be noted that transfecting mN1 lines with an equivalent amount of EV, instead of cis-JAG1, did not result in reduced activation levels. Furthermore, Notch activation was only seen when using B16 ligand-expressing cells, not when using B16 WT control cells (Figure

4.1C).

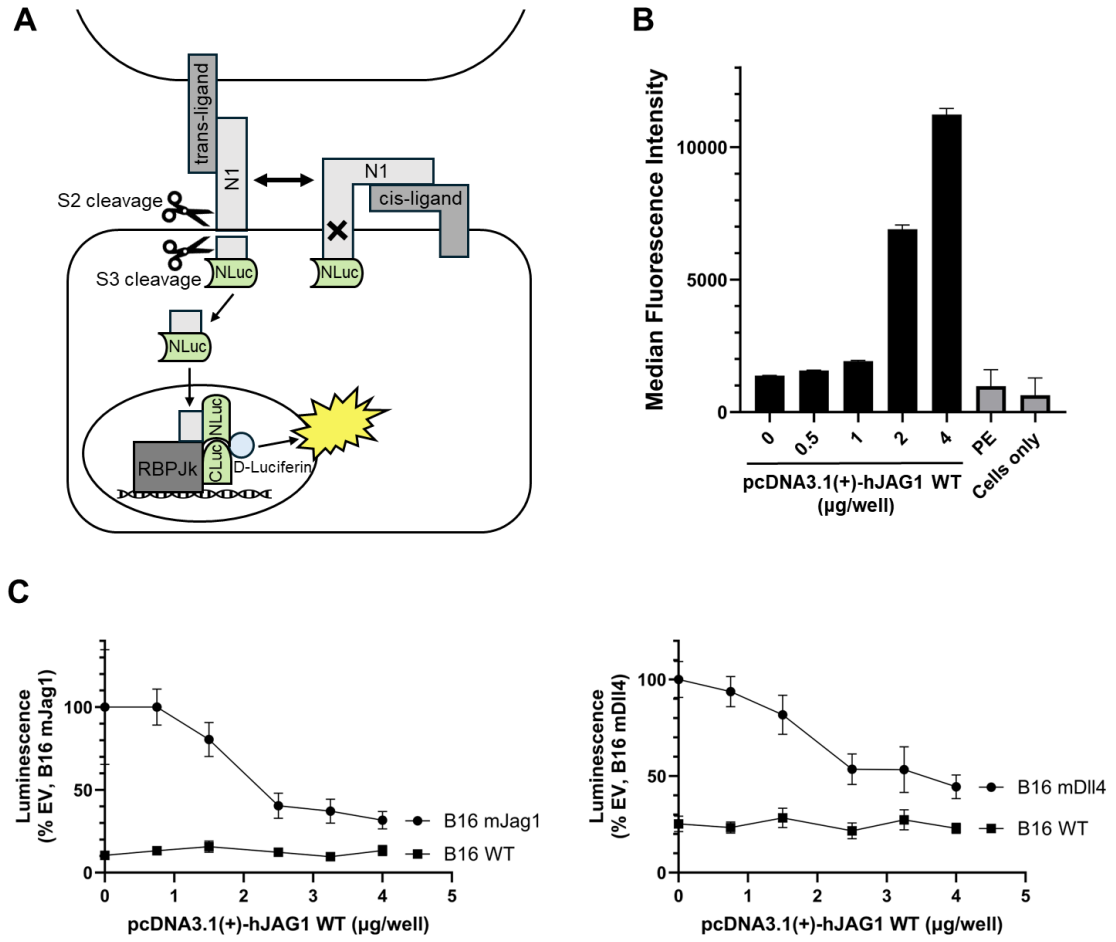


Figure 4.1. Optimisation for cis-inhibition assay using cis-JAG1.

(A) HEK-RBP mN1 cells were transfected with pcDNA3.1(+) plasmids encoding either full-length JAG1 or DLL4, producing ligands that can cis-inhibit mN1 and reduce the N1 activation level. This schematic shows the cis-complex at the cell surface and in one conformation, but this is not proven. (B) mN1 WT cells were transfected with 0-4 µg of cis-JAG1 WT plasmid per well in a 6-well plate and stained with anti-JAG1 (J1-65D) primary antibody and a PE-conjugated secondary antibody. The median PE fluorescence intensity for each cell was quantified by flow cytometry. Data presented as mean ± SD. (C) mN1 WT cells transfected with 0-4 µg of cis-JAG1 WT plasmid per well were co-cultured either with B16 WT control cells or B16 cells expressing mJag1 (left panel) or mDll4 (right panel). Luminescence signal produced in each case is shown relative to cells transfected with an equal quantity of EV and co-cultured with ligand-expressing B16 cells. Data presented as mean ± SD.

4.3 *JAG1* RNA expression verification

Since the transfections for cis-inhibition analysis were transient, it was important to verify that the quantity of cis-JAG1 expressed in each cell line was reproducible to allow comparative analyses. RT-PCRs (see Section 2.4) using cDNA-specific primers (see Appendix A) were performed for mN1 WT and variant cell lines transfected with cis-JAG1 or EV and examined by gel electrophoresis to confirm transfection efficiency and RNA expression. For cells transfected with plasmids encoding cis-JAG1 WT or a receptor binding-deficient F207A/E228K (cis-JAG1 FAEK) double variant (Meng *et al.*, 2022), RT-PCRs for *JAG1* RNA expression produced bands of 250 bp with equivalent intensity, suggesting comparable *JAG1* RNA expression (Figure 4.2). RT-PCR analysis of EV cells produced a minor band of 250 bp, suggesting some JAG1 was produced endogenously in the mN1 line at a low level (<10% cis-JAG1 transfected). RT-PCRs for *mN1* RNA expression were also performed on RNA samples of mN1 lines transfected with cis-plasmid (Figure 4.3). This resulted in a specific band of 337 bp of similar intensity in each sample, irrespective of whether or not cis-JAG1 or EV plasmid was transfected, This showed that transient transfection/expression of cis-JAG1 did not affect stable mN1 expression. RT-PCRs for *GAPDH*, a constitutively expressed gene, which produced a band of 237 bp, were performed alongside to ensure each reverse transcription reaction was performed with the same starting concentration of RNA (Figure 4.4). No bands were observed for PCR amplification of RNA samples without reverse transcription, suggesting there was no DNA contamination in the RNA samples.

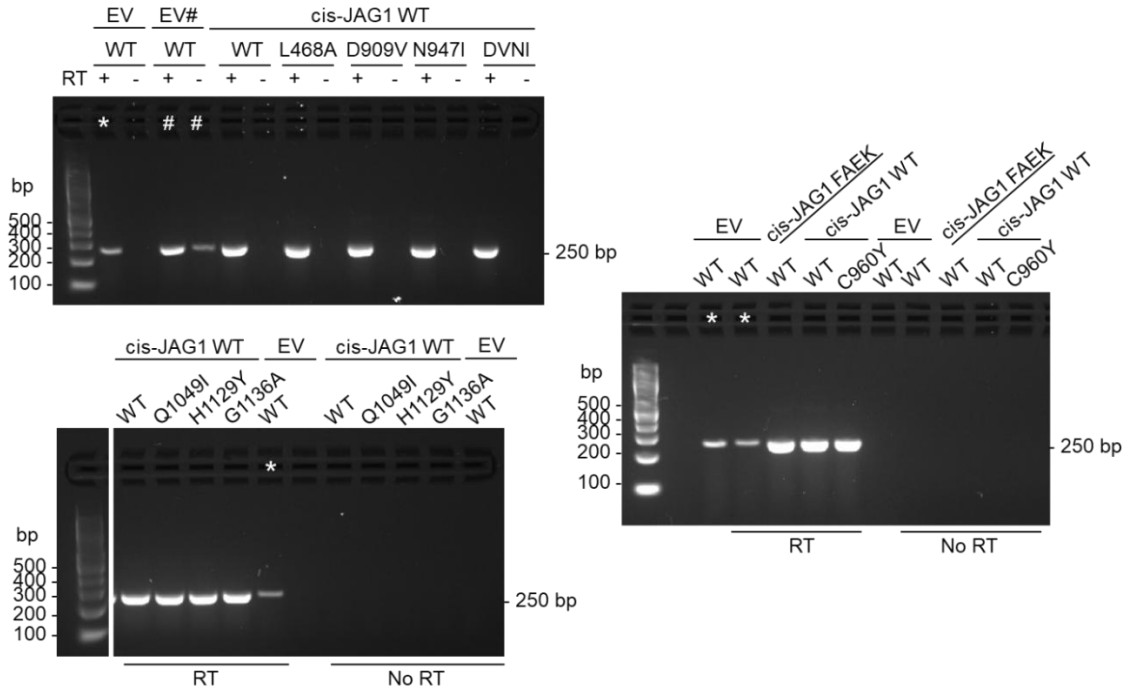


Figure 4.2. RT-PCR for *JAG1* expressed in mN1 cells transfected with cis-JAG1 plasmid.

RNA was extracted from HEK-RBP mN1 WT and Ax variant (D909V, N947I, DVNI, C960Y, Q1049I, H1129Y, G1136A) cells transfected with pcDNA3.1(+) plasmids encoding JAG1 WT or JAG1 FAEK variant or EV (indicated by labels). PCRs to amplify a 250 bp region in *JAG1* cDNA were performed for RNA samples with and without RT (indicated by labels). Note the presence of a small amount of *JAG1* RNA in EV lanes (white asterisk) which corresponds to a low level of endogenous JAG1 expression in the host cell line. RNA sample with DNA contamination is indicated with "#" and was not used for further RT-PCR analysis. PCR products were run on a 2.5% agarose TBE gel.

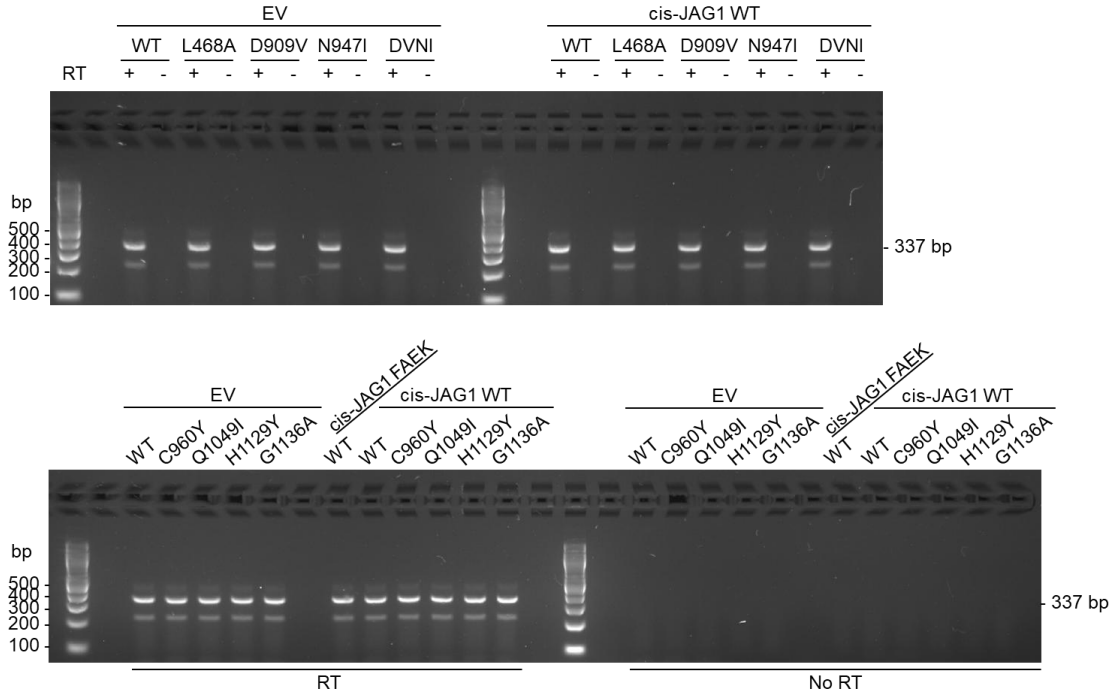


Figure 4.3. RT-PCR for *mN1* expressed in mN1 cells transfected with cis-JAG1 plasmid.

RNA was extracted from HEK-RBP mN1 WT, L468A and Ax variant (D909V, N947I, DVNI, C960Y, Q1049I, H1129Y, G1136A) cells transfected with pcDNA3.1(+) plasmids encoding JAG1 WT or JAG1 FAEK variant or EV (indicated by labels). PCRs to amplify a 337 bp region in *mN1* cDNA were performed for RNA samples with and without RT (indicated by labels). PCR products were run on a 2.5% agarose TBE gel.

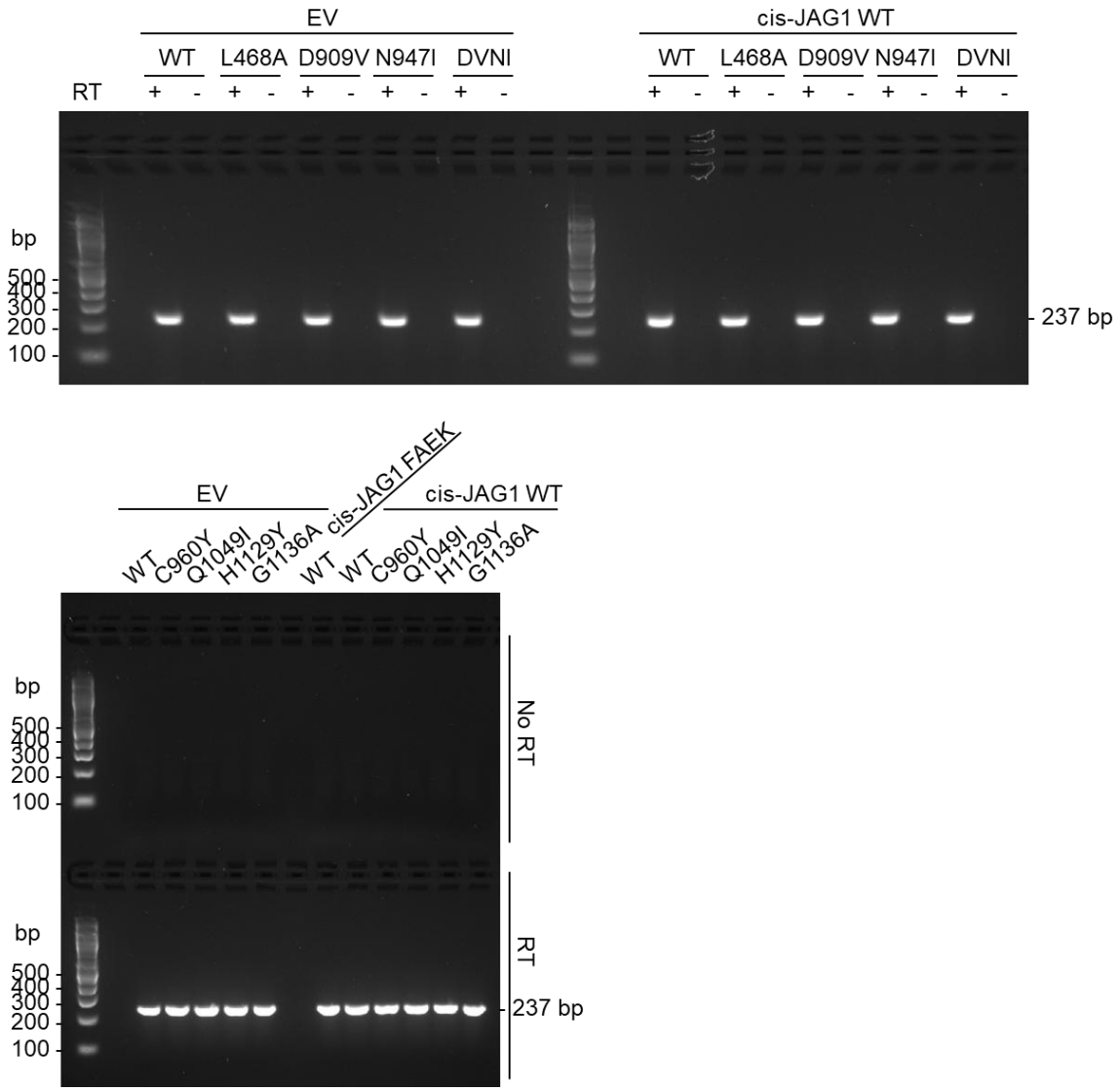


Figure 4.4. RT-PCR for *GAPDH* expressed in mN1 cells transfected with cis-JAG1 plasmid.

RNA was extracted from HEK-RBP mN1 WT, L468A and Ax variant (D909V, N947I, DVNI, C960Y, Q1049I, H1129Y, G1136A) cells transfected with pcDNA3.1(+) plasmids encoding JAG1 WT or JAG1 FAEK variant or EV (indicated by labels). PCRs to amplify a 237 bp region in *GAPDH* cDNA were performed for RNA samples with and without RT (indicated by labels). PCR products were run on a 2.5% agarose TBE gel.

4.4 Effect of cis-JAG1 expression on N1 WT activation

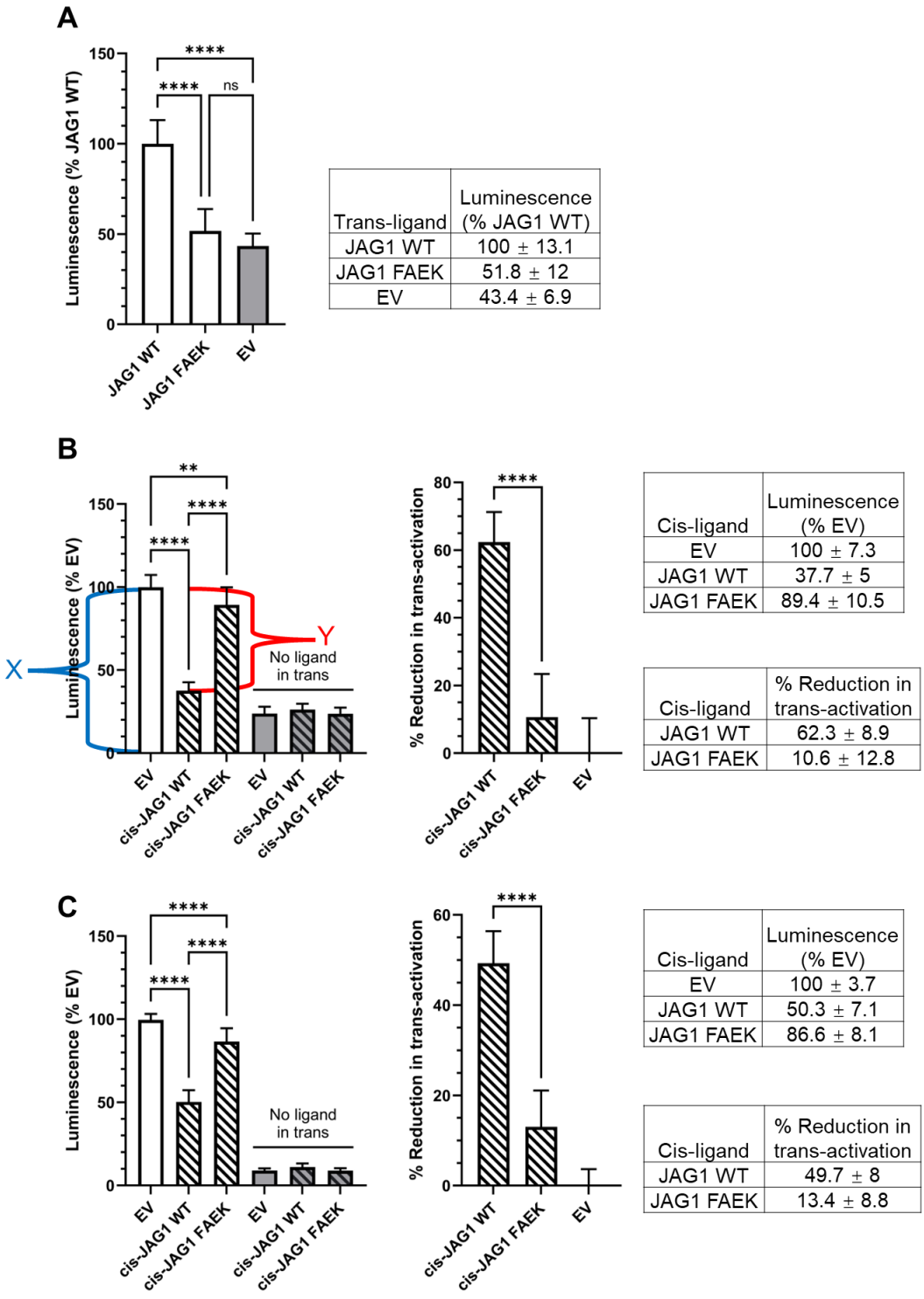
Transient transfections of mN1 WT cells were performed to study the behaviour of JAG1 WT and the FAEK variants in cis-inhibition. Initially, plasmids encoding each of these

were transfected into HEK293T cells and tested in a trans-activation assay by co-culturing with the mN1 WT reporter line. These data showed that compared to JAG1 WT, the FAEK variant was unable to induce mN1 trans-activation, with no significant difference in activation level compared to EV (Figure 4.5A).

Subsequently, the mN1 reporter line was transfected with cis-JAG1 WT (Figure 4.1A). When co-cultured with mJag1-expressing B16 cells, luminescence was reduced to around 40% of levels seen with EV (Figure 4.5B). A similar trend was observed when mDll4-expressing B16 cells were used (Figure 4.5C), suggesting in both cases cis-inhibition was achieved. However, cis-JAG1 WT was somewhat less effective at inhibiting mN1 activation in the presence of trans-Dll4 (~50% reduction in luminescence compared with ~60% reduction seen with trans-Jag1). Cis-JAG1 FAEK was ineffective at cis-inhibition irrespective of trans-ligand used, with the reporter cell line retaining 85-90% of the luminescence levels seen with EV.

As a direct measurement of the strength of cis-inhibition observed, % reduction in trans-activation was calculated for mN1 WT using the equation *(Luminescence with EV – Luminescence with cis-ligand)/Luminescence with EV x100* (Y/X x100 in Figure 4.5B). A high % reduction in trans-activation value corresponds to strong cis-inhibition. While cis-JAG1 WT expression in the mN1 WT line resulted in strong cis-inhibition ~60% (trans-mJag1) and ~50% (trans-Dll4) respectively, cis-JAG1 FAEK expression only resulted in very weak cis-inhibition of ~10-15% for both trans-ligands (Figure 4.5B and C). When

grown with B16 WT control cells, mN1 cells transfected with EV, cis-JAG1 WT or cis-JAG1 FAEK had similar basal levels of activation (see Figure 4.5 B and C, no ligand in trans). These assays were also performed using plate-coated ligand NE3 proteins instead of co-culture with ligand-expressing B16 cells. Similar results were obtained (Appendix F, Figure F.1), although as observed in Chapter 3, error bars were wider for plate-coated ligands.



Trans-ligand	Luminescence (% JAG1 WT)
JAG1 WT	100 ± 13.1
JAG1 FAEK	51.8 ± 12
EV	43.4 ± 6.9

Cis-ligand	Luminescence (% EV)
EV	100 ± 7.3
JAG1 WT	37.7 ± 5
JAG1 FAEK	89.4 ± 10.5

Cis-ligand	% Reduction in trans-activation
JAG1 WT	62.3 ± 8.9
JAG1 FAEK	10.6 ± 12.8

Cis-ligand	Luminescence (% EV)
EV	100 ± 3.7
JAG1 WT	50.3 ± 7.1
JAG1 FAEK	86.6 ± 8.1

Cis-ligand	% Reduction in trans-activation
JAG1 WT	49.7 ± 8
JAG1 FAEK	13.4 ± 8.8

Figure 4.5. Trans-activation of mN1 WT cells transfected with cis-JAG1 plasmid.

(A) Activation of mN1 WT cells by co-culturing overnight with HEK293T cells transfected with pcDNA3.1(+) plasmids encoding JAG1 WT, JAG1 FAEK or EV (see Section 2.6.3). Signal in each case is shown relative to cells co-cultured with JAG1 WT-expressing HEK293T. (B, C) Cis-inhibition assays by cis-JAG1 WT and FAEK for mN1 WT cells grown with B16 cells expressing (B) mJag1 or (C) mDll4 or B16 WT control cells (indicated by “No ligand in trans”).

Graph (left panel) and table (right panel) show the combined results of four independent plates, each with five repeat wells. Luminescence signal in each case is shown relative to cells transfected with EV. As a measure of the extent of cis-inhibition of mN1, % reduction in trans-activation was calculated by *(Luminescence with EV – Luminescence with cis-ligand)/Luminescence with EV x 100,* which was equivalent to Y/X (x100) as indicated in (B). Data presented as mean ± SD. Statistical significance was determined in (A) by Kruskal-Wallis test and Dunn's post hoc test, in (B) and (C) by Welch's ANOVA and Dunnett's post hoc test (Luminescence) or unpaired two-tailed t test (% reduction in trans-activation) (ns = not significant, ** = P < 0.01, **** = P < 0.0001).

4.5 Cis-inhibition of Ax variants by JAG1

After testing the effect of cis-JAG1 expression in the mN1 WT cell line, the assay was performed using Ax variant lines. When cis-JAG1 WT was expressed, activation levels of all N1 Ax variants, when co-cultured with either B16 cells expressing mJag1 (Figure 4.6A) or mDll4 (Figure 4.7A), were reduced significantly compared to the EV control, indicating that some cis-inhibition was induced in each case.

For *Ax N* suppressor variant cell lines (D909V, N947I, DVNI) transfected with cis-JAG1, similar results were observed when co-cultured with both trans-ligands. Upon cis-JAG1 expression, activation levels of *N* suppressor variants were similar to or higher than WT cells (Figure 4.6A and 4.7A). Considering these variants showed reduced trans-activation in the absence of cis-JAG1 (see Chapter 3 and EV datasets in Figure 4.6A and 4.7A), these results suggested that they were less responsive to the inhibitory effect of cis-JAG1. Otherwise, the overall activity levels observed would be lower than those of N1 WT. In support of this, % reduction in trans-activation indicating strength of cis-

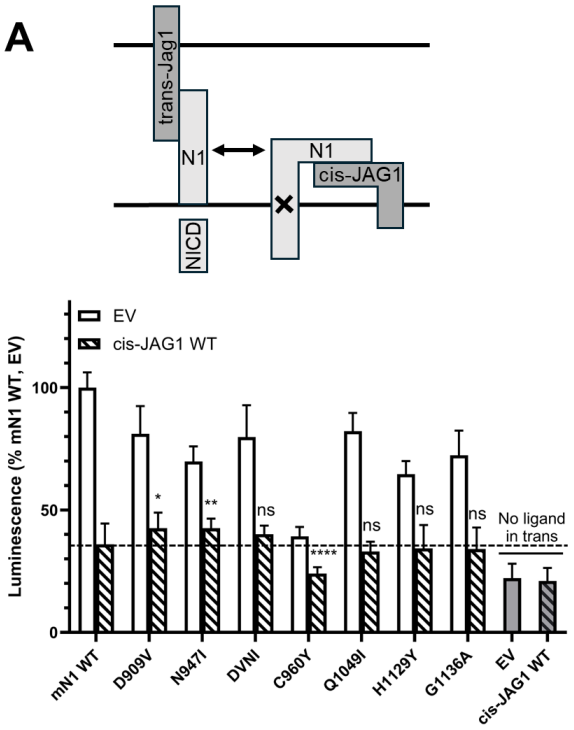
inhibition was <50% (B16 mJag1, Figure 4.6B) and <45% (B16 mDll4, Figure 4.7B) for *N* suppressor variants compared to ~65% (B16 mJag1) and ~55% (B16 mDll4) for N1 WT.

For *Ax N* enhancer variant cell lines (Q1049I, H1129Y, G1136A) transfected with cis-JAG1, different results were observed when co-cultured with the two trans-ligands. Overall activation levels of these variants showed no significant difference to that of N1 WT when grown with B16 mJag1 (Figure 4.6A). In addition, H1129Y and G1136A showed less cis-inhibition than observed in WT as indicated by % reduction in trans-activation by B16 mJag1 (from 65% observed in N1 WT to less than 50%; Figure 4.6B). This suggested that these two variants, like the *N* suppressor variants, negatively affected the ability of JAG1 to cis-inhibit. However, when grown with B16 mDll4, *N* enhancer variants showed lower activation levels in the presence of cis-JAG1 (Figure 4.7A), and, strikingly, no significant difference to N1 WT in % reduction in trans-activation, distinguishing them from *N* suppressor behaviour (Figure 4.7B).

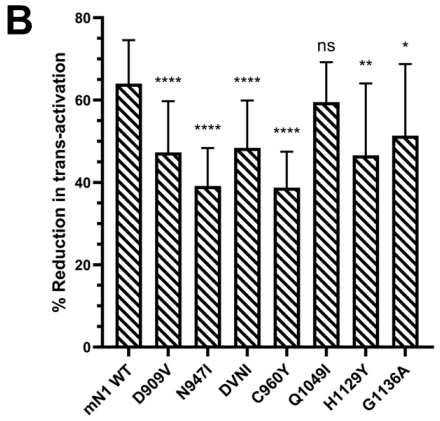
The homozygous lethal variant C960Y, which showed a lower cell surface level than N1 WT (see Section 3.4.2), showed significantly lower activation levels than N1 WT in the presence of either trans-ligand when cis-JAG1 was present (Figure 4.6A and 4.7A). It still displayed some cis-inhibition by both trans-ligands (>40%) as indicated by % reduction in trans-activation values (Figure 4.6B and 4.7B).

Cis-inhibition assays were also performed using plate-coated ligand NE3 fragments for ligand-dependent activation instead of cell surface expressed ligand in co-culture. Similar luminescence results for all variants were demonstrated using hJAG1 NE3 as obtained by co-culture (compare Appendix F, Figure F.2A with Figure 4.6A), with the exception of the Q1049I variant. For hDLL4 NE3, there were some differences, with the *N* enhancer variants showing higher levels of activity/luminescence (compared to WT) in the presence of cis-JAG1, than in co-culture (compare Appendix F, Figure F.3A with Figure 4.7A), although this did not alter their cis-inhibition profiles (compare Appendix F, Figure F.3B with Figure 4.7B). As previously noted (see Chapter 3) activation measurements generally showed wider SD values for experiments performed with plate-coated purified ligands which made it more difficult to establish statistical significance. This may explain some of the differences observed and provide further evidence for using a more native-like co-culture system for Notch activation.

Additionally, raw luminescence levels of cell lines transfected with cis-JAG1 and grown in the absence of trans-ligands were measured to check whether cis-JAG1 induced auto-activation of Ax variants (Appendix F, Figure F.4). Results suggested that Ax variants had similar activation levels to N1 WT when transfected with cis-JAG1 and grown without trans-ligands, indicating no excess activation was induced.



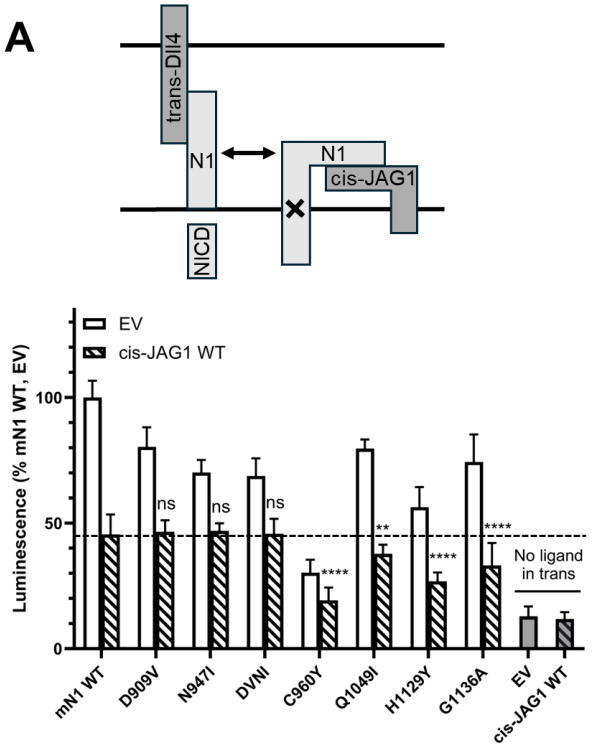
Cell line	Luminescence (% mN1 WT, EV)		Statistical significance (cis-JAG1 WT)
	EV	cis-JAG1 WT	
mN1 WT	100 ± 6.3	36 ± 8.5	
D909V	81.2 ± 11.3	42.5 ± 6.4	*
N947I	69.8 ± 6.2	42.6 ± 3.9	**
DVNI	79.8 ± 13	40.2 ± 3.5	ns
C960Y	39.3 ± 3.8	24.1 ± 2.5	****
Q1049I	82.2 ± 7.4	33.1 ± 4	ns
H1129Y	64.7 ± 5.4	34.4 ± 9.5	ns
G1136A	72.4 ± 10.1	34.1 ± 8.8	ns



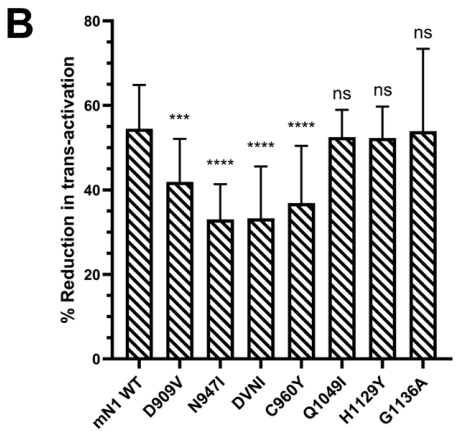
Cell line	% Reduction in trans-activation	Statistical significance
mN1 WT	64 ± 10.6	
D909V	47.3 ± 12.4	****
N947I	39.1 ± 9.3	****
DVNI	48.4 ± 11.5	****
C960Y	38.7 ± 8.7	****
Q1049I	59.5 ± 9.7	ns
H1129Y	46.6 ± 17.5	**
G1136A	51.4 ± 17.4	*

Figure 4.6. Trans-activation of cis-JAG1-expressing mN1 Ax variant cells by B16 mJag1.

(A) Cis-inhibition assay by cis-JAG1 WT for mN1 WT and Ax variant cells grown with B16 mJag1 cells or B16 WT control cells (indicated by "No ligand in trans") (cartoon in upper panel, results in lower panel). Luminescence signal in each case is shown relative to mN1 WT cells transfected with the EV. (B) % reduction in trans-activation caused by cis-JAG1 was calculated by *(Luminescence with EV – Luminescence with cis-ligand)/Luminescence with EV x 100*. Graph (left panel) and table (right panel) show the combined results of four independent plates, each with five repeat wells. Data presented as mean ± SD. Statistical significance compared to mN1 WT transfected with cis-JAG1 was determined in (A) by Kruskal-Wallis test and Dunn's post hoc test and in (B) by Welch's ANOVA and Dunnett's post hoc test (ns = not significant, * = P < 0.05, ** = P < 0.01, **** = P < 0.0001).



Cell line	Luminescence (% mN1 WT, EV)		Statistical significance (cis-JAG1 WT)
	EV	cis-JAG1 WT	
mN1 WT	100 ± 6.7	45.5 ± 7.9	
D909V	80.4 ± 7.8	46.6 ± 4.6	ns
N947I	70.1 ± 5	46.9 ± 3	ns
DVNI	68.8 ± 7	45.8 ± 5.9	ns
C960Y	30.3 ± 5.1	19.3 ± 5.1	****
Q1049I	79.6 ± 3.7	37.8 ± 3.7	**
H1129Y	56.3 ± 8	26.8 ± 3.5	****
G1136A	74.3 ± 11	33.2 ± 8.9	****



Cell line	% Reduction in trans-activation	Statistical significance
mN1 WT	54.5 ± 10.3	
D909V	41.9 ± 10.2	***
N947I	33 ± 8.3	****
DVNI	33.3 ± 12.3	****
C960Y	36.9 ± 13.6	****
Q1049I	52.5 ± 6.5	ns
H1129Y	52.3 ± 7.5	ns
G1136A	53.9 ± 19.5	ns

Figure 4.7. Trans-activation of cis-JAG1-expressing mN1 Ax variant cells by B16 mDll4.

(A) Cis-inhibition assay by cis-JAG1 WT for mN1 WT and Ax variant cells grown with B16 mDll4 cells or B16 WT control cells (indicated by "No ligand in trans") (cartoon in upper panel, results in lower panel). Luminescence signal in each case is shown relative to mN1 WT cells transfected with the EV. (B) % reduction in trans-activation caused by cis-JAG1 was calculated by *(Luminescence with EV – Luminescence with cis-ligand)/Luminescence with EV x 100*. Graph (left panel) and table (right panel) show the combined results of four independent plates, each with five repeat wells. Data presented as mean ± SD. Statistical significance compared to mN1 WT transfected with cis-JAG1 was determined in (A) by Kruskal-Wallis test and Dunn's post hoc test and in (B) by Welch's ANOVA and Dunnett's post hoc test (ns = not significant, ** = P < 0.01, *** = P < 0.001, **** = P < 0.0001).

4.6 Discussion

Significant levels of cis-inhibition with JAG1 were achieved

In this chapter, JAG1 cis-inhibition assays were developed. The activation of N1 in cells transfected with cis-JAG1 was compared with cells transfected with EV (Table 4.1) to determine whether or not cis-inhibition was occurring. In addition, the % reduction in trans-activation was calculated for each Notch variant to quantify the extent of cis-inhibition. Under optimised assay conditions, cis-inhibition, shown by a reduction in luminescence by 50-60% upon transfection with plasmid encoding cis-JAG1 compared to the signal obtained with EV, was achieved (Table 4.1, Figure 4.5). This reduction in Notch activation correlated with an increase in concentration of cis-plasmid transfected and therefore was consistent with the formation of a cis-inhibitory complex (Figure 4.1).

Since the readout for the assay was dependent on measuring Notch activity utilising a trans-ligand, some receptors in the cell populations transfected with cis-ligand were still susceptible to activation by trans-ligands. This might be due to some cells remaining untransfected, transient transfection might not induce high cis-ligand levels sufficient to “saturate” receptors on the cell surface and/or competition between cis- and trans-complexes may occur.

Table 4.1. Summary for N1 WT trans-activation and cis-inhibition by JAG1.

Luminescence signals measured for mN1 WT cells in trans-activation and cis-inhibition assays using JAG1 WT and JAG1 FAEK. For trans-activation assay, signal in mN1 WT cells co-cultured with trans-JAG1 WT is shown as 100% (Figure 4.5A). For cis-inhibition assay, signal in mN1 WT cells transfected with EV and co-cultured with trans-ligand is shown as 100% (Figure 4.5B and C). Values obtained with cis-JAG1 are expressed relative to this.

Plasmid	Trans-activation	Cis-JAG1 vs trans-Jag1	Cis-JAG1 vs trans-Dll4
EV	43	100	100
JAG1 WT	100	38	50
JAG1 FAEK	52	89	87

Interaction between ligand DSL and N1 receptor was essential for trans-activation and cis-inhibition

JAG1 FAEK variant, which was designed to abolish the interaction between the ligand DSL domain and EGF11 of N1 (Cordle *et al.*, 2008; Luca *et al.*, 2015, Meng et al., 2022), was unable to activate N1 above background levels when utilised as trans-ligand (Figure 4.5A). When tested for its ability to cis-inhibit the receptor, JAG1 FAEK was much less effective than JAG1 WT, irrespective of the trans-ligand used (Table 4.1, Figure 4.5B and C). This suggested that the DSL Notch binding patch in which F207 and E228 are located is required for N1 inhibition by cis-JAG1.

Ax N suppressor variants showed less inhibition by cis-JAG1 than WT

The effect of JAG1-mediated cis-inhibition on Ax variants was tested. Upon transfection with cis-JAG1, *N* suppressor variants (D909V, N947I and DVNI) showed similar or higher levels of luminescence than WT but a significantly lower % reduction in trans-activation (indicative of less cis-inhibition) compared to WT, when co-cultured with either trans-

ligand (Table 4.2 and 4.3, Figure 4.6 and 4.7). Together, these data suggested that the Ca^{2+}-dependent rod-like structure of EGF23-24 and 24-25 between the LBR and NRR, which the *N* suppressor substitutions perturb is required for both trans-activation and cis-inhibition.

Table 4.2. Summary of effects of cis-JAG1 expression on Jag1-mediated trans-activation of Ax variants.

The results of JAG1-mediated cis-inhibition assays for mN1 Ax variants co-cultured with trans-Jag1. Luminescence signals of mN1 WT and Ax variants cells transfected with cis-JAG1 are shown relative to mN1 WT cells transfected with the EV, which is set as 100% (Figure 4.6A). % reduction in trans-activation caused by cis-JAG1 was calculated by *(Luminescence with EV – Luminescence with cis-ligand)/Luminescence with EV x 100* (Figure 4.6B). Results for Ax variants that show significant differences to those of mN1 WT are coloured red.

Cell line	cis-JAG1 vs trans-Jag1	
	Luminescence	% reduction in trans-activation
N1 WT (no cis-JAG1)	100	0
N1 WT	36	64
D909V	43	47
N947I	43	39
DVNI	40	48
C960Y	24	39
Q1049I	33	60
H1129Y	34	47
G1136A	34	51

Table 4.3. Summary of effects of cis-JAG1 expression on Dll4-mediated trans-activation of Ax variants.

The results of JAG1-mediated cis-inhibition assays for mN1 Ax variants co-cultured with trans-Dll4. Luminescence signals of mN1 WT and Ax variants cells transfected with cis-JAG1 are shown relative to mN1 WT cells transfected with the EV, which is set as 100% (Figure 4.7A). % reduction in trans-activation caused by cis-JAG1 was calculated by *(Luminescence with EV – Luminescence with cis-ligand)/Luminescence with EV x 100* (Figure 4.7B). Results for Ax variants that show significant differences to those of mN1 WT are coloured red.

Cell line	cis-JAG1 vs trans-Dll4	
	Luminescence	% reduction in trans-activation
N1 WT (no cis-JAG1)	100	0
N1 WT	46	54
D909V	47	42
N947I	47	33
DVNI	46	33
C960Y	19	37
Q1049I	38	53
H1129Y	27	52
G1136A	33	54

Ax N enhancer variants were less inhibited by cis-JAG1 compared to WT when co-cultured with trans-Jag1, but this effect was not seen with trans-Dll4

When transfected with cis-JAG1 and co-cultured with Jag1-expressing B16 cells, *N* enhancer variants H1129Y and G1136A showed higher than expected activation levels (considering their ability to be trans-activated was reduced without cis-JAG1) (see Chapter 3 and Figure 4.6A) and less cis-inhibition than seen in WT (Figure 4.6B). They therefore showed some similarity in behaviour to *N* suppressors (Figure 4.6). These data suggest that the substitutions within the EGF29 region can perturb cis-N1/JAG1 inhibitory complex formation.

In contrast, when co-cultured with mDll4-expressing B16 cells, activation levels of all *N* enhancer variants tested in the presence of cis-JAG1 were lower than WT and showed no difference in % reduction in trans-activation (Figure 4.7A, B). Under these conditions, cis-inhibition of *N* enhancer variants appears more similar to WT and may suggest that trans-Dll4 competes less readily with the cis-JAG1/*N* enhancer inhibitory complex than trans-Jag1. Irrespective of the mechanism, *N* enhancer variants H1129Y and G1136A reveal differences in cis-inhibition in a ligand-dependent manner which are not seen with *N* suppressor variants.

5 Investigating the role of the Abruptex region in Notch1 cis-inhibition by DLL4

5.1 Introduction

Chapter 4 established a protocol for measuring cis-inhibition of Notch and suggested that Ax substitutions can reduce the ability of N1 to be inhibited by cis-JAG1. To explore the effect of Ax substitutions on N1 cis-inhibition by a Delta family ligand, a cis-inhibition assay was established using mN1 WT reporter cell lines transiently transfected to express either cis-DLL4 WT or a receptor binding-deficient variant. Experiments were then performed using Ax variant lines.

5.2 DLL4 cis-inhibition assay design and optimisation

Similar to the JAG1 cis-inhibition assay (see Chapter 4), HEK-RBP mN1 cells were transiently transfected with a pcDNA3.1(+) plasmid encoding full-length hDLL4 or EV and co-cultured overnight with non-ligand expressing B16 WT control cells or B16 cells expressing mJag1 or mDll4 (Figure 4.1A) (see Section 2.9.3). In preliminary experiments, using conditions established for the JAG1 cis-inhibition assay (40,000 mN1 cells per well), co-culture with B16 WT control cells resulted unexpectedly in an increase (>2.5-fold) in apparent activation of mN1 WT cells transfected with cis-DLL4 WT compared with those transfected with EV or cis-DLL4 F195A/Y216A (FAYA), a receptor binding-deficient variant of DLL4 equivalent to JAG1 FAEK (Feng et al. unpublished data) (Figure 5.1A and B, No ligand in trans). This apparent raised activation level in the absence of trans-ligand on B16 cells might theoretically be caused by trans-interaction between cis-DLL4 WT and available mN1 receptor on the cell surface of a neighbouring cell, and/or cis-

activation of mN1 by DLL4 WT expressed in the same cell. Irrespective of the cause, mN1 WT cell numbers were titrated to examine their effect on this higher-than-expected “background” value.

Titration results suggested that when 10,000 or fewer mN1 WT cells were added per well, the difference between activation levels of N1 cells transfected with EV and cis-DLL4 WT and co-cultured with B16 WT control cells was much lower than observed when 40,000 cells were used (Figure 5.1A and B, No ligand in trans). 10,000 mN1 cells per well were therefore selected as this condition, when compared with conditions using fewer than 10,000 mN1 WT cells, not only reduced “background” activation but also produced a larger difference between activation levels of cells transfected with EV and cis-DLL4 WT when co-cultured with trans-ligands. Titrations of cis-DLL4 WT plasmid transiently transfected were then performed, which showed that the trans-activation level of mN1 WT cells gradually decreased and started to plateau at around 2.5 µg plasmid per well when incubated with B16 ligand-expressing cells (Figure 5.1C). Therefore, 2.5 µg cis-DLL4 plasmid per well was used for transfection in a 6-well plate and 10,000 transfected cells were grown in each well in a 96-well plate for co-culture with B16 cells.

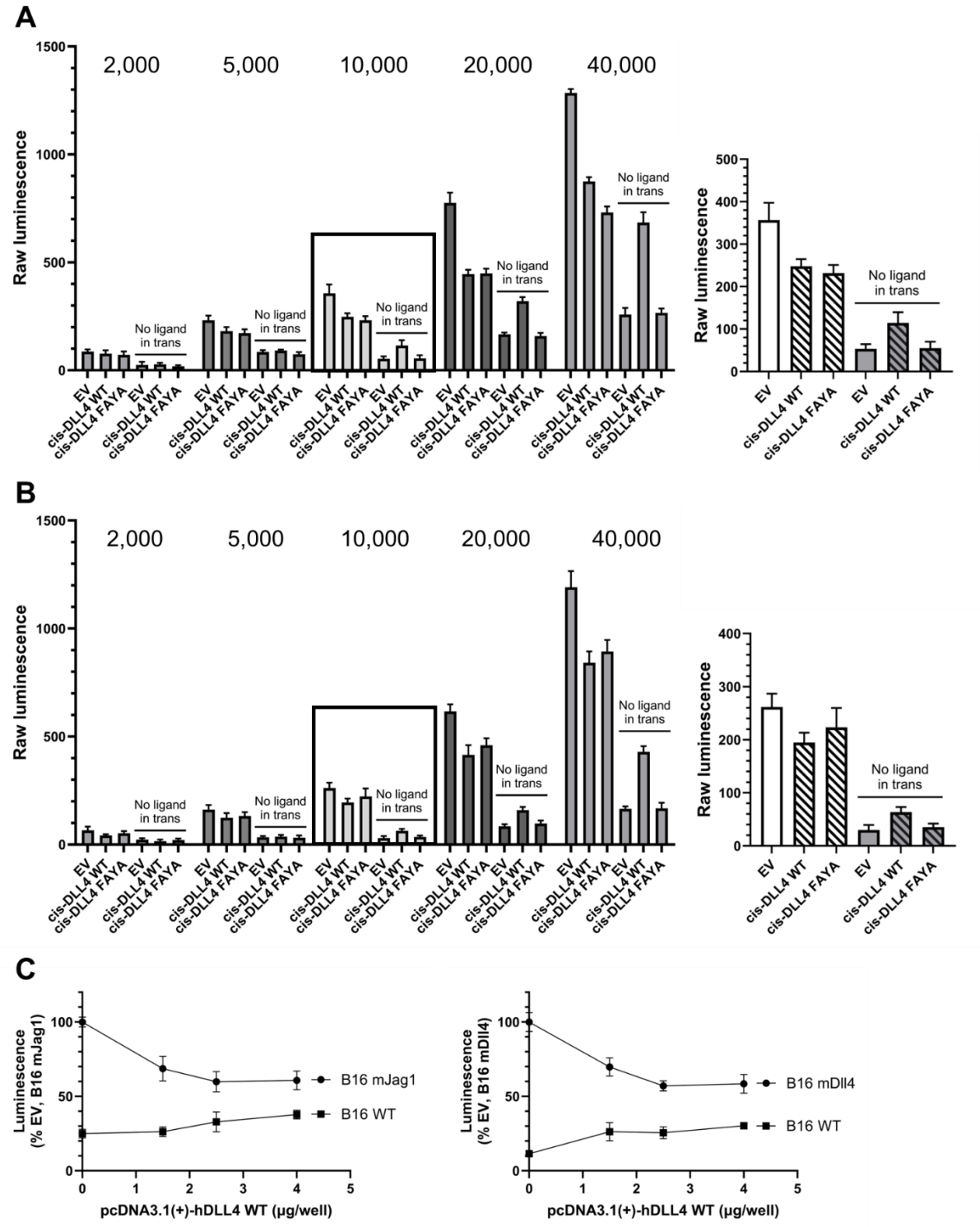


Figure 5.1. Optimisation for cis-inhibition assay using cis-DLL4.

Cis-inhibition assays performed when 2,000 to 40,000 (indicated by labels) mN1 WT cells transfected with cis-DLL4 WT or cis-DLL4 FAYA or EV were co-cultured with 40,000 (A) mJag1-expressing or (B) mDLL4-expressing B16 cells alongside B16 WT control cells (no ligand in trans) in each well of a 96-well plate. Raw luminescence measured was presented as mean ± SD of 5 repeat wells. 10,000 mN1 cells per well (indicated with a frame in the left

panel and enlarged in the right panel) were selected for use in subsequent assays. (C) mN1 WT cells transfected with 0-4 µg of cis-DLL4 WT plasmid per well in a 6-well plate were co-cultured either with B16 control cells or B16 cells expressing mJag1 (left panel) or mDll4 (right panel) or B16 WT control. Luminescence signal produced in each case is shown relative to cells transfected with an equal quantity of EV and co-cultured with ligand-expressing B16 cells. Data presented as mean ± SD.

5.3 *DLL4* RNA expression verification

To verify that the quantity of cis-DLL4 mRNA expressed in each cell line was reproducible, RT-PCRs (see Section 2.4) using cDNA-specific primers (see Appendix A) were performed for mN1 WT and Ax variant cells transfected with cis-DLL4 or EV and examined by gel electrophoresis (Figure 5.2). For cells transfected with plasmids encoding cis-DLL4 WT or cis-DLL4 FAYA, RT-PCRs for *DLL4* RNA expression produced bands of 139 bp with similar intensity, suggesting comparable RNA expression levels (Figure 5.2A). RT-PCRs for *mN1* RNA expression in mN1 cells transfected with either EV or cis-DLL4 produced bands of 337 bp with similar intensity, indicating that, as for cis-JAG1 previously (see Section 4.3), the expression of cis-DLL4 did not appear to affect *mN1* expression at the RNA level (Figure 5.2B). RT-PCRs for *GAPDH*, producing bands of 237 bp with similar intensity, confirmed that the same starting concentration of RNA was used in each reverse transcription reaction (Figure 5.2C). PCR amplification of RNA samples without reverse transcription, which showed no band, confirmed the RNA samples were not contaminated with DNA.

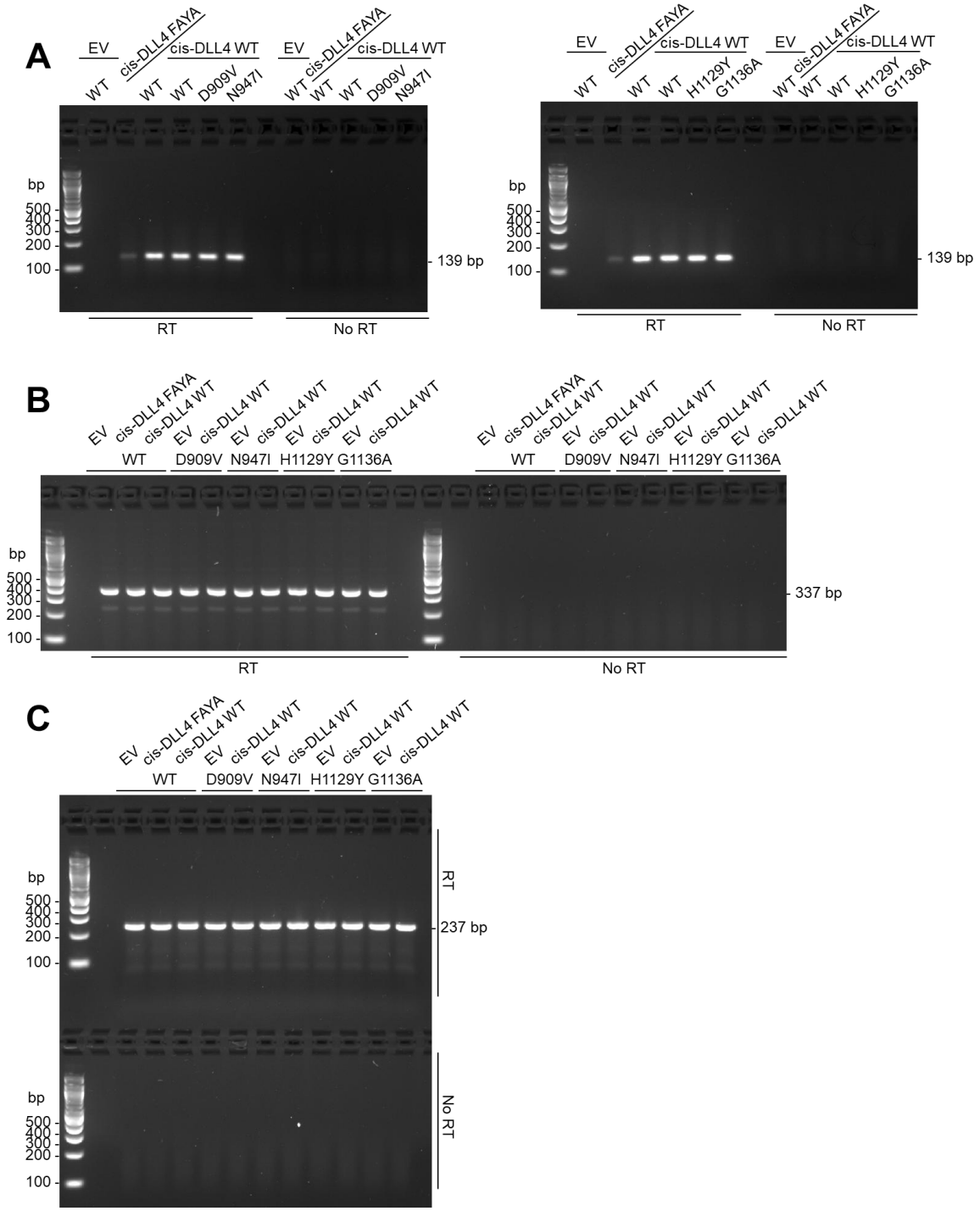
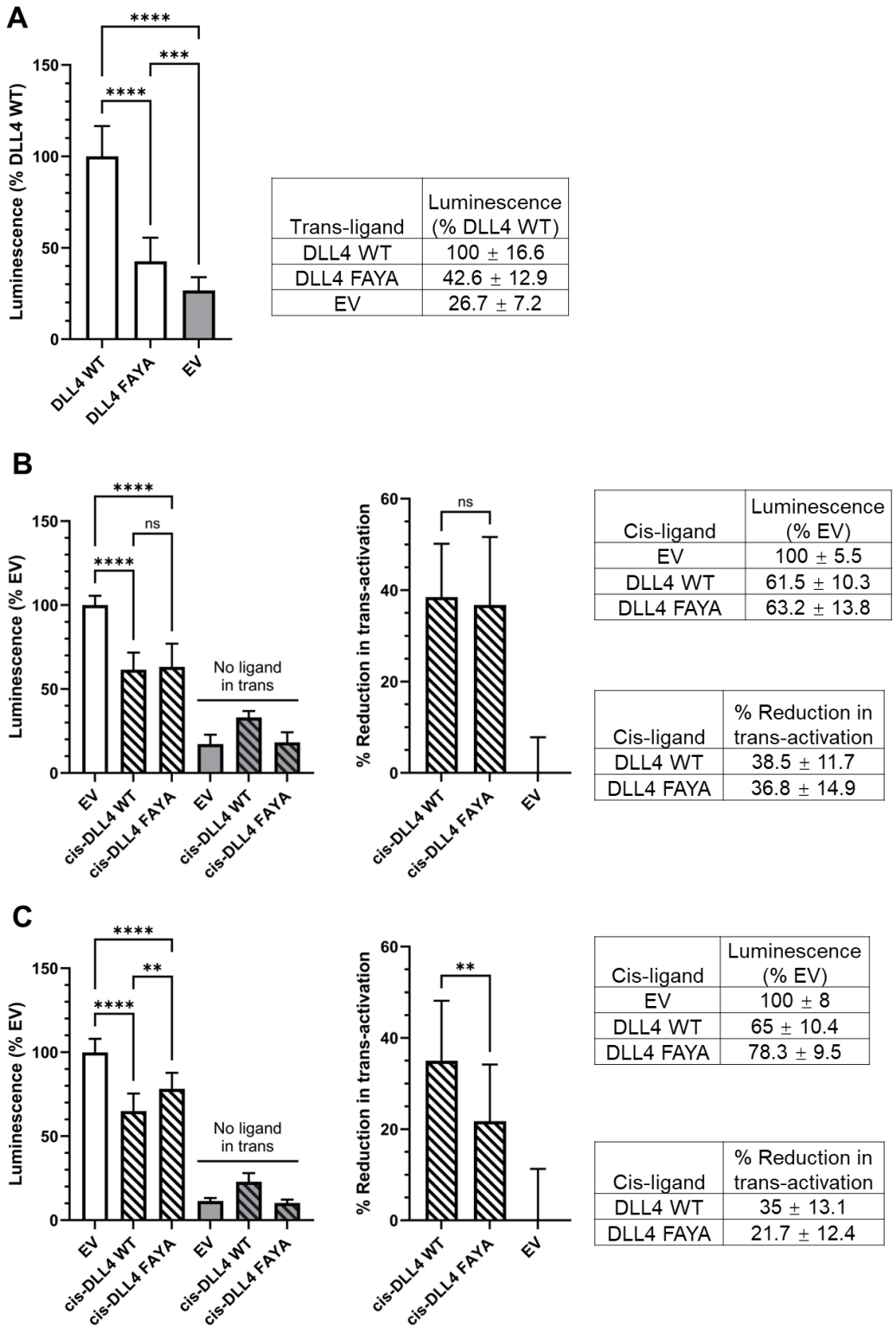


Figure 5.2. RT-PCR of mN1 cells transfected with cis-DLL4 plasmid.

RNA was extracted from HEK-RBP mN1 WT and Ax variants cells transfected with pcDNA3.1(+) plasmids encoding DLL4 WT or DLL4 FAYA variant or EV (indicated by labels). PCRs to amplify (A) a 139 bp region in *DLL4* cDNA, (B) a 337 bp region in *mN1* cDNA, and (C) a 237 bp region in *GAPDH* cDNA were performed for RNA samples with and without RT (indicated by labels). PCR products were run on a 2.5% agarose TBE gel.

5.4 Effect of cis-DLL4 expression on N1 WT activation

When plasmids encoding full-length DLL4 were transfected into HEK293T cells and tested with mN1 WT reporter cells, WT DLL4 was able to elicit strong trans-activation compared to EV, whilst the Notch-binding-negative DLL4 FAYA variant only induced ~40% WT trans-activation (Figure 5.3A). Subsequently, when DLL4 WT was expressed in cis, mN1 WT cells showed a reduction in overall N1 activation with luminescence levels at 60-65% of cells transfected with EV when co-cultured with either trans-ligand (Figure 5.3B and C), suggesting cis-inhibition was achieved to some extent. However, unlike JAG1 FAEK (see Section 4.4), DLL4 FAYA was unable to rescue the observed inhibitory effect of cis-DLL4, and both WT and FAYA cis-constructs reduced overall trans-activation, irrespective of trans-ligand (Figure 5.3B and C). Whilst mN1 WT cells transfected with cis-DLL4 WT showed a moderate 35% reduction in trans-activation (cis-inhibition) with both trans-ligands (Figure 5.3B and C), cis-DLL4 FAYA led to a milder cis-inhibitory effect with % reduction in trans-activation of ~20% in presence of trans-Dll4, suggesting that the FAYA substitutions did have a small effect on N1 cis-inhibition (Figure 5.3C). This is also evident when overall luminescence is compared, with cell lines transfected with cis-DLL4 FAYA and activated by trans-DLL4 producing a statistically significant increase in activity compared to levels achieved with cis-DLL4 WT (Figure 5.3C).



Trans-ligand	Luminescence (% DLL4 WT)
DLL4 WT	100 ± 16.6
DLL4 FAYA	42.6 ± 12.9
EV	26.7 ± 7.2

Cis-ligand	Luminescence (% EV)
EV	100 ± 5.5
DLL4 WT	61.5 ± 10.3
DLL4 FAYA	63.2 ± 13.8

Cis-ligand	% Reduction in trans-activation
DLL4 WT	38.5 ± 11.7
DLL4 FAYA	36.8 ± 14.9

Cis-ligand	Luminescence (% EV)
EV	100 ± 8
DLL4 WT	65 ± 10.4
DLL4 FAYA	78.3 ± 9.5

Cis-ligand	% Reduction in trans-activation
DLL4 WT	35 ± 13.1
DLL4 FAYA	21.7 ± 12.4

Figure 5.3. Trans-activation of mN1 WT cells transfected with cis-DLL4 plasmid.

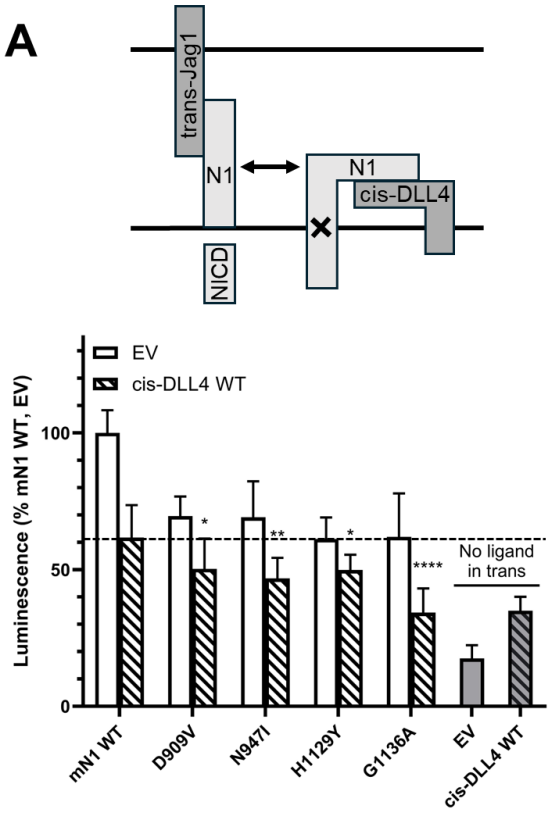
(A) Activation of mN1 WT cells by co-culturing overnight with HEK293T cells transfected with pcDNA3.1(+) plasmids encoding DLL4 WT, DLL4 FAYA or EV (see Section 2.6.3). Graph (left panel) and table (right panel) show the combined results of four independent plates, each with five repeat wells. Signal in each case is shown relative to cells co-cultured with DLL4

WT-expressing HEK293T. (B, C) Cis-inhibition assays by cis-DLL4 WT and FAYA for mN1 WT cells grown with B16 cells expressing (B) mJag1 or (C) mDll4 alongside B16 WT control cells (indicated by "No ligand in trans"). Graph (left panel) and table (right panel) show the combined results of three independent plates, each with five repeat wells. Luminescence signal in each case is shown relative to cells transfected with EV. % reduction in trans-activation was calculated by *(Luminescence with EV – Luminescence with cis-ligand)/Luminescence with EV x100*. Data presented as mean ± SD. Statistical significance in (A) was determined by ordinary one-way ANOVA and Tukey's post hoc test. Statistical significance for luminescence in (B) and (C) was determined by Welch's ANOVA or ordinary one-way ANOVA along with Dunnett's post hoc test. Statistical significance for % reduction in trans-activation in (B) and (C) was determined by unpaired two-tailed t test. (ns = not significant, ** = P < 0.01, *** = P < 0.001, **** = P < 0.0001)

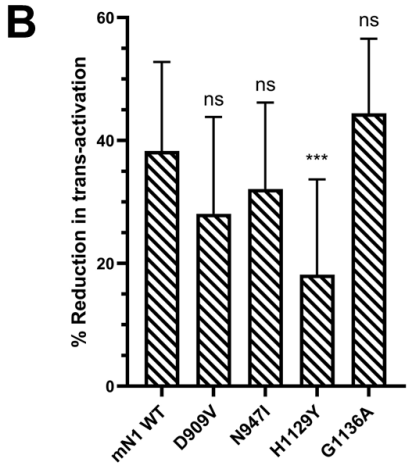
5.5 Cis-inhibition of Ax variants by DLL4

Cis-inhibition assays were tested on a subset of Ax lines representing the *N* suppressor (D909V, N947I) and *N* enhancer (H1129Y, G1136A) classes. Analysis showed that trans-activation levels of mN1 Ax variant cell lines transfected with cis-DLL4, and co-cultured with B16 cells expressing either mJag1 (Figure 5.4A) or mDll4 (Figure 5.5A) were reduced significantly, indicating that cis-inhibition was induced. In each case, the negative effects of these variants on mN1 trans-activation observed previously (see Chapter 3) were seen in the presence of EV, and luminescence was reduced further in the presence of cis-DLL4 to levels still lower than N1 WT. While D909V, N947I and G1136A showed no effect on % reduction in trans-activation compared to N1 WT, the *N* enhancer H1129Y showed a statistically significant lower value of 16-18% reduction in the presence of either trans-ligand compared to 36-38% reduction observed in N1 WT (Figure 5.4B and 5.5B). This suggested that H1129Y reduced the cis-inhibitory effect of

cis-DLL4 under current assay conditions to some extent. Raw luminescence levels of all cell lines transfected with cis-DLL4 and grown in the absence of trans-ligands were also measured to confirm that these Ax variants had similar auto-activation levels to mN1 WT (Appendix F, Figure F.4).



Cell line	Luminescence (% mN1 WT, EV)		Statistical significance (cis-DLL4 WT)
	EV	cis-DLL4 WT	
mN1 WT	100 ± 8.3	61.7 ± 11.9	
D909V	69.6 ± 7.2	50.3 ± 11.1	*
N947I	69.2 ± 13.1	46.8 ± 7.5	**
H1129Y	61.2 ± 7.9	49.8 ± 5.6	*
G1136A	62 ± 15.9	34.3 ± 8.8	****

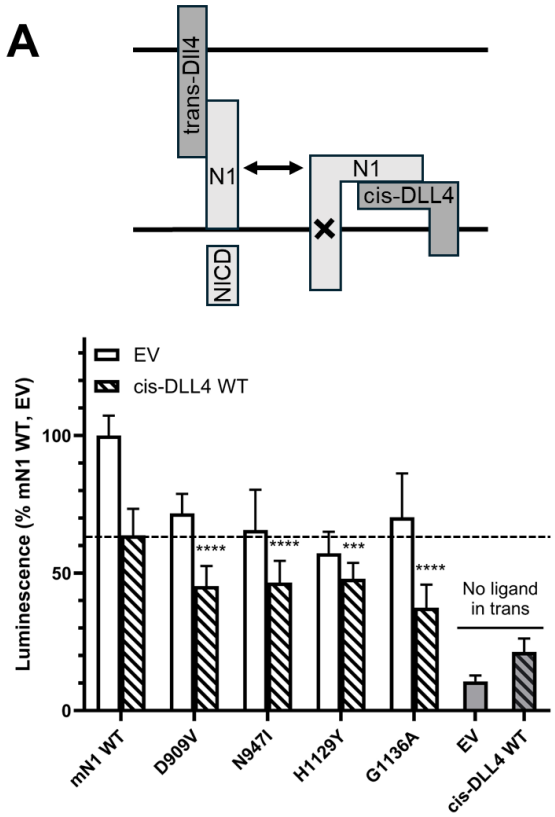


Cell line	% Reduction in trans-activation	Statistical significance
mN1 WT	38.3 ± 14.5	
D909V	28.1 ± 15.8	ns
N947I	32.1 ± 14.1	ns
H1129Y	18.2 ± 15.5	***
G1136A	44.4 ± 12.1	ns

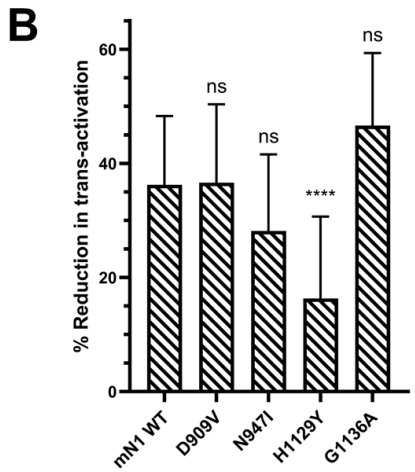
Figure 5.4. Trans-activation of cis-DLL4-expressing mN1 Ax variant cells by B16 mJag1.

(A) Cis-inhibition assay by cis-DLL4 WT for mN1 WT and Ax variant cells grown with B16 cells expressing mJag1 or B16 WT control cells (indicated by "No ligand in trans") (cartoon in upper panel, results in lower panel). Luminescence signal in each case is shown relative to mN1 WT cells transfected with the EV. (B) % reduction in trans-activation caused by cis-DLL4 was calculated by *(Luminescence with EV – Luminescence with cis-ligand)/Luminescence with EV x 100*. Graph (left panel) and table (right panel) show the combined results of three independent plates, each with five repeat wells. Data presented as

mean ± SD. Statistical significance compared to mN1 WT transfected with cis-DLL4 was determined in (A) by Kruskal-Wallis test and Dunn's post hoc test and in (B) by ordinary one-way ANOVA and Dunnett's post hoc test (ns = not significant, * = P < 0.05, ** = P < 0.01, *** = P < 0.001, **** = P < 0.0001).



Cell line	Luminescence (% mN1 WT, EV)		Statistical significance (cis-DLL4 WT)
	EV	cis-DLL4 WT	
mN1 WT	100 ± 7.2	63.8 ± 9.6	
D909V	71.8 ± 7	45.3 ± 7.3	****
N947I	65.6 ± 14.7	46.6 ± 7.8	****
H1129Y	57.2 ± 7.8	47.9 ± 5.8	***
G1136A	70.3 ± 15.9	37.4 ± 8.4	****



Cell line	% Reduction in trans-activation	Statistical significance
mN1 WT	36.3 ± 12	
D909V	36.6 ± 13.7	ns
N947I	28.2 ± 13.4	ns
H1129Y	16.3 ± 14.4	***
G1136A	46.6 ± 12.7	ns

Figure 5.5. Trans-activation of cis-DLL4-expressing mN1 Ax variant cells by B16 mDll4.

(A) Cis-inhibition assay by cis-DLL4 WT for mN1 WT and Ax variant cells grown with B16 cells expressing mDll4 or B16 WT control cells (indicated by "No ligand in trans") (cartoon in upper panel, results in lower panel). Luminescence signal in each case is shown relative to mN1 WT cells transfected with the EV. (B) % reduction in trans-activation caused by cis-DLL4 was calculated by *(Luminescence with EV – Luminescence with cis-ligand)/Luminescence with EV x 100*. Graph (left panel) and table (right panel) show the combined results of three independent plates, each with five repeat wells. Data presented as mean ± SD. Statistical significance compared to mN1 WT transfected with cis-DLL4 was determined in (A) by Kruskal-Wallis test and Dunn's post hoc test and in (B) by ordinary one-

way ANOVA and Dunnett's post hoc test (ns = not significant, *** = P < 0.001, **** = P < 0.0001).

5.6 Discussion

Significant levels of DLL4-mediated cis-inhibition were achieved for N1

In this chapter, DLL4 cis-inhibition assay was developed and tested on a subset of Ax variants. Compared to JAG1 cis-inhibition assay developed in Chapter 4, a lower number of mN1 cells was used due to the high levels of activation observed for cis-DLL4-expressing cells in the absence of trans-ligand (Figure 5.1). Initially, mN1 WT cells transfected with cis-DLL4 WT or cis-DLL4 FAYA were compared with cells transfected with EV (Table 5.1) (Figure 5.3). Under optimised assay conditions, cis-inhibition was achieved to some extent, shown by a 35-40% reduction in trans-activation of mN1 WT cells upon transfection with plasmid encoding cis-DLL4 WT. This was lower than cis-inhibition (50-60% reduction in trans-activation) achieved in the cis-JAG1 assay (compare Figure 4.5 with Figure 5.3), which may be caused by differences in assay conditions or in the cis-inhibitory ability of the two ligands.

Table 5.1. Summary for N1 WT trans-activation and cis-inhibition by DLL4.

Luminescence signals measured for mN1 WT cells in trans-activation and cis-inhibition assays using DLL4 WT and DLL4 FAYA. For trans-activation assay, signal in mN1 WT cells co-cultured with trans-DLL4 WT is shown as 100% (Figure 5.3A). For cis-inhibition assay, signal in mN1 WT cells transfected with EV and co-cultured with trans-ligand is shown as 100% (Figure 5.3B and C). Values obtained with cis-DLL4 are expressed relative to this.

Plasmid	Trans-activation	Cis-DLL4 vs trans-Jag1	Cis-DLL4 vs trans-Dll4
EV	27	100	100
DLL4 WT	100	62	65
DLL4 FAYA	43	63	78

The interaction between DLL4 DSL and N1 receptor facilitated trans-activation but appeared less important for cis-inhibition

The DLL4 FAYA variant, which was designed to abolish the interaction between the ligand DSL domain and EGF11 of N1 (Luca *et al.*, 2015, Feng *et al.* unpublished data), was effective in trans-activation assays, showing reduced ability (~20% of WT) to trans-activate N1 (Figure 5.3A). In contrast, DLL4 WT and FAYA induced a similar level of cis-inhibition when co-cultured with trans-Jag1, and to some extent with trans-Dll4 (Figure 5.3B and C, Table 5.1). These data suggest that the DSL domain in DLL4 may be less involved in mediating a cis-inhibitory interaction of N1, at least under the assay conditions used.

It should be noted that the ratio of ligand-expressing B16 cells to mN1 reporter cells used in cis-DLL4 experiments (40,000 B16 cells grown with 10,000 mN1 cells per well) is larger than in cis-JAG experiments (40,000 B16 cells grown with 40,000 mN1 cells per well) (see Section 2.9.3), and therefore greater competition between trans- and cis-

complexes may reduce the apparent effectiveness of the receptor-binding negative variant. Alternatively, the DSL-EGF11 interaction site of DLL4/N1 may have less of a role to play in any cis-inhibitory complex formed, with other interaction sites dominating. It is of interest that when co-cultured with trans-Dll4, the strength of cis-inhibition by DLL4 was reduced slightly by cis-DLL4 FAYA, suggesting that trans-Dll4 might be a more effective competitor than trans-Jag1.

Ax N suppressor variants did not affect N1 cis-inhibition by DLL4

The effect of DLL4-mediated cis-inhibition on Ax variants was tested (Table 5.2 and 5.3). Upon cis-DLL4 expression, *N* suppressor variants (D909V and N947I) showed % reduction in trans-activation levels similar to WT when co-cultured with either trans-ligand (Figure 5.4 and 5.5). This suggested that the Ca^{2+}-binding-dependent structure of EGF24-25 disrupted by *N* suppressor substitutions plays a less important role in cis-inhibition by DLL4 than seen with JAG1.

Table 5.2. Summary of effects of cis-DLL4 expression on Jag1-mediated trans-activation of Ax variants.

The results of DLL4-mediated cis-inhibition assays for mN1 Ax variants co-cultured with trans-Jag1. Luminescence signals of mN1 WT and Ax variants cells transfected with cis-DLL4 are shown relative to mN1 WT cells transfected with the EV, which is set as 100% (Figure 5.4A). % reduction in trans-activation caused by cis-DLL4 was calculated by *(Luminescence with EV – Luminescence with cis-ligand)/Luminescence with EV x 100* (Figure 5.4B). Results for Ax variants that show significant differences to those of mN1 WT are coloured red.

Cell line	cis-DLL4 vs trans-Jag1	
	Luminescence	% reduction in trans-activation
N1 WT (no cis-DLL4)	100	0
N1 WT	62	38
D909V	50	28
N947I	47	32
H1129Y	50	18
G1136A	34	44

Table 5.3. Summary of effects of cis-DLL4 expression on Dll4-mediated trans-activation of Ax variants.

The results of DLL4-mediated cis-inhibition assays for mN1 Ax variants co-cultured with trans-Dll4. Luminescence signals of mN1 WT and Ax variants cells transfected with cis-DLL4 are shown relative to mN1 WT cells transfected with the EV, which is set as 100% (Figure 5.5A). % reduction in trans-activation caused by cis-DLL4 was calculated by *(Luminescence with EV – Luminescence with cis-ligand)/Luminescence with EV x 100* (Figure 5.5B). Results for Ax variants that show significant differences to those of mN1 WT are coloured red.

Cell line	cis-DLL4 vs trans-Dll4	
	Luminescence	% reduction in trans-activation
N1 WT (no cis-DLL4)	100	0
N1 WT	64	36
D909V	45	37
N947I	47	28
H1129Y	48	16
G1136A	37	47

Ax N enhancer variant H1129Y reduced N1 cis-inhibition by DLL4

For *N* enhancer variants, upon cis-DLL4 expression, H1129Y gave a statistically significant decrease in % reduction in trans-activation compared to N1 WT when co-cultured with either trans-ligand, whilst G1136A did not (Table 5.2 and 5.3, Figure 5.4 and 5.5). Both *N* enhancer substitutions tested are located in EGF29. These data show whilst both affect the ability of Notch to be trans-activated, H1129Y has a selective effect on DLL4-mediated cis-inhibition of N1. This suggests that the property of EGF29 affected by H1129Y may be different from that of G1136A during N1 inhibition by cis-DLL4.

In EGF29, H1129 is located between Cys3 and Cys4 and closer to EGF28 while G1136 is located between Cys5 and Cys6 and pointing towards EGF30 (Figure 5.6). H1129Y which replaces histidine with the aromatic residue tyrosine may create new hydrophobic interactions or disturb existing packing with residues in EGF28. G1136A affects the glycine residue required for a conserved β-turn in the core EGF structure (Campbell *et al.*, 1990; Baron *et al.*, 1992) and the consensus sequence of O-GlcNAcylation (Tsukamoto *et al.*, 2022), thus may affect the stability and conformation of EGF29 and its interface with EGF30.

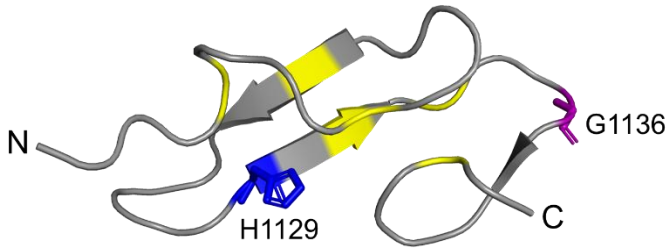


Figure 5.6. Locations of *N* enhancer mutations in N1 EGF29.

The locations of H1129 (blue) and G1136 (purple) in N1 EGF29 (model based on N1 EGF6, PDB: 5FMA). Canonical cysteine residues are shown in yellow. H1129 is located between Cys3 and Cys4. G1136 is located between Cys5 and Cys6.

6 Studying the response of Ax variants to Fringe expression

6.1 Introduction

During passage through the secretory pathway to the cell membrane, the extracellular domain of the Notch receptor can be O-glycosylated in the ER by O-glycosyltransferases at appropriate enzyme recognition sites containing consensus sequences (see Section 1.2.8). The O-glycans can be further modified by other glycosyltransferases in the Golgi. Expression of Fng, a glycosyltransferase in the Golgi that adds GlcNAc onto O-fucose (Figure 6.1), has been shown to regulate the strength of Notch signalling during development (Irvine and Wieschaus, 1994; Fleming, Gu and Hukriede, 1997; Klein and Arias, 1998) (see Section 1.2.8.3). For example, during the formation of the D/V boundary of *Drosophila* wing and eye, the expression of Fng enhanced Notch activation by Dl but reduced dN activation by Ser (Panin *et al.*, 1997) (see Section 1.2.8.3). While both dorsal and ventral cells expressed dN, Fng was found to be exclusively expressed in dorsal cells, which only expressed Ser, but not in ventral cells, which only expressed Dl (Celis, Garcia-Bellido and Bray, 1996; Doherty *et al.*, 1996). Either of the two cell populations appeared to only activate Notch in the other population (Fleming, Gu and Hukriede, 1997; Klein and Arias, 1998). As a result, a high level of Notch activity was observed at the interface of dorsal and ventral cells, i.e. along the D/V axis, inducing the expression of Wg and Cut and maintaining the boundary (de Celis and Bray, 1997; Becam and Milán, 2008).

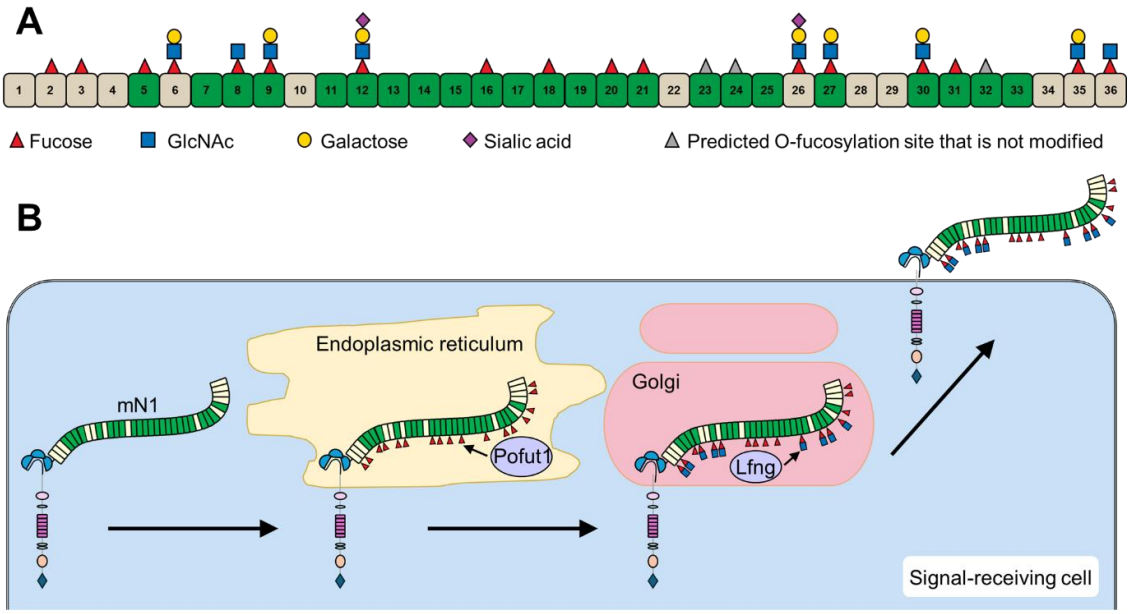


Figure 6.1. Schematic illustration of Lfng modifications of O-fucose on mN1.

(A) Schematic diagrams showing the O-fucosylation sites in the EGF repeats of mN1 ECDs predicted by Pofut1 recognition consensus sequence matching. Predicted sites that have been confirmed as unmodified are indicated by grey triangles (Kakuda and Haltiwanger, 2017). The most abundant type of O-fucose glycan found by Kakuda and Haltiwanger (2017) upon Lfng expression at each O-fucosylation site is shown. Only some of the O-fucosylation sites contain the GlcNAc moiety specifically added by Lfng. (B) EGF domains in mN1 with the appropriate consensus sequence are O-fucosylated (indicated with red triangles) by Pofut1 in the ER. Subsequently, mN1 is translocated to the Golgi, where some O-fucose-modified residues are extended by Lfng, which adds GlcNAc (indicated with blue square) onto O-fucose. The sites of O-fucosylation and Lfng modification in mN1 are shown as previously identified (Kakuda and Haltiwanger, 2017).

In addition, by studying how well dN variants with substitutions abolishing O-fucosylation sites in certain EGFs rescue the phenotypes caused by Notch haploinsufficiency, Fng-mediated enhancement of dN trans-activation by Dl was shown to regulate wing vein development (Pandey *et al.*, 2019). Moreover, Fng was found to regulate wing margin development by reducing Notch cis-inhibition by Ser (LeBon *et al.*, 2014; Pandey *et al.*, 2019). As Ax variants of dN led to interrupted wing veins and fewer sensory bristles along

the wing margin (see Section 1.2.4) (Foster, 1975; Portin, 1975), studying the effects of Ax variants on Notch signalling in the presence of Fng will help to explore the molecular basis of how these variants lead to the unique *Ax* phenotypes.

While *Drosophila* only has one Fng, there are three Fngs (Lfng, Mfng and Rfng) in mammals, each having different effects on Notch signalling (see Section 1.2.8.3). In this chapter, to study the effects of Fng on N1 trans-activation in a mammalian system, activation assays were performed using mN1 WT or Ax variants reporter cell lines transiently transfected to express Lfng. Lfng was selected from the three mammalian Fng because previous studies suggested the effects of Lfng expression on the trans-activation of N1 were similar to those observed for *Drosophila* Fng, which enhanced dN trans-activation by Dl but reduced that by Ser (Panin *et al.*, 1997; LeBon *et al.*, 2014; Kakuda and Haltiwanger, 2017). Subsequently, cis-JAG1 was co-expressed with Lfng in reporter cell lines to study the effect on cis-inhibition of N1 WT and Ax variants.

6.1.1 Overall assay design

Mouse Lfng and three trans-ligands expressed either by B16 cells (B16 mJag1 and mDll4) or CHO-K1 cells (CHO-K1 hDLL1) were tested in this chapter to study the effects of Lfng expression on N1 activation. Previous studies showed that Lfng had different effects on N1 trans-activation dependent upon the specific canonical ligand used (Table 6.1) (LeBon *et al.*, 2014; Kakuda and Haltiwanger, 2017; Kakuda *et al.*, 2020; Kuintzle, Santat and Elowitz, 2023). In previous studies, while Lfng reduced N1 trans-activation by JAG1, it increased N1 trans-activation by DLL1. The effects of Lfng on N1 trans-activation by

DLL4 appeared to depend on the cell type, as no effect was detected in NIH3T3 cells whereas a positive effect was observed in CHO-K1 cells (Kakuda *et al.*, 2020; Kuintzle, Santat and Elowitz, 2023). Previous studies also suggested that Lfng affected the strength of the cis-interaction (shown by the amount of trans-Dll1 bound to each cell upon cis-ligand expression) of N1 with Jag1 and Dll1 (Table 6.1) (LeBon *et al.*, 2014). In this chapter, following examination of the effects of Lfng alone on the mN1 reporter cells' response to trans-ligands, cis-JAG1 was introduced in the presence and absence of Lfng.

Table 6.1. Effects of Lfng expression on N1 activation by different trans-ligands and the strength of interactions between N1 and different cis-ligands (LeBon *et al.*, 2014; Kakuda and Haltiwanger, 2017; Kakuda *et al.*, 2020; Kuintzle, Santat and Elowitz, 2023). For effects on N1 trans-activation, "↓" or "↑" represent reduced or increased trans-activation. "=" represents no effect on trans-activation. For effects on N1 cis-interaction with cis-Jag1, a "↑" represents an increased amount of trans-Dll1 bound indicative of a weaker cis-inhibitory complex formed in the presence of Fng. Conversely, with cis-Dll1, fewer trans-Dll1 (indicated by "↓") were bound suggesting a stronger cis-inhibitory complex.

Trans/Cis-ligand	Effects on N1 trans-activation	Effects on N1 cis-interaction
JAG1	↓	↑ binding to trans-Dll1
DLL4	= (NIH3T3) or ↑ (CHO-K1)	Not tested
DLL1	↑	↓ binding to trans-Dll1

6.1.2 Experimental setup

mN1 reporter cells were transiently transfected simultaneously with 2 µg of pAPtag2 plasmid encoding either Lfng or EV (gift from Prof. Robert S. Haltiwanger) and 2 µg of pcDNA3.1(+) plasmid encoding cis-JAG1 or EV dependent upon the experiment (Figure 6.2) (see Section 2.6.3). Four different combinations of plasmids were used for transient transfection:

1. mN1 cells co-transfected with EVs of pAPtag2 (pAPtag2-EV) and pcDNA3.1(+) (pcDNA3.1-EV) were used as the double negative control (Figure 6.2A).
2. mN1 cells co-transfected with pAPtag2 plasmid encoding Lfng and pcDNA3.1-EV were used to study the effects of Lfng expression on N1 trans-activation (Figure 6.2B).
3. mN1 cells co-transfected with pAPtag2-EV and pcDNA3.1(+)-hJAG1 were used as the positive control for N1 cis-inhibition by JAG1 without Lfng modifications (Figure 6.2C).
4. mN1 cells co-transfected with pAPtag2-Lfng and pcDNA3.1(+)-hJAG1 were used to study N1 cis-inhibition by JAG1 in the presence of Lfng (Figure 6.2D).

Transfected mN1 reporter cells were co-cultured with ligand-expressing cells (B16 mJag1, B16 mDll4, or CHO-K1 hDLL1) or control cells (B16 WT or CHO-K1 WT). The luminescence produced was measured after 24 hours of co-culture (see Section 2.9.3). Assays were first performed for mN1 WT reporter cells and subsequently for two cell lines expressing either the *N* suppressor variant N947I or the *N* enhancer variant H1129Y. When co-cultured with control cells in the absence of trans-ligand, similar auto-activation of all three cell lines transfected with Lfng and pAPtag2-EV was observed (Appendix G, Figure G.1), indicating that the expression of Lfng did not affect the background activation level. RT-PCRs were also performed for transfected cells as before (see Section 4.3) for *cis-JAG1* and *mN1* with the additional amplification for a 350 bp fragment of *Lfng* to show that the quantity of RNA expressed in each cell line was consistent to

allow comparative analyses (Appendix G, Figure G.2-5). In all cases, specific amplification of the expected band was seen.

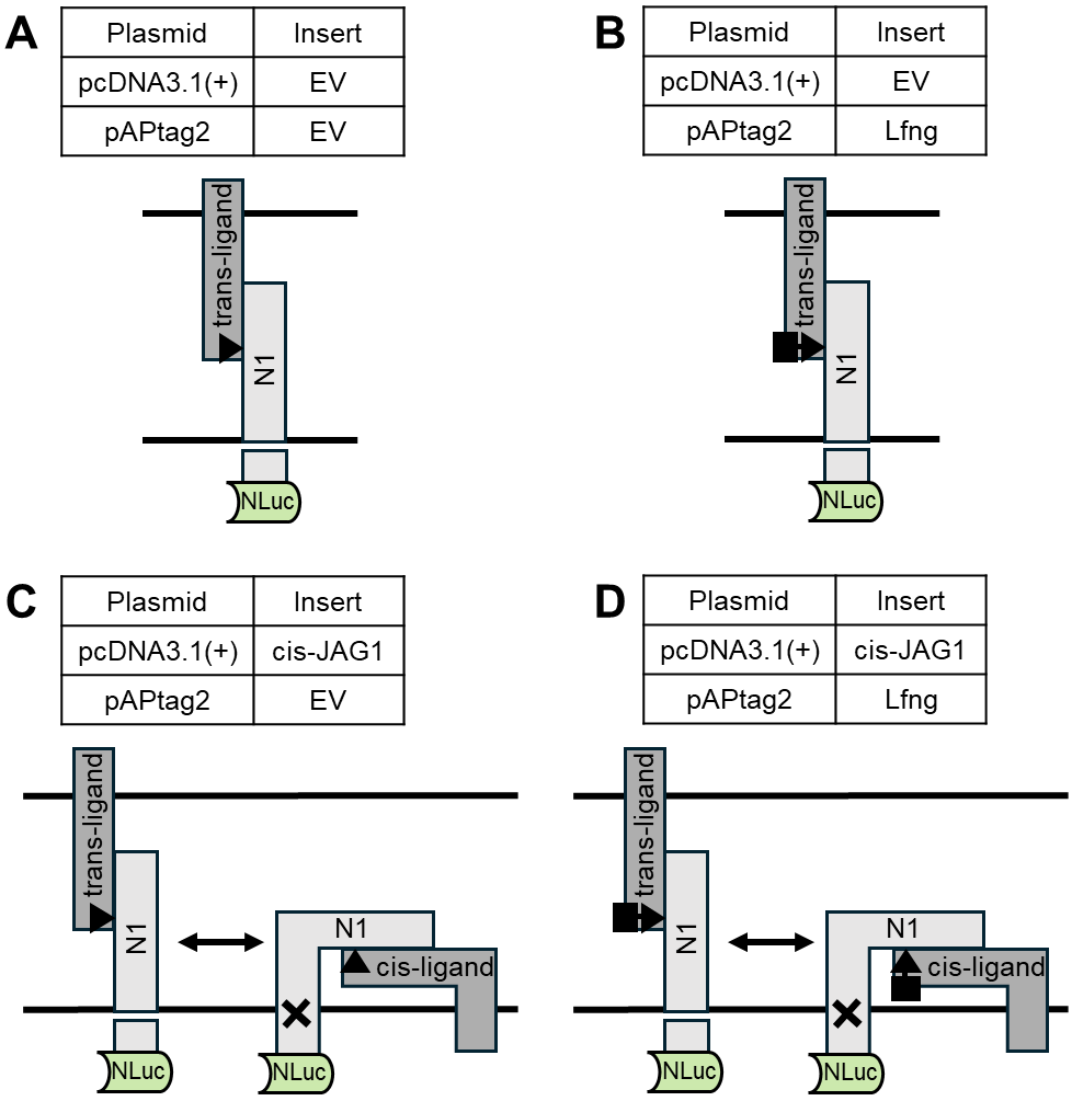


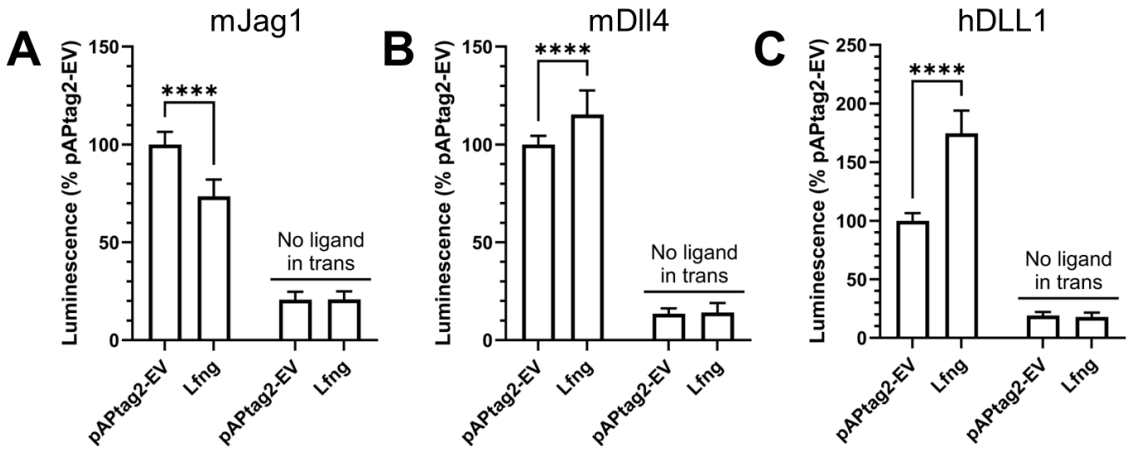
Figure 6.2. Plasmids used to study Lfng's effects on Notch activation and cis-inhibition.

Four combinations of plasmids were used for transient transfection of mN1 reporter cells. (A) Cells transfected with EVs of pcDNA3.1(+) and pAPtag2 were used to show N1 trans-activation in the absence of both Lfng and cis-JAG1. (B) Cells transfected with EV of pcDNA3.1(+) and pAPtag2 plasmid encoding Lfng were used to study N1 trans-activation upon Lfng modifications in the absence of cis-JAG1. (C) Cells transfected with pcDNA3.1(+) plasmid encoding cis-JAG1 and EV of pAPtag2 were used to show N1 cis-inhibition by JAG1 in the absence of Lfng. (D) Cells transfected with pcDNA3.1(+) plasmid encoding cis-JAG1 and pAPtag2 plasmid encoding Lfng were used to study N1 cis-inhibition by JAG1 upon Lfng modifications.

6.2 Studying the effects of Lfng expression on N1 trans-activation

6.2.1 Effects of Lfng expression on N1 WT trans-activation

In the absence of cis-inhibition, the activity level of WT mN1 reporter cells transfected with either pAPtag2-Lfng or the control plasmid pAPtag2-EV (Figure 6.3) were compared. Lfng expression reduced Jag1-mediated N1 trans-activation by ~25% (Figure 6.3A), whereas Lfng enhanced Dll4- (Figure 6.3B) and DLL1-mediated (Figure 6.3C) trans-activation by ~15% and ~75% respectively.



Plasmid	Luminescence (% pAPtag2-EV)
pAPtag2-EV	100 ± 6.7
Lfng	73.5 ± 8.6

Plasmid	Luminescence (% pAPtag2-EV)
pAPtag2-EV	100 ± 4.5
Lfng	115.3 ± 12.3

Plasmid	Luminescence (% pAPtag2-EV)
pAPtag2-EV	100 ± 6.5
Lfng	174.6 ± 19.4

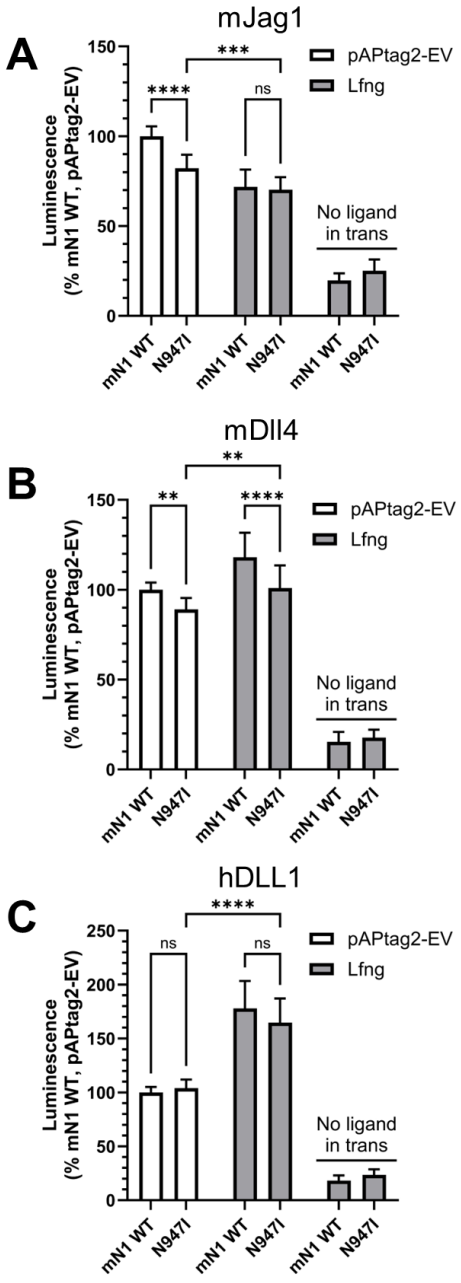
Figure 6.3. Trans-activation of mN1 WT cells transfected with Lfng plasmid.

Activation assays for mN1 WT cells transiently transfected with either pAPtag2-Lfng (Lfng) or pAPtag2-EV. Transfected cells were grown with (A) B16 mJag1 cells, (B) B16 mDll4 cells, (C) CHO-K1 hDLL1 cells or control cells (B16 WT or CHO-K1 WT, indicated by “No ligand in trans”). Graph (upper panel) and table (lower panel) show the combined results of at least eight independent plates, each with four repeat wells. Luminescence signal in each case is shown relative to cells transfected with pAPtag2-EV. Data presented as mean ± SD. Statistical significance compared to pAPtag2-EV was determined in (A) by two-tailed unpaired t test and in (B) and (C) by two-tailed unpaired Welch’s test (**** = $P < 0.0001$).

6.2.2 Effects of Lfng expression on trans-activation of Ax variants

Similar to the results of previous co-culture trans-activation assays (see Section 3.6.2), in the absence of Fng, the *N* suppressor variant N947I (Figure 6.4) and the *N* enhancer variant H1129Y (Figure 6.5) both showed lower activation levels than WT when co-cultured with B16 mJag1 (Figure 6.4A and 6.5A) and B16 mDll4 (Figure 6.4B and 6.5B). When co-cultured with CHO-K1 hDLL1, which had not been tested previously, N947I and H1129Y showed WT activation levels (Figure 6.4C and 6.5C).

Upon Lfng expression, N1 WT activation was reduced with trans-Jag1, but increased with trans-Dll4 and trans-DLL1 (Fig 6.3). The direction of change in trans-activation levels of N947I and H1129Y was similar to those observed in N1 WT for all three trans-ligands used. (Fig 6.4 and 6.5). However, in the presence of trans-Jag1, the magnitude of change in activity for both N947I and H1129Y was substantially smaller than WT (Figure 6.4A and 6.5A), suggesting that the response to Lfng was largely lost or ineffective. This was in contrast to the magnitude of change seen in the Lfng-transfected Ax cell lines activated by trans-Dll4 and trans-DLL1, which were very similar to WT (Figure 6.4B, C and 6.5B, C). Therefore both Ax variants showed a selective loss of the Lfng effect in response to trans-Jag1 only.



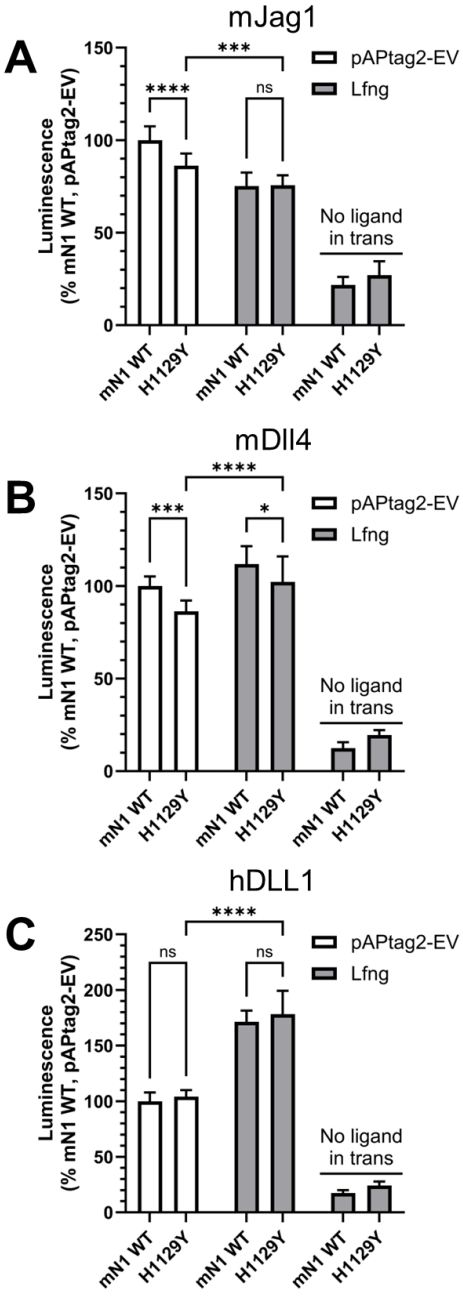
Plasmid	Luminescence (% mN1 WT, pAPtag2-EV)	
	mN1 WT	N947I
pAPtag2-EV	100 ± 5.5	82.2 ± 7.5
Lfng	71.8 ± 9.7	70.2 ± 7

Plasmid	Luminescence (% mN1 WT, pAPtag2-EV)	
	mN1 WT	N947I
pAPtag2-EV	100 ± 4	89.1 ± 6.4
Lfng	118.1 ± 13.7	100.9 ± 12.6

Plasmid	Luminescence (% mN1 WT, pAPtag2-EV)	
	mN1 WT	N947I
pAPtag2-EV	100 ± 5.1	104 ± 7.9
Lfng	177.9 ± 25.5	164.8 ± 22.3

Figure 6.4. Trans-activation of mN1 N947I cells transfected with Lfng plasmid.

Activation assays for mN1 WT and N947I cells transfected with pcDNA3.1-EV and pAPtag2-EV or Lfng. Cells were grown with (A) B16 mJag1 cells, (B) B16 mDll4 cells, (C) CHO-K1 hDLL1 cells or control cells (B16 WT or CHO-K1 WT, indicated by “No ligand in trans”). Graph (left panel) and table (right panel) show the combined results of at least four independent plates, each with four repeat wells. Luminescence signal in each case is shown relative to cells transfected with pAPtag2-EV. Data presented as mean ± SD. Statistical significance was determined by ordinary two-way ANOVA and Šídák’s post hoc test (ns = not significant, ** = $P < 0.01$, *** = $P < 0.001$, **** = $P < 0.0001$). Note the effect of Lfng on Jag1-mediated trans-activation was weaker in N947I than in WT.



Plasmid	Luminescence (% mN1 WT, pAPtag2-EV)	
	mN1 WT	H1129Y
pAPtag2-EV	100 ± 7.5	86.2 ± 6.5
Lfng	75.2 ± 7.2	75.6 ± 5.5

Plasmid	Luminescence (% mN1 WT, pAPtag2-EV)	
	mN1 WT	H1129Y
pAPtag2-EV	100 ± 5.1	86.4 ± 5.8
Lfng	111.8 ± 9.6	102.2 ± 13.8

Plasmid	Luminescence (% mN1 WT, pAPtag2-EV)	
	mN1 WT	H1129Y
pAPtag2-EV	100 ± 7.8	104.2 ± 5.7
Lfng	171.4 ± 10.1	178.3 ± 21

Figure 6.5. Trans-activation of mN1 H1129Y cells transfected with Lfng plasmid.

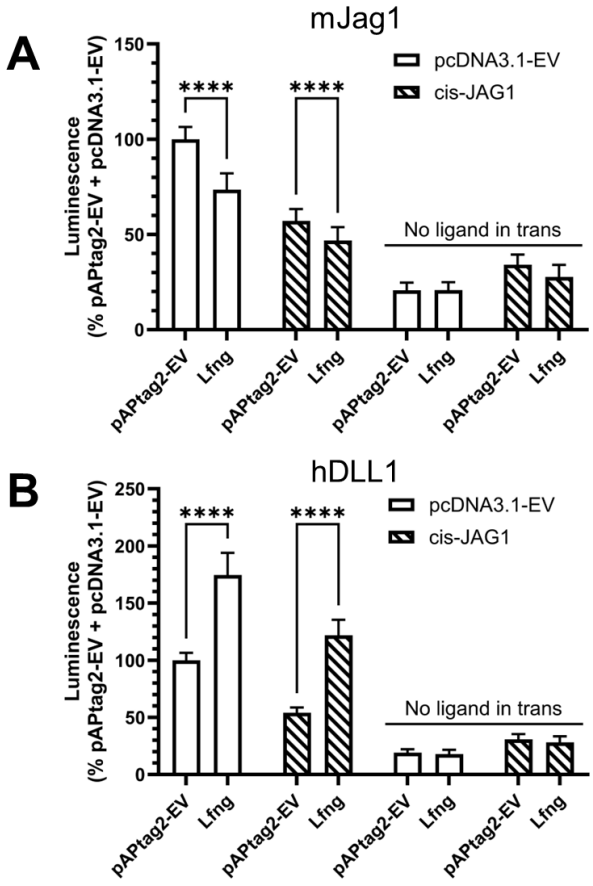
Activation assays for mN1 WT and H1129Y cells transfected with pcDNA3.1-EV and pAPtag2-EV or Lfng. Cells were grown with (A) B16 mJag1 cells, (B) B16 mDll4 cells, (C) CHO-K1 hDLL1 cells or control cells (B16 WT or CHO-K1 WT, indicated by "No ligand in trans"). Graph (left panel) and table (right panel) show the combined results of four independent plates, each with four repeat wells. Luminescence signal in each case is shown relative to cells transfected with pAPtag2-EV. Data presented as mean ± SD. Statistical significance was determined by ordinary two-way ANOVA and Šídák's post hoc test (ns = not significant, * = $P < 0.05$, *** = $P < 0.001$, **** = $P < 0.0001$). Note the effect of Lfng on Jag1-mediated trans-activation was weaker in H1129Y than in WT.

6.3 Studying the effects of Lfng expression on N1 cis-inhibition by JAG1

6.3.1 Effects of Lfng expression on N1 WT cis-inhibition by JAG1

The activity level of WT cells co-transfected with cis-JAG1 and Lfng was compared with that of WT cells co-transfected with cis-JAG1 and pAPtag2-EV. Under current assay conditions without Lfng co-transfection, >40% reduction in Jag1- and DLL1-mediated N1 trans-activation was obtained upon cis-JAG1 expression (Figure 6.6). The reduction in trans-activation is smaller than that observed previously for cis-inhibition in the presence of trans-Jag1 (Chapter 4, Figure 4.5), likely due to a lower concentration of cis-JAG1 plasmid used during transfection. Upon Lfng expression Jag1-mediated N1 activation was further reduced by ~10% (Figure 6.6A), suggesting the cis-inhibitory response might be increased slightly. Conversely, DLL1-mediated N1 activation increased by over 60% suggesting the cis-inhibitory response was reduced (Figure 6.6B).

Since very low levels of cis-inhibition (<20%) were obtained with and without Lfng expression under the current experimental setup, the data for trans-Dll4-mediated N1 activation upon co-expression of cis-JAG1 and Lfng is shown in Appendix G (Figure G.6) and not discussed in depth in this chapter. These data suggest that the GlcNAc extension has only minor modulatory effects on the Notch response to trans-Dll4, irrespective of whether or not cis-JAG1 is present.



Plasmid	Luminescence (% pAPtag2-EV + pcDNA3.1-EV)	
	pcDNA3.1-EV	cis-JAG1
pAPtag2-EV	100 ± 6.7	56.1 ± 6.3
Lfng	73.5 ± 8.6	46.3 ± 7

Plasmid	Luminescence (% pAPtag2-EV + pcDNA3.1-EV)	
	pcDNA3.1-EV	cis-JAG1
pAPtag2-EV	100 ± 6.5	54.1 ± 4.6
Lfng	174.6 ± 19.4	121.8 ± 13.6

Figure 6.6. Trans-activation of mN1 WT cells transfected with cis-JAG1 and Lfng plasmids.

Jag1-mediated cis-inhibition assays for mN1 WT cells transfected with pcDNA3.1-EV or cis-JAG1 and pAPtag2-EV or Lfng. Cells were grown with (A) B16 mJag1 cells or (B) CHO-K1 hDLL1 cells or control cells (B16 WT or CHO-K1 WT, indicated by “No ligand in trans”). Graph (left panel) and table (right panel) show the combined results of at least eight independent plates, each with four repeat wells. Luminescence signal in each case is shown relative to cells transfected with pcDNA3.1-EV and pAPtag2-EV. Data presented as mean ± SD. Statistical significance was determined by ordinary two-way ANOVA and Šídák’s post hoc test (**** = $P < 0.0001$).

6.3.2 Effects of Lfng expression on cis-inhibition of Ax variants by JAG1

6.3.2.1 Cis-Inhibition of N947I and H1129Y in the absence of Fng

In the absence of Fng, trends similar to the previous cis-inhibition assay (see Section

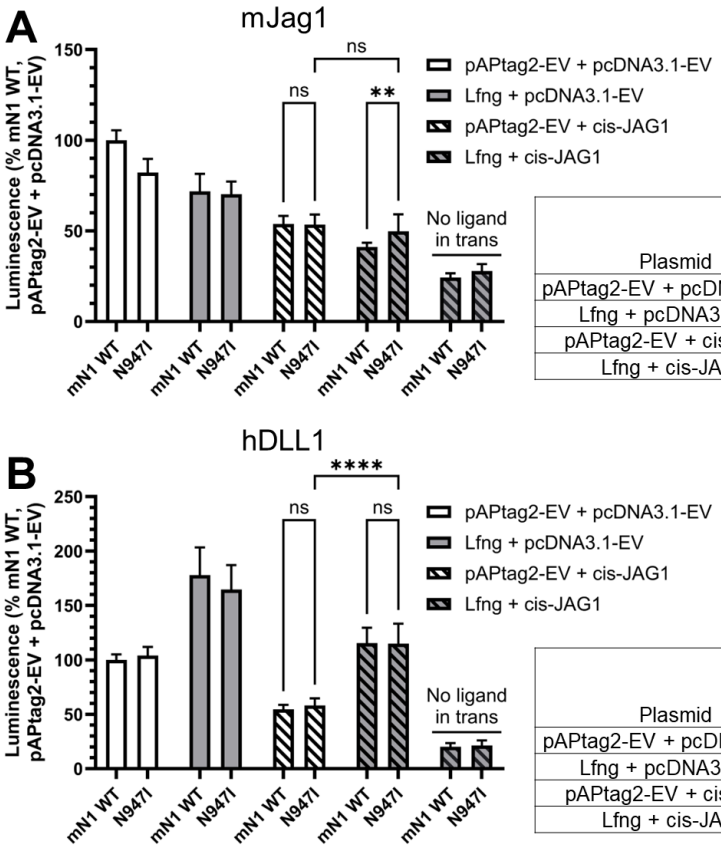
4.5) were observed for N947I and H1129Y demonstrating as for WT that transfection of the control plasmid pAPtag2 did not impact receptor activity. Upon expression of cis-JAG1, the activation levels of N947I (Figure 6.7A) and H1129Y (Figure 6.8A) were similar to or higher than N1 WT when co-cultured with trans-Jag1 despite showing reduced trans-activation compared to N1 WT in the absence of cis-JAG1. When co-cultured with trans-DLL1, both Ax variants showed similar trans-activation levels to N1 WT (Figure 6.7B and 6.8B). Upon cis-JAG1 expression, N947I showed similar activity to N1 WT (Figure 6.7B) while H1129Y showed increased activity by ~25% (Figure 6.8B). These data suggest that the the inhibitory effect of cis-JAG1 on N947I is unaffected in the presence of trans-DLL1, whilst the H1129Y substitution reduces the cis-inhibitory effect leading to higher activation than WT.

6.3.2.2 Cis-Inhibition of N947I in the presence of Lfng

Upon Lfng expression, trans-Jag1-mediated activation of N947I in the presence of cis-JAG1 was unaffected, whilst that of N1 WT was reduced by ~10% (Figure 6.7A). As a result, when grown with trans-Jag1, N947I showed higher activity than N1 WT upon co-expression of cis-JAG1 and Lfng. In contrast, when grown with trans-DLL1 (Figure 6.7B) in the presence of cis-JAG1, Lfng expression led to a substantial increase (~60%) in the activity of N947I, indistinguishable from N1 WT.

6.3.2.3 Cis-inhibition of H1129Y in the presence of Lfng

Similar to trends observed for N1 WT, Lfng expression in the presence of cis-JAG1 reduced trans-Jag1-mediated activation of H1129Y by ~10% (Figure 6.8A) such that the activity of H1129Y remained higher than that of N1 WT. For DLL1-mediated activation of H1129Y (Figure 6.8B) Lfng expression in the presence of cis-JAG1 substantially enhanced H1129Y activity (~60%), as seen for WT, with the Ax variant having higher activity than WT overall.

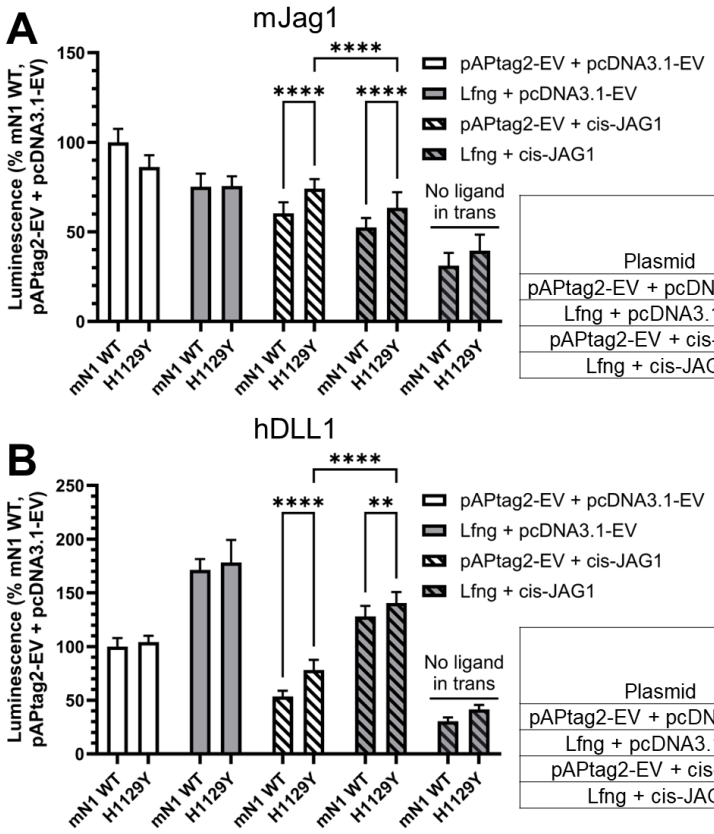


Plasmid	Luminescence (% mN1 WT, pAPtag2-EV + pcDNA3.1-EV)	
	mN1 WT	N947I
pAPtag2-EV + pcDNA3.1-EV	100 ± 5.5	82.2 ± 7.5
Lfng + pcDNA3.1-EV	71.8 ± 9.7	70.2 ± 7
pAPtag2-EV + cis-JAG1	53.8 ± 4.5	53.5 ± 5.6
Lfng + cis-JAG1	41.1 ± 2.3	49.8 ± 9.4

Plasmid	Luminescence (% mN1 WT, pAPtag2-EV + pcDNA3.1-EV)	
	mN1 WT	N947I
pAPtag2-EV + pcDNA3.1-EV	100 ± 5.1	104 ± 7.9
Lfng + pcDNA3.1-EV	177.9 ± 25.5	164.8 ± 22.3
pAPtag2-EV + cis-JAG1	54.6 ± 4	58.2 ± 6.4
Lfng + cis-JAG1	115.4 ± 14.1	115 ± 18.3

Figure 6.7. Trans-activation of mN1 N947I cells transfected with cis-JAG1 and Lfng.

Jag1-mediated cis-inhibition assays for mN1 WT and N947I cells transfected with pcDNA3.1-EV or cis-JAG1 and pAPtag2-EV or Lfng. Cells were grown with (A) B16 mJag1 cells or (B) CHO-K1 hDLL1 cells or control cells (B16 WT or CHO-K1 WT, indicated by “No ligand in trans”). Graph (left panel) and table (right panel) show the combined results of at least four independent plates, each with four repeat wells. Luminescence signal in each case is shown relative to mN1 WT cells transfected with pcDNA3.1-EV and pAPtag2-EV. Data presented as mean ± SD. Statistical significance was determined by ordinary two-way ANOVA and Šídák’s post hoc test (ns = not significant, ** = P < 0.01, **** = P < 0.0001).



Plasmid	Luminescence (% mN1 WT, pAPtag2-EV + pcDNA3.1-EV)	
	mN1 WT	H1129Y
pAPtag2-EV + pcDNA3.1-EV	100 ± 7.5	86.2 ± 6.5
Lfng + pcDNA3.1-EV	75.2 ± 7.2	75.6 ± 5.5
pAPtag2-EV + cis-JAG1	60.4 ± 6.2	74.1 ± 5.4
Lfng + cis-JAG1	52.5 ± 5.3	63.4 ± 8.7

Plasmid	Luminescence (% mN1 WT, pAPtag2-EV + pcDNA3.1-EV)	
	mN1 WT	H1129Y
pAPtag2-EV + pcDNA3.1-EV	100 ± 7.8	104.2 ± 5.7
Lfng + pcDNA3.1-EV	171.4 ± 10.1	178.3 ± 21
pAPtag2-EV + cis-JAG1	53.6 ± 5.2	78.3 ± 9.4
Lfng + cis-JAG1	128.1 ± 9.8	140.5 ± 10.2

Figure 6.8. Trans-activation of mN1 H1129Y cells transfected with cis-JAG1 and Lfng.

Jag1-mediated cis-inhibition assays for mN1 WT and H1129Y cells transfected with pcDNA3.1-EV or cis-JAG1 and pAPtag2-EV or Lfng. Cells were grown with (A) B16 mJag1 cells or (B) CHO-K1 hDLL1 cells or control cells (B16 WT or CHO-K1 WT, indicated by “No ligand in trans”). Graph (left panel) and table (right panel) show the combined results of four independent plates, each with four repeat wells. Luminescence signal in each case is shown relative to mN1 WT cells transfected with pcDNA3.1-EV and pAPtag2-EV. Data presented as mean ± SD. Statistical significance was determined by ordinary two-way ANOVA and Šídák’s post hoc test (** = P < 0.01, **** = P < 0.0001).

6.4 Discussion

Lfng reduced N1 WT trans-activation by Jag1 but increased it by Dll4 and DLL1

The effects of Lfng expression on the trans-activation of N1 WT and Ax variants tested in this chapter are summarised in Table 6.2. Upon expression of Lfng, When co-cultured

with trans-Jag1, the trans-activation level of N1 WT decreased (Figure 6.3, Table 6.2). When co-cultured with trans-Dll4 or trans-DLL1, the activation level of N1 WT increased upon expression of Lfng (Figure 6.3). The positive effect of Lfng expression on the trans-activation of N1 WT by DLL1 (~75%) was much greater than that for Dll4 (~15%) (compare Figure 6.3B and C). These results are consistent with the trends observed in previous studies (Table 6.1) and suggest that the cellular assay used here is a suitable system to probe the effects of O-glycan PTMs on trans-activatory and cis-inhibitory responses of N1 WT and Ax variants (Kakuda and Haltiwanger, 2017; Kakuda *et al.*, 2020; Kuintzle, Santat and Elowitz, 2023).

Table 6.2. Effects of Lfng expression on the trans-activation of mN1 WT and Ax variants.

Activation levels of mN1 WT and Ax variant cell lines transfected with no Fng or Lfng and co-cultured with three different trans-ligands (as indicated by labels) (Figure 6.3, 6.4, 6.5). The activities measured for N1 WT cells transfected without Fng are shown as 100%. The results are coloured red when the activity of the Ax variant is significantly different from that of N1 WT tested under the same conditions.

Cell line	Trans-Jag1		Trans-Dll4		Trans-DLL1	
	No Fng	Lfng	No Fng	Lfng	No Fng	Lfng
N1 WT	100	74	100	115	100	175
N947I	82	70	89	101	104	165
H1129Y	86	76	86	102	104	178

For N1 WT, Lfng caused a small increase in JAG1-mediated cis-inhibition with trans-Jag1, but an apparent reduction with trans-DLL1

When cis-JAG1 was present, Lfng expression reduced Jag1-mediated activation of N1 WT by ~10% compared to cells without Lfng (Figure 6.6, Table 6.3). This showed that Lfng modification of N1 strengthened the cis-inhibitory response when trans- and cis-

ligands were both JAG1. Since Jag1-mediated trans-activation was reduced by Lfng (Table 6.2), the cis-inhibitory ability of JAG1 appeared to be unchanged or reduced to a smaller extent by Lfng.

Table 6.3. Changes in Jag1-mediated trans-activation of mN1 WT and Ax variants upon co-expression of cis-JAG1 and Lfng.

Trans-Jag1-mediated activation levels of mN1 WT and Ax variant cell lines transfected with no Fng or Lfng upon expression of cis-JAG1 (Figure 6.6, 6.7, 6.8). The activity measured for N1 WT cells transfected with no cis-JAG1 or Fng is shown as 100%. The results are coloured red when the activity of the Ax variant is significantly different from that of N1 WT tested under the same conditions.

Cell line	Trans-Jag1		
	No cis-JAG1 No Fng	cis-Jag1 No Fng	cis-Jag1 Lfng
N1 WT	100	56	46
N947I	82	53	50
H1129Y	86	74	63

When grown with trans-DLL1, higher activity (>60% increase) was observed for N1 WT cells co-expressing cis-JAG1 and Lfng, than cells only expressing cis-JAG1 (Figure 6.6, Table 6.4). This is a very similar increase in N1 activity to that seen when the Lfng effect on trans-activation alone was measured (Table 6.2), and suggests that Lfng enhancement of DLL1-mediated trans-activation reverses the negative effect of cis-JAG1. This is consistent with a higher amount of trans-Dll1 bound to N1 cells expressing Lfng and cis-Jag1 as observed previously (LeBon *et al.*, 2014) (Table 6.1).

Table 6.4. Changes in DLL1-mediated trans-activation of mN1 WT and Ax variants upon co-expression of cis-JAG1 and Lfng.

Trans-DLL1-mediated activation levels of mN1 WT and Ax variant cell lines transfected with no Fng or Lfng upon expression of cis-JAG1 (Figure 6.6, 6.7, 6.8). The activity measured for N1 WT cells transfected with no cis-JAG1 or Fng is shown as 100%. The results are coloured red when the activity of the Ax variant is significantly different from that of N1 WT tested under the same conditions.

Cell line	Trans-DLL1		
	No cis-JAG1 No Fng	cis-Jag1 No Fng	cis-Jag1 Lfng
N1 WT	100	54	122
N947I	104	58	115
H1129Y	104	78	141

N947I and H1129Y variants were less sensitive than N1 WT to the negative effect of Lfng on Jag1-mediated trans-activation

The two Ax variants tested, N947I and H1129Y, both showed an increase in activity similar to those observed for WT upon Lfng expression when co-cultured with trans-Dll4 or trans-DLL1 (Figure 6.4, 6.5, Table 6.2). However, when grown with trans-Jag1, both variants showed only a ~10% decrease in activity, which was less than that observed for N1 WT (~25%). This suggested that both these substitutions in the Ax region may reduce, to some extent, the negative effect of Lfng on N1 trans-activation by Jag1 (Figure 6.4, 6.5). While showing reduced Jag1-mediated trans-activation compared to N1 WT in the absence of Lfng, it should be noted that these two variants showed similar overall activities to N1 WT when Lfng was expressed (Figure 6.4, 6.5, Table 6.2).

Lfng expression did not change the level of Jag1-mediated trans-activation of N947I when cis-JAG1 was expressed

Similar to N1 WT, when cis-JAG1 was present, Lfng expression led to a small (~10%) reduction in Jag1-mediated activation of H1129Y (Figure 6.8, Table 6.3). On the other hand, N947I showed similar Jag1-mediated activation when cis-JAG1 was co-expressed with and without Lfng (Figure 6.7). Therefore, the small negative effect of Lfng on JAG1-mediated cis-inhibition appeared to be cancelled out by its effect on N947I trans-activation by Jag1, thereby generating an overall activity level similar to cis-inhibited cells without Lfng.

N947I and H1129Y both showed higher Jag1-mediated activation than N1 WT when Lfng was expressed in the presence of cis-JAG1

Co-expression of Lfng and cis-JAG1 reduced Jag1-mediated activation level for WT, but not for N947I, compared to cis-JAG1-transfected cells alone, resulting in ~10% higher overall activity of this Ax variant (Figure 6.7). The Jag1-mediated activation of H1129Y was higher than that of N1 WT when cis-JAG1 was expressed either in the absence or presence of Lfng (Figure 6.8). Therefore, upon Lfng expression, while showing similar Jag1-mediated activation to N1 WT in the absence of cis-JAG1, N947I and H1129Y showed higher activation in the presence of cis-JAG1.

When grown with trans-DLL1, Lfng reduced JAG1-mediated cis-inhibition of N1 WT, N947I and H1129Y to a similar extent

Lfng expression resulted in similar increases in activities for N1 WT, N947I and H1129Y cell lines transfected with cis-JAG1 and co-cultured with trans-DLL1 (Figure 6.7 and 6.8, Table 6.4). Taking into consideration that N947I and H1129Y did not change Lfng's positive effect on trans-activation by DLL1, this suggested that Lfng's apparent negative effect on cis-inhibition is mediated primarily through the enhanced trans-activation response.

H1129Y showed higher DLL1-mediated activation than N1 WT and N947I upon co-expression of cis-JAG1 and Lfng

DLL1-mediated activation of H1129Y was higher than that of N1 WT when cis-JAG1 was expressed in the absence of Lfng (Figure 6.8, Table 6.4). This is in contrast to N947I which showed activity indistinguishable from WT (Figure 6.7). Furthermore, although WT and the two Ax variants all showed substantial enhancements in activity when Lfng was co-expressed with cis-JAG1, because of the higher activity of H1129Y in the cis-JAG1-only condition, its overall activity was considerably higher than either WT or N947I when Lfng was expressed (Figure 6.8, Table 6.4).

7 Low-resolution structural analysis of the Abruptex region

7.1 Introduction

Though commonly presented as a straight rod in simplified schematic figures, the actual structure of NECD is not completely known. The narrow dimensions of tandem EGF repeats increase the difficulty of getting high-resolution structures by cryo-electron microscopy (Kelly *et al.*, 2010). Previous X-ray crystallography and NMR studies of fragments of N1ECD revealed structures of EGF4-13, which showed an angle of 80-90° between EGF5 and EGF6, a flexible linker between EGF9 and EGF10 and a rod-like rigid structure of EGF11-13 (Cordle, Johnson, *et al.*, 2008; Weisshuhn *et al.*, 2016) (Figure 7.1). Also, recent X-ray crystallography studies performed by our collaborator showed a near-linear structure of EGF20-24 with Ca^{2+}-dependent flexibility at the interface of EGF20-21 due to a relatively weak Ca^{2+}-binding affinity of EGF21 (Bo *et al.*, 2024) (Figure 7.1). The structure of the rest of the EGF repeats in the NECD, including the Ax region, remains unknown. Previous attempts by our lab to determine the structure of the Ax region by X-ray crystallography were unsuccessful. In this chapter, following the purification of hN1 EGF20-27 and EGF20-29 fragments, size exclusion chromatography small angle X-ray scattering (SEC-SAXS) was used to study the structures of these constructs in solution and generate a low-resolution structural model of the Ax region.

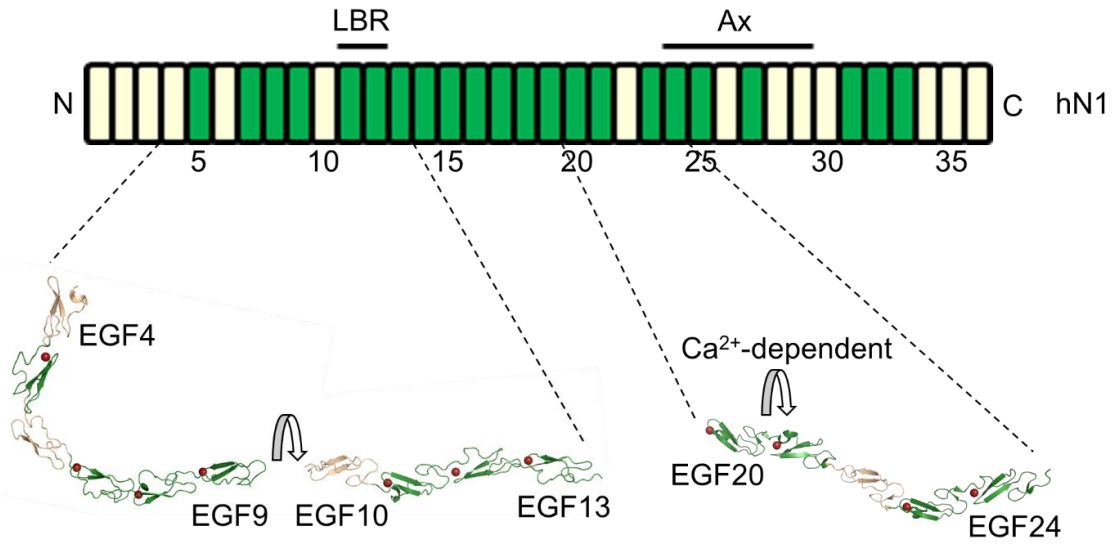


Figure 7.1. Existing structural models of hN1ECD.

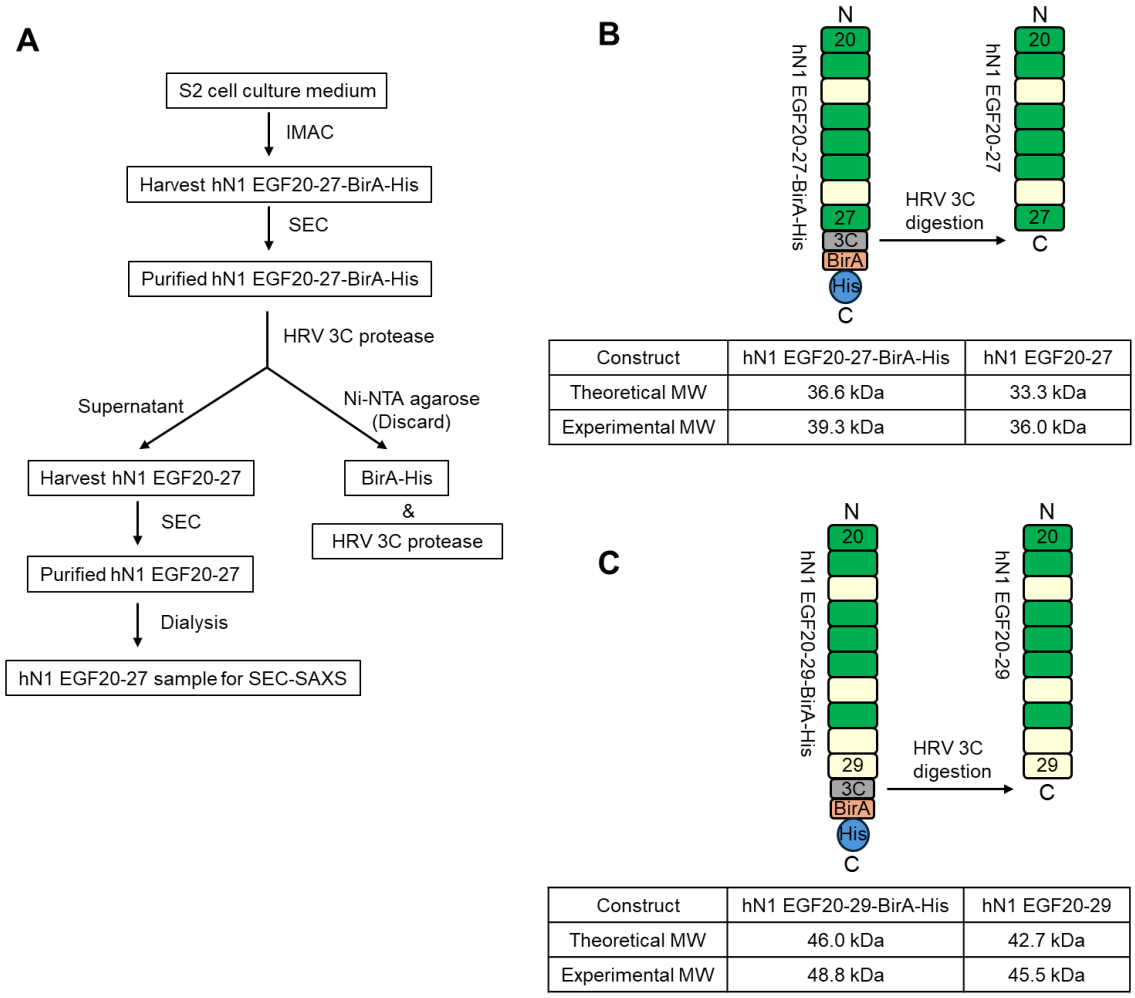
X-ray structures of EGF4–7 (PDB: 5FMA) and EGF10–13 (PDB: 2VJ3) and RDC measurements were employed to construct the model for EGF4-13 by Weisshuhn et al. (2016), which suggested a flexible linker between EGF9 and 10 (Cordle, Johnson, *et al.*, 2008; Weisshuhn *et al.*, 2016). The X-ray structure of EGF20-24 (PDB: 9B3N) showed a near-linear structure with Ca^{2+}-dependent flexibility at the interface of EGF20-21 (Bo *et al.*, 2024). Non-Ca^{2+}-binding EGF domains are shown in wheat, cbEGF domains are shown in green and the Ca^{2+} ions are shown as red spheres.

7.2 SEC-SAXS sample preparation

7.2.1 Protein purification strategy

The method employed to prepare protein samples for SEC-SAXS is shown in Figure 7.2A (see Section 2.7). hN1 EGF20-27 and EGF20-29 constructs with a C-terminal BirA-His tag (see Appendix H, Table H.1) were expressed by stably-transfected S2 cells (see Section 2.6.4, S2 hN1 EGF20-27 cells were maintained by Dr Hilman Nurmahdi, University of Oxford). The BirA-His-tagged constructs contain an HRV 3C protease cleavage site (LEVLFQ/GP) between the hN1 fragment and the BirA-His tag (Figure

7.2B). To harvest the BirA-His-tagged proteins, the S2 cell culture medium was filtered and subjected initially to IMAC. The protein sample eluted from the IMAC column was then purified by SEC. To remove the BirA-His tag, protein samples were then digested with His-tagged HRV 3C protease. The released BirA-His tag and His-tagged HRV 3C protease (and any uncleaved BirA-His-tagged protein) were captured by Ni-NTA agarose and removed by centrifugation. The supernatant containing the hN1 fragment without BirA-His tag was subjected to further purification by SEC.



Construct	hN1 EGF20-27-BirA-His	hN1 EGF20-27
Theoretical MW	36.6 kDa	33.3 kDa
Experimental MW	39.3 kDa	36.0 kDa

Construct	hN1 EGF20-29-BirA-His	hN1 EGF20-29
Theoretical MW	46.0 kDa	42.7 kDa
Experimental MW	48.8 kDa	45.5 kDa

Figure 7.2. Preparation of protein samples for SEC-SAXS.

(A) Method employed to prepare samples for SEC-SAXS using hN1 EGF20-27 as an example. hN1 EGF20-27-BirA-His construct was produced by S2 cells and harvested by IMAC. The protein eluted from the IMAC column was further purified by SEC. The hN1 EGF20-27-BirA-His construct was digested with HRV 3C protease and treated with Ni-NTA agarose which captured the released BirA-His tag and His-tagged protease. The supernatant containing the cleaved hN1 EGF20-27 was subjected to purification by SEC. The purified hN1 EGF20-27 protein was dialysed overnight in SAXS buffer to prepare the sample for SEC-SAXS. (B) Schematic illustration of hN1 EGF20-27(-BirA-His) constructs before and after HRV 3C protease digestion. (C) Schematic illustration of hN1 EGF20-29(-BirA-His) constructs before and after HRV 3C protease digestion. Theoretical MWs calculated without PTMs (Expasy ProtParam) and experimental MWs measured by ESI-MS (performed by Dr David Staunton, University of Oxford) are shown in the tables below the illustrations. Non-Ca^{2+}-binding EGF domains are shown in wheat. cbEGF domains are shown in green.

7.2.2 Purification of hN1 EGF20-27 and EGF20-29

The protein samples of hN1 EGF20-27 and EGF20-29 were analysed by western blot or SDS-PAGE between each stage of the purification protocol (Figure 7.3 and 7.4). The SEC chromatogram of hN1 EGF20-27-BirA-His sample after IMAC showed a major peak with a few minor peaks on both sides (Figure 7.3B). Analysis of SEC samples by SDS-PAGE and western blot showed that the major peak contained the protein with MW (between 34 and 43 kDa) similar to the theoretical MW of hN1 EGF20-27-BirA-His (36.6 kDa) (Figure 7.3C). The SEC chromatogram of hN1 EGF20-29-BirA-His sample after IMAC also showed a major peak with a few minor peaks (Figure 7.4B). Analysis of SEC samples by SDS-PAGE and western blot showed that the major peak contained the protein with MW (between 43 and 55 kDa) similar to the theoretical MW of hN1 EGF20-29-BirA-His (46 kDa) (Figure 7.4C). His-tagged proteins with higher MWs were detected in minor peaks collected before the major peak of both constructs. This suggested the constructs may interact to form large MW complexes with itself or other cellular proteins.

The protein samples corresponding to the major peaks were collected as BirA-His constructs of hN1 EGF20-27 and EGF20-29 and were subjected to HRV 3C protease digestion and further purification by SEC. Western blot of the digested samples before and after SEC showed the absence of His-tagged protein, suggesting complete removal of BirA-His tag from the constructs (Figure 7.3D and 7.4D). Also, SDS-PAGE showed that samples after SEC were relatively pure (Figure 7.3D and 7.4D). Electron spray ionisation mass spectrometry (ESI-MS, performed by Dr David Staunton, University of

Oxford) for hN1 EGF20-27 and EGF20-29 constructs before and after removal of the BirA-His tag showed higher MWs than the theoretical MWs estimated without PTMs (Figure 7.2B), which is expected since these constructs might be post-translational modified by glycosyltransferases in the secretory pathway of S2 cells.

.

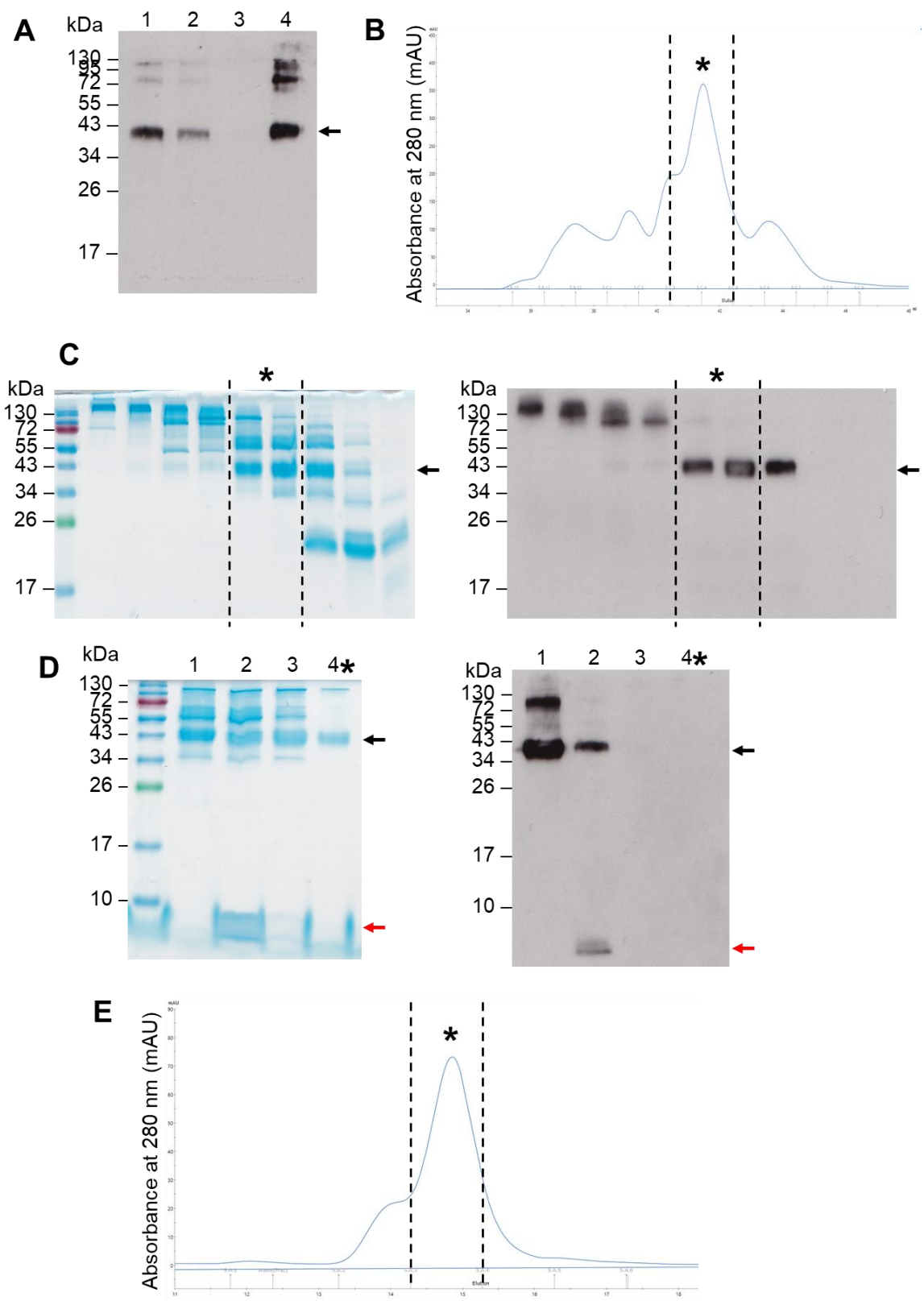


Figure 7.3. Purification of hN1 EGF20-27.

(A) Western blot using anti-His-tag antibody for IMAC samples of hN1 EGF20-27-BirA-His. Lane 1) cell culture medium; Lane 2) cell culture medium after IMAC; Lane 3) washing of Ni column before elution; Lane 4) eluate. The presence of His-tagged proteins with an MW

(indicated by a black arrow) close to the theoretical MW showed that the target protein was successfully produced and purified. (B) SEC chromatograms showing the peaks collected for one injection of the protein sample eluted from the IMAC Ni column. The major peak was indicated by an asterisk. (C) Non-reducing SDS-PAGE and Coomassie staining (left panel) and His-tag western blot (right panel) for peaks collected by SEC. The major peak in SEC, which contains the target band (indicated by a black arrow) was indicated by an asterisk. (D) Non-reducing SDS-PAGE and Coomassie staining (left panel) and His-tag western blot (right panel) for HRV 3C protease digestion of hN1 EGF20-27-BirA-His sample. Lane 1) undigested sample; Lane 2) digested sample; Lane 3) digested sample after treatment with Ni-NTA agarose; Lane 4) SEC-purified hN1 EGF20-27 sample. The band of hN1 EGF20-27 is indicated by a black arrow. The band of BirA-His tag removed from the hN1 construct is indicated by a red arrow. E) SEC chromatograms showing the peaks collected for one injection of the protein sample digested by HRV 3C protease and treated with Ni-NTA agarose. The major peak was indicated by an asterisk.

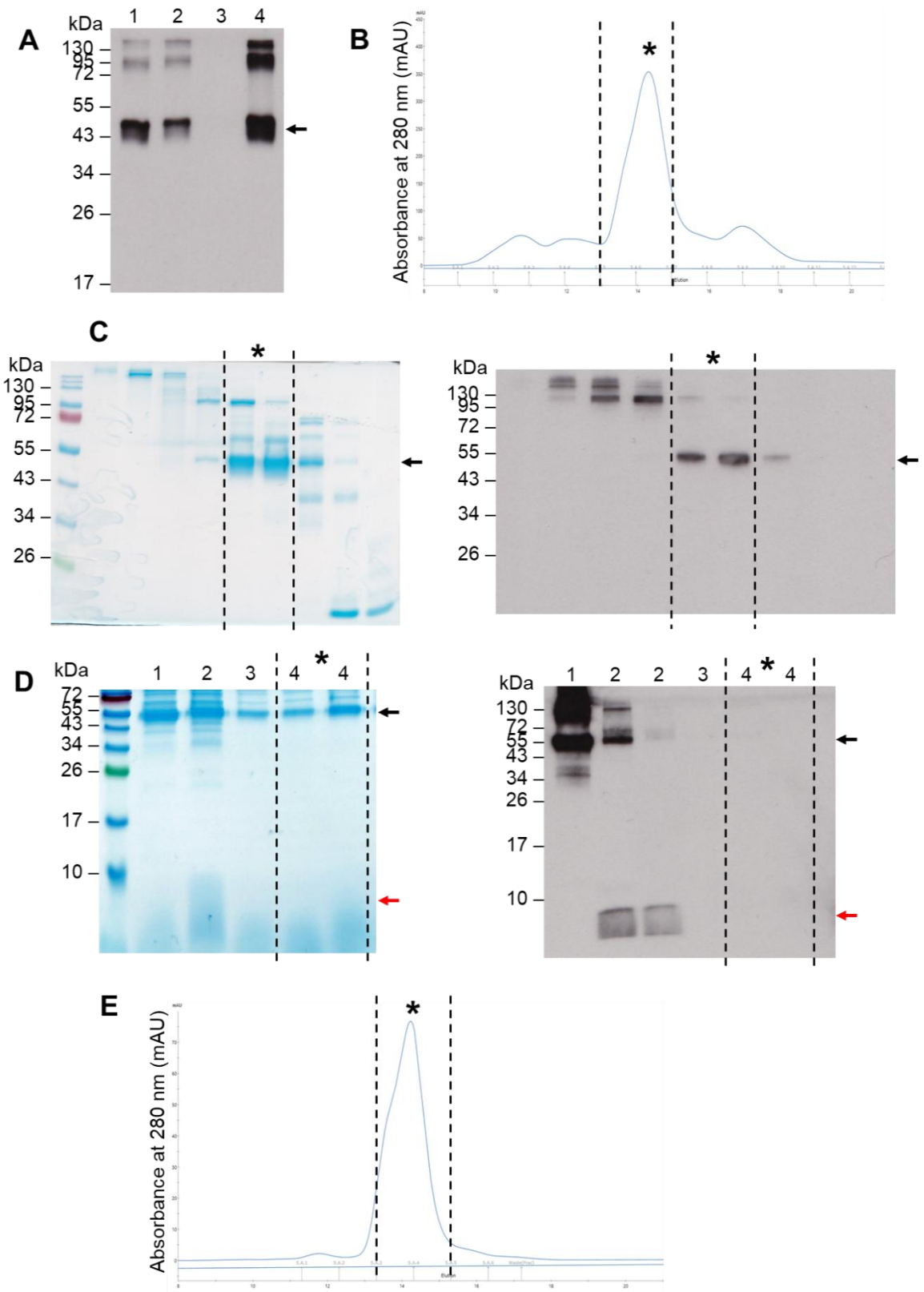


Figure 7.4. Purification of hN1 EGF20-29.

(A) Western blot using anti-His-tag antibody for IMAC samples of hN1 EGF20-29-BirA-His. Lane 1) cell culture medium; Lane 2) cell culture medium after IMAC; Lane 3) washing of Ni column before elution; Lane 4) eluate. The presence of His-tagged proteins with an MW

(indicated by a black arrow) close to the theoretical MW showed the target protein was successfully produced and purified. (B) SEC chromatograms showing the peaks collected for one injection of the protein sample eluted from the IMAC Ni column. The major peak was indicated by an asterisk. (C) Non-reducing SDS-PAGE and Coomassie staining (left panel) and His-tag western blot (right panel) for peaks collected by SEC. The major peak in SEC, which contains the target band (indicated by a black arrow) was indicated by an asterisk. (D) Non-reducing SDS-PAGE and Coomassie staining (left panel) and His-tag western blot (right panel) for HRV 3C protease digestion of hN1 EGF20-29-BirA-His sample. Lane 1) undigested sample; Lane 2) digested sample; Lane 3) digested sample after treatment with Ni-NTA agarose; Lane 4) SEC-purified hN1 EGF20-29 sample. The band of hN1 EGF20-29 is indicated by a black arrow. The band of BirA-His tag removed from the hN1 construct is indicated by a red arrow. E) SEC chromatograms showing the peaks collected for one injection of the protein sample digested by HRV 3C protease and treated with Ni-NTA agarose. The major peak was indicated by an asterisk.

7.2.3 SEC-SAXS preparation

To prepare the protein samples for SEC-SAXS, purified hN1 EGF20-27 and EGF20-29 constructs were dialysed overnight in SAXS buffer (5 mM Tris pH 7.5, 15 mM $CaCl_2$), and concentrated to 2.5 mg/ml (see Section 2.13). SDS-PAGE for samples before and after dialysis showed that dialysis did not change the MWs or purity of the protein samples (Figure 7.5). It should be noted that the purity of the hN1 EGF20-29 sample was lower than that of hN1 EGF20-27.

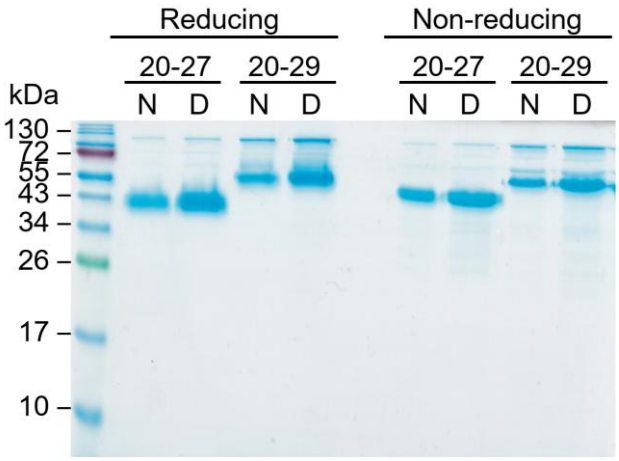


Figure 7.5. SDS-PAGE for hN1 constructs after dialysis.

Reducing and non-reducing SDS-PAGE and Coomassie staining for hN1 EGF20-27 and EGF20-29 samples before (indicated by "N") and after (indicated by "D") dialysis in SAXS buffer.

7.3 SEC-SAXS for hN1 constructs

7.3.1 SEC-SAXS

SAXS involved probing a sample in solution with a monochromatic X-ray beam. When the beam hits the sample, while most radiation passes through the sample, some radiation is scattered at a small angle by the atoms in the sample (Figure 7.6A). The angle and intensity of the scattering waves are detected by a two-dimensional detector to build the scattering pattern. The scattering pattern generated is radially symmetric as molecules are randomly oriented in the solution. The scattering pattern is radially averaged to generate a one-dimensional scattering curve (Figure 7.6C), where the y-axis records the intensity (I) of the scattered waves and the x-axis shows the transformation of the scattering angle ($S = \frac{4\pi}{\lambda}\sin\theta$, λ = wavelength of the X-ray beam, θ = half of the scattering angle). After subtracting the background scatter of the buffer

(Figure 7.6B), the gradients and shapes of the scattering curve can be used to determine the molecular dimensions, volume and shape of the sample (Svergun *et al.*, 2013; Chaudhuri *et al.*, 2017). To improve background subtraction and the purity and homogeneity of the protein crossing the X-ray beam, SAXS is coupled with SEC, which resolves samples by size and allows isolation of the scattering data of the target peak. SEC-SAXS for hN1 EGF20-27 and EGF20-29 was performed in collaboration with Dr Edward D. Lowe (University of Oxford) with Ca^{2+}-containing SAXS buffer (5 mM Tris pH 7.5, 15 mM $CaCl_2$) to ensure the Ca^{2+}-binding sites were saturated in the constructs (see Section 2.13.1).

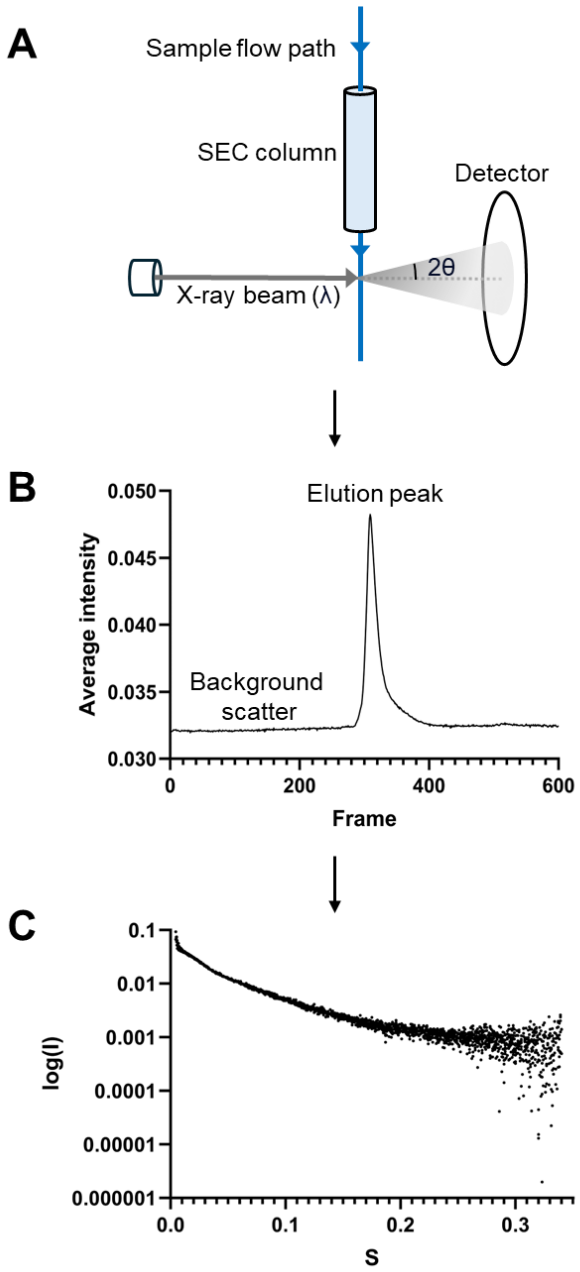


Figure 7.6. SEC-SAXS data collection.

(A) Protein sample in SAXS buffer is loaded onto a Shodex 402.5 analytical SEC column. Eluate from the column was passed through an X-ray beam of wavelength λ (Beamline B21, Diamond Light Source). The scattering pattern, including the scattering angle (θ) and intensity, is recorded by a detector. (B) The scattering pattern is collected over the elution from the SEC column and used to generate the scattering curve. (C) The scattering curve after subtraction of the background scatter is used for analysis of protein structure. The intensity (I) of the scattering is shown on the y-axis, and the transformation of the scattering angle ($S = \frac{4\pi}{\lambda}\sin\theta$, λ = wavelength of the X-ray beam, θ = half of the scattering angle) is shown on the x-axis.

7.3.2 Data analysis pipeline

SEC-SAXS data was visualised and analysed using the ATSAS 3.0 software package (Manalastas-Cantos *et al.*, 2021) in collaboration with Dr Edward D. Lowe (University of Oxford) (see Section 2.13.2). Initially, the SEC chromatograms of hN1 EGF20-27 and EGF20-29 were checked to ensure only a single elution peak was presented in each sample (Figure 7.7A). The middle of the elution peak was selected to extract the scattering curve of the protein. The edges of the peak may reduce the homogeneity of the scattering curve and thus were excluded. Scattering data of a flat region in elution coming out of the column before the peak was selected to show the background scatter, which was subtracted from the scattering curve of the protein (Figure 7.7A). The scattering curve was then checked to ensure the intensities, especially at small angles, did not have too much noise or fluctuations that could affect the reliability of the curve (Figure 7.7B). The scattering curves of both constructs showed low noise at small angles ($S < 0.15$). The noise in the scattering curve of hN1 EGF20-29 was higher than that of hN1 EGF20-27 (Figure 7.7B), which might be due to a lower purity of the hN1 EGF20-29 sample (Figure 7.5) and a wider elution peak observed during SEC (Figure 7.7A, right panel).

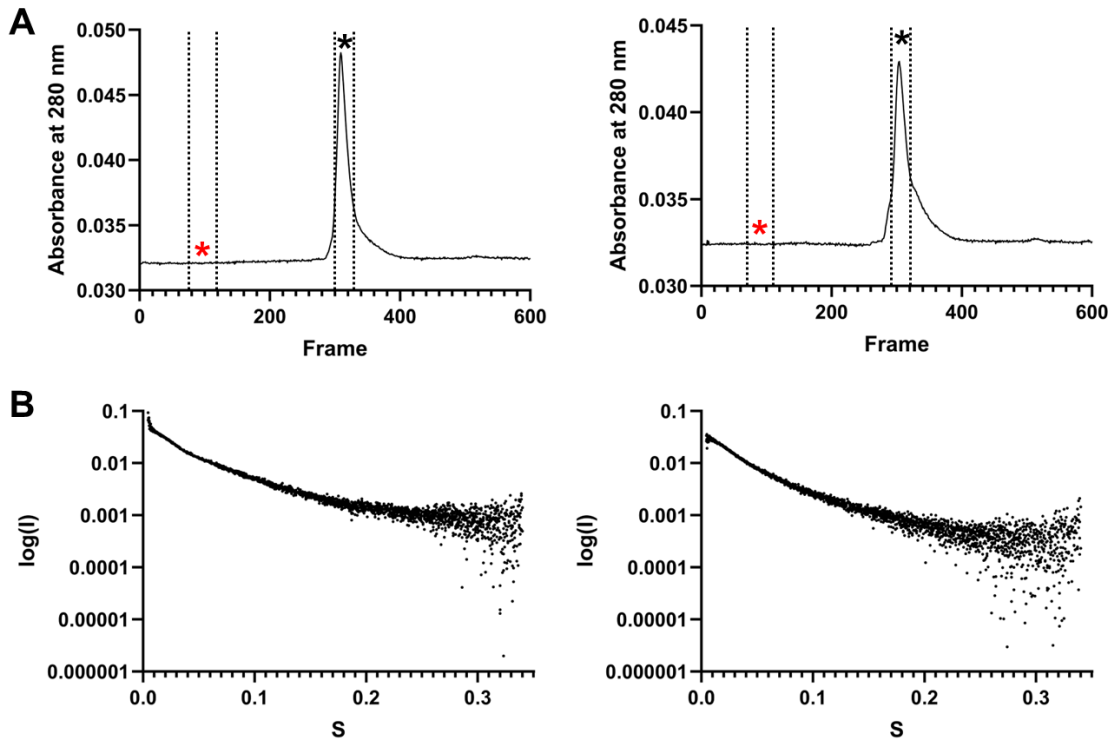


Figure 7.7. Quality check for SEC-SAXS data.

(A) SEC chromatograms and (B) scattering curves of hN1 EGF20-27 (left panel) and hN1 EGF20-29 (right panel). The fraction of the SEC elution used to show the background scatter of the SAXS buffer is indicated by a red asterisk. The fraction of the elution peak used to analyse the scattering curve of the protein construct is indicated by a black asterisk.

After inspecting the quality of the scattering data, to study the shape and foldedness of the construct, the Kratky plot and the pair distance (P(r)) distribution curve were generated from the scattering data. The Kratky plot ($I*S^2$ as a function of S) is commonly employed to study whether the particle has a folded or globular structure (Glatter and Kratky, 1982). For folded globular protein, a sharp peak is usually observed (Figure 7.8A, orange curve). For rigid partially-folded or extended proteins, the curve usually forms a smooth peak which gradually decreases after the peak (Figure 7.8A, grey curve). For unfolded or intrinsically disordered proteins, the curve may continue increasing (Figure 7.8A, blue curve).

The P(r) distribution curve of the protein construct, which shows the frequency distribution of the distances (r) between all pairs of scattering elements within the particle, was determined using a suitable maximum dimension of the particle (D_{max}) (Figure 7.8B, grey curve) (Feigin and Svergun, 1987; Svergun *et al.*, 2013). If the D_{max} is set too small, the P(r) distribution curve will show an abrupt decrease when P(r) is approaching 0 (Figure 7.8B, orange curve). If the D_{max} is set too large, the P(r) distribution curve will show a long trailing tail when P(r) is approaching 0 (Figure 7.8B, blue curve). In addition, P(r) may be unstable and oscillate around the x-axis generating negative values if D_{max} is set too large or small. The P(r) distribution not only provides information for the maximum length of the particle but also provides information for the shape of the particle. For example, a curve that peaks at a small distance and gradually decreases to form an extended tail suggests the particle has an extended rod-like structure (Figure 7.8C, grey curve). A normal distribution across the distance suggests the particle has a globular structure (Figure 7.8C, orange curve). Multiple peaks in the curve suggest the particle has multiple structured domains with rigid linkers (Figure 7.8C, blue curve).

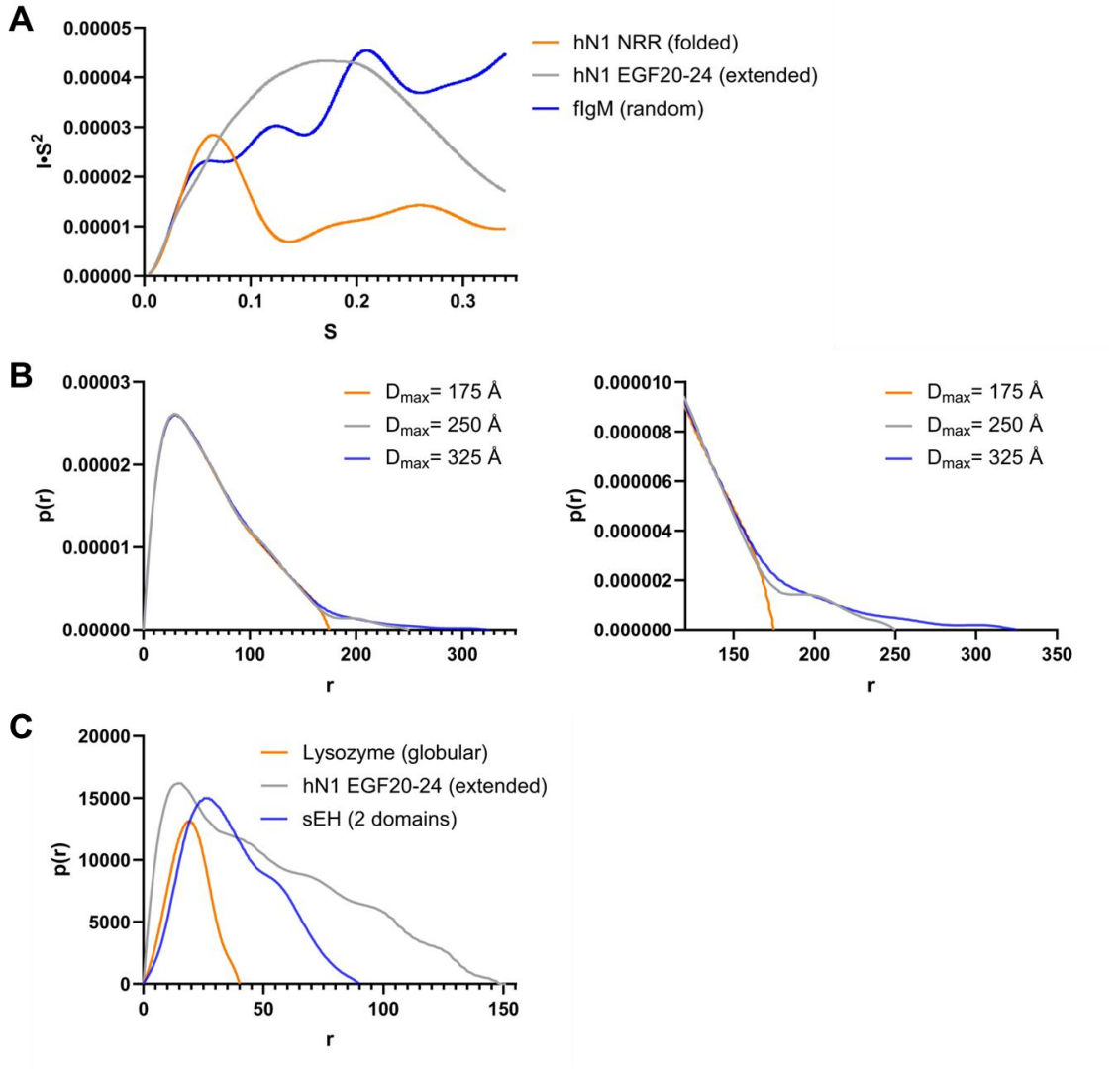


Figure 7.8. Determination of the shape and foldedness of a construct by SAXS.

(A) Kratky plots derived from computed SAXS data (Schneidman-Duhovny *et al.*, 2013, 2016) of hN1 NRR (PDB: 3ETO, orange) (Gordon *et al.*, 2009), hN1 EGF20-24 (PDB: 9B3N, grey) (Bo *et al.*, 2024) and flgM (AlphaFold model, blue) (Jumper *et al.*, 2021; Varadi *et al.*, 2024), which are used as examples of folded particle, rigid extended particle and intrinsically disordered particle respectively. (B) P(r) distribution curves (left panel) derived from the scattering curve of hN1 EGF20-29 using different D_{max} (orange = 175 Å, grey = 250 Å, blue = 325 Å). An enlargement of the curves at large r is shown in the right panel. (C) P(r) distribution curves derived from computed SAXS data (Schneidman-Duhovny *et al.*, 2013, 2016) of lysozyme (PDB: 1REX, orange) (Muraki *et al.*, 1996), hN1 EGF20-24 (PDB: 9B3N, grey) (Bo *et al.*, 2024) and sEH (PDB: 3WK4, blue) (Amano, Yamaguchi and Tanabe, 2014), which are used as examples of globular particle, extended particle and particle with two domains respectively.

To create structural models for hN1 EGF20-27 and EGF20-29, initial models of the fragments were created by adding free-hanging EGF domains C-terminal to the X-ray structure of hN1 EGF20-24 (PDB: 9B3N) (Bo *et al.*, 2024) using the Coot software (Emsley *et al.*, 2010). Since the structure of EGF domains is highly conserved, existing structures of EGF domains were used as models for EGF25-EGF29. The initial models were fed into the SREFLEX program in the ATSAS package (Panjkovich and Svergun, 2016) alongside the scattering curves collected from the constructs. SREFLEX utilised normal mode analysis to rearrange the positions of pseudo-domains (domains of fixed structures that are only allowed to move in position) to improve the agreement of the refined model with the scattering curve. The refined model provided information on how EGF24-29 was linked together and the overall shape of the Ax region. In addition, AlphaFold2 was used to predict models for hN1 EGF20-27 and EGF20-29 (Jumper *et al.*, 2021). These computed models were compared with those generated by SREFLEX.

7.3.3 SEC-SAXS for hN1 EGF20-27

7.3.3.1 Foldedness and length

The Kratky plot of hN1 EGF20-27 showed an initial increase in $I*S^2$ at small S followed by a plateau (Figure 7.9A). This pattern is between the smooth peak for a partially folded (or extended) protein and the continuously increasing curve for an unfolded protein. It is commonly considered to represent either an ideal Gaussian chain or an extended thin

chain (Kikhney and Svergun, 2015). Since the X-ray structure of hN1 EGF20-24 showed a Ca^{2+}-dependent rigid extended structure (Bo *et al.*, 2024), it is more likely that EGF20-27 shows an extended structure rather than an unfolded structure. The P(r) distribution of EGF20-27 showed a D_{max} between 230-240 Å (Figure 7.9B). As a completely extended construct formed by 8 EGF domains would be expected to have a D_{max} of ~240 Å based on the length of ~30 Å per EGF domain, this D_{max} estimation supported the prediction that EGF20-27 has an extended near-linear structure. Also, the P(r) distribution showed a curve that peaks at a small distance and gradually decreases to form an extended tail, which suggested that EGF20-27 has a single-domain rod-like structure.

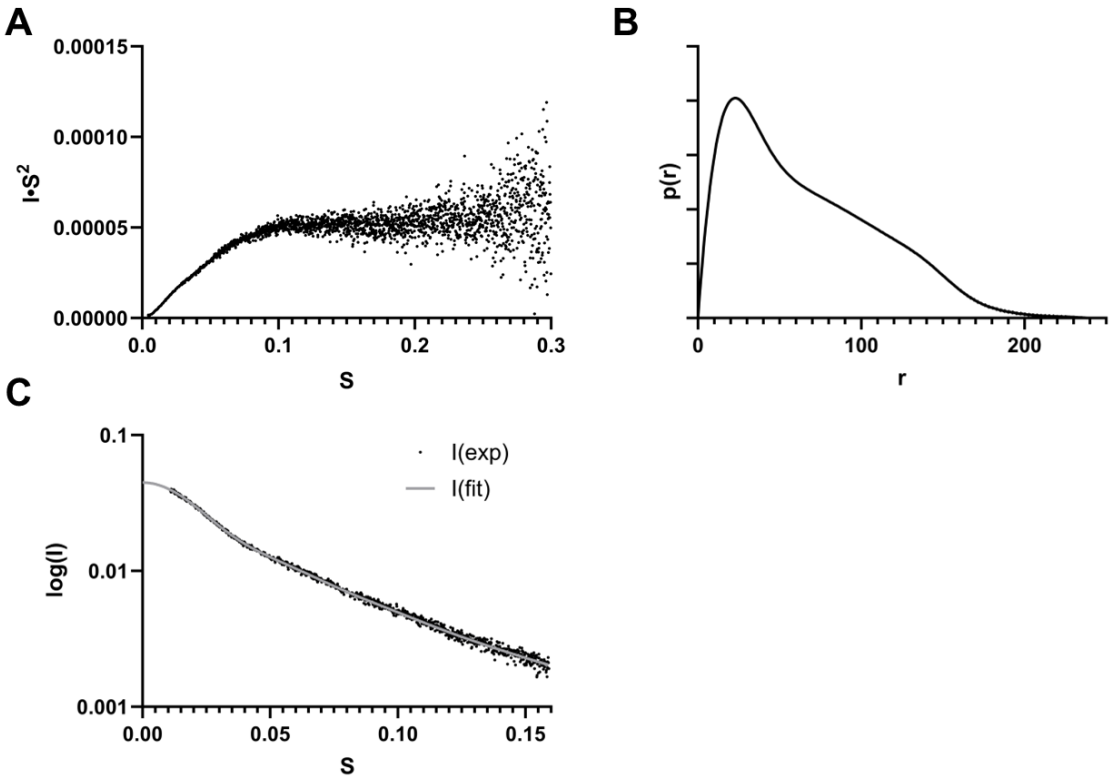


Figure 7.9. Prediction of the foldedness and length of hN1 EGF20-27.

(A) Kratky plot and (B) P(r) distribution derived from the scattering curve collected from hN1 EGF20-27. D_{max} was set as 235 Å. (C) The artificial scattering curve computed using the P(r) distribution of hN1 EGF20-27 (I(fit)) is aligned with the experimental scattering curve collected from hN1 EGF20-27 (I(exp)). The two curves show good alignment.

7.3.3.2 Structural model generated by SREFLEX

The X-ray structures of EGF11, 12 and 13 (PDB: 3ETO) (Cordle, Johnson, *et al.*, 2008) were used as independent models for EGF25, 26 and 27 respectively and added C-terminal to the X-ray structure of EGF20-24 (PDB: 9B3N) (Bo *et al.*, 2024) to form the 4-pseudo-domain initial model of hN1 EGF20-27 (Figure 7.10A). An optimised structural model that showed an extended near-linear structure of EGF20-27 (Figure 7.10B) was generated by SREFLEX based on the initial model. This optimised model had a good fit for the scattering curve collected from hN1 EGF20-27, with a χ^2 of 1.96 (Panjkovich and Svergun, 2016) (Figure 7.10C).

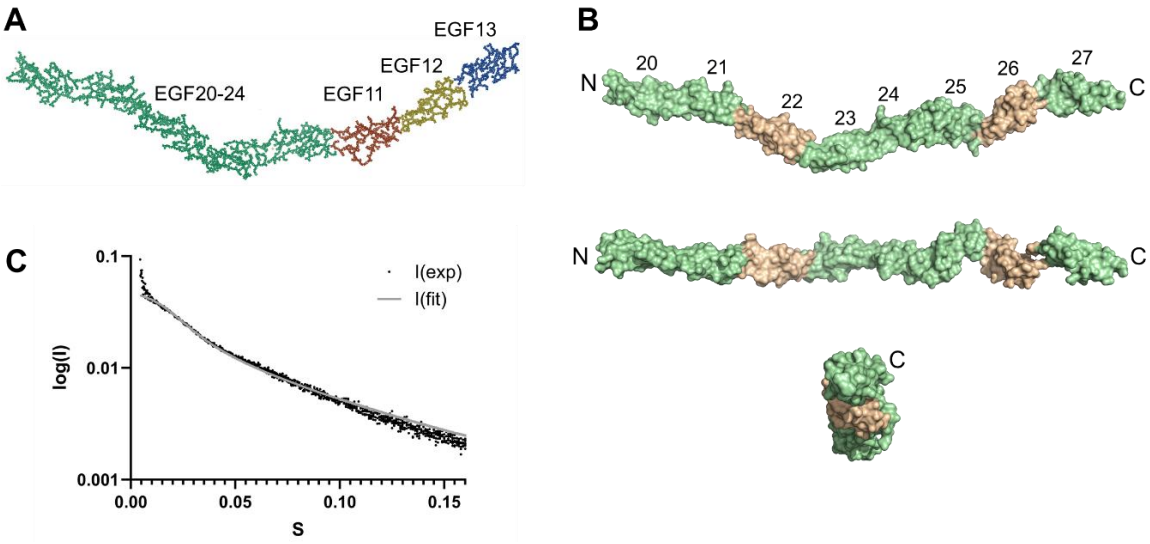


Figure 7.10. Structural model of hN1 EGF20-27 generated by SREFLEX.

(A) Initial model of hN1 EGF20-27 formed by the X-ray structure of EGF20-24 (PDB: 9B3N) (green), EGF11 (PDB: 2VJ3) for EGF25 (red), EGF12 (PDB: 2VJ3) for EGF26 (yellow) and EGF13 (PDB: 2VJ3) for EGF27 (blue). (B) Optimised model of hN1 EGF20-27 generated by SREFLEX based on the initial model. The model is shown from 3 different angles. Non-Ca^{2+}-binding EGF domains are shown in wheat and cbEGF domains are shown in green. (C) The artificial scattering curve computed for the optimised model (I(fit)) is aligned with the experimental scattering curve collected from hN1 EGF20-27 (I(exp)). The two curves show good agreement.

7.3.3.3 Structural model generated by AlphaFold2

The AlphaFold2 model of hN1 EGF20-27 (Jumper *et al.*, 2021) showed an extended structure similar to that generated by SREFLEX (Figure 7.11A). The two models aligned well between EGF22-24 but deviated at the two ends (Figure 7.11B). Also, the AlphaFold2 model was slightly more extended than the SREFLEX model (Figure 7.11B). As assessed by the CRYSOL program in the ATSAS package (Franke *et al.*, 2017), the AlphaFold2 model had a χ^2 of 3.35 when fitted to the SAXS scattering curve collected from hN1 EGF20-27, which was worse than that of the SREFLEX model (χ^2 = 1.96).

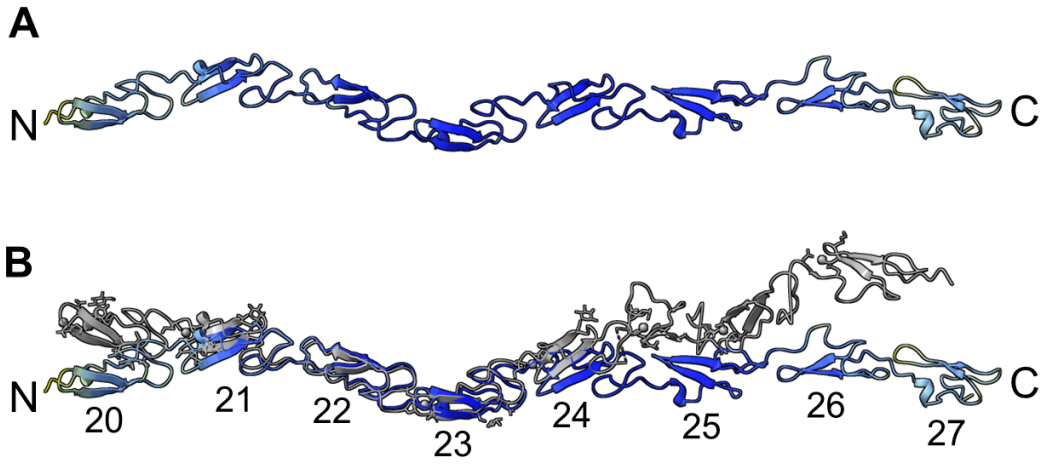


Figure 7.11. Structural model of hN1 EGF20-27 generated by AlphaFold2.

(A) The highest-ranked AlphaFold2 model generated for hN1 EGF20-27 (Jumper *et al.*, 2021). Colouring is based on the pLDDT confidence score (high confidence in dark blue, low confidence in red). (B) The AlphaFold2 model is aligned with the SREFLEX model (shown in grey) (Figure 7.10B) generated from the scattering curve of hN1 EGF20-27.

7.3.4 SEC-SAXS for hN1 EGF20-29

7.3.4.1 Foldedness and length

The Kratky plot of hN1 EGF20-29 showed an initial increase in $I*S^2$ at small S followed by a plateau (Figure 7.12A), which is similar to that of hN1 EGF20-27. Since EGF20-27 was predicted to have an extended structure by SAXS analysis (see Section 7.3.3), it is predicted that EGF20-29 also shows an extended structure. The P(r) distribution of EGF20-29 suggested a D_{max} between 250-260 Å (Figure 7.12B). D_{max} higher than 260 Å was also used to plot the P(r) distribution of EGF20-29, which showed a long trailing tail when P(r) approached 0, and the P(r) value became negative (<0) at high r values when D_{max} was set at 280Å (Appendix H, Figure H.1), suggesting it is less likely for EGF20-29

to have a D_{max} over 260 Å.

The difference between the D_{max} of EGF20-29 and EGF20-27 (230-240 Å, Figure 7.9B) is ~20 Å, which is smaller than the length of a single EGF domain (~30 Å). This suggested that despite having an extended structure, EGF20-29 may show a tilt after EGF27. The P(r) distribution of EGF20-29 showed a curve that peaks at a small distance and gradually decreases to form an extended tail. A small peak was observed at the tail of the curve. This pattern suggested that EGF20-29 has a rod-like structure, potentially with a small “second domain” at one end of the rod, which may be caused by a bending between EGF27-29.

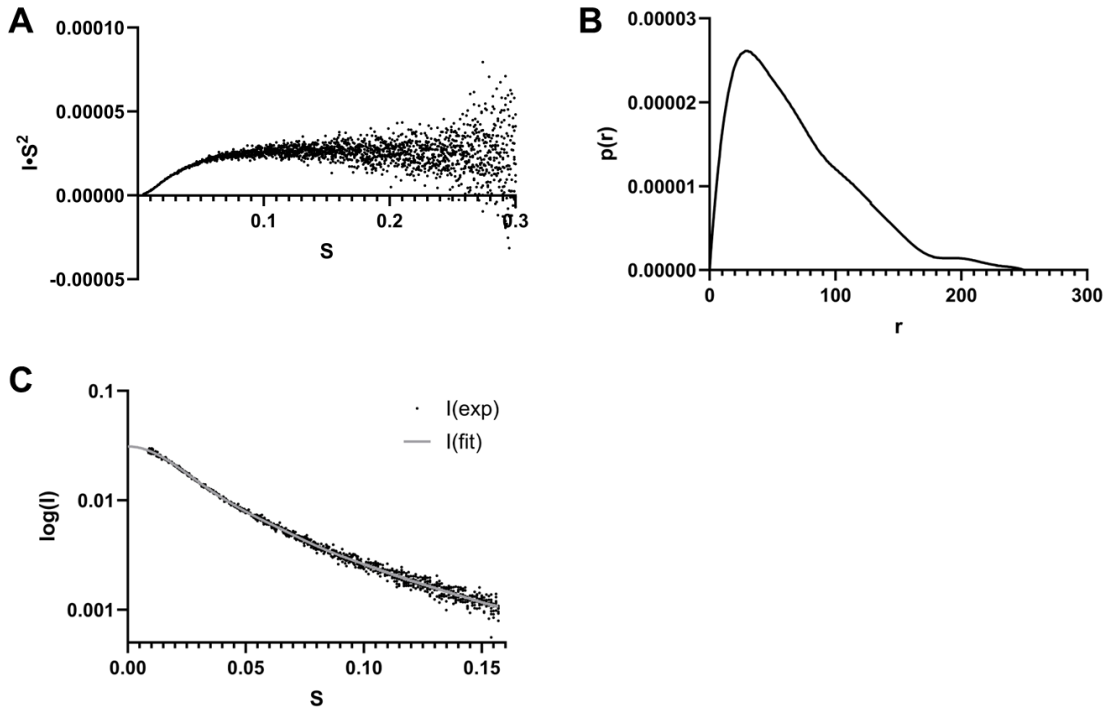


Figure 7.12. Prediction of the foldedness and length of hN1 EGF20-29.

(A) Kratky plot and (B) P(r) distribution derived from the scattering curve collected from hN1 EGF20-29. D_{max} was set as 250 Å. (C) The artificial scattering curve computed using the P(r) distribution of hN1 EGF20-29 (I(fit)) is aligned with the experimental scattering curve collected from hN1 EGF20-29 (I(exp)). The two curves show good agreement.

7.3.4.2 Structural model generated by SREFLEX

The X-ray structure of EGF5 and EGF6 (PDB: 5FMA) (Weisshuhn *et al.*, 2016) were used as independent models for EGF28 and EGF29 respectively and added C-terminal to the SREFLEX-generated structure of EGF20-27 (Figure 7.10B) to form the 3-pseudo-domain initial model of hN1 EGF20-29 (Figure 7.13A). The optimised model of EGF20-29 generated by SREFLEX based on the initial model showed bending at the interfaces of EGF27-28 and EGF28-29 (Figure 7.13B). EGF28 was shown to fold back on EGF29. However, this optimised model of EGF20-29 showed relatively poor agreement with the scattering curve (χ^2 = 5.18) (Figure 7.13C). Therefore, caution should be taken when

referring to this model of EGF20-29.

Initial models were also built using EGF12 and EGF13 (PDB: 3ETO) (Cordle, Johnson, *et al.*, 2008) or EGF6 and EGF7 (PDB: 5FMA) (Weisshuhn *et al.*, 2016) as models for EGF28 and EGF29 (Appendix H, Figure H.2). The SREFLEX models based on these initial models showed even worse agreement with the scattering data ($\chi^2 > 5.9$) and were not considered.

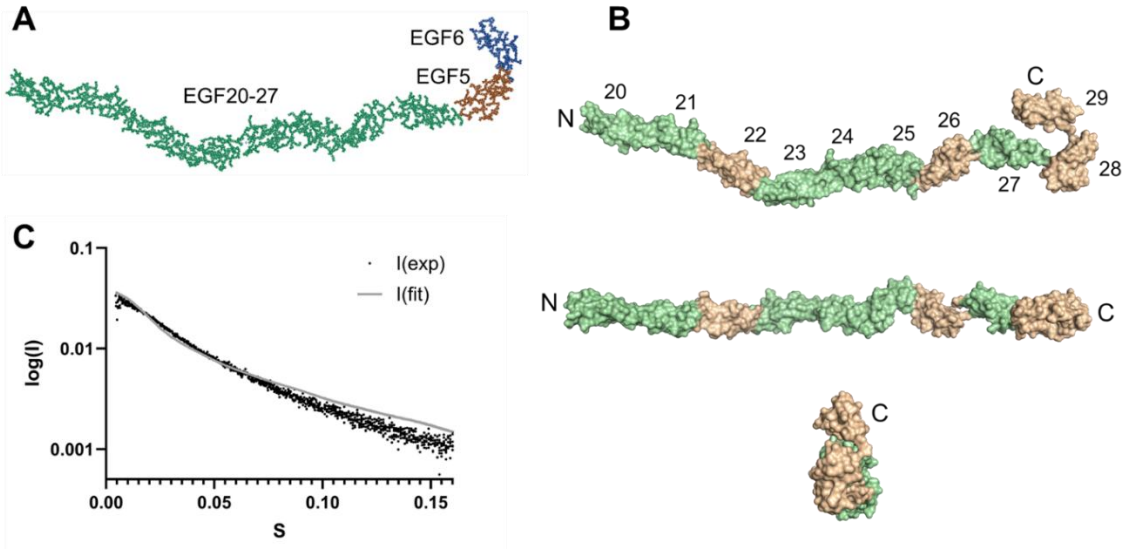


Figure 7.13. Structural model of hN1 EGF20-29 generated by SREFLEX.

(A) Initial model of hN1 EGF20-29 formed by the SREFLEX-generated structure of EGF20-27 (green), EGF5 (PDB: 5FMA) for EGF28 (red) and EGF6 (PDB: 5FMA) for EGF29 (blue). (B) Optimised model of hN1 EGF20-29 generated by SREFLEX based on the initial model. The model is shown from 3 different angles. Non-Ca^{2+}-binding EGF domains are shown in wheat and cbEGF domains are shown in green. (C) The artificial scattering curve computed for the optimised model (I(fit)) is aligned with the experimental scattering curve collected from hN1 EGF20-29 (I(exp)). The two curves show poor agreement, especially at large S.

7.3.4.3 Structural model generated by AlphaFold2

The AlphaFold2 model of hN1 EGF20-29 (Jumper *et al.*, 2021) showed an extended structure from EGF20-28 and a bending between EGF28 and EGF29 (Figure 7.14A). This was similar to the SREFLEX model of EGF20-29 (Figure 7.13B) except that the interface between EGF27 and EGF28 shows a bend in the SREFLEX model. The two models aligned well between EGF22-24 but deviated significantly at the C terminus with the AlphaFold2 model more extended than the SREFLEX model (Figure 7.14B). As assessed by the CRYSOL program in the ATSAS package (Franke *et al.*, 2017), the AlphaFold2 model had a χ^2 of 8.23 when fitted to the SAXS scattering curve collected from hN1 EGF20-29, which was worse than that of the SREFLEX model (χ^2 = 5.18).

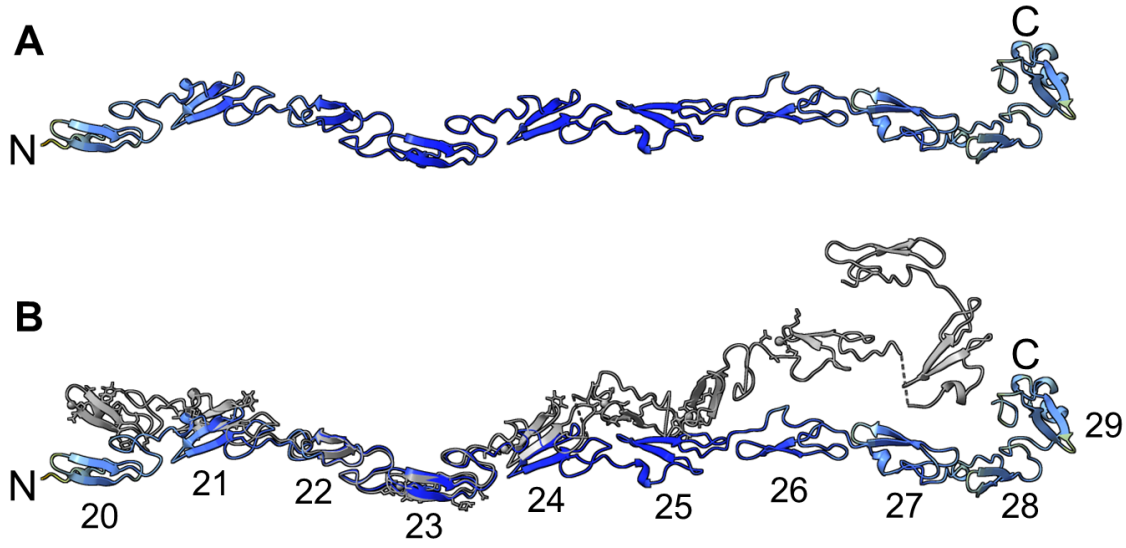


Figure 7.14. Structural model of hN1 EGF20-29 generated by AlphaFold2.
(A) The highest-ranked AlphaFold2 model generated for hN1 EGF20-29 (Jumper *et al.*, 2021). Colouring is based on the pLDDT confidence score (high confidence in dark blue, low confidence in red). (B) The AlphaFold2 model is aligned with the SREFLEX model (shown in grey) (Figure 7.13B) generated from the scattering curve of hN1 EGF20-29.

7.4 Discussion

SREFLEX models agreed with AlphaFold2 models of hN1 EGF20-27 and EGF20-29

SREFLEX models of hN1 EGF20-27 and EGF20-29 derived from scattering curves of protein samples showed similar structures to their AlphaFold2 models, giving confidence to the models. SREFLEX models also showed better agreement than the AlphaFold2 models with the SAXS scattering data collected from the two protein constructs. A structural model of the Ax region in hN1 (EGF24-29) could be extracted from the SREFLEX model of EGF20-29 (Figure 7.15).

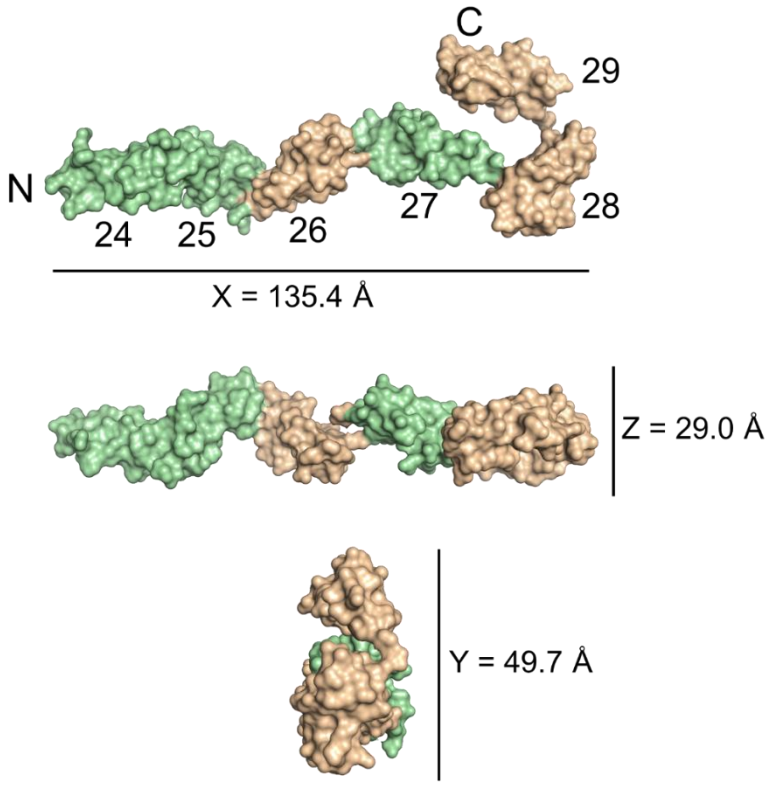


Figure 7.15. Structural model of hN1 Ax region.

SREFLEX model of the Ax region (EGF24-29) in hN1 extracted from SREFLEX model of hN1 EGF20-29 (Figure 7.13B). The model is shown from 3 different angles with dimensions indicated. Non-Ca^{2+}-binding EGF domains are shown in wheat and cbEGF domains are shown in green. Note the structural model for EGF28-29 showed low agreement with the SAXS data and should be treated with caution.

EGF24-27 showed an extended structure

SAXS analysis and AlphaFold2 modelling suggested with high confidence (Figure 7.10B and 7.11A) that hN1 EGF20-27 had an extended structure with a length of 230-240 Å in solution, suggesting that the N terminal EGF24-27 of the Ax region also had an extended structure. As EGF24, 25 and 27 have Ca^{2+} binding consensus sequences (see Section 1.2.2.2), Ca^{2+} binding may confer rigidity at the interfaces of EGF23-24, EGF24-25 and EGF26-27 (see Section 1.2.2.3). SAXS analysis or limited proteolysis assay (Cordle, Redfield, *et al.*, 2008; Chillakuri *et al.*, 2013) performed with titration of Ca^{2+} or EGTA for Ca^{2+} chelation, or study of constructs carrying mutations that abolish Ca^{2+} binding in these EGF domains, may be conducted in future to confirm the impact of Ca^{2+} binding on the rigidity of the structure.

Though EGF26 does not have a Ca^{2+} binding consensus sequence and should not bind Ca^{2+}, a linear interface was detected between EGF25 and EGF26, which was also observed between EGF21 and the non-Ca^{2+}-binding EGF22 (PDB: 9B3N) (Bo *et al.*, 2024) (Figure 7.16A). No sharp bend within EGF20-27 was detected, suggesting the non-canonical cysteines in EGF25 and EGF27 (see Section 3.2) do not form interdomain disulfide bonds.

EGF27-29 may have a bent or flexible structure

Since EGF28 and EGF29 do not have the consensus sequence for Ca^{2+} binding, the interfaces of EGF27-28 and EGF28-29 have the possibility to be linear as between hN1

EGF21-22 (Bo *et al.*, 2024), bent as between hN1 EGF5-6 (90°) (Weisshuhn *et al.*, 2016) and between EGFs at the C terminus of merozoite surface protein 1 (MSP-1) (180°) (Morgan *et al.*, 1999), or flexible as between hN1 EGF9-10 (Weisshuhn *et al.*, 2016) (Figure 7.16). SAXS analysis showed that hN1 EGF20-29 had a length of 250-260 Å, which, when assuming EGF20-27 has an extended structure, suggested an angle may be presented within EGF27-29. SREFLEX and AlphaFold2 modelling showed that hN1 EGF20-29 was bent between EGF28 and EGF29 (and EGF27 and 28 in the SREFLEX model) (Figure 7.13B and 7.14A). However, it should be noted that these models have relatively poor agreements with the scattering data of EGF20-29, so the interdomain angles within EGF27-29 may not be accurate in the models generated.

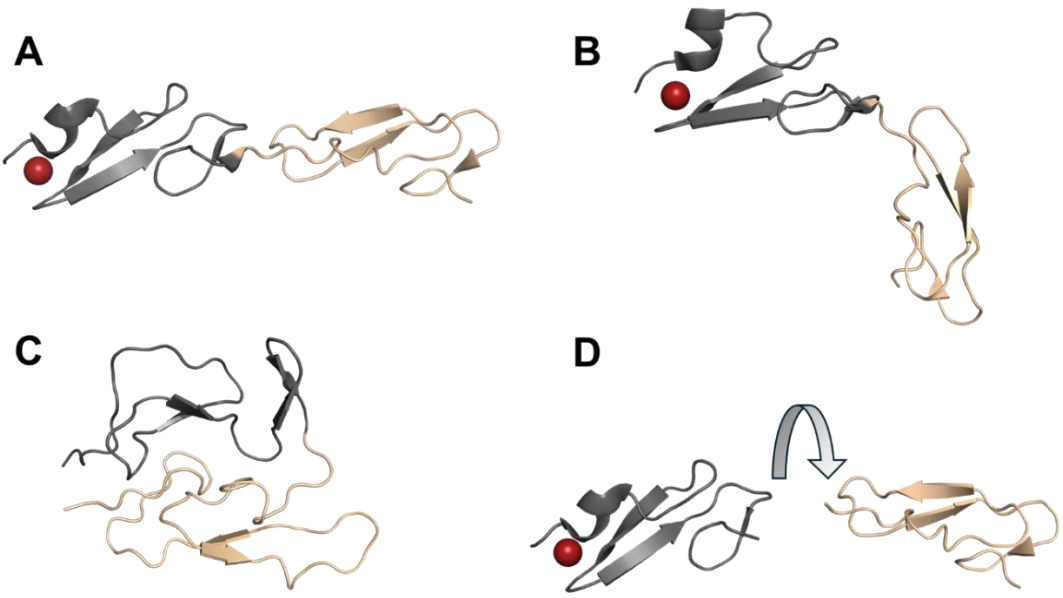


Figure 7.16. Structures of (cb)EGF-EGF pairs.

(A) The structure of hN1 EGF21-22 (PDB: 9B3N) showed a near-linear conformation (Bo *et al.*, 2024). (B) The structure of hN1 EGF5-6 (PDB: 5FMA) showed an angle of 80-90° between the two EGF domains (Weisshuhn *et al.*, 2016). (C) The structure of the two EGF domains at the C terminus of MSP-1 showed a U-shaped conformation (Morgan *et al.*, 1999). (D) RDC measurements suggested a flexible linker between hN1 EGF9 and 10 (Weisshuhn *et al.*, 2016). Flexibility is indicated by an arrow. The first EGF domains of the pairs are shown in grey. The second EGF domains of the pairs, which are non-Ca^{2+}-binding, are shown in wheat. Ca^{2+} ions are shown as red spheres.

Alternatively, there may be a flexible linker between EGF27 and EGF28 or EGF28 and EGF29, which could lead to averaging of the scattering data and make the contribution of the EGF28-29 region to the scattering data “noisier”. This might result in a decrease in D_{max} estimated for P(r) distribution (Figure 7.12). Since the SREFLEX modelling assumes a single rigid structure, the presence of flexible linkers in EGF27-29 would decrease the accuracy of the model generated and reduce the agreement of the model to the SAXS data (Figure 7.13C). Due to the lower quality of SAXS data collected from

hN1 EGF20-29 and structural models that showed poor agreement with the SAXS data, further experiments are needed to confirm the structure of EGF27-29.

8 Discussion

8.1 Aim of this thesis

The aim of this thesis was to study the functions and structure of the Ax region (EGF24-29) in the Notch receptor. Cell-based functional assays were developed to measure the cell surface level, ligand binding, trans-activation, and cis-inhibition of N1. These assays were employed to examine the effects of Ax substitutions on Notch signalling in a mammalian context both in the absence and presence of Lfng. SEC-SAXS analysis of N1 fragments was performed to study the structure of the Ax region in low resolution. The structural and functional data were combined to interpret possible explanations for Notch-enhancing phenotypes caused by the Ax variants in *Drosophila*.

8.2 Assessment of experimental approaches employed in this project

8.2.1 Assay systems to test N1 signalling

Cellular assays employed in this project utilised a receptor with the native sequence of N1 and an additional luciferase domain connected to the C terminus of the NICD. Control experiments with ligand/receptor-binding deficient N1 variant (L468A, see Chapter 3) and ligand variants (JAG1 FAEK and DLL4 FAYA, see Chapter 4 and 5) showed low levels of ligand binding, Notch trans-activation and cis-inhibition as suggested by previous studies (Fleming *et al.*, 2013; Whiteman *et al.*, 2013; Luca *et al.*, 2015; Meng *et al.*, 2022). Also, assays of N1 WT activity in response to different trans-ligands in the presence of Lfng with and without cis-JAG1 recapitulated other published studies (LeBon

et al., 2014; Kakuda and Haltiwanger, 2017; Kuintzle, Santat and Elowitz, 2023) (see Chapter 6). These results suggest that the addition of the luciferase domain did not affect ligand binding and the effect of Fng modification on trans-activation and cis-inhibition of N1. With a direct quantification of Notch activity, the cellular assays act as reliable tools to study the effect of mutations in N1ECD and ligands on Notch signalling. It should be noted that further validation is needed before using this system to study mutations in the N1ICD. It is unclear whether the luciferase domain will affect the interaction of the intracellular domains of N1 and cis-ligand, which was detected between N1 and cis-Jag1 in proximity ligation assays of cells in the intra-aortic hematopoietic clusters (Thambyrajah *et al.*, 2024).

RT-PCRs were performed to validate the expression of N1 and cis-ligands in the reporter cells. However, they did not provide a direct measurement of protein level, and thus might overlook the effects of mutations on protein stability and turnover rate. In addition, mutations may affect trafficking, endocytosis and recycling of receptors and ligands. Experiments to study protein level and localisation, such as western blot, immunofluorescence and flow cytometry, can be performed alongside current assays to further characterise the effects of mutations.

The ligand binding assay used in this project, although detecting gross changes in binding, is avidity-driven, which may mask smaller changes in binding. A biophysics assay, such as SPR using purified monomeric ligand and N1 protein constructs, could

be performed to check changes in the strength (K_d) of binding. Also, since ligand NE3 constructs were used in current ligand binding assays, binding or cell aggregation assays, which utilise full-length ligands, can be performed in future to study ligand binding in a more native context.

Assays employed in this project quantified Notch activation and inhibition at fixed time points and provided minimal information on the dynamics of receptor-ligand interaction. labelling of single receptor and ligand molecules or specific motifs in the proteins, such as by biarsenical-tetracysteine labelling (Martin *et al.*, 2005) or aptamer-based probing (Klussmann, 2006) may be accompanied by live-cell imaging to explore how variants behave and interact with ligands in real time.

8.2.2 Low-resolution structural analysis of N1

SEC-SAXS, which provided information about large-scale bulk microstructure within a sample, was employed to explore the structure of the Ax region in low resolution. SAXS data provided information on the length and foldedness of protein constructs, which were used to generate structural models. SAXS is suitable for studying materials with partially ordered structures, which, based on the knowledge that hN1 EGF20-24 has a rigid extended structure (Bo *et al.*, 2024), suits the investigation of EGF20-27 and EGF20-29 constructs. On the other hand, data analysis and model generation based on SAXS data usually assume all particles within the sample have the same structure. Therefore, when particles have regions of high flexibility, structural features derived from SAXS data may

be unreliable, and models generated may have low confidence. While the model of hN1 EGF20-27 showed an extended structure with a good fit for its SAXS data, the model generated in this project for the hN1 EGF20-29 construct showed a relatively poor agreement with its SAXS data. Our result suggested EGF27-29 may have a bent or flexible structure, which needs to be confirmed by other experimental approaches, such as Hydrogen/Deuterium eXchange mass spectrometry and NMR of smaller fragments.

8.3 Structure of the Ax region

The SEC-SAXS data collected from the hN1 EGF20-27 and EGF20-29 constructs, the structural models generated based on the scattering data by SREFLEX, and the Alphafold2 models collectively showed that the Ax region in N1 has an extended structure for the N-terminal EGF24-27 but the C terminal EGF27-29 may be bent or flexible (see Chapter 7). Due to the limited resolution and data quality of the SAXS data and the poor agreement of the SREFLEX and AlphaFold2 models of hN1 EGF20-29 with SAXS data, the exact structure of EGF28-29 was unclear and needs further investigations. The structure of the Ax region described in this thesis can be added to the existing structural models of other regions of hN1 to help understand the organisation of the NECD (Figure 8.1A). The NECD likely has a non-linear structure that can be flexible in certain regions (Figure 8.1B). The Ax region that is located between the LBR and the NRR and comprises both extended and bent/flexible regions may serve an important role in organising the structure of the receptor during interaction with other components

of the Notch signalling pathway, such as the canonical ligands and PTM enzymes.

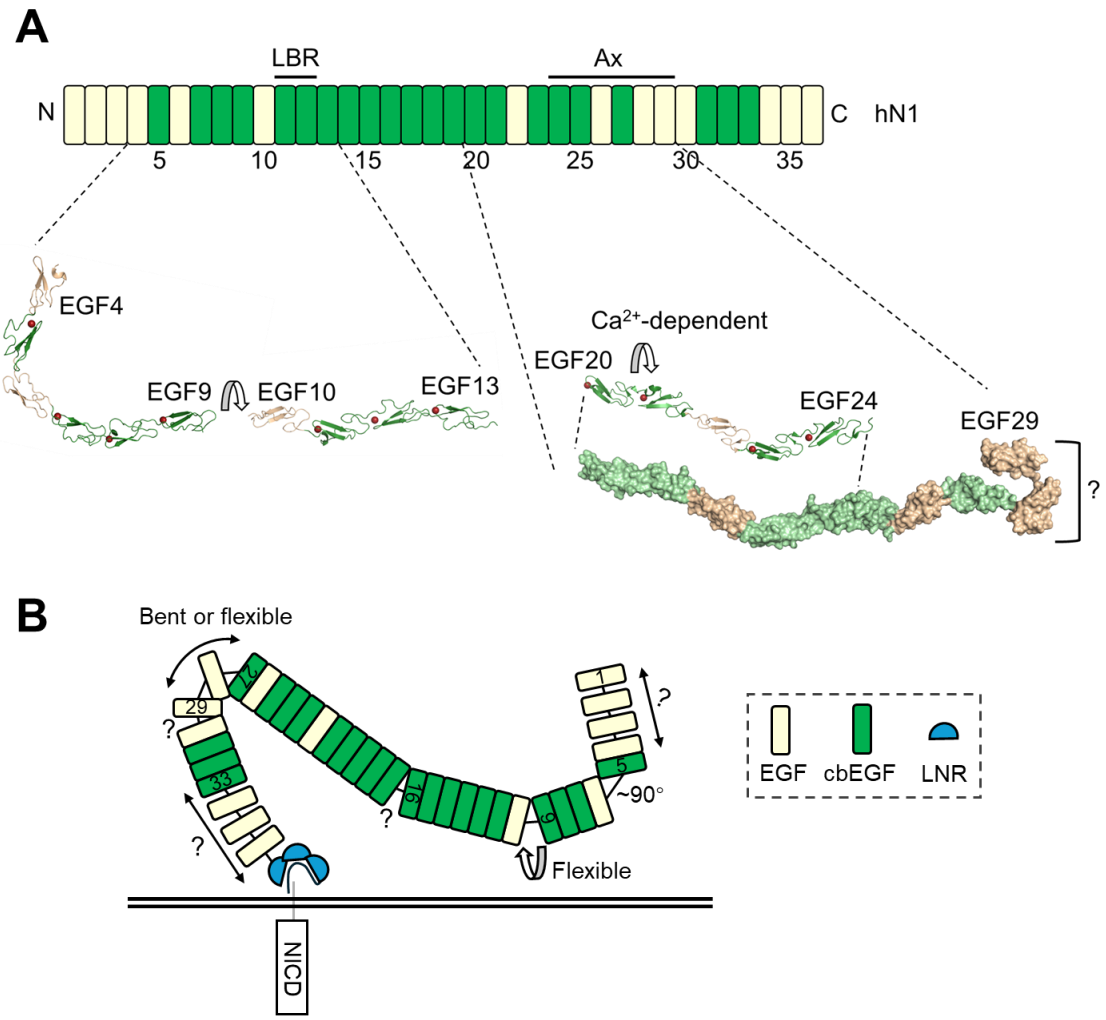


Figure 8.1. Structure of hN1ECD.

(A) Existing structural models of hN1ECD. X-ray structures of EGF4–7 (PDB: 5FMA) and EGF10–13 (PDB: 2VJ3) and RDC measurements were employed to construct the model for EGF4-13 by Weisshuhn et al. (2016), which suggested a flexible linker between EGF9 and 10 (Cordle, Johnson, *et al.*, 2008; Weisshuhn *et al.*, 2016). The X-ray structure of EGF20-24 (PDB: 9B3N) showed a near-linear structure with Ca^{2+}-dependent flexibility at the interface of EGF20-21 (Bo *et al.*, 2024). The structure of EGF20-29 was generated in this project (see Chapter 7) by SREFLEX modelling of SEC-SAXS data. The exact structure of EGF28-29 was unclear (indicated by "?"), due to a relatively poor agreement between the model and the SAXS data. Non-Ca^{2+}-binding EGF domains are shown in wheat, cbEGF domains are shown in green and the Ca^{2+} ions are shown as red spheres. (B) Schematic illustration of a possible conformation of hN1ECD. Consecutive cbEGF repeats, such as EGF10-16, EGF17-

21 and EGF30-33, and EGF20-27 (based on SAXS SREFLEX model, see Chapter 7) are shown as rod-like structures (see Section 1.2.2.3). Regions that have been shown by existing structural models to be flexible or bent are labelled (Cordle, Johnson, *et al.*, 2008; Weisshuhn *et al.*, 2016). Regions of unknown structure and have the potential to be flexible or bent are indicated by "?". Note due to the absence of the conserved aromatic residue at the end of EGF16, the interface of EGF16 and EGF17 cannot be predicted despite both EGFs being Ca^{2+}-binding. The figure was not drawn to scale.

8.4 The role of the Ax region in Notch signalling

8.4.1 Misfolding of EGF24-25 affected receptor trafficking

mN1 homologues of dN *Ax* homozygous lethal variants (C933S and C960Y) and S990N identified in ageing oesophageal and skin tissues showed reduced expression levels on the cell surface and reduced ligand binding and trans-activation (see Chapter 3).

Since C933S and C960Y affect the conserved cysteine residues essential for forming the disulfide bonds in EGF24 and 25 (Figure 1.17), the reduced cell surface level of these variants was likely due to protein misfolding, subsequent protein aggregation and reduced transportation or increased proteasomal degradation, as observed for cysteine substitutions in other EGF-containing proteins and in N3 in CADASIL patients (Joutel *et al.*, 2000; Opherk *et al.*, 2009; Jensen *et al.*, 2015; Young *et al.*, 2022). A previous study suggested that dN C999Y, which is homologous to mN1 C960Y, had reduced cell surface availability in *Drosophila* S2 cells (Pérez *et al.*, 2005). Additionally, a recent study on missense mutations in *dN* discovered that C972S substitution in EGF25 increased dN accumulation in the ER (Nurmahdi *et al.*, 2022). These results suggest changes to

cysteine residues in the Ax region may, as a consequence of misfolding, disrupt the normal trafficking of Notch to the cell surface and trap the receptor in the secretory pathway. These speculations can be tested by studies of the structure and cellular localisation of these variants. However, the finding that the cysteine substitutions reduced trans-activation cannot explain why they induced Notch-enhancing phenotypes in the *Drosophila* wing, suggesting alternative mechanisms apart from trans-activation.

Though S990N does not affect the residue involved in forming the core EGF fold, the asparagine substitution creates an N-X-C motif which can be associated with post-translational N-glycosylation (Lowenthal *et al.*, 2016) (see Section 1.2.8.6). It is possible that the addition of a non-native N-glycan to EGF26 disrupts folding. Additionally, the negative effect of this variant on Notch signalling supports the hypothesis that the accumulation of loss of function Notch mutations is associated with ageing oesophageal tissue (Martincorena *et al.*, 2018).

8.4.2 The Ax region facilitates trans-activation of N1

Ax substitutions reduced N1 trans-activation by Jag1 and Dll4

mN1 homologues of dN *Ax N* suppressor and *N* enhancer variants reduced N1 trans-activation by Jag1 and Dll4 by ~30% without reducing the cell surface level of N1 (see Chapter 3). However, this reduction was less significant than that caused by a mutation (L468A) in the LBR that abolished ligand binding. This suggests that though less critical than the LBR, the native property of the Ax region optimises N1 trans-activation by Jag1

and Dll4. Interestingly, the two Ax variants (*N* suppressor N947I and *N* enhancer H1129Y) tested in trans-activation assay using DLL1 as the trans-ligand showed WT activation level (see Chapter 6), which was different to the trend observed in assays using trans-Jag1 or trans-Dll4. This suggests that these Ax variants played a minor function in the trans-interaction between N1 and DLL1.

The rigid linear structure of EGF23-25 may facilitate N1 trans-activation

The *N* suppressor variants (D909V and N947I) in EGF24 and EGF25 affect residues involved in Ca^{2+} binding and were shown to reduce Ca^{2+} binding affinity in NMR titration studies (Bo *et al.*, 2024). *N* suppressor variants may disrupt the rigid linear structure at the N terminus of the Ax region formed by Ca^{2+}-stabilised hydrophobic packing interactions at the interfaces of EGF23-24 and EGF24-25 (see Section 1.2.2.3) (Downing *et al.*, 1996; Hambleton *et al.*, 2004; Cordle, Johnson, *et al.*, 2008; Cordle, Redfield, *et al.*, 2008). This may lead to changes in conformation and increase structural flexibility.

The property of EGF27-29 affected by *N* enhancers enhances N1 trans-activation

N enhancer variants (Q1049I, H1129Y and G1136A) in EGF27 and EGF29 do not affect Ca^{2+} binding. Q1049I replaces glutamine, which has a polar side chain, with isoleucine, which has a hydrophobic side chain. H1129Y replaces histidine, which has a positive side chain, with the aromatic residue tyrosine. G1136A affects the glycine residue required for a conserved β-turn in the core EGF structure (Campbell *et al.*, 1990; Baron *et al.*, 1992) and the consensus sequence of O-GlcNAcylation (Tsukamoto *et al.*, 2022), thus may affect the stability and conformation of EGF29. The structural model generated

by AlphaFold2 suggested that Q1049 and G1136 may be located close to the interfaces of EGF27-28 and 29-30 respectively (Figure 8.2) (Jumper *et al.*, 2021). H1129 may be located at the centre of a cluster of hydrophobic residues at the N terminus of EGF29 close to the interface with EGF28 (Figure 8.2). Therefore, these substitutions by residues with hydrophobic side chains may disturb existing hydrophobic interactions in EGF27-30 or create new hydrophobic packings. As SAXS analysis suggested that EGF27-29 has a bent/flexible structure, these variants may affect the flexibility or angle of the interfaces of EGF27-28 (Q1049I), 28-29 (H1129Y) or 29-30 (G1136A), leading to changes in the flexibility and structure of the receptor.

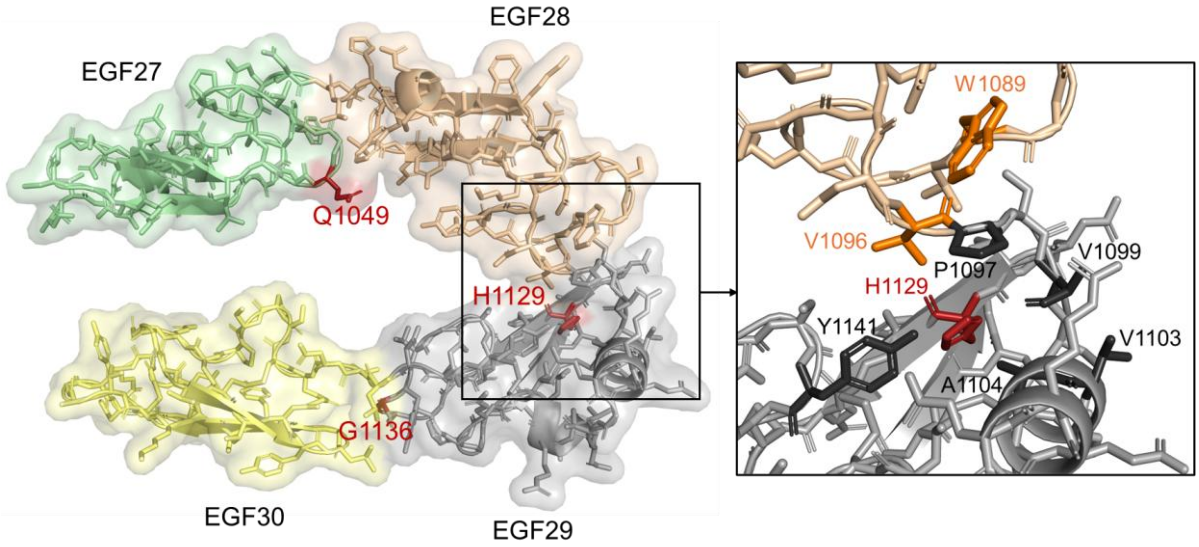


Figure 8.2. Structural model of hN1 EGF27-30 generated by AlphaFold2.

The highest-ranked AlphaFold2 model generated for hN1 EGF27-30 (Jumper *et al.*, 2021). Residues affected by *Ax N* enhancer variants are labelled and coloured in red. The interface of EGF28-29 (indicated with a frame in the left panel) is enlarged in the right panel. Hydrophobic residues at the interface are labelled and coloured in orange (for EGF28) and black (for EGF29).

Potential mechanism underlying the negative effects of *N* suppressor and enhancer substitutions on trans-activation

Since *N* suppressor and *N* enhancer mutations did not reduce the amount of ligand NE3 constructs bound to the cell, the negative effects of these Ax variants on N1 activation are unlikely a result of reduced levels of ligand binding. Since these variants may affect the structure of N1, they may reduce N1 trans-activation by increasing the structural flexibility of the receptor and reducing the amount of pulling force (generated by ligand-NECD trans-endocytosis, see Section 1.4.2) transmitted to the NRR. Consequently, a stronger pulling force is needed to activate these variants. Alternatively, the structural effects of Ax mutations may limit the movement of the receptor to seek and bind ligands expressed on neighbouring cells. Therefore, stronger ligand binding affinity and pulling force, or a smaller cell-to-cell distance, may be required to fully activate Ax variants. In addition, previous studies showed that while receptors and ligands are mobile and diffuse laterally in the cell membrane in the absence of cell contact, Notch synapses, which show accumulation of receptors and ligands, are formed at the contact sites between receptor-expressing and ligand-expressing cells (Fehon *et al.*, 1990; Chapman *et al.*, 2016; Tveriakhina *et al.*, 2024). Ax variants may have reduced ability to migrate to the Notch synapse and have lower chances to interact with trans-ligands that accumulate at the Notch synapse.

Previous studies using N1 fragments suggested that the Ax region can interact with the LBR but not with ligands (Pei and Baker, 2008; Sharma, Rangarajan and Dighe, 2013).

In full-length N1, the LBR may potentially interact inter- or intramolecularly with the Ax region in the same receptor or a neighbouring receptor. Also, a competition of N1 EGF21-30 with the extracellular domain of JAG1 for binding to EGF11-20 was detected by previous in vitro assays (Sharma, Rangarajan and Dighe, 2013), suggesting the ligand may compete with the Ax region for binding to the LBR. The Ax mutations may enhance the interaction between Ax and LBR and reduce the strength of binding of ligands to the LBR, thus reducing the amount of receptor activated by ligands. Structural analysis, SPR or XL-MS can be performed on constructs containing the LBR and Ax regions to investigate inter- or intramolecular interactions between these regions and the effect of Ax mutations on the interactions.

8.4.3 The Ax region regulates cis-inhibition of N1

N suppressor substitutions affected N1 cis-inhibition by JAG1 but not DLL4

Ax N suppressor and *N* enhancer variants behaved differently in cis-inhibition assays (see Chapter 4 and 5). *N* suppressor substitutions reduced N1 cis-inhibition by cis-JAG1 when co-cultured with trans-Jag1 or trans-Dll4 (see Chapter 4), but did not affect cis-inhibition by cis-DLL4 when co-cultured with either trans-ligand (see Chapter 5) (Table 8.1). These results suggest that the Ca^{2+}-binding-dependent structure of EGF24-25, which is disrupted by *N* suppressor variants, facilitates cis-inhibition of N1 by cis-JAG1 but plays a less important role in cis-inhibition by cis-DLL4. The interaction of N1 with ligands of different families may require different interfaces or properties of the receptor.

Table 8.1. Summary of the effects of N1 Ax mutations on cis-inhibition.

The effects of Ax mutations on the levels of JAG1- or DLL4-mediated cis-inhibition of N1 when grown with trans-Jag1, trans-Dll4 or trans-DLL1 (see Chapter 4, 5 and 6). The effects of receptor-binding deficient cis-ligands (cis-JAG1 FAEK, cis-DLL4 FAYA) on cis-inhibition of N1 WT are also shown. "↓" indicates a decrease in cis-inhibition within 50% of that in N1 WT (or that by WT cis-ligand in the case of cis-ligand variants). "↓↓" indicates a decrease in cis-inhibition over 50% of that generated by WT cis-ligand. "ns" indicates no significant difference to N1 WT (in the case of Ax variants) or WT cis-ligand (in the case of cis-ligand variants). "N/A" indicates an experiment is not applicable.

EGF	Mutation	Type	Cis-inhibition by JAG1			Cis-inhibition by DLL4	
			Trans-Jag1	Trans-Dll4	Trans-DLL1	Trans-Jag1	Trans-Dll4
Cis-JAG1 FAEK		Receptor-binding deficient	↓↓	↓↓	Not tested	N/A	N/A
Cis-DLL4 FAYA		Receptor-binding deficient	N/A	N/A	N/A	ns	↓
24	D909V	*Ax N* suppressor	↓	↓	Not tested	ns	ns
25	N947I	*Ax N* suppressor	↓	↓	ns	ns	ns
24-25	DVNI	*Ax N* suppressor double variant	↓	↓	Not tested	Not tested	Not tested
27	Q1049I	*Ax N* enhancer	ns	ns	Not tested	Not tested	Not tested
29	H1129Y	*Ax N* enhancer	↓	ns	↓	↓	↓
29	G1136A	*Ax N* enhancer	↓	ns	Not tested	ns	ns

<u>*N* enhancer substitutions in EGF29 affected N1 cis-inhibition by both JAG1 and DLL4</u>

N enhancer substitutions in EGF29, H1129Y and G1136A, reduced N1 cis-inhibition by JAG1 when co-cultured with trans-Jag1 whilst Q1049I in EGF27 did not (see Chapter 4) (Table 8.1). On the other hand, all *N* enhancer variants tested showed no effect on N1 cis-inhibition by cis-JAG1 when co-cultured with trans-Dll4 (see Chapter 4) (Table 8.1). This suggests that the native property of EGF29 may facilitate competition of cis-JAG1 with trans-Jag1 but not trans-Dll4. H1129Y reduced receptor cis-inhibition by cis-DLL4 when co-cultured with either trans-ligand, whilst G1136A and *N* suppressors did not (see

Chapter 5) (Table 8.1). However, similar to trends observed in the absence of cis-ligand, activation levels of H1129Y (and other Ax variants tested) were still lower than that of N1 WT upon expression of cis-DLL4 (Appendix I).

N suppressors and enhancers may show different responses to trans-DLL1 upon cis-inhibition

N suppressor N947I and *N* enhancer H1129Y were tested in a cis-inhibition assay using cis-JAG1 and trans-DLL1. Compared to N1 WT, N947I showed a similar level of cis-inhibition by cis-JAG1 while H1129Y showed a reduced level of cis-inhibition (see Chapter 6) (Table 8.1). This suggests the two classes of mutations may have different effects on the trans-activation of N1 by DLL1 upon inhibition by cis-JAG1. Additional experiments testing the other Ax variants and using other cis-ligands may be performed in future to explore potential differential responses of *N* suppressors and enhancers to trans- and cis-DLL1.

N suppressor and enhancer variants showed different effects on receptor-ligand interactions during cis-inhibition

N suppressor and *N* enhancer variants showed different responses to cis-JAG1 and cis-DLL4 when grown with different trans-ligands. These results show that the properties of the receptor affected by *N* suppressors may be different to those affected by *N* enhancers. Therefore, the rigid extended N terminus of the Ax region may play a different role in receptor-ligand cis-interactions compared to EGF29 at the C terminus of the Ax region.

The differences in results obtained with ligands of different families show the complexity of the effects of these Ax substitutions on Notch signalling. Variations in the cis-inhibition level obtained using the same cis-ligand paired with different trans-ligands suggest that competition between trans-ligand and cis-ligand on the cell surface is likely to take place.

Ax substitutions that reduced the level of cis-inhibition should have a stronger negative effect on the receptor-ligand interaction in cis than on that in trans, shifting the competition or equilibrium of interactions towards the trans-activatory state. By changing the conformation of the receptor, Ax substitutions may increase the difficulty for N1 to orient itself at the cell membrane, thus reducing the chance to interact with a cis-ligand. Alternatively, they may make the structure of N1 less suitable for binding to cis-ligands and decrease the strength and stability of binding between N1 and cis-ligands. As a result, more receptors are released from the constraints of forming the inhibitory complex with cis-ligands.

8.5 Ax variants in the presence of Lfng

Lfng was shown to reduce Jag1-mediated trans-activation of N1 while enhancing Dll4- and DLL1-mediated trans-activation (see Chapter 6). Also, as reduced N1 WT activity was detected in cells expressing both cis-JAG1 and Lfng compared with cells only expressing cis-JAG1, the negative effect of Lfng expression on activation of N1 WT by trans-Jag1 seems to be stronger than that on inhibition by cis-JAG1.

Lfng offset the negative effect of Ax variants on N1 trans-activation by Jag1

Ax variants tested (N947I and H1129Y) were less sensitive than N1 WT to the negative effect of Lfng on N1 trans-activation by Jag1 and showed a similar activation level compared to N1 WT upon Lfng expression (see Chapter 6) (Figure 8.3). This observation supports the previous finding that the *Ax* alleles N986I (homolog of N1 N947I) and G1174A (homolog of N1 G1136A) were insensitive to Fng expression when it functions to inhibit Notch signalling in the *Drosophila* wing disc (De Celis and Bray, 2000). Previous glycoproteomic analysis of N1 EGF24-28 fragment found that modifications of O-fucose by Mfng were downregulated in this fragment carrying D909V (*N* suppressor), suggesting that this mutation may prevent Fng from recognising the Ax region (Shao, Moloney and Haltiwanger, 2003). The effects of Ax substitutions on the structure of N1 may lead to a similar downregulation of Lfng modifications. For example, *N* suppressors, which have reduced Ca^{2+} binding at EGF23-25, may have a more flexible structure in the Golgi that has a Ca^{2+} concentration (~0.3 mM) (Pinton, Pozzan and Rizzuto, 1998) significantly lower than that in the extracellular region (~1.5 mM) (Jones and Keep, 1987). The new structure formed may reduce Fng recognition of the receptor or block sites of Fng modification. Alternatively, Ax substitutions may change the interface for Jag1 interaction and reduce the impacts of Lfng modifications on it by shifting the relative positions of receptor and ligand.

Lfng had similar effects on Dll4- and DLL1-mediated trans-activation of N1 WT and Ax

variants (see Chapter 6). Since previous studies suggested that Lfng enhances N1 activation by extending O-fucose in EGF8 and EGF12 (Kakuda and Haltiwanger, 2017), Ax substitutions may not affect the amount or the impact of Lfng-mediated extension of these O-fucose.

Compared with N1 WT, Ax variants showed higher activation by trans-Jag1 and/or trans-DLL1 upon co-expression of cis-JAG1 and Lfng

When cis-JAG1 and Lfng were co-expressed, both Ax variants tested showed higher Jag1-mediated activation than N1 WT (see Chapter 6) (Figure 8.3). The expression of Lfng appeared to offset the negative effect of Ax substitutions on N1 trans-activation by Jag1 while not affecting the negative effect of Ax substitutions on N1 cis-inhibition by JAG1. This leads to overall weaker JAG1-mediated cis-inhibition in Ax variants than WT when grown with trans-Jag1. In addition, *N* enhancer H1129Y showed higher DLL1-mediated activation than N1 WT and *N* suppressor N947I upon JAG1-mediated cis-inhibition both in the presence and absence of Lfng (see Chapter 6) (Figure 8.3).

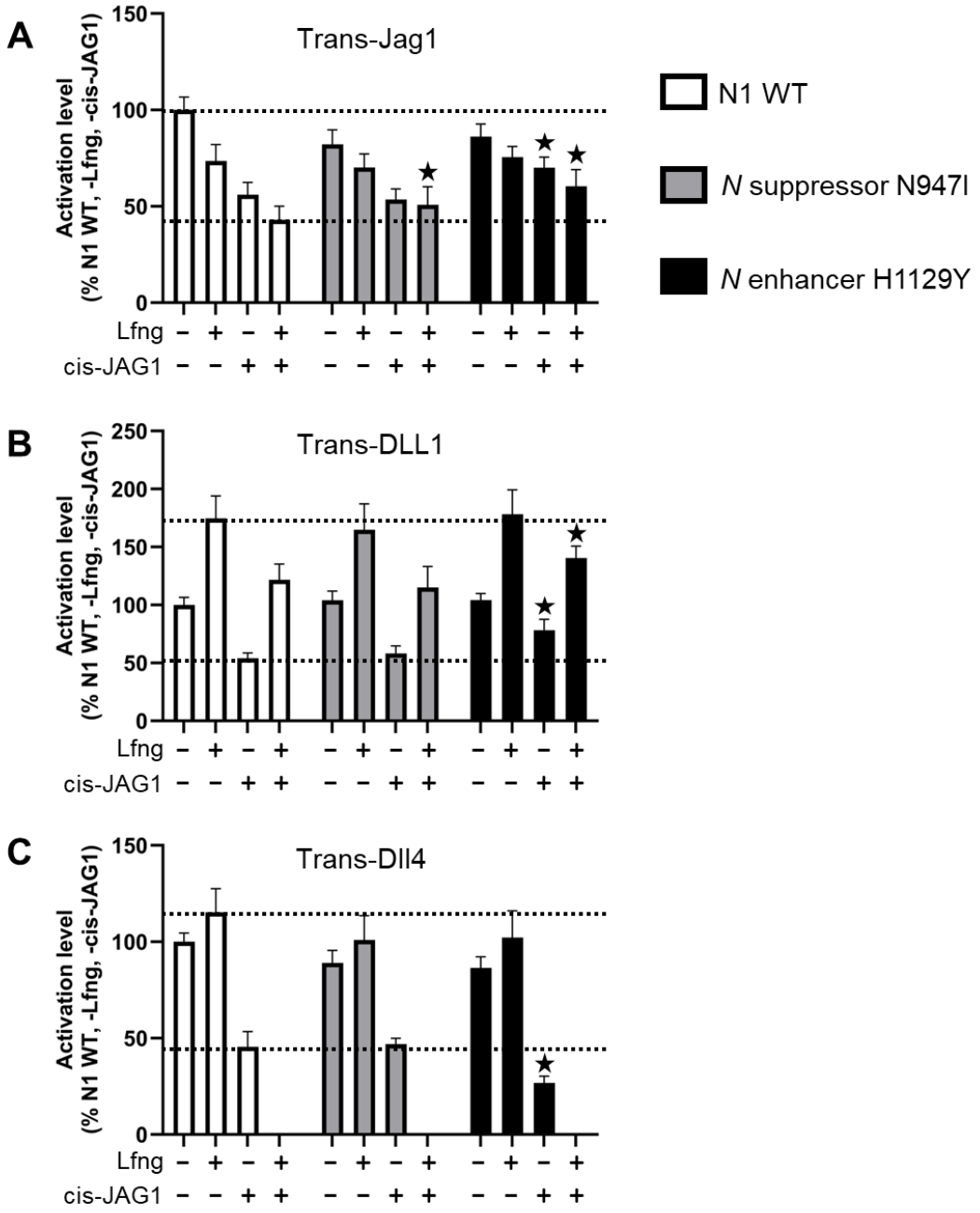


Figure 8.3. Activation of N1 WT and Ax variants by different trans-ligands under conditions with and without Lfng and cis-JAG1.

Activation levels of N1 WT, *N* suppressor N947I and *N* enhancer H1129Y in the absence ("-") and presence ("+") of Lfng and cis-JAG1. Cells were grown with (A) trans-Jag1, (B) trans-DLL1 or (C) trans-Dll4. Signals are shown relative to N1 WT in the absence of Lfng or cis-JAG1. Data were presented as mean ± SD (extracted from Figure 4.6, 4.7, 6.4, 6.5, 6.7, 6.8). The dashed lines indicate the highest and lowest levels of activation of N1 WT by each trans-ligand. Activation levels of Ax variants that are statistically different to that of N1 WT in the presence of cis-JAG1 are indicated by stars.

8.6 Ax variants and the *Ax* phenotype

The *Ax* phenotype, including interrupted wing veins and fewer bristles on the wing margin, is commonly considered to be caused by hyperactivation of Notch signalling that generates similar effects to deficiencies in cis-Dl and cis-Ser (De Celis and Bray, 2000). *Drosophila* Fng, which generates similar effects on Notch activation as Lfng (Panin *et al.*, 1997), was found to be expressed during the development of the *Drosophila* wing (Doherty *et al.*, 1996; de Celis and Bray, 1997; Becam and Milán, 2008). Also, dN inhibition by cis-Dl and cis-Ser was found to regulate wing vein and margin development (LeBon *et al.*, 2014). Considering *Drosophila* as a model organism which shares conserved systems with mammals, similar to the trend observed for N1 variants tested with trans-Jag1 and cis-JAG1 in the presence of Lfng (see Chapter 6) (Figure 8.3), the Ax variants may show higher levels of Ser-mediated activation upon cis-inhibition by Ser in Fng-expressing *Drosophila* cells. *N* enhancers may also show higher levels of Dl-mediated activation upon expression of cis-Ser similar to that observed with trans-DLL1 and cis-JAG1 for N1 variant (see Chapter 6) (Figure 8.3). Under these trans- and cis-ligand combinations, Ax variants may have higher Notch activation levels than WT, which may contribute to the *Ax* phenotype in the *Drosophila* wing.

While *N* suppressors and *N* enhancers are both viable when combined with Ax variants of the same class, previous studies suggested that the combinations of *N* suppressors with *N* enhancers lead to lethality (Foster, 1975; Portin, 1975). This suggests that these

variants may affect different properties of the receptor, which is supported by our findings that *N* suppressors and *N* enhancers responded differently to different combinations of trans- and cis-ligands in cis-inhibition assays (see Section 8.4.3) and affected regions of different structures in the Ax region as shown by SAXS analyses (see Section 8.3). However, the mechanism leading to the negative complementation of Ax variants from different classes remains unclear. In addition, when in combination with a null allele of dN, it is unclear how *N* suppressors reduce nicks in the wing margin while *N* enhancers enhance nicking (Foster, 1975; Portin, 1975; Kelley *et al.*, 1987). *N* enhancers showed lower Dll4-mediated activation than N1 WT and *N* suppressors upon inhibition by cis-JAG1 (see Chapter 4) (Figure 8.3). A similar mechanism may be responsible for the lower Notch signalling level represented by enhanced wing nicking when the *N* enhancer and the null allele are combined.

Since this project focused on studying the effect of Ax mutations on ligand-dependent trans-activation and cis-inhibition of Notch, further experiments can be performed to study the impacts of these mutations on ligand-independent activation of Notch. Previous studies showed that mutations in Lethal (2) giant discs protein, endosomal sorting complex required for transport, and the E3 ubiquitin ligase Suppressor of dx, as well as overexpression of Dx, which increased the fraction of Notch on the limiting membrane of mature endosomes or lysosomes, can induce ligand-independent Notch activation (Wilkin *et al.*, 2008; Hori *et al.*, 2011; Troost *et al.*, 2012; Schneider *et al.*, 2013). These studies proposed that in the lumen of mature endosomes and lysosomes, NECD may be

degraded by hydrolases, or the low pH and Ca^{2+} level may induce a conformational change of the NECD, leading to dissociation of the NECD and subsequent γ-secretase-mediated S3 cleavage (Rand *et al.*, 2000; Wilkin *et al.*, 2008; Hori *et al.*, 2011; Troost *et al.*, 2012; Schneider *et al.*, 2013). As a result, NICD is released, leading to activation of Notch signalling.

Previous studies have shown that the loss of function of Dx can suppress the gain of function phenotypes of some Ax variants and rescue the lethal combinations of Ax variants, suggesting that the way those Ax variants enhance Notch signalling involves Notch ubiquitination and endocytosis (Xu and Artavanis-Tsakonas, 1990; Gorman and Girton, 1992; Busseau *et al.*, 1994; Diederich *et al.*, 1994). Ax mutations, by altering structural properties, may affect endocytosis and recycling of the receptor, and increase the accumulation of receptors in mature endosomes or lysosomes, thus leading to increased ligand-independent Notch activation. Ax homozygous lethal mutations, which may affect the conserved EGF fold and lead to aggregation, may increase retention of the receptor in endocytic vesicles and facilitate the sorting of Notch within early endosomes to late endosomes.

8.7 Future work

The SAXS data analysis pipeline employed in this project (see Chapter 7) can be used to study other regions in Notch receptors that fail to be crystallised. Fragments including

and after the Ax region, such as hN1 EGF25-32 or EGF25-36 could be subjected to SAXS analysis or X-ray crystallography to confirm the bent or flexible structure of EGF27-29. Also, NMR and RDC analysis of shorter protein fragments could be employed to determine the interdomain orientations within the Ax region, especially for interfaces of EGF27-28 and EGF28-29.

Further work could be done in the future to explore the mechanisms underlying the downregulated trans-activation and cis-inhibition of Ax variants. Additional experiments (as described in Table 8.2) could be performed on N1 protein constructs and reporter cells to study the effects of Ax substitutions on (1) the structure and flexibility of the receptor; (2) the pulling force needed for receptor activation; (3) receptor-ligand binding affinity and kinetics; (4) interaction of the Ax region with LBR.

Ax variants tested in this project showed reduced responses to the negative effect of Lfng on N1 trans-activation by trans-Jag1. To study whether this mitigated response is caused by reduced PTMs by Lfng, mass-spectrometry-based glycoproteomic analysis could be conducted for protein fragments of N1 WT and Ax variants produced by Lfng-expressing cells to assess the extent of Lfng-mediated O-fucose elongation at different EGF repeats. In addition, further experiments can be performed to study the structure, ligand binding and mechanical force needed for activation of Lfng-modified Ax variants.

Table 8.2. Proposed experiments to further characterise the effects of Ax substitutions on Notch signalling.

Investigation	Materials	Proposed methodology
The effect of Ax substitutions on the structure and flexibility of the receptor	Ax variant protein constructs	SAXS, NMR, X-ray crystallography
The effect of Ax substitutions on the pulling force needed to activate the receptor	Ligand protein constructs Ax variant reporter cell lines	Tension gauge tether assay, magnetic tweezers assay
The effect of Ax substitutions on receptor-ligand binding affinity and kinetics	Ax variant protein constructs Ligand protein constructs Ax variant reporter cell lines Ligand-expressing cell lines	SPR, biolayer interferometry, force-clamp spectroscopy, binding assays with live cells expressing full-length ligands
The effect of Ax substitutions on the interaction of the Ax region with LBR	Ax variant protein constructs LBR protein constructs Ax variant reporter cell lines	SPR, biolayer interferometry, binding assays

Since human and mouse N1 and ligands were tested in protein- or cell-based experiments in this project, similar assays or tissue-based studies could be performed for dN, *Drosophila* ligands and Fng to confirm the mechanism leading to the *Ax* phenotypes in the original context. Along with the *Drosophila* wing, other tissues where Notch signalling plays a known role, such as gut and eye (Miller, Lyons and Herman, 2009; Takashima *et al.*, 2011; Guo and Ohlstein, 2015), may be employed to study the effects of Ax mutations in tissues.

The cell-based luciferase assays developed in this project could be helpful for future

studies of Notch cis-inhibition. Previous studies showed that deletions of each EGF in EGF4-6 of Ser and EGF8 of DLL4, which might generate large structural changes of the ligand, reduced cis-inhibition but not trans-activation of the receptor (Fleming *et al.*, 2013; Chen *et al.*, 2023) (see Section 1.5.3). Cis-inhibition assays using cis-ligands carrying point mutations affecting different structural characteristics of these EGF domains may be performed to explore the roles of these domains in Notch signalling. When combined with genome-wide CRISPR screens, cis-inhibition assays could be used to identify potential genes, proteins and mutations that modulate Notch signalling via changing cis-inhibition. The effects of EGF16 variants that generated *Ax* phenotype in *Drosophila* on cis-inhibition could be studied to explore the role of EGF16 in N1 cis-inhibition. Flow cytometry-based assay could be employed to quantify changes in cell surface levels of Notch and cis-ligand upon co-expression. Also, to track movements of receptors and cis-ligands, explore cellular localisation of receptor-ligand cis-complexes, and probe the interactions between trans- and cis-ligands and receptors on the cell surface, immunofluorescence techniques (e.g., fluorescence resonance energy transfer, fluorescein arsenical hairpin technique and proximity ligation assay) could be used to study the (co-)localisation of receptors and trans- and cis-ligands.

9 Bibliography

Acar, M. *et al.* (2008) 'Rumi is a CAP10 domain glycosyltransferase that modifies Notch and is required for Notch signaling.', *Cell*, 132(2), pp. 247–258. Available at: https://doi.org/10.1016/j.cell.2007.12.016.

Adams, F.H. and Oliver, C.P. (1945) 'Hereditary deformities in man', *Journal of Heredity*, 36(1), pp. 3–7. Available at: https://doi.org/10.1093/oxfordjournals.jhered.a105415.

Agrawal, N. *et al.* (2011) 'Exome sequencing of head and neck squamous cell carcinoma reveals inactivating mutations in NOTCH1', *Science (New York, N.Y.)*, 333(6046), pp. 1154–1157. Available at: https://doi.org/10.1126/SCIENCE.1206923.

del Álamo, D., Rouault, H. and Schweisguth, F. (2011) 'Mechanism and Significance of cis-Inhibition in Notch Signalling', *Current Biology*, 21(1), pp. R40–R47. Available at: https://doi.org/10.1016/j.cub.2010.10.034.

Albrecht, T. *et al.* (2015) 'Fluorescent biosensors illuminate calcium levels within defined beta-cell endosome subpopulations', *Cell Calcium*, 57(4), pp. 263–274. Available at: https://doi.org/10.1016/j.ceca.2015.01.008.

Alcolea, M.P. *et al.* (2014) 'Differentiation imbalance in single Oesophageal progenitor cells causes clonal immortalization and field change', *Nature cell biology*, 16(6), p. 615. Available at: https://doi.org/10.1038/NCB2963.

Amano, Y., Yamaguchi, T. and Tanabe, E. (2014) 'Structural insights into binding of inhibitors to soluble epoxide hydrolase gained by fragment screening and X-ray crystallography', *Bioorganic & Medicinal Chemistry*, 22(8), pp. 2427–2434. Available at: https://doi.org/10.1016/j.bmc.2014.03.001.

Andrawes, M.B. *et al.* (2013) 'Intrinsic selectivity of Notch 1 for Delta-like 4 over Delta-like 1.', *The Journal of biological chemistry*, 288(35), pp. 25477–25489. Available at: https://doi.org/10.1074/jbc.M113.454850.

Artavanis-Tsakonas, S. (1999) 'Notch Signaling: Cell Fate Control and Signal Integration in Development', *Science*, 284(5415), pp. 770–776. Available at: https://doi.org/10.1126/science.284.5415.770.

Aster, J.C., Pear, W.S. and Blacklow, S.C. (2017) 'The Varied Roles of Notch in Cancer', *Annual Review of Pathology: Mechanisms of Disease*, 12, pp. 245–275. Available at: https://doi.org/10.1146/annurev-pathol-052016-100127.

Austin, J. and Kimble, J. (1989) 'Transcript analysis of glp-1 and lin-12, homologous genes required for cell interactions during development of C. elegans', *Cell*, 58(3), pp. 565–71. Available at: https://doi.org/10.1016/0092-8674(89)90437-6.

Baek, C. *et al.* (2018) 'Mib1 prevents Notch Cis-inhibition to defer differentiation and preserve neuroepithelial integrity during neural delamination', *PLoS Biology*, 16(4), p. e2004162. Available at: https://doi.org/10.1371/journal.pbio.2004162.

Bailey, P. *et al.* (2016) 'Genomic analyses identify molecular subtypes of pancreatic cancer', *Nature 2016 531:7592*, 531(7592), pp. 47–52. Available at: https://doi.org/10.1038/nature16965.

Barolo, S. *et al.* (2002) 'Default repression and Notch signaling: Hairless acts as an adaptor to recruit the corepressors Groucho and dCtBP to Suppressor of Hairless', *Genes & Development*, 16(15), pp. 1964–1976. Available at: https://doi.org/10.1101/gad.987402.

Baron, M. *et al.* (1992) 'The three-dimensional structure of the first EGF-like module of human factor IX: comparison with EGF and TGF-alpha.', *Protein science : a publication of the Protein Society*, 1(1), pp. 81–90. Available at: https://doi.org/10.1002/pro.5560010109.

Basmanav, F.B. *et al.* (2014) 'Mutations in POGLUT1, encoding protein O-glucosyltransferase 1, cause autosomal-dominant Dowling-Degos disease.', *American journal of human genetics*, 94(1), pp. 135–143. Available at: https://doi.org/10.1016/j.ajhg.2013.12.003.

Bauer, R.C. *et al.* (2010) 'Jagged1 (JAG1) mutations in patients with tetralogy of fallot or pulmonic stenosis', *Human Mutation*, 31(5), pp. 594–601. Available at: https://doi.org/10.1002/HUMU.21231.

Bause, E. and Hettkamp, H. (1979) 'Primary structural requirements for N-glycosylation of peptides in rat liver', *FEBS letters*, 108(2), pp. 341–344. Available at: https://doi.org/10.1016/0014-5793(79)80559-1.

Beà, S. *et al.* (2013) 'Landscape of somatic mutations and clonal evolution in mantle cell lymphoma.', *Proceedings of the National Academy of Sciences of the United States of America*, 110(45), pp. 18250–18255. Available at: https://doi.org/10.1073/pnas.1314608110.

Becam, I. *et al.* (2010) 'A role of receptor Notch in ligand cis-inhibition in Drosophila.', *Current biology : CB*, 20(6), pp. 554–560. Available at: https://doi.org/10.1016/j.cub.2010.01.058.

Becam, I. and Milán, M. (2008) 'A permissive role of Notch in maintaining the DV affinity boundary of the Drosophila wing', *Developmental Biology*, 322(1), pp. 190–198. Available at: https://doi.org/10.1016/j.ydbio.2008.07.028.

Bernasconi-Elias, P. *et al.* (2016) 'Characterization of activating mutations of NOTCH3 in T cell acute lymphoblastic leukemia and anti-leukemic activity of NOTCH3 inhibitory antibodies', *Oncogene*, 35(47), p. 6077. Available at: https://doi.org/10.1038/ONC.2016.133.

Berndt, N. *et al.* (2017) 'Ubiquitylation-independent activation of Notch signalling by Delta', *eLife*, 6. Available at: https://doi.org/10.7554/ELIFE.27346.

Bertagna, A. *et al.* (2008) ‘The effects of conformational heterogeneity on the binding of the Notch intracellular domain to effector proteins: a case of biologically tuned disorder.’, *Biochemical Society transactions*, 36(Pt 2), pp. 157–66. Available at: https://doi.org/10.1042/BST0360157.

Bierkamp, C. and Campos-Ortega, J.A. (1993) ‘A zebrafish homologue of the Drosophila neurogenic gene Notch and its pattern of transcription during early embryogenesis’, *Mech Dev*, 43(2–3), pp. 87–100. Available at: https://doi.org/10.1016/0925-4773(93)90027-u.

Blaumueller, C.M. *et al.* (1997) ‘Intracellular cleavage of Notch leads to a heterodimeric receptor on the plasma membrane’, *Cell*, 90(2), pp. 281–291. Available at: https://doi.org/10.1016/S0092-8674(00)80336-0.

Bo, Z. *et al.* (2024) ‘Structural and functional studies of the EGF20-27 region reveal new features of the human Notch receptor important for optimal activation’, *Structure* [Preprint]. Available at: https://doi.org/10.1016/j.str.2024.10.012.

Boareto, M. *et al.* (2015) ‘Jagged mediates differences in normal and tumor angiogenesis by affecting tip-stalk fate decision’, *Proceedings of the National Academy of Sciences*, 112(29), pp. E3836–E3844. Available at: https://doi.org/10.1073/pnas.1511814112.

Bonfiglio, F. *et al.* (2022) ‘Genetic and phenotypic attributes of splenic marginal zone lymphoma’, *Blood*, 139(5), pp. 732–747. Available at: https://doi.org/10.1182/BLOOD.2021012386.

Brat, D.J. *et al.* (2015) ‘Comprehensive, Integrative Genomic Analysis of Diffuse Lower-Grade Gliomas.’, *The New England journal of medicine*, 372(26), pp. 2481–2498. Available at: https://doi.org/10.1056/NEJMoa1402121.

Bray, S. (1998) ‘Notch signalling in Drosophila: Three ways to use a pathway’, *Seminars in Cell and Developmental Biology* [Preprint]. Available at: https://doi.org/10.1006/scdb.1998.0262.

Bray, S.J. (2016) ‘Notch signalling in context’, *Nature Reviews Molecular Cell Biology*, 17(11), pp. 722–735. Available at: https://doi.org/10.1038/nrm.2016.94.

Bray, S.J. and Gomez-Lamarca, M. (2018) ‘Notch after cleavage’, *Current Opinion in Cell Biology*, 51, pp. 103–109. Available at: https://doi.org/10.1016/J.CEB.2017.12.008.

Brennan, K. *et al.* (1999) ‘The Abruptex Mutations of Notch Disrupt the Establishment of Proneural Clusters in Drosophila’, *Developmental Biology*, 216(1), pp. 230–242. Available at: https://doi.org/10.1006/dbio.1999.9501.

Brou, C. *et al.* (2000) ‘A Novel Proteolytic Cleavage Involved in Notch Signaling: The Role of the Disintegrin-Metalloprotease TACE’, *Molecular Cell*, 5(2), pp. 207–216. Available at: https://doi.org/10.1016/S1097-2765(00)80417-7.

Brückner, K. *et al.* (2000) 'Glycosyltransferase activity of Fringe modulates Notch–Delta interactions', *Nature*, 406(6794), pp. 411–415. Available at: https://doi.org/10.1038/35019075.

Bulman, M.P. *et al.* (2000) 'Mutations in the human Delta homologue, DLL3, cause axial skeletal defects in spondylocostal dysostosis', *Nature Genetics*, 24(4), pp. 438–441. Available at: https://doi.org/10.1038/74307.

Busseau, I. *et al.* (1994) 'A Member of the Notch Group of Interacting Loci, Deltex Encodes a Cytoplasmic Basic Protein', *Genetics*, 136(2), p. 585. Available at: https://doi.org/10.1093/GENETICS/136.2.585.

Campbell, I.D. *et al.* (1990) 'Structure-function relationships in epidermal growth factor (egf) and transforming growth factor-alpha (TGF-α)', *Biochemical Pharmacology*, 40(1), pp. 35–40. Available at: https://doi.org/10.1016/0006-2952(90)90175-K.

Canalis, E. and Zanotti, S. (2016) 'HAJDU CHENEY SYNDROME, A DISEASE ASSOCIATED WITH NOTCH2 MUTATIONS', *Current osteoporosis reports*, 14(4), pp. 126–131. Available at: https://doi.org/10.1007/s11914-016-0311-6.

Cancer Genome Atlas Research Network (2012) 'Comprehensive genomic characterization of squamous cell lung cancers.', *Nature*, 489(7417), pp. 519–525. Available at: https://doi.org/10.1038/nature11404.

Cantarini, M.C. *et al.* (2006) 'Aspartyl-asparagyl β hydroxylase over-expression in human hepatoma is linked to activation of insulin-like growth factor and notch signaling mechanisms', *Hepatology*, 44(2), pp. 446–457. Available at: https://doi.org/10.1002/hep.21272.

Carrieri, F.A. *et al.* (2019) 'CDK 1 and CDK 2 regulate NICD 1 turnover and the periodicity of the segmentation clock', *EMBO reports*, 20(7). Available at: https://doi.org/10.15252/embr.201846436.

de Celis, J.F. and Bray, S. (1997) 'Feed-back mechanisms affecting Notch activation at the dorsoventral boundary in the Drosophila wing.', *Development (Cambridge, England)*, 124(17), pp. 3241–3251. Available at: https://doi.org/10.1242/dev.124.17.3241.

Celis, J.F. de, Garcia-Bellido, A. and Bray, S.J. (1996) 'Activation and function of Notch at the dorsal-ventral boundary of the wing imaginal disc', *Development*, 122(1), pp. 339–369. Available at: https://doi.org/10.1242/dev.122.1.359.

Chabriat, H. *et al.* (2009) 'Cadasil.', *The Lancet. Neurology*, 8(7), pp. 643–653. Available at: https://doi.org/10.1016/S1474-4422(09)70127-9.

Chapman, G. *et al.* (2011) 'Notch inhibition by the ligand DELTA-LIKE 3 defines the mechanism of abnormal vertebral segmentation in spondylocostal dysostosis', *Human Molecular Genetics*, 20(5), pp. 905–916. Available at: https://doi.org/10.1093/hmg/ddq529.

Chapman, G. *et al.* (2016) 'Notch1 endocytosis is induced by ligand and is required for signal

transduction', *Biochimica et biophysica acta*, 1863(1), pp. 166–177. Available at: https://doi.org/10.1016/J.BBAMCR.2015.10.021.

Chastagner, P., Rubinstein, E. and Brou, C. (2017) 'Ligand-activated Notch undergoes DTX4-mediated ubiquitylation and bilateral endocytosis before ADAM10 processing', *Science signaling*, 10(483). Available at: https://doi.org/10.1126/SCISIGNAL.AAG2989.

Chaudhuri, B. *et al.* (eds) (2017) *Biological Small Angle Scattering: Techniques, Strategies and Tips*. Singapore: Springer (Advances in Experimental Medicine and Biology). Available at: https://doi.org/10.1007/978-981-10-6038-0.

Chen, D. *et al.* (2023) 'A new model of Notch signalling: Control of Notch receptor cis-inhibition via Notch ligand dimers', *PLOS Computational Biology*, 19(1), p. e1010169. Available at: https://doi.org/10.1371/journal.pcbi.1010169.

Chen, H. *et al.* (2009) 'Embryonic arrest at midgestation and disruption of Notch signaling produced by the absence of both epsin 1 and epsin 2 in mice', *Proceedings of the National Academy of Sciences of the United States of America*, 106(33), p. 13838. Available at: https://doi.org/10.1073/PNAS.0907008106.

Chen, J., Moloney, D.J. and Stanley, P. (2001) 'Fringe modulation of Jagged1-induced Notch signaling requires the action of β4galactosyltransferase-1', *Proceedings of the National Academy of Sciences of the United States of America*, 98(24), p. 13716. Available at: https://doi.org/10.1073/PNAS.241398098.

Chillakuri, C.R. *et al.* (2013) 'Structural Analysis Uncovers Lipid-Binding Properties of Notch Ligands', *CellReports*, 5, pp. 861–867. Available at: https://doi.org/10.1016/j.celrep.2013.10.029.

Choi, J.H. *et al.* (2008) 'Jagged-1 and Notch3 Juxtacrine Loop Regulates Ovarian Tumor Growth and Adhesion', *Cancer Research*, 68(14), pp. 5716–5723. Available at: https://doi.org/10.1158/0008-5472.CAN-08-0001.

Chu, Q., Liu, L. and Wang, W. (2013) 'Overexpression of hCLP46 enhances Notch activation and regulates cell proliferation in a cell type-dependent manner.', *Cell proliferation*, 46(3), pp. 254–262. Available at: https://doi.org/10.1111/cpr.12037.

Clustal Omega < EMBL-EBI (no date). Available at: https://www.ebi.ac.uk/jdispatcher/msa/clustalo (Accessed: 17 March 2024).

Coffman, C., Harris, W. and Kintner, C. (1990) 'Xotch, the Xenopus homolog of Drosophila notch', *Science*, 249(4975), pp. 1438–41. Available at: https://doi.org/10.1126/science.2402639.

Cohen, B. *et al.* (1997) 'Fringe boundaries coincide with Notch-dependent patterning centres in mammals and alter Notch-dependent development in Drosophila.', *Nature genetics*, 16(3), pp. 283–288. Available at: https://doi.org/10.1038/ng0797-283.

Collins, K.J., Yuan, Z. and Kovall, R.A. (2014) 'Structure and Function of the CSL-KyoT2 Corepressor Complex – a Negative Regulator of Notch Signaling', *Structure (London, England : 1993)*, 22(1), pp. 70–81. Available at: https://doi.org/10.1016/j.str.2013.10.010.

Cooke, R.M. *et al.* (1987) 'The solution structure of human epidermal growth factor', *Nature*, 327(6120), pp. 339–341. Available at: https://doi.org/10.1038/327339a0.

Coppens, S. *et al.* (2021) 'A form of muscular dystrophy associated with pathogenic variants in JAG2', *The American Journal of Human Genetics*, 108(5), pp. 840–856. Available at: https://doi.org/10.1016/j.ajhg.2021.03.020.

Corbalan-Garcia, S. and Gómez-Fernández, J.C. (2014) 'Signaling through C2 domains: More than one lipid target', *Biochimica et Biophysica Acta (BBA) - Biomembranes*, 1838(6), pp. 1536–1547. Available at: https://doi.org/10.1016/J.BBAMEM.2014.01.008.

Cordle, J., Johnson, S., *et al.* (2008) 'A Conserved Face of the Jagged/Serrate DSL Domain is Involved in Notch Trans-Activation and Cis-Inhibition', *Nature Structural & Molecular Biology*, pp. 849–857. Available at: https://doi.org/10.1038/nsmb.1457.

Cordle, J., Redfield, C., *et al.* (2008) 'Localization of the delta-like-1-binding site in human Notch-1 and its modulation by calcium affinity', *Journal of Biological Chemistry*, 283(17), pp. 11785–11793. Available at: https://doi.org/10.1074/jbc.M708424200.

De Celis, J.F. and Bray, S.J. (2000) 'The Abruptex domain of Notch regulates negative interactions between Notch, its ligands and Fringe', *Development*, 127(6), pp. 1291–1302. Available at: https://doi.org/10.1242/dev.127.6.1291.

De Celis, J.F. and Garcia-Bellido, A. (1994) 'Modifications of the Notch function by Abruptex mutations in Drosophila melanogaster', *Genetics*, 136(1), pp. 183–194.

De Strooper, B. *et al.* (1999) 'A presenilin-1-dependent γ-secretase-like protease mediates release of Notch intracellular domain', *Nature*, 398(6727), pp. 518–522. Available at: https://doi.org/10.1038/19083.

Debiec, R.M. *et al.* (2022) 'Contribution of NOTCH1 genetic variants to bicuspid aortic valve and other congenital lesions', *Heart*, 108(14), pp. 1114–1120. Available at: https://doi.org/10.1136/heartjnl-2021-320428.

Deblandre, G.A., Lai, E.C. and Kintner, C. (2001) 'Xenopus neuralized is a ubiquitin ligase that interacts with XDelta1 and regulates Notch signaling', *Developmental cell*, 1(6), pp. 795–806. Available at: https://doi.org/10.1016/s1534-5807(01)00091-0.

Del Amo, F.F. *et al.* (1992) 'Expression pattern of Motch, a mouse homolog of Drosophila Notch, suggests an important role in early postimplantation mouse development', *Development (Cambridge, England)*, 115(3), pp. 737–44. Available at: https://doi.org/10.1242/dev.115.3.737.

Dexter, J.S. (1914) 'The Analysis of a Case of Continuous Variation in Drosophila by a Study of Its Linkage Relations', *The American Naturalist*, 48(576), pp. 712–758. Available at: https://doi.org/10.1086/279446.

Di Ianni, M. *et al.* (2009) 'A new genetic lesion in B-CLL: a NOTCH1 PEST domain mutation.', *British journal of haematology*, 146(6), pp. 689–691. Available at: https://doi.org/10.1111/j.1365-2141.2009.07816.x.

Diederich, R.J. *et al.* (1994) 'Cytosolic interaction between deltex and Notch ankyrin repeats implicates deltex in the Notch signaling pathway', *Development (Cambridge, England)*, 120(3), pp. 473–481. Available at: https://doi.org/10.1242/DEV.120.3.473.

Dinchuk, J.E. *et al.* (2002) 'Absence of post-translational aspartyl β-hydroxylation of epidermal growth factor domains in mice leads to developmental defects and an increased incidence of intestinal neoplasia', *Journal of Biological Chemistry*, 277(15), pp. 12970–12977. Available at: https://doi.org/10.1074/jbc.M110389200.

Doherty, D. *et al.* (1996) 'Delta is a ventral to dorsal signal complementary to Serrate, another Notch ligand, in Drosophila wing formation', *Genes & Development*, 10(4), pp. 421–434. Available at: https://doi.org/10.1101/gad.10.4.421.

Dong, X. *et al.* (2015) 'Aspartate β-Hydroxylase expression promotes a malignant pancreatic cellular phenotype', *Oncotarget*, 6(2), pp. 1231–1248. Available at: https://doi.org/10.18632/oncotarget.2840.

Downing, A.K. *et al.* (1996) 'Solution structure of a pair of calcium-binding epidermal growth factor-like domains: implications for the Marfan syndrome and other genetic disorders.', *Cell*, 85(4), pp. 597–605. Available at: https://doi.org/10.1016/s0092-8674(00)81259-3.

D'Souza, B., Meloty-Kapella, L. and Weinmaster, G. (2010) 'Chapter Three - Canonical and Non-Canonical Notch Ligands', in R. Kopan (ed.) *Current Topics in Developmental Biology*. Academic Press (Notch Signaling), pp. 73–129. Available at: https://doi.org/10.1016/S0070-2153(10)92003-6.

D'souza, B., Miyamoto, A. and Weinmaster, G. (2008) 'The many facets of Notch ligands', *Oncogene* [Preprint]. Available at: https://doi.org/10.1038/onc.2008.229.

Durinck, S. *et al.* (2011) 'Temporal dissection of tumorigenesis in primary cancers.', *Cancer discovery*, 1(2), pp. 137–143. Available at: https://doi.org/10.1158/2159-8290.CD-11-0028.

Duvall, K. *et al.* (2022) 'Revisiting the role of Notch in nephron segmentation confirms a role for proximal fate selection during mouse and human nephrogenesis', *Development*, 149(10). Available at: https://doi.org/10.1242/dev.200446.

Eiraku, M. *et al.* (2002) 'Delta/Notch-like Epidermal Growth Factor (EGF)-related Receptor, a Novel EGF-like Repeat-containing Protein Targeted to Dendrites of Developing and Adult Central Nervous System Neurons*', *Journal of Biological Chemistry*, 277(28), pp. 25400–

25407. Available at: https://doi.org/10.1074/jbc.M110793200.

Eldadah, Z.A. *et al.* (2001) 'Familial Tetralogy of Fallot caused by mutation in the jagged1 gene', *Human Molecular Genetics*, 10(2), pp. 163–169.

Ellisen, L.W. *et al.* (1991) 'TAN-1, the human homolog of the Drosophila notch gene, is broken by chromosomal translocations in T lymphoblastic neoplasms', *Cell*, 66(4), pp. 649–61. Available at: https://doi.org/10.1016/0092-8674(91)90111-b.

Emsley, P. *et al.* (2010) 'Features and development of Coot', *Acta Crystallographica Section D: Biological Crystallography*, 66(Pt 4), pp. 486–501. Available at: https://doi.org/10.1107/S0907444910007493.

Falo-Sanjuan, J. *et al.* (2019) 'Enhancer Priming Enables Fast and Sustained Transcriptional Responses to Notch Signaling.', *Developmental cell*, 50(4), pp. 411-425.e8. Available at: https://doi.org/10.1016/j.devcel.2019.07.002.

Fehon, R.G. *et al.* (1990) 'Molecular interactions between the protein products of the neurogenic loci Notch and Delta, two EGF-homologous genes in Drosophila', *Cell*, 61(3), pp. 523–534. Available at: https://doi.org/10.1016/0092-8674(90)90534-l.

Feigin, L.A. and Svergun, D.I. (1987) *Structure Analysis by Small-Angle X-Ray and Neutron Scattering*. Edited by G.W. Taylor. Boston, MA: Springer US. Available at: https://doi.org/10.1007/978-1-4757-6624-0.

Fernandez-Valdivia, R. *et al.* (2011) 'Regulation of mammalian Notch signaling and embryonic development by the protein O-glucosyltransferase Rumi.', *Development (Cambridge, England)*, 138(10), pp. 1925–1934. Available at: https://doi.org/10.1242/dev.060020.

Fischer, A. and Gessler, M. (2003) 'Hey Genes in Cardiovascular Development', *Trends in Cardiovascular Medicine*, 13(6), pp. 221–226. Available at: https://doi.org/10.1016/S1050-1738(03)00082-3.

Fiuza, U.-M. *et al.* (2010) 'Mechanisms of ligand-mediated inhibition in Notch signaling activity in *Drosophila*', *Developmental Dynamics*, 239(3), pp. 798–805. Available at: https://doi.org/10.1002/dvdy.22207.

Fleming, R.J. *et al.* (1990) 'The gene Serrate encodes a putative EGF-like transmembrane protein essential for proper ectodermal development in Drosophila melanogaster.', *Genes & Development*, 4(12a), pp. 2188–2201. Available at: https://doi.org/10.1101/gad.4.12a.2188.

Fleming, R.J. *et al.* (2013) 'An extracellular region of Serrate is essential for ligand-induced cis-inhibition of Notch signaling', *Development (Cambridge, England)*, 140(9), pp. 2039–2049. Available at: https://doi.org/10.1242/DEV.087916.

Fleming, R.J. (2020) 'Ligand-Induced Cis-Inhibition of Notch Signaling: The Role of an

Extracellular Region of Serrate', in J. Reichrath and S. Reichrath (eds) *Notch Signaling in Embryology and Cancer: Molecular Biology of Notch Signaling*. Cham: Springer International Publishing (Advances in Experimental Medicine and Biology), pp. 29–49. Available at: https://doi.org/10.1007/978-3-030-36422-9_3.

Fleming, R.J., Gu, Y. and Hukriede, N.A. (1997) 'Serrate-mediated activation of Notch is specifically blocked by the product of the gene fringe in the dorsal compartment of the Drosophila wing imaginal disc', *Development*, 124(15), pp. 2973–2981. Available at: https://doi.org/10.1242/dev.124.15.2973.

FlySox « Russell Lab (no date). Available at: https://flypress.gen.cam.ac.uk/?page_id=21 (Accessed: 28 June 2021).

Foster, G.G. (1975) 'Negative complementation at the notch locus of Drosophila melanogaster', *Genetics*, 81(1), pp. 99–120. Available at: https://doi.org/10.1093/GENETICS/81.1.99.

Franke, D. *et al.* (2017) 'ATSAS 2.8: a comprehensive data analysis suite for small-angle scattering from macromolecular solutions', *Journal of Applied Crystallography*, 50(Pt 4), pp. 1212–1225. Available at: https://doi.org/10.1107/S1600576717007786.

Friedmann, D.R., Wilson, J.J. and Kovall, R.A. (2008) 'RAM-induced Allostery Facilitates Assembly of a Notch Pathway Active Transcription Complex', *The Journal of Biological Chemistry*, 283(21), p. 14781. Available at: https://doi.org/10.1074/jbc.M709501200.

Fryer, C.J., White, J.B. and Jones, K.A. (2004) 'Mastermind Recruits CycC:CDK8 to Phosphorylate the Notch ICD and Coordinate Activation with Turnover', *Molecular Cell*, 16(4), pp. 509–520. Available at: https://doi.org/10.1016/j.molcel.2004.10.014.

Fryxell, K.J., Soderlund, M. and Jordan, T.V. (2001) 'An animal model for the molecular genetics of CADASIL', *Stroke*, 32(1), pp. 6–11. Available at: https://doi.org/10.1161/01.STR.32.1.6.

Gao, J. *et al.* (2011) 'Up-regulated expression of Notch1 and Jagged1 in human colon adenocarcinoma', *Pathologie Biologie*, 59(6), pp. 298–302. Available at: https://doi.org/10.1016/J.PATBIO.2010.11.001.

Garg, V. *et al.* (2005) 'Mutations in NOTCH1 cause aortic valve disease', *Nature*, 437(7056), pp. 270–274. Available at: https://doi.org/10.1038/nature03940.

Gasteiger, E. *et al.* (2005) 'Protein Identification and Analysis Tools on the ExPASy Server', in J.M. Walker (ed.) *The Proteomics Protocols Handbook*. Totowa, NJ: Humana Press, pp. 571–607. Available at: https://doi.org/10.1385/1-59259-890-0:571.

Del Gaudio, F., Liu, D. and Lendahl, U. (2022) 'Notch signalling in healthy and diseased vasculature', *Open Biology*, 12(4). Available at: https://doi.org/10.1098/rsob.220004.

Geffers, I. *et al.* (2007) 'Divergent functions and distinct localization of the Notch ligands DLL1 and DLL3 in vivo', *J Cell Biol*, 178(3), pp. 465–76. Available at: https://doi.org/10.1083/jcb.200702009.

George, J. *et al.* (2015) 'Comprehensive genomic profiles of small cell lung cancer', *Nature*, 524(7563), p. 47. Available at: https://doi.org/10.1038/NATURE14664.

Gerhardt, D.M. *et al.* (2014) 'The Notch1 transcriptional activation domain is required for development and reveals a novel role for Notch1 signaling in fetal hematopoietic stem cells', *Genes & Development*, 28(6), pp. 576–593. Available at: https://doi.org/10.1101/gad.227496.113.

Glatter, O. and Kratky, O. (1982) *Small angle x-ray scattering*. London ; Academic Press.

Glittenberg, M. *et al.* (2006) 'Role of conserved intracellular motifs in Serrate signalling, cis-inhibition and endocytosis', *The EMBO Journal*, 25(20), p. 4697. Available at: https://doi.org/10.1038/SJ.EMBOJ.7601337.

Gomez-Lamarca, M.J. *et al.* (2018) 'Activation of the Notch Signaling Pathway In Vivo Elicits Changes in CSL Nuclear Dynamics', *Developmental Cell*, 44(5), pp. 611-623.e7. Available at: https://doi.org/10.1016/j.devcel.2018.01.020.

Gordon, W.R. *et al.* (2009) 'Structure of the Notch1-negative regulatory region: implications for normal activation and pathogenic signaling in T-ALL', *Blood*, 113(18), p. 4381. Available at: https://doi.org/10.1182/BLOOD-2008-08-174748.

Gordon, W.R. *et al.* (2015) 'Mechanical Allostery: Evidence for a Force Requirement in the Proteolytic Activation of Notch', *Developmental Cell*, 33(6), pp. 729–736. Available at: https://doi.org/10.1016/j.devcel.2015.05.004.

Gorman, M.J. and Girton, J.R. (1992) 'A genetic analysis of deltex and its interaction with the Notch locus in Drosophila melanogaster', *Genetics*, 131(1), pp. 99–112. Available at: https://doi.org/10.1093/GENETICS/131.1.99.

Gozlan, O. and Sprinzak, D. (2023) 'Notch signaling in development and homeostasis', *Development*, 150(4). Available at: https://doi.org/10.1242/dev.201138.

Guarnaccia, C. *et al.* (2009) 'The tetralogy of Fallot-associated G274D mutation impairs folding of the second epidermal growth factor repeat in Jagged-1', *FEBS Journal*, 276(21), pp. 6247–6257. Available at: https://doi.org/10.1111/j.1742-4658.2009.07333.x.

Gubina, E. *et al.* (1999) 'Assignment of DLK1 to human chromosome band 14q32 by in situ hybridization', *Cytogenetics and Cell Genetics*, 84(3–4), pp. 206–207. Available at: https://doi.org/10.1159/000015259.

Gundogan, F. *et al.* (2011) 'SiRNA inhibition of aspartyl-asparaginyl β-hydroxylase expression impairs cell motility, Notch signaling, and fetal growth', *Pathology Research and Practice*,

207(9). Available at: https://doi.org/10.1016/j.prp.2011.06.001.

Guo, D. *et al.* (2009) 'Down-regulation of Notch-1 increases co-cultured Jurkat cell sensitivity to chemotherapy', *https://doi.org/10.1080/10428190802553257*, 50(2), pp. 270–278. Available at: https://doi.org/10.1080/10428190802553257.

Guo, M., Jan, L.Y. and Jan, Y.N. (1996) 'Control of daughter cell fates during asymmetric division: Interaction of Numb and Notch', *Neuron* [Preprint]. Available at: https://doi.org/10.1016/S0896-6273(00)80278-0.

Guo, Z. and Ohlstein, B. (2015) 'Bidirectional Notch signaling regulates Drosophila intestinal stem cell multipotency', *Science*, 350(6263), p. aab0988. Available at: https://doi.org/10.1126/science.aab0988.

Gupta-Rossi, N. *et al.* (2004) 'Monoubiquitination and endocytosis direct γ-secretase cleavage of activated Notch receptor', *Journal of Cell Biology*, 166(1), pp. 73–83. Available at: https://doi.org/10.1083/jcb.200310098.

Hambleton, S. *et al.* (2004) 'Structural and functional properties of the human notch-1 ligand binding region.', *Structure (London, England : 1993)*, 12(12), pp. 2173–2183. Available at: https://doi.org/10.1016/j.str.2004.09.012.

Hammerman, P.S. *et al.* (2012) 'Comprehensive genomic characterization of squamous cell lung cancers', *Nature*, 489(7417), pp. 519–525. Available at: https://doi.org/10.1038/NATURE11404.

Handford, P. *et al.* (1995) 'The Calcium Binding Properties and Molecular Organization of Epidermal Growth Factor-like Domains in Human Fibrillin-1 (∗)', *Journal of Biological Chemistry*, 270(12), pp. 6751–6756. Available at: https://doi.org/10.1074/jbc.270.12.6751.

Handford, P.A. *et al.* (1990) 'The first EGF-like domain from human factor IX contains a high-affinity calcium binding site.', *The EMBO Journal*, 9(2), pp. 475–480.

Handford, P.A. *et al.* (1991) 'Key residues involved in calcium-binding motifs in EGF-like domains', *Nature*, 351(6322), pp. 164–167. Available at: https://doi.org/10.1038/351164a0.

Harvey, B.M. *et al.* (2016) 'Mapping Sites of O-Glycosylation and Fringe Elongation on Drosophila Notch.', *The Journal of biological chemistry*, 291(31), pp. 16348–16360. Available at: https://doi.org/10.1074/jbc.M116.732537.

Hassed, S. *et al.* (2017) 'Adams–Oliver syndrome review of the literature: Refining the diagnostic phenotype', *American Journal of Medical Genetics Part A*, 173(3), pp. 790–800. Available at: https://doi.org/10.1002/ajmg.a.37889.

Hassed, S.J. *et al.* (2012) 'RBPJ mutations identified in two families affected by Adams-Oliver syndrome.', *American journal of human genetics*, 91(2), pp. 391–395. Available at: https://doi.org/10.1016/j.ajhg.2012.07.005.

Heitzler, P. and Simpson, P. (1993) ‘Altered epidermal growth factor-like sequences provide evidence for a role of Notch as a receptor in cell fate decisions’, *Development*, 117(3), pp. 1113–1123. Available at: https://doi.org/10.1242/dev.117.3.1113.

Henrique, D. and Schweisguth, F. (2019) ‘Mechanisms of Notch signaling: a simple logic deployed in time and space’, *Development*, 146(3). Available at: https://doi.org/10.1242/dev.172148.

Hirano, K.-I. *et al.* (2020) ‘Delta-like 1 and Delta-like 4 differently require their extracellular domains for triggering Notch signaling in mice’, *Elife*, 9, p. e50979. Available at: https://doi.org/10.7554/eLife.50979.

Ho, A.S. *et al.* (2013) ‘The mutational landscape of adenoid cystic carcinoma’, *Nature Genetics 2013 45:7*, 45(7), pp. 791–798. Available at: https://doi.org/10.1038/ng.2643.

Holdener, B.C. and Haltiwanger, R.S. (2019) ‘Protein O-fucosylation: structure and function’, *Current Opinion in Structural Biology*, 56, pp. 78–86. Available at: https://doi.org/10.1016/J.SBI.2018.12.005.

Hori, K. *et al.* (2011) ‘Synergy between the ESCRT-III complex and Deltex defines a ligand-independent Notch signal’, *The Journal of cell biology*, 195(6), pp. 1005–1015. Available at: https://doi.org/10.1083/JCB.201104146.

Hu, N. and Zou, L. (2022) ‘Multiple functions of Hes genes in the proliferation and differentiation of neural stem cells’, *Annals of Anatomy - Anatomischer Anzeiger*, 239, p. 151848. Available at: https://doi.org/10.1016/j.aanat.2021.151848.

Ilagan, M.X.G. *et al.* (2011) ‘Real-time imaging of notch activation with a luciferase complementation-based reporter’, *Science signaling*, 4(181), pp. rs7–rs7. Available at: https://doi.org/10.1126/scisignal.2001656.

Irvine, K.D. and Wieschaus, E. (1994) ‘fringe, a Boundary-specific signaling molecule, mediates interactions between dorsal and ventral cells during Drosophila wing development.’, *Cell*, 79(4), pp. 595–606. Available at: https://doi.org/10.1016/0092-8674(94)90545-2.

Isidor, B. *et al.* (2011) ‘Truncating mutations in the last exon of NOTCH2 cause a rare skeletal disorder with osteoporosis’, *Nature Genetics*, 43(4), pp. 306–308. Available at: https://doi.org/10.1038/ng.778.

Iso, T., Kedes, L. and Hamamori, Y. (2003) ‘HES and HERP families: Multiple effectors of the notch signaling pathway’, *Journal of Cellular Physiology*, 194(3), pp. 237–255. Available at: https://doi.org/10.1002/jcp.10208.

Itoh, M. *et al.* (2003) ‘Mind bomb is a ubiquitin ligase that is essential for efficient activation of Notch signaling by Delta’, *Developmental cell*, 4(1), pp. 67–82. Available at: https://doi.org/10.1016/s1534-5807(02)00409-4.

Iwagami, K. *et al.* (2016) ‘Anti-Tumor Effects of Second Generation β-Hydroxylase Inhibitors on Cholangiocarcinoma Development and Progression’, *PLoS ONE*, 11(3). Available at: https://doi.org/10.1371/journal.pone.0150336.

Jafar-Nejad, H., Leonardi, J. and Fernandez-Valdivia, R. (2010) ‘Role of glycans and glycosyltransferases in the regulation of Notch signaling.’, *Glycobiology*, 20(8), pp. 931–949. Available at: https://doi.org/10.1093/glycob/cwq053.

Jensen, S.A. *et al.* (2005) ‘Ca2+-dependent Interface Formation in Fibrillin-1*’, *Journal of Biological Chemistry*, 280(14), pp. 14076–14084. Available at: https://doi.org/10.1074/jbc.M412832200.

Jensen, S.A. *et al.* (2015) ‘A microfibril assembly assay identifies different mechanisms of dominance underlying Marfan syndrome, stiff skin syndrome and acromelic dysplasias’, *Hum Mol Genet*, 24(15), pp. 4454–4463. Available at: https://doi.org/10.1093/hmg/ddv181.

Johnston, S.H. *et al.* (1997) ‘A family of mammalian Fringe genes implicated in boundary determination and the Notch pathway.’, *Development (Cambridge, England)*, 124(11), pp. 2245–2254. Available at: https://doi.org/10.1242/dev.124.11.2245.

Jones, H.C. and Keep, R.F. (1987) ‘The control of potassium concentration in the cerebrospinal fluid and brain interstitial fluid of developing rats.’, *The Journal of Physiology*, 383(1), pp. 441–453. Available at: https://doi.org/10.1113/jphysiol.1987.sp016419.

Joutel, A. *et al.* (1996) ‘Notch3 mutations in CADASIL, a hereditary adult-onset condition causing stroke and dementia’, *Nature*, 383(6602), pp. 707–10. Available at: https://doi.org/10.1038/383707a0.

Joutel, A. *et al.* (2000) ‘The ectodomain of the Notch3 receptor accumulates within the cerebrovasculature of CADASIL patients’, *Journal of Clinical Investigation*, 105(5), pp. 597–605. Available at: https://doi.org/10.1172/JCI8047.

Jubb, A.M. *et al.* (2012) ‘Expression of vascular Notch ligands Delta-like 4 and Jagged-1 in glioblastoma’, *Histopathology*, 60(5), pp. 740–747. Available at: https://doi.org/10.1111/J.1365-2559.2011.04138.X.

Jumper, J. *et al.* (2021) ‘Highly accurate protein structure prediction with AlphaFold’, *Nature*, 596(7873), pp. 583–589. Available at: https://doi.org/10.1038/s41586-021-03819-2.

Kakuda, S. *et al.* (2020) ‘Canonical Notch ligands and Fringes have distinct effects on NOTCH1 and NOTCH2’, *The Journal of Biological Chemistry*, 295(43), pp. 14710–14722. Available at: https://doi.org/10.1074/jbc.RA120.014407.

Kakuda, S. and Haltiwanger, R.S. (2017) ‘Deciphering the Fringe-Mediated Notch Code: Identification of Activating and Inhibiting Sites Allowing Discrimination between Ligands.’, *Developmental cell*, 40(2), pp. 193–201. Available at: https://doi.org/10.1016/j.devcel.2016.12.013.

Kang, K. *et al.* (2012) 'The E3 Ligase Mind Bomb-1 (Mib1) Modulates Delta-Notch Signaling to Control Neurogenesis and Gliogenesis in the Developing Spinal Cord *'. Available at: https://doi.org/10.1074/jbc.M112.398263.

Kelley, M.R. *et al.* (1987) 'Mutations altering the structure of epidermal growth factor-like coding sequences at the Drosophila Notch locus', *Cell*, 51(4), pp. 539–548. Available at: https://doi.org/10.1016/0092-8674(87)90123-1.

Kelly, D.F. *et al.* (2010) 'Molecular Structure and Dimeric Organization of the Notch Extracellular Domain as Revealed by Electron Microscopy', *PLOS ONE*, 5(5), p. e10532. Available at: https://doi.org/10.1371/journal.pone.0010532.

Kershaw, N.J. *et al.* (2015) 'Notch ligand delta-like1: X-ray crystal structure and binding affinity.', *The Biochemical journal*, 468(1), pp. 159–166. Available at: https://doi.org/10.1042/BJ20150010.

Kiel, M.J. *et al.* (2012) 'Whole-genome sequencing identifies recurrent somatic NOTCH2 mutations in splenic marginal zone lymphoma', *The Journal of Experimental Medicine*, 209(9), p. 1553. Available at: https://doi.org/10.1084/JEM.20120910.

Kiernan, A.E. (2013) 'Notch signaling during cell fate determination in the inner ear', *Seminars in Cell & Developmental Biology*, 24(5), pp. 470–479. Available at: https://doi.org/10.1016/j.semcdb.2013.04.002.

Kikhney, A.G. and Svergun, D.I. (2015) 'A practical guide to small angle X-ray scattering (SAXS) of flexible and intrinsically disordered proteins', *FEBS Letters*, 589(19PartA), pp. 2570–2577. Available at: https://doi.org/10.1016/j.febslet.2015.08.027.

Kim, E.J. *et al.* (2015) 'Epidermal growth factor receptor variant III renders glioma cancer cells less differentiated by JAGGED1', *Tumor Biology*, 36(4), pp. 2921–2928. Available at: https://doi.org/10.1007/S13277-014-2922-9/FIGURES/4.

Kim, J., Irvine, K.D. and Carroll, S.B. (1995) 'Cell recognition, signal induction, and symmetrical gene activation at the dorsal-ventral boundary of the developing drosophila wing', *Cell* [Preprint]. Available at: https://doi.org/10.1016/0092-8674(95)90476-X.

Klein, T. and Arias, A.M. (1998) 'Interactions among Delta, Serrate and Fringe modulate Notch activity during Drosophila wing development', *Development (Cambridge, England)*, 125(15), pp. 2951–2962. Available at: https://doi.org/10.1242/dev.125.15.2951.

Klein, T., Brennan, K. and Arias, A.M. (1997) 'An intrinsic dominant negative activity of serrate that is modulated during wing development in Drosophila.', *Developmental biology*, 189(1), pp. 123–134. Available at: https://doi.org/10.1006/dbio.1997.8564.

Klinakis, A. *et al.* (2011) 'A novel tumour-suppressor function for the Notch pathway in myeloid leukaemia.', *Nature*, 473(7346), pp. 230–233. Available at: https://doi.org/10.1038/nature09999.

Klueg, K.M. and Muskavitch, M.A.T. (1999) ‘Ligand-receptor interactions and trans-endocytosis of Delta, Serrate and Notch: members of the Notch signalling pathway in Drosophila’, *Journal of cell science*, 112 (Pt 1(19), pp. 3289–3297. Available at: https://doi.org/10.1242/JCS.112.19.3289.

Klussmann, S. (2006) *The Aptamer Handbook: Functional Oligonucleotides and Their Applications*. John Wiley & Sons.

Kobia, F.M. *et al.* (2020) ‘Notch dimerization and gene dosage are important for normal heart development, intestinal stem cell maintenance, and splenic marginal zone B-cell homeostasis during mite infestation’, *PLOS Biology*. Edited by B.-K. Koo, 18(10), p. e3000850. Available at: https://doi.org/10.1371/journal.pbio.3000850.

Kohsaka, T. *et al.* (2002) ‘The significance of human jagged 1 mutations detected in severe cases of extrahepatic biliary atresia’, *Hepatology*, 36(4), pp. 904–912. Available at: https://doi.org/10.1053/jhep.2002.35820.

Komatsu, H. *et al.* (2008) ‘OSM-11 Facilitates LIN-12 Notch Signaling during Caenorhabditis elegans Vulval Development’, *PLoS Biology*, 6(8), p. e196. Available at: https://doi.org/10.1371/journal.pbio.0060196.

Kopan, R. and Ilagan, M.X.G. (2009) ‘The Canonical Notch Signaling Pathway: Unfolding the Activation Mechanism’, *Cell*, 137(2), pp. 216–233. Available at: https://doi.org/10.1016/j.cell.2009.03.045.

Korioth, F., Gieffers, C. and Frey, J. (1994) ‘Cloning and characterization of the human gene encoding aspartyl beta-hydroxylase’, *Gene*, 150(2), pp. 395–399. Available at: https://doi.org/10.1016/0378-1119(94)90460-x.

Kridel, R. *et al.* (2012) ‘Whole transcriptome sequencing reveals recurrent NOTCH1 mutations in mantle cell lymphoma.’, *Blood*, 119(9), pp. 1963–1971. Available at: https://doi.org/10.1182/blood-2011-11-391474.

Kuintzle, R., Santat, L.A. and Elowitz, M.B. (2023) ‘Diversity in Notch ligand-receptor signaling interactions’, *eLife*, 12. Available at: https://doi.org/10.7554/eLife.91422.1.

Ladi, E. *et al.* (2005) ‘The divergent DSL ligand Dll3 does not activate Notch signaling but cell autonomously attenuates signaling induced by other DSL ligands’, *J Cell Biol*, 170(6), pp. 983–92. Available at: https://doi.org/10.1083/jcb.200503113.

Lai, E.C. *et al.* (2005) ‘The ubiquitin ligase Drosophila Mind bomb promotes Notch signaling by regulating the localization and activity of Serrate and Delta’, *Development (Cambridge, England)*, 132(10), pp. 2319–32. Available at: https://doi.org/10.1242/dev.01825.

Le Borgne, R. (2005) ‘The roles of receptor and ligand endocytosis in regulating Notch signaling’, *Development*, 132(8), pp. 1751–1762. Available at: https://doi.org/10.1242/dev.01789.

LeBon, L. *et al.* (2014) ‘Fringe proteins modulate Notch-ligand cis and trans interactions to specify signaling states.’, *eLife*, 3, p. e02950. Available at: https://doi.org/10.7554/eLife.02950.

Lee, S.S.J. *et al.* (2004) ‘Structure of the integrin binding fragment from fibrillin-1 gives new insights into microfibril organization.’, *Structure (London, England : 1993)*, 12(4), pp. 717–729. Available at: https://doi.org/10.1016/j.str.2004.02.023.

Lee, T.V. *et al.* (2013) ‘Negative Regulation of Notch Signaling by Xylose’, *PLoS Genetics*, 9(6), p. e1003547. Available at: https://doi.org/10.1371/journal.pgen.1003547.

Lehmann, R. *et al.* (1983) *On the Phenotype and Development of Mutants of Early Neurogenesis in Drosophila melanogaster*, pp. 62–74. Available at: https://link.springer.com/content/pdf/10.1007%2FBF00848482.pdf.

Leonardi, J. *et al.* (2011) ‘Multiple O-glucosylation sites on Notch function as a buffer against temperature-dependent loss of signaling.’, *Development (Cambridge, England)*, 138(16), pp. 3569–3578. Available at: https://doi.org/10.1242/dev.068361.

Li, M. *et al.* (2013) ‘Mutations in POFUT1, encoding protein O-fucosyltransferase 1, cause generalized Dowling-Degos disease.’, *American journal of human genetics*, 92(6), pp. 895–903. Available at: https://doi.org/10.1016/j.ajhg.2013.04.022.

Lieber, T. *et al.* (1992) ‘Single amino acid substitutions in EGF-like elements of notch and delta modify drosophila development and affect cell adhesion in vitro’, *Neuron*, 9(5), pp. 847–859. Available at: https://doi.org/10.1016/0896-6273(92)90238-9.

Lin, Q. *et al.* (2019) ‘ASPH-notch Axis guided Exosomal delivery of Prometastatic Secretome renders breast Cancer multi-organ metastasis’, *Molecular Cancer*, 18(1). Available at: https://doi.org/10.1186/s12943-019-1077-0.

Lloyd-Evans, E. and Waller-Evans, H. (2020) ‘Lysosomal Ca2+ Homeostasis and Signaling in Health and Disease’, *Cold Spring Harbor Perspectives in Biology*, 12(6), p. a035311. Available at: https://doi.org/10.1101/cshperspect.a035311.

Logeat, F. *et al.* (1998) ‘The Notch1 receptor is cleaved constitutively by a furin-like convertase’, *Proceedings of the National Academy of Sciences of the United States of America*, 95(14), pp. 8108–8112. Available at: https://doi.org/10.1073/PNAS.95.14.8108/ASSET/009C6B77-98CE-4BE0-BC51-0E6FB5E43A39/ASSETS/GRAPHIC/PQ1481625005.JPEG.

Logeay, R. *et al.* (2022) ‘Mechanisms underlying the cooperation between loss of epithelial polarity and Notch signaling during neoplastic growth in *Drosophila*’, *Development*, 149(3). Available at: https://doi.org/10.1242/dev.200110.

Lowenthal, M.S. *et al.* (2016) ‘Identification of novel N-glycosylation sites at non-canonical protein consensus motifs’, *Journal of proteome research*, 15(7), pp. 2087–2101. Available at:

https://doi.org/10.1021/acs.jproteome.5b00733.

Lubman, O.Y. *et al.* (2007) 'Quantitative Dissection of the Notch:CSL Interaction: Insights into the Notch Transcriptional Switch', *Journal of molecular biology*, 365(3), pp. 577–589. Available at: https://doi.org/10.1016/j.jmb.2006.09.071.

Luca, V.C. *et al.* (2015) 'Structural basis for Notch1 engagement of Delta-like 4', *Science*, 347(6224), pp. 847–853. Available at: https://doi.org/10.1126/science.1261093.

Luca, V.C. *et al.* (2017) 'Notch-Jagged complex structure implicates a catch bond in tuning ligand sensitivity', *Science*, 355(6331), pp. 1320–1324. Available at: https://doi.org/10.1126/science.aaf9739.

Ma, W. *et al.* (2011) 'hCLP46 regulates U937 cell proliferation via Notch signaling pathway.', *Biochemical and biophysical research communications*, 408(1), pp. 84–88. Available at: https://doi.org/10.1016/j.bbrc.2011.03.124.

Madeira, F. *et al.* (2022) 'Search and sequence analysis tools services from EMBL-EBI in 2022', *Nucleic acids research*, 50(W1), pp. W276–W279. Available at: https://doi.org/10.1093/nar/gkac240.

Manalastas-Cantos, K. *et al.* (2021) 'ATSAS 3.0: expanded functionality and new tools for small-angle scattering data analysis', *Journal of Applied Crystallography*, 54(Pt 1), pp. 343–355. Available at: https://doi.org/10.1107/S1600576720013412.

Martin, B.R. *et al.* (2005) 'Mammalian cell–based optimization of the biarsenical-binding tetracysteine motif for improved fluorescence and affinity', *Nature Biotechnology*, 23(10), pp. 1308–1314. Available at: https://doi.org/10.1038/nbt1136.

Martincorena, I. *et al.* (2018) 'Somatic mutant clones colonize the human esophagus with age.', *Science (New York, N.Y.)*, 362(6417), pp. 911–917. Available at: https://doi.org/10.1126/science.aau3879.

Masiero, M. *et al.* (2019) 'Development of Therapeutic Anti-JAGGED1 Antibodies for Cancer Therapy', *Molecular cancer therapeutics*, 18(11), pp. 2030–2042. Available at: https://doi.org/10.1158/1535-7163.MCT-18-1176.

Matsumoto, K. *et al.* (2016) 'Dual Roles of O-Glucose Glycans Redundant with Monosaccharide O-Fucose on Notch in Notch Trafficking', *The Journal of Biological Chemistry*, 291(26), pp. 13743–13752. Available at: https://doi.org/10.1074/jbc.M115.710483.

Matsumoto, K., Luther, K.B. and Haltiwanger, R.S. (2021) 'Diseases related to Notch glycosylation', *Molecular Aspects of Medicine*, 79, p. 100938. Available at: https://doi.org/10.1016/J.MAM.2020.100938.

Matsuura, A. *et al.* (2008) 'O-linked N-acetylglucosamine is present on the extracellular domain of notch receptors.', *The Journal of biological chemistry*, 283(51), pp. 35486–35495.

Available at: https://doi.org/10.1074/jbc.M806202200.

Meester, J.A. *et al.* (2015) 'Heterozygous Loss-of-Function Mutations in DLL4 Cause Adams-Oliver Syndrome', *American journal of human genetics*, 97(3), pp. 475–82. Available at: https://doi.org/10.1016/j.ajhg.2015.07.015.

Meloty-Kapella, L. *et al.* (2012) 'Notch Ligand Endocytosis Generates Mechanical Pulling Force Dependent on Dynamin, Epsins and Actin', *Developmental Cell*, 22(6), p. 1299. Available at: https://doi.org/10.1016/J.DEVCEL.2012.04.005.

Meng, Y. *et al.* (2022) 'An N-glycan on the C2 domain of JAGGED1 is important for Notch activation.', *Science signaling*, 15(755), p. eabo3507. Available at: https://doi.org/10.1126/scisignal.abo3507.

Meng, Y. *et al.* (2023) 'The Notch Signaling Pathway: Mechanistic Insights in Health and Disease', *Engineering* [Preprint]. Available at: https://doi.org/10.1016/j.eng.2023.11.011.

Micchelli, C.A. and Blair, S.S. (1999) 'Dorsoventral lineage restriction in wing imaginal discs requires Notch', *Nature*, 401(6752), pp. 473–476. Available at: https://doi.org/10.1038/46779.

Micchelli, C.A., Rulifson, E.J. and Blair, S.S. (1997) 'The function and regulation of cut expression on the wing margin of Drosophila: Notch, Wingless and a dominant negative role for Delta and Serrate.', *Development (Cambridge, England)*, 124(8), pp. 1485–1495. Available at: https://doi.org/10.1242/dev.124.8.1485.

Miller, A.C., Lyons, E.L. and Herman, T.G. (2009) 'cis-Inhibition of Notch by endogenous Delta biases the outcome of lateral inhibition.', *Current biology : CB*, 19(16), pp. 1378–1383. Available at: https://doi.org/10.1016/j.cub.2009.06.042.

Mohamed, S.A. *et al.* (2006) 'Novel missense mutations (p.T596M and p.P1797H) in NOTCH1 in patients with bicuspid aortic valve', *Biochemical and Biophysical Research Communications*, 345(4), pp. 1460–1465. Available at: https://doi.org/10.1016/J.BBRC.2006.05.046.

Moloney, D.J., Panin, V.M., *et al.* (2000) 'Fringe is a glycosyltransferase that modifies Notch.', *Nature*, 406(6794), pp. 369–375. Available at: https://doi.org/10.1038/35019000.

Moloney, D.J., Shair, L.H., *et al.* (2000) 'Mammalian Notch1 is modified with two unusual forms of O-linked glycosylation found on epidermal growth factor-like modules', *The Journal of Biological Chemistry*, 275(13), pp. 9604–9611. Available at: https://doi.org/10.1074/jbc.275.13.9604.

Morgan, T.H. (1917) 'The Theory of the Gene', *The American Naturalist*, 51(609), pp. 513–544.

Morgan, W.D. *et al.* (1999) 'Solution structure of an EGF module pair from the *Plasmodium falciparum* merozoite surface protein 11', *Journal of Molecular Biology*, 289(1), pp. 113–122.

Available at: https://doi.org/10.1006/jmbi.1999.2753.

Mosquera, J.-M. *et al.* (2013) 'Novel MIR143-NOTCH fusions in benign and malignant glomus tumors.', *Genes, chromosomes & cancer*, 52(11), pp. 1075–1087. Available at: https://doi.org/10.1002/gcc.22102.

Müller, J. *et al.* (2014) 'O-fucosylation of the Notch Ligand mDLL1 by POFUT1 Is Dispensable for Ligand Function', *PLoS ONE*. Edited by T. Brand, 9(2), p. e88571. Available at: https://doi.org/10.1371/journal.pone.0088571.

Müller, R., Jenny, A. and Stanley, P. (2013) 'The EGF repeat-specific O-GlcNAc-transferase Eogt interacts with notch signaling and pyrimidine metabolism pathways in Drosophila.', *PloS one*, 8(5), p. e62835. Available at: https://doi.org/10.1371/journal.pone.0062835.

Muraki, M. *et al.* (1996) 'Origin of Carbohydrate Recognition Specificity of Human Lysozyme Revealed by Affinity Labeling', *Biochemistry*, 35(42), pp. 13562–13567. Available at: https://doi.org/10.1021/bi9613180.

Nam, Y. *et al.* (2006) 'Structural basis for cooperativity in recruitment of MAML coactivators to Notch transcription complexes.', *Cell*, 124(5), pp. 973–83. Available at: https://doi.org/10.1016/j.cell.2005.12.037.

Nandagopal, N., Santat, L.A. and Elowitz, M.B. (2019) 'Cis-activation in the Notch signaling pathway', *eLife*, 8. Available at: https://doi.org/10.7554/eLife.37880.

Nasarenko, J. (1930) 'Ein Fall wahrscheinlicher Verdoppelung eines Chromosomsttlckes bei Drosophila melanogaster', *Biology Zentr* [Preprint]. Available at: https://scholar.google.com/scholar_lookup?journal=Biol+Zentr&title=Ein+Fall+wahrscheinlicher+Verdoppelung+eines+Chromosomsttlckes+bei+Drosophila+melanogaster&author=JJ+Nasarenko&volume=50&publication_year=1930&pages=385-392& (Accessed: 28 June 2021).

Neumann, M. *et al.* (2013) 'Whole-exome sequencing in adult ETP-ALL reveals a high rate of DNMT3A mutations.', *Blood*, 121(23), pp. 4749–4752. Available at: https://doi.org/10.1182/blood-2012-11-465138.

Nichols, J.T. *et al.* (2007) 'DSL ligand endocytosis physically dissociates Notch1 heterodimers before activating proteolysis can occur', *The Journal of cell biology*, 176(4), pp. 445–458. Available at: https://doi.org/10.1083/JCB.200609014.

Nurmahdi, H. *et al.* (2022) 'Notch Missense Mutations in Drosophila Reveal Functions of Specific EGF-like Repeats in Notch Folding, Trafficking, and Signaling', *Biomolecules 2022, Vol. 12, Page 1752*, 12(12), p. 1752. Available at: https://doi.org/10.3390/BIOM12121752.

Ogawa, K. *et al.* (2020) 'Prometastatic secretome trafficking via exosomes initiates pancreatic cancer pulmonary metastasis', *Cancer Letters*, 481, pp. 63–75. Available at: https://doi.org/10.1016/j.canlet.2020.02.039.

Ogawa, M. *et al.* (2018) 'Structural Divergence in O-GlcNAc Glycans Displayed on Epidermal Growth Factor-like Repeats of Mammalian Notch1.', *Molecules (Basel, Switzerland)*, 23(7). Available at: https://doi.org/10.3390/molecules23071745.

Ogawa, M. and Okajima, T. (2019) 'Structure and function of extracellular O-GlcNAc.', *Current opinion in structural biology*, 56, pp. 72–77. Available at: https://doi.org/10.1016/j.sbi.2018.12.002.

Ohlin, A.K. *et al.* (1988) 'Beta-hydroxyaspartic acid in the first epidermal growth factor-like domain of protein C. Its role in Ca2+ binding and biological activity.', *Journal of Biological Chemistry*, 263(35), pp. 19240–19248. Available at: https://doi.org/10.1016/S0021-9258(18)37415-5.

Okajima, T. *et al.* (2008) 'Contributions of chaperone and glycosyltransferase activities of O-fucosyltransferase 1 to Notch signaling', *BMC biology*, 6. Available at: https://doi.org/10.1186/1741-7007-6-1.

Okajima, T. and Irvine, K.D. (2002) 'Regulation of notch signaling by o-linked fucose.', *Cell*, 111(6), pp. 893–904. Available at: https://doi.org/10.1016/s0092-8674(02)01114-5.

Okamura, Y. and Saga, Y. (2008) 'Pofut1 is required for the proper localization of the Notch receptor during mouse development.', *Mechanisms of development*, 125(8), pp. 663–673. Available at: https://doi.org/10.1016/j.mod.2008.04.007.

O'Neil, J. *et al.* (2007) 'FBW7 mutations in leukemic cells mediate NOTCH pathway activation and resistance to γ-secretase inhibitors', *The Journal of Experimental Medicine*, 204(8), pp. 1813–1824. Available at: https://doi.org/10.1084/jem.20070876.

Opherk, C. *et al.* (2009) 'CADASIL mutations enhance spontaneous multimerization of NOTCH3', *Hum. Mol. Genet.*, 18(15), pp. 2761–2767. Available at: https://doi.org/10.1093/hmg/ddp211.

Oswald, F. *et al.* (2002) 'SHARP is a novel component of the Notch/RBP-Jκ signalling pathway', *The EMBO Journal*, 21(20), pp. 5417–5426. Available at: https://doi.org/10.1093/emboj/cdf549.

Oswald, F. and Kovall, R.A. (2018) 'CSL-Associated Corepressor and Coactivator Complexes.', *Advances in experimental medicine and biology*, 1066, pp. 279–295. Available at: https://doi.org/10.1007/978-3-319-89512-3_14.

Pancewicz, J. *et al.* (2010) 'Notch signaling contributes to proliferation and tumor formation of human T-cell leukemia virus type 1-associated adult T-cell leukemia.', *Proceedings of the National Academy of Sciences of the United States of America*, 107(38), pp. 16619–16624. Available at: https://doi.org/10.1073/pnas.1010722107.

Pandey, A. *et al.* (2019) 'Glycosylation of Specific Notch EGF Repeats by O-Fut1 and Fringe Regulates Notch Signaling in Drosophila', *Cell Rep*, 29(7), pp. 2054-2066.e6. Available at:

https://doi.org/10.1016/j.celrep.2019.10.027.

Pandey, A., Niknejad, N. and Jafar-Nejad, H. (2021) 'Multifaceted regulation of Notch signaling by glycosylation', *Glycobiology*, 31(1), pp. 8–28. Available at: https://doi.org/10.1093/glycob/cwaa049.

Panin, V.M. *et al.* (1997) 'Fringe modulates Notch-ligand interactions.', *Nature*, 387(6636), pp. 908–912. Available at: https://doi.org/10.1038/43191.

Panin, V.M. *et al.* (2002) 'Notch ligands are substrates for protein O-fucosyltransferase-1 and Fringe.', *The Journal of biological chemistry*, 277(33), pp. 29945–29952. Available at: https://doi.org/10.1074/jbc.M204445200.

Panjkovich, A. and Svergun, D.I. (2016) 'Deciphering conformational transitions of proteins by small angle X-ray scattering and normal mode analysis', *Physical Chemistry Chemical Physics*, 18(8), pp. 5707–5719. Available at: https://doi.org/10.1039/C5CP04540A.

Papayannopoulos, V. *et al.* (1998) 'Dorsal-ventral signaling in the Drosophila eye.', *Science (New York, N.Y.)*, 281(5385), pp. 2031–4. Available at: https://doi.org/10.1126/science.281.5385.2031.

Parks, A.L. *et al.* (2000) 'Ligand endocytosis drives receptor dissociation and activation in the Notch pathway', *Development (Cambridge, England)*, 127(7), pp. 1373–1385. Available at: https://doi.org/10.1242/DEV.127.7.1373.

Pei, Z. and Baker, N.E. (2008) 'Competition between Delta and the Abruptex domain of Notch', *BMC Developmental Biology*, 8. Available at: https://doi.org/10.1186/1471-213X-8-4.

Pennarubia, F. *et al.* (2022) 'Cancer-associated Notch receptor variants lead to O-fucosylation defects that deregulate Notch signaling', *The Journal of biological chemistry*, 298(12). Available at: https://doi.org/10.1016/J.JBC.2022.102616.

Perdigoto, C.N., Schweisguth, F. and Bardin, A.J. (2011) 'Distinct levels of Notch activity for commitment and terminal differentiation of stem cells in the adult fly intestine.', *Development (Cambridge, England)*, 138(21), pp. 4585–4595. Available at: https://doi.org/10.1242/dev.065292.

Pérez, L. *et al.* (2005) 'Ligand-binding and signaling properties of the Ax[M1] form of Notch', *Mechanisms of Development*, 122(4), pp. 479–486. Available at: https://doi.org/10.1016/j.mod.2004.12.007.

Pfeffer, I. *et al.* (2019) 'Aspartate/asparagine-β-hydroxylase crystal structures reveal an unexpected epidermal growth factor-like domain substrate disulfide pattern', *Nature Communications*, 10(1), p. 4910. Available at: https://doi.org/10.1038/s41467-019-12711-7.

Pinton, P., Pozzan, T. and Rizzuto, R. (1998) 'The Golgi apparatus is an inositol 1,4,5-trisphosphate-sensitive Ca2+ store, with functional properties distinct from those of the

endoplasmic reticulum', *The EMBO Journal*, 17(18), pp. 5298–5308. Available at: https://doi.org/10.1093/emboj/17.18.5298.

Porcheri, C. *et al.* (2020) 'Notch ligand Dll4 impairs cell recruitment to aortic clusters and limits blood stem cell generation', *The EMBO Journal*, 39(8), p. e104270. Available at: https://doi.org/10.15252/embj.2019104270.

Portin, P. (1975) 'Allelic negative complementation at the Abruptex locus of Drosophila melanogaster', *Genetics*, 81(1), pp. 121–133. Available at: https://doi.org/10.1093/genetics/81.1.121.

Preuße, K. *et al.* (2015) 'Context-Dependent Functional Divergence of the Notch Ligands DLL1 and DLL4 In Vivo', *PLoS Genetics*, 11(6), p. e1005328. Available at: https://doi.org/10.1371/journal.pgen.1005328.

Puente, X.S. *et al.* (2011) 'Whole-genome sequencing identifies recurrent mutations in chronic lymphocytic leukaemia.', *Nature*, 475(7354), pp. 101–105. Available at: https://doi.org/10.1038/nature10113.

Puente, X.S. *et al.* (2015) 'Non-coding recurrent mutations in chronic lymphocytic leukaemia.', *Nature*, 526(7574), pp. 519–524. Available at: https://doi.org/10.1038/nature14666.

Raffaello, A. *et al.* (2016) 'Calcium at the center of cell signaling: interplay between endoplasmic reticulum, mitochondria and lysosomes', *Trends in biochemical sciences*, 41(12), pp. 1035–1049. Available at: https://doi.org/10.1016/j.tibs.2016.09.001.

Ramkumar, N. *et al.* (2015) 'Protein O-Glucosyltransferase 1 (POGLUT1) Promotes Mouse Gastrulation through Modification of the Apical Polarity Protein CRUMBS2.', *PLoS genetics*, 11(10), p. e1005551. Available at: https://doi.org/10.1371/journal.pgen.1005551.

Rampal, R. *et al.* (2005) 'Lunatic fringe, manic fringe, and radical fringe recognize similar specificity determinants in O-fucosylated epidermal growth factor-like repeats.', *The Journal of biological chemistry*, 280(51), pp. 42454–42463. Available at: https://doi.org/10.1074/jbc.M509552200.

Rampias, T. *et al.* (2014) 'A new tumor suppressor role for the Notch pathway in bladder cancer', *Nature Medicine 2014 20:10*, 20(10), pp. 1199–1205. Available at: https://doi.org/10.1038/nm.3678.

Rand, M.D. *et al.* (2000) 'Calcium depletion dissociates and activates heterodimeric notch receptors', *Molecular and cellular biology*, 20(5), pp. 1825–1835. Available at: https://doi.org/10.1128/MCB.20.5.1825-1835.2000.

Rao, Z. *et al.* (1995) 'The structure of a Ca(2+)-binding epidermal growth factor-like domain: its role in protein-protein interactions.', *Cell*, 82(1), pp. 131–41. Available at: https://doi.org/10.1016/0092-8674(95)90059-4.

Rebay, I. *et al.* (1991) 'Specific EGF repeats of Notch mediate interactions with Delta and serrate: Implications for notch as a multifunctional receptor', *Cell* [Preprint]. Available at: https://doi.org/10.1016/0092-8674(91)90064-6.

Reedijk, M. *et al.* (2005) 'High-level Coexpression of JAG1 and NOTCH1 Is Observed in Human Breast Cancer and Is Associated with Poor Overall Survival', *Cancer Research*, 65(18), pp. 8530–8537. Available at: https://doi.org/10.1158/0008-5472.CAN-05-1069.

Robinson, D.R. *et al.* (2011) 'Functionally recurrent rearrangements of the MAST kinase and Notch gene families in breast cancer.', *Nature medicine*, 17(12), pp. 1646–1651. Available at: https://doi.org/10.1038/nm.2580.

Rossi, D. *et al.* (2012) 'The coding genome of splenic marginal zone lymphoma: activation of NOTCH2 and other pathways regulating marginal zone development.', *The Journal of experimental medicine*, 209(9), pp. 1537–1551. Available at: https://doi.org/10.1084/jem.20120904.

Sakaidani, Y. *et al.* (2011) 'O-linked-N-acetylglucosamine on extracellular protein domains mediates epithelial cell-matrix interactions.', *Nature communications*, 2, p. 583. Available at: https://doi.org/10.1038/ncomms1591.

Sakaidani, Y. *et al.* (2012) 'O-linked-N-acetylglucosamine modification of mammalian Notch receptors by an atypical O-GlcNAc transferase Eogt1.', *Biochemical and biophysical research communications*, 419(1), pp. 14–19. Available at: https://doi.org/10.1016/j.bbrc.2012.01.098.

Sakamoto, K. *et al.* (2002) 'Intracellular cell-autonomous association of Notch and its ligands: A novel mechanism of Notch signal modification', *Developmental Biology* [Preprint]. Available at: https://doi.org/10.1006/dbio.2001.0517.

Sanchez-Irizarry, C. *et al.* (2004) 'Notch Subunit Heterodimerization and Prevention of Ligand-Independent Proteolytic Activation Depend, Respectively, on a Novel Domain and the LNR Repeats', *Molecular and Cellular Biology*, 24(21), pp. 9265–9273. Available at: https://doi.org/10.1128/mcb.24.21.9265-9273.2004.

Santagata, S. *et al.* (2004) 'JAGGED1 expression is associated with prostate cancer metastasis and recurrence', *Cancer research*, 64(19), pp. 6854–6857. Available at: https://doi.org/10.1158/0008-5472.CAN-04-2500.

Sawaguchi, S. *et al.* (2017) 'O-GlcNAc on NOTCH1 EGF repeats regulates ligand-induced Notch signaling and vascular development in mammals', *eLife*, 6. Available at: https://doi.org/10.7554/ELIFE.24419.

Sawangarun, W. *et al.* (2018) 'Loss of Notch1 predisposes oro-esophageal epithelium to tumorigenesis', *Experimental cell research*, 372(2), pp. 129–140. Available at: https://doi.org/10.1016/J.YEXCR.2018.09.019.

Schneider, M. *et al.* (2013) 'Activation of Notch in lgd mutant cells requires the fusion of late endosomes with the lysosome', *Journal of cell science*, 126(Pt 2), pp. 645–656. Available at: https://doi.org/10.1242/JCS.116590.

Schneidman-Duhovny, D. *et al.* (2013) 'Accurate SAXS Profile Computation and its Assessment by Contrast Variation Experiments', *Biophysical Journal*, 105(4), pp. 962–974. Available at: https://doi.org/10.1016/j.bpj.2013.07.020.

Schneidman-Duhovny, D. *et al.* (2016) 'FoXS, FoXSDock and MultiFoXS: Single-state and multi-state structural modeling of proteins and their complexes based on SAXS profiles', *Nucleic Acids Research*, 44(W1), pp. W424–W429. Available at: https://doi.org/10.1093/nar/gkw389.

Schroeter, E.H., Kisslinger, J.A. and Kopan, R. (1998) 'Notch-1 signalling requires ligand-induced proteolytic release of intracellular domain', *Nature*, 393(6683), pp. 382–386. Available at: https://doi.org/10.1038/30756.

Serth, K. *et al.* (2015) 'O-Fucosylation of DLL3 Is Required for Its Function during Somitogenesis', *PLOS ONE*. Edited by D. Henrique, 10(4), p. e0123776. Available at: https://doi.org/10.1371/journal.pone.0123776.

Servián-Morilla, E. *et al.* (2016) 'A POGLUT1 mutation causes a muscular dystrophy with reduced Notch signaling and satellite cell loss.', *EMBO molecular medicine*, 8(11), pp. 1289–1309. Available at: https://doi.org/10.15252/emmm.201505815.

Servián-Morilla, E. *et al.* (2020) 'POGLUT1 biallelic mutations cause myopathy with reduced satellite cells, α-dystroglycan hypoglycosylation and a distinctive radiological pattern.', *Acta neuropathologica*, 139(3), pp. 565–582. Available at: https://doi.org/10.1007/s00401-019-02117-6.

Seymour, P.A. *et al.* (2020) 'Jag1 Modulates an Oscillatory Dll1-Notch-Hes1 Signaling Module to Coordinate Growth and Fate of Pancreatic Progenitors', *Developmental Cell*, 52(6), pp. 731-747.e8. Available at: https://doi.org/10.1016/j.devcel.2020.01.015.

Shaheen, R. *et al.* (2013) 'Mutations in EOGT confirm the genetic heterogeneity of autosomal-recessive Adams-Oliver syndrome.', *American journal of human genetics*, 92(4), pp. 598–604. Available at: https://doi.org/10.1016/j.ajhg.2013.02.012.

Shao, L., Moloney, D.J. and Haltiwanger, R. (2003) 'Fringe Modifies O-Fucose on Mouse Notch1 at Epidermal Growth Factor-like Repeats within the Ligand-binding Site and the Abruptex Region *', *Journal of Biological Chemistry*, 278(10), pp. 7775–7782. Available at: https://doi.org/10.1074/jbc.M212221200.

Sharma, A., Rangarajan, A. and Dighe, R.R. (2013) 'Antibodies against the extracellular domain of human Notch1 receptor reveal the critical role of epidermal-growth-factor-like repeats 25-26 in ligand binding and receptor activation', *Biochemical Journal*, 449(2), pp. 519–530. Available at: https://doi.org/10.1042/BJ20121153.

Shi, S. and Stanley, P. (2003) ‘Protein O-fucosyltransferase 1 is an essential component of Notch signaling pathways.’, *Proceedings of the National Academy of Sciences of the United States of America*, 100(9), pp. 5234–5239. Available at: https://doi.org/10.1073/pnas.0831126100.

Shimizu, D. *et al.* (2007) ‘Detection of NOTCH1 mutations in adult T-cell leukemia/lymphoma and peripheral T-cell lymphoma.’, *International journal of hematology*, 85(3), pp. 212–218. Available at: https://doi.org/10.1532/IJH97.06165.

Sievers, F. and Higgins, D.G. (2021) ‘The Clustal Omega Multiple Alignment Package’, in K. Katoh (ed.) *Multiple Sequence Alignment: Methods and Protocols*. New York, NY: Springer US, pp. 3–16. Available at: https://doi.org/10.1007/978-1-0716-1036-7_1.

Simpson, M.A. *et al.* (2011) ‘Mutations in NOTCH2 cause Hajdu-Cheney syndrome, a disorder of severe and progressive bone loss’, *Nature Genetics*, 43(4), pp. 303–305. Available at: https://doi.org/10.1038/ng.779.

Singh, A. and Choi, K.-W. (2003) ‘Initial state of the Drosophila eye before dorsoventral specification is equivalent to ventral’, *Development*, 130(25), pp. 6351–6360. Available at: https://doi.org/10.1242/dev.00864.

Song, Y. *et al.* (2014) ‘Identification of genomic alterations in oesophageal squamous cell cancer.’, *Nature*, 509(7498), pp. 91–95. Available at: https://doi.org/10.1038/nature13176.

Sorensen, E.B. and Conner, S.D. (2010) ‘γ secretase-dependent cleavage initiates Notch signaling from the plasma membrane’, *Traffic (Copenhagen, Denmark)*, 11(9), p. 1234. Available at: https://doi.org/10.1111/J.1600-0854.2010.01090.X.

Southgate, L. *et al.* (2015) ‘Haploinsufficiency of the NOTCH1 Receptor as a Cause of Adams–Oliver Syndrome With Variable Cardiac Anomalies’, *Circulation: Cardiovascular Genetics*, 8(4), pp. 572–581. Available at: https://doi.org/10.1161/CIRCGENETICS.115.001086.

Sportoletti, P. *et al.* (2010) ‘NOTCH1 PEST domain mutation is an adverse prognostic factor in B-CLL.’, *British journal of haematology*, 151(4), pp. 404–406. Available at: https://doi.org/10.1111/j.1365-2141.2010.08368.x.

Sprinzak, D. *et al.* (2010) ‘Cis-interactions between Notch and Delta generate mutually exclusive signalling states’, *Nature*, 465(7294), pp. 86–90. Available at: https://doi.org/10.1038/nature08959.

Sprinzak, D. *et al.* (2011) ‘Mutual Inactivation of Notch Receptors and Ligands Facilitates Developmental Patterning’, *PLoS Computational Biology*, 7(6), p. e1002069. Available at: https://doi.org/10.1371/journal.pcbi.1002069.

Sprinzak, D. and Blacklow, S.C. (2021) ‘Biophysics of Notch Signaling’, *Annu Rev Biophys*, 50, pp. 157–189. Available at: https://doi.org/10.1146/annurev-biophys-101920-082204.

Stanley, P. (2007) 'Regulation of Notch Signaling by Glycosylation', *Current opinion in structural biology*, 17(5), pp. 530–535. Available at: https://doi.org/10.1016/j.sbi.2007.09.007.

Stenflo, J. *et al.* (1988) 'beta-Hydroxyaspartic acid or beta-hydroxyasparagine in bovine low density lipoprotein receptor and in bovine thrombomodulin.', *Journal of Biological Chemistry*, 263(1), pp. 21–24. Available at: https://doi.org/10.1016/S0021-9258(19)57350-1.

Stenflo, J. *et al.* (1989) 'Hydroxylation of aspartic acid in domains homologous to the epidermal growth factor precursor is catalyzed by a 2-oxoglutarate-dependent dioxygenase.', *Proceedings of the National Academy of Sciences of the United States of America*, 86(2), pp. 444–447.

Stephens, P.J. *et al.* (2013) 'Whole exome sequencing of adenoid cystic carcinoma', *The Journal of Clinical Investigation*, 123(7), p. 2965. Available at: https://doi.org/10.1172/JCI67201.

Stephenson, N.L. and Avis, J.M. (2012) 'Direct observation of proteolytic cleavage at the S2 site upon forced unfolding of the Notch negative regulatory region', *Proceedings of the National Academy of Sciences*, 109(41), pp. E2757–E2765. Available at: https://doi.org/10.1073/pnas.1205788109.

Stittrich, A.-B. *et al.* (2014) 'Mutations in NOTCH1 cause Adams-Oliver syndrome.', *American journal of human genetics*, 95(3), pp. 275–284. Available at: https://doi.org/10.1016/j.ajhg.2014.07.011.

Stoeck, A. *et al.* (2014) 'Discovery of biomarkers predictive of GSI response in triple-negative breast cancer and adenoid cystic carcinoma.', *Cancer discovery*, 4(10), pp. 1154–1167. Available at: https://doi.org/10.1158/2159-8290.CD-13-0830.

Stransky, N. *et al.* (2011) 'The mutational landscape of head and neck squamous cell carcinoma', *Science (New York, N.Y.)*, 333(6046), pp. 1157–1160. Available at: https://doi.org/10.1126/SCIENCE.1208130.

Strati, T.M. *et al.* (2017) 'Prognostic Subcellular Notch2, Notch3 and Jagged1 Localization Patterns in Early Triple-negative Breast Cancer', *Anticancer research*, 37(5), pp. 2323–2334. Available at: https://doi.org/10.21873/ANTICANRES.11570.

Streb, H. *et al.* (1983) 'Release of Ca2+ from a nonmitochondrial intracellular store in pancreatic acinar cells by inositol-1,4,5-trisphosphate', *Nature*, 306(5938), pp. 67–69. Available at: https://doi.org/10.1038/306067a0.

Struhl, G. and Adachi, A. (2000) 'Requirements for Presenilin-Dependent Cleavage of Notch and Other Transmembrane Proteins', *Molecular Cell*, 6(3), pp. 625–636. Available at: https://doi.org/10.1016/S1097-2765(00)00061-7.

Suckling, R.J. *et al.* (2017) 'Structural and functional dissection of the interplay between lipid and Notch binding by human Notch ligands', *The EMBO Journal*, 36(15), pp. 2204–2215.

Available at: https://doi.org/10.15252/embj.201796632.

Sugiyama, Masakazu *et al.* (2016) 'High expression of the Notch ligand Jagged-1 is associated with poor prognosis after surgery for colorectal cancer', *Cancer Science*, 107(11), pp. 1705–1716. Available at: https://doi.org/10.1111/CAS.13075.

Sullivan, J.M. *et al.* (2020) 'Dominant mutations of the Notch ligand Jagged1 cause peripheral neuropathy.', *The Journal of clinical investigation*, 130(3), pp. 1506–1512. Available at: https://doi.org/10.1172/JCI128152.

Sutherland, E.W. and Rall, T.W. (1958) 'Fractionation and characterization of a cyclic adenine ribonucleotide formed by tissue particles', *The Journal of Biological Chemistry*, 232(2), pp. 1077–1091.

Svergun, D., Barberato, C. and Koch, M.H.J. (1995) 'CRYSOL– a Program to Evaluate X-ray Solution Scattering of Biological Macromolecules from Atomic Coordinates', *Journal of Applied Crystallography*, 28(6), pp. 768–773. Available at: https://doi.org/10.1107/S0021889895007047.

Svergun, D.I. *et al.* (eds) (2013) *Small Angle X-Ray and Neutron Scattering from Solutions of Biological Macromolecules*. Oxford University Press. Available at: https://doi.org/10.1093/acprof:oso/9780199639533.002.0003.

Takashima, S. *et al.* (2011) 'Development of the *Drosophila* entero-endocrine lineage and its specification by the Notch signaling pathway', *Developmental Biology*, 353(2), pp. 161–172. Available at: https://doi.org/10.1016/j.ydbio.2011.01.039.

Takeuchi, H. *et al.* (2011) 'Rumi functions as both a protein O-glucosyltransferase and a protein O-xylosyltransferase.', *Proceedings of the National Academy of Sciences of the United States of America*, 108(40), pp. 16600–16605. Available at: https://doi.org/10.1073/pnas.1109696108.

Takeuchi, H. *et al.* (2017) 'O-Glycosylation modulates the stability of epidermal growth factor-like repeats and thereby regulates Notch trafficking', *The Journal of biological chemistry*, 292(38), pp. 15964–15973. Available at: https://doi.org/10.1074/JBC.M117.800102.

Takeuchi, H. *et al.* (2018) 'Two novel protein O-glucosyltransferases that modify sites distinct from POGLUT1 and affect Notch trafficking and signaling.', *Proceedings of the National Academy of Sciences of the United States of America*, 115(36), pp. E8395–E8402. Available at: https://doi.org/10.1073/pnas.1804005115.

Takeuchi, H. and Haltiwanger, R.S. (2014) 'Significance of glycosylation in Notch signaling', *Biochemical and biophysical research communications*, 453(2), pp. 235–242. Available at: https://doi.org/10.1016/j.bbrc.2014.05.115.

Tamura, K. *et al.* (1995) 'Physical interaction between a novel domain of the receptor Notch and the transcription factor RBP-Jκ/Su(H)', *Current Biology*, 5(12), pp. 1416–1423. Available

at: https://doi.org/10.1016/S0960-9822(95)00279-X.

Tani, S. *et al.* (2001) 'The N- and C-terminal regions of RBP-J interact with the ankyrin repeats of Notch1 RAMIC to activate transcription', *Nucleic Acids Research*, 29(6), pp. 1373–1380.

Taylor, P. *et al.* (2014) 'Fringe-mediated extension of O-linked fucose in the ligand-binding region of Notch1 increases binding to mammalian Notch ligands.', *Proceedings of the National Academy of Sciences of the United States of America*, 111(20), pp. 7290–5. Available at: https://doi.org/10.1073/pnas.1319683111.

Thakurdas, S.M. *et al.* (2016) 'Jagged1 heterozygosity in mice results in a congenital cholangiopathy which is reversed by concomitant deletion of one copy of Poglut1 (Rumi).', *Hepatology (Baltimore, Md.)*, 63(2), pp. 550–565. Available at: https://doi.org/10.1002/hep.28024.

Thambyrajah, R. *et al.* (2024) 'Cis inhibition of NOTCH1 through JAGGED1 sustains embryonic hematopoietic stem cell fate', *Nature Communications*, 15(1), p. 1604. Available at: https://doi.org/10.1038/s41467-024-45716-y.

Trøen, G. *et al.* (2008) 'NOTCH2 mutations in marginal zone lymphoma.', *Haematologica*, 93(7), pp. 1107–1109. Available at: https://doi.org/10.3324/haematol.11635.

Troost, T. *et al.* (2012) 'The tumour suppressor Lethal (2) giant discs is required for the function of the ESCRT-III component Shrub/CHMP4', *Journal of Cell Science*, 125(3), pp. 763–776. Available at: https://doi.org/10.1242/JCS.097261.

Troost, T. *et al.* (2023) 'Cis-inhibition suppresses basal Notch signaling during sensory organ precursor selection', *Proceedings of the National Academy of Sciences*, 120(23), p. e2214535120. Available at: https://doi.org/10.1073/pnas.2214535120.

Tsukamoto, Y. *et al.* (2022) 'Glycoproteomics of NOTCH1 EGF repeat fragments overexpressed with different glycosyltransferases in HEK293T cells reveals insights into O-GlcNAcylation of NOTCH1', *Glycobiology*, 32(7), pp. 616–628. Available at: https://doi.org/10.1093/glycob/cwac015.

Tsunematsu, R. *et al.* (2004) 'Mouse Fbw7/Sel-10/Cdc4 is required for notch degradation during vascular development', *The Journal of Biological Chemistry*, 279(10), pp. 9417–9423. Available at: https://doi.org/10.1074/jbc.M312337200.

Tveriakhina, L. *et al.* (2018) 'The ectodomains determine ligand function in vivo and selectivity of DLL1 and DLL4 toward NOTCH1 and NOTCH2 in vitro.', *eLife*, 7. Available at: https://doi.org/10.7554/eLife.40045.

Tveriakhina, L. *et al.* (2024) 'Temporal dynamics and stoichiometry in human Notch signaling from Notch synaptic complex formation to nuclear entry of the Notch intracellular domain', *Developmental Cell*, 59(11), pp. 1425-1438.e8. Available at:

https://doi.org/10.1016/j.devcel.2024.03.021.

Umair, M. *et al.* (2022) 'Clinical genetics of spondylocostal dysostosis: A mini review.', *Frontiers in genetics*, 13, p. 996364. Available at: https://doi.org/10.3389/fgene.2022.996364.

Urata, Y. *et al.* (2020) 'Xylosyl Extension of O-Glucose Glycans on the Extracellular Domain of NOTCH1 and NOTCH2 Regulates Notch Cell Surface Trafficking', *Cells*, 9(5), p. 1220. Available at: https://doi.org/10.3390/cells9051220.

Urata, Y. and Takeuchi, H. (2020) 'Effects of Notch glycosylation on health and diseases', *Development, Growth & Differentiation*, 62(1), pp. 35–48. Available at: https://doi.org/10.1111/dgd.12643.

Vaccari, T. *et al.* (2008) 'Endosomal entry regulates Notch receptor activation in Drosophila melanogaster', *The Journal of Cell Biology*, 180(4), p. 755. Available at: https://doi.org/10.1083/JCB.200708127.

Vaish, V., Kim, J. and Shim, M. (2017) 'Jagged-2 (JAG2) enhances tumorigenicity and chemoresistance of colorectal cancer cells', *Oncotarget*, 8(32), p. 53262. Available at: https://doi.org/10.18632/ONCOTARGET.18391.

Van Vlierberghe, P. *et al.* (2011) 'ETV6 mutations in early immature human T cell leukemias.', *The Journal of experimental medicine*, 208(13), pp. 2571–2579. Available at: https://doi.org/10.1084/jem.20112239.

Varadi, M. *et al.* (2024) 'AlphaFold Protein Structure Database in 2024: providing structure coverage for over 214 million protein sequences', *Nucleic Acids Research*, 52(D1), pp. D368–D375. Available at: https://doi.org/10.1093/nar/gkad1011.

Varshney, S. and Stanley, P. (2018) 'Multiple roles for O-glycans in Notch signalling.', *FEBS letters*, 592(23), pp. 3819–3834. Available at: https://doi.org/10.1002/1873-3468.13251.

Vässin, H. *et al.* (1987) 'The neurogenic gene Delta of Drosophila melanogaster is expressed in neurogenic territories and encodes a putative transmembrane protein with EGF-like repeats', *The EMBO Journal*, 6(11), pp. 3431–3440. Available at: https://doi.org/10.1002/j.1460-2075.1987.tb02666.x.

Vitt, U.A., Hsu, S.Y. and Hsueh, A.J.W. (2001) 'Evolution and Classification of Cystine Knot-Containing Hormones and Related Extracellular Signaling Molecules', *Molecular Endocrinology*, 15(5), pp. 681–694. Available at: https://doi.org/10.1210/mend.15.5.0639.

Voas, M.G. and Rebay, I. (2004) 'Signal integration during development: Insights from the Drosophila eye', *Developmental Dynamics*, 229(1), pp. 162–175. Available at: https://doi.org/10.1002/dvdy.10449.

Wang, N.J. *et al.* (2011) 'Loss-of-function mutations in Notch receptors in cutaneous and lung squamous cell carcinoma', *Proceedings of the National Academy of Sciences of the United*

States of America, 108(43), pp. 17761–17766. Available at: https://doi.org/10.1073/PNAS.1114669108/-/DCSUPPLEMENTAL.

Wang, W. and Struhl, G. (2004) 'Drosophila Epsin mediates a select endocytic pathway that DSL ligands must enter to activate Notch', *Development*, 131(21). Available at: https://doi.org/10.1242/dev.01413.

Wang, W. and Struhl, G. (2005) 'Distinct roles for Mind bomb, Neuralized and Epsin in mediating DSL endocytosis and signaling in Drosophila', *Development (Cambridge, England)*, 132(12), pp. 2883–2894. Available at: https://doi.org/10.1242/DEV.01860.

Wang, X. and Ha, T. (2013) 'Defining Single Molecular Forces Required to Activate Integrin and Notch Signaling', *Science*, 340(6135), pp. 991–994. Available at: https://doi.org/10.1126/science.1231041.

Wang, Y. *et al.* (1996) 'Identification of a GDP-L-fucose:polypeptide fucosyltransferase and enzymatic addition of O-linked fucose to EGF domains.', *Glycobiology*, 6(8), pp. 837–842. Available at: https://doi.org/10.1093/glycob/6.8.837.

Wang, Y. *et al.* (2001) 'Modification of epidermal growth factor-like repeats with O-fucose. Molecular cloning and expression of a novel GDP-fucose protein O-fucosyltransferase.', *The Journal of biological chemistry*, 276(43), pp. 40338–40345. Available at: https://doi.org/10.1074/jbc.M107849200.

Wang, Y. *et al.* (2017) 'Uncontrolled angiogenic precursor expansion causes coronary artery anomalies in mice lacking Pofut1.', *Nature communications*, 8(1), p. 578. Available at: https://doi.org/10.1038/s41467-017-00654-w.

Weinmaster, G., Roberts, V.J. and Lemke, G. (1991) 'A homolog of Drosophila Notch expressed during mammalian development', *Development (Cambridge, England)*, 113(1), pp. 199–205. Available at: https://doi.org/10.1242/dev.113.1.199.

Weisshuhn, P.C. *et al.* (2016) 'Non-Linear and Flexible Regions of the Human Notch1 Extracellular Domain Revealed by High-Resolution Structural Studies', *Structure (London, England : 1993)*, 24(4), pp. 555–566. Available at: https://doi.org/10.1016/j.str.2016.02.010.

Weng, A.P. *et al.* (2004) 'Activating mutations of NOTCH1 in human T cell acute lymphoblastic leukemia', *Science*, 306(5694), pp. 269–271. Available at: https://doi.org/10.1126/SCIENCE.1102160/SUPPL_FILE/WENG_SOM.PDF.

Westhoff, B. *et al.* (2009) 'Alterations of the Notch pathway in lung cancer', *Proceedings of the National Academy of Sciences of the United States of America*, 106(52), p. 22293. Available at: https://doi.org/10.1073/PNAS.0907781106.

Wharton, K.A. *et al.* (1985) 'Nucleotide sequence from the neurogenic locus notch implies a gene product that shares homology with proteins containing EGF-like repeats', *Cell*, 43(3 Pt 2), pp. 567–81. Available at: https://doi.org/10.1016/0092-8674(85)90229-6.

Whiteman, P. *et al.* (2013) 'Molecular basis for Jagged-1/Serrate ligand recognition by the Notch receptor.', *The Journal of biological chemistry*, 288(10), pp. 7305–12. Available at: https://doi.org/10.1074/jbc.M112.428854.

Wilkin, M. *et al.* (2008) 'Drosophila HOPS and AP-3 Complex Genes Are Required for a Deltex-Regulated Activation of Notch in the Endosomal Trafficking Pathway', *Developmental Cell*, 15(5), pp. 762–772. Available at: https://doi.org/10.1016/j.devcel.2008.09.002.

Williamson, D.B. and Haltiwanger, R.S. (2022) 'Identification, function, and biological relevance of POGLUT2 and POGLUT3', *Biochemical Society Transactions*, 50(2), pp. 1003–1012. Available at: https://doi.org/10.1042/BST20210850.

Wilson, J.J. and Kovall, R.A. (2006) 'Crystal structure of the CSL-Notch-Mastermind ternary complex bound to DNA.', *Cell*, 124(5), pp. 985–96. Available at: https://doi.org/10.1016/j.cell.2006.01.035.

Windler, S.L. and Bilder, D. (2010) 'Endocytic internalization routes required for delta/notch signaling', *Current biology : CB*, 20(6), pp. 538–543. Available at: https://doi.org/10.1016/J.CUB.2010.01.049.

Wouters, M.A. *et al.* (2005) 'Evolution of distinct EGF domains with specific functions', *Protein Science : A Publication of the Protein Society*, 14(4), pp. 1091–1103. Available at: https://doi.org/10.1110/ps.041207005.

Xie, X., Cho, B. and Fischer, J.A. (2012) 'Drosophila Epsin's role in Notch ligand cells requires three Epsin protein functions: The lipid binding function of the ENTH domain, a single Ubiquitin interaction motif, and a subset of the C-terminal protein binding modules', *Developmental Biology*, 363(2). Available at: https://doi.org/10.1016/j.ydbio.2012.01.004.

Xu, T. *et al.* (1990) *The Notch locus and the genetic circuitry involved in early Drosophila neurogenesis*. Available at: http://genesdev.cshlp.org/content/4/3/464.full.pdf.

Xu, T. and Artavanis-Tsakonas, S. (1990) 'deltex, a locus interacting with the neurogenic genes, Notch, Delta and mastermind in Drosophila melanogaster', *Genetics*, 126(3), pp. 665–677. Available at: https://doi.org/10.1093/GENETICS/126.3.665.

Xu, X. *et al.* (2015) 'Insights into Autoregulation of Notch3 from Structural and Functional Studies of Its Negative Regulatory Region.', *Structure (London, England : 1993)*, 23(7), pp. 1227–1235. Available at: https://doi.org/10.1016/j.str.2015.05.001.

Xu, X. *et al.* (2023) 'Jag1-Notch cis-interaction determines cell fate segregation in pancreatic development', *Nature Communications*, 14(1), p. 348. Available at: https://doi.org/10.1038/s41467-023-35963-w.

Yamamoto, S. *et al.* (2012) 'A mutation in EGF repeat-8 of notch discriminates between serrate/jagged and delta family ligands', *Science*, 338(6111), pp. 1229–1232. Available at: https://doi.org/10.1126/science.1228745.

Yao, D. *et al.* (2011) ‘Protein O-fucosyltransferase 1 (Pofut1) regulates lymphoid and myeloid homeostasis through modulation of Notch receptor ligand interactions.’, *Blood*, 117(21), pp. 5652–5662. Available at: https://doi.org/10.1182/blood-2010-12-326074.

Yochem, J., Weston, K. and Greenwald, I. (1988) ‘The Caenorhabditis elegans lin-12 gene encodes a transmembrane protein with overall similarity to Drosophila Notch’, *Nature*, 335(6190), pp. 547–50. Available at: https://doi.org/10.1038/335547a0.

Yokoi, Y. and Nishimura, S.I. (2020) ‘Effect of Site-Specific O-Glycosylation on the Structural Behavior of NOTCH1 Receptor Extracellular EGF-like Domains 11 and 10’, *Chemistry - A European Journal*, 26(54). Available at: https://doi.org/10.1002/chem.202002652.

Young, K.Z. *et al.* (2022) ‘Oligomerization, trans-reduction, and instability of mutant NOTCH3 in inherited vascular dementia’, *Communications Biology 2022 5:1*, 5(1), pp. 1–12. Available at: https://doi.org/10.1038/s42003-022-03259-2.

Yuan, L. *et al.* (2024) ‘CADASIL: A *NOTCH3*-associated cerebral small vessel disease’, *Journal of Advanced Research* [Preprint]. Available at: https://doi.org/10.1016/j.jare.2024.01.001.

Yuan, X. *et al.* (2015) ‘Meta-analysis reveals the correlation of Notch signaling with non-small cell lung cancer progression and prognosis’, *Scientific Reports*, 5. Available at: https://doi.org/10.1038/SREP10338.

Yuan, Z. *et al.* (2016) ‘Structure and Function of the Su(H)-Hairless Repressor Complex, the Major Antagonist of Notch Signaling in Drosophila melanogaster’, *PLoS Biology*, 14(7), p. e1002509. Available at: https://doi.org/10.1371/journal.pbio.1002509.

Zeronian, M.R. *et al.* (2021) ‘Notch–Jagged signaling complex defined by an interaction mosaic’, *Proceedings of the National Academy of Sciences*, 118(30), p. e2102502118. Available at: https://doi.org/10.1073/pnas.2102502118.

Zhang, J. *et al.* (2012) ‘The genetic basis of early T-cell precursor acute lymphoblastic leukaemia.’, *Nature*, 481(7380), pp. 157–163. Available at: https://doi.org/10.1038/nature10725.

Zheng, C.G. *et al.* (2015) ‘Immunohistochemical expression of Notch1, Jagged1, NF-κB and MMP-9 in colorectal cancer patients and the relationship to clinicopathological parameters’, *Cancer Biomarkers*, 15(6), pp. 889–897. Available at: https://doi.org/10.3233/CBM-150533.